



**HAL**  
open science

## Multinuclear NMR in Polypeptide Liquid Crystals: Three Fertile Decades of Methodological Developments and Analytical Challenges

Philippe Lesot, Christie Aroulanda, Philippe Berdagué, Abdelkrim Meddour,  
Denis Merlet, Jonathan Farjon, Nicolas Giraud, Olivier Lafon

### ► To cite this version:

Philippe Lesot, Christie Aroulanda, Philippe Berdagué, Abdelkrim Meddour, Denis Merlet, et al.. Multinuclear NMR in Polypeptide Liquid Crystals: Three Fertile Decades of Methodological Developments and Analytical Challenges. Progress in Nuclear Magnetic Resonance Spectroscopy, 2019, Progress in Nuclear Magnetic Resonance Spectroscopy, 116, pp.85-154. 10.1016/j.pnmrs.2019.10.001 . hal-02351278

**HAL Id: hal-02351278**

**<https://hal.science/hal-02351278v1>**

Submitted on 17 Nov 2020

**HAL** is a multi-disciplinary open access archive for the deposit and dissemination of scientific research documents, whether they are published or not. The documents may come from teaching and research institutions in France or abroad, or from public or private research centers.

L'archive ouverte pluridisciplinaire **HAL**, est destinée au dépôt et à la diffusion de documents scientifiques de niveau recherche, publiés ou non, émanant des établissements d'enseignement et de recherche français ou étrangers, des laboratoires publics ou privés.

# Multinuclear NMR in Polypeptide Liquid Crystals: Three Fertile Decades of Methodological Developments and Analytical Challenges

Philippe Lesot<sup>a,b,\*</sup>  Christie Aroulanda<sup>a</sup>, Philippe Berdagué<sup>a</sup>, Abdelkrim Meddour<sup>a</sup>, Denis Merlet<sup>a</sup>, Jonathan Farjon<sup>b,c</sup>, Nicolas Giraud<sup>d</sup> and Olivier Lafon<sup>e,f</sup>

<sup>a</sup> Université Paris Sud/Université Paris-Saclay, UMR CNRS 8182, Institut de Chimie Moléculaire et des Matériaux d'Orsay, ICMMO, Equipe RMN en Milieu Orienté, Bât. 410, 15 rue du Doyen Georges Poitou, F-91405 Orsay cedex, France.

<sup>b</sup> Centre National de la Recherche Scientifique (CNRS), 3 rue Michel Ange, F-75016 Paris, France.

<sup>c</sup> Faculté des Sciences et Techniques de Nantes, UMR CNRS 6230, Chimie et Interdisciplinarité, Synthèse, Analyse, Modélisation, CEISAM, Equipe EBSI, BP 92208, 2 rue de la Houssinière, F-44322 Nantes cedex 3, France.

<sup>d</sup> Université Paris Descartes, Sorbonne Paris Cité, UMR CNRS 8601, Laboratory of Pharmacological and Toxicological Chemistry and Biochemistry, LPTCB, 45 rue des Saints Pères, F-75006 Paris, France.

<sup>e</sup> Université de Lille, CNRS, Centrale Lille, ENSCL, Univ. Artois, UMR CNRS 8181, Unité de Catalyse et Chimie du Solide, UCCS, F-59000 Lille, France.

<sup>f</sup> Institut Universitaire de France, 1 rue Descartes, F-75231 Paris, France.

*Dedication: This article is dedicated to the 75<sup>th</sup> anniversary of Prof. Jacques Courtieu*

## ABSTRACT :

NMR spectroscopy of oriented samples makes accessible residual anisotropic intramolecular NMR interactions, such as chemical shift anisotropy (RCSA), dipolar coupling (RDC), and quadrupolar coupling (RQC), while preserving high spectral resolution. In addition, in a chiral aligned environment, enantiomers of chiral molecules or enantiopic elements of prochiral compounds adopt different average orientations on the NMR timescale, and hence produce distinct NMR spectra or signals. NMR spectroscopy in chiral aligned media is a powerful analytical tool, and notably provides unique information on (pro)chirality analysis, natural isotopic fractionation, stereochemistry, as well as molecular conformation and configuration. Significant progress has been made in this area over the three last decades, particularly using polypeptide-based chiral liquid crystals (CLCs) made of organic solutions of helically chiral polymers (as PBLG) in organic solvents. This review presents an overview of NMR in polymeric LCs. In particular, we describe the theoretical tools and the major NMR methods that have been developed and applied to study (pro)chiral molecules dissolved in such oriented solvents. We also discuss the representative applications illustrating the analytical potential of this original NMR tool. This overview article is dedicated to thirty years of original contributions to the development of NMR spectroscopy in polypeptide-based chiral liquid crystals.


## KEYWORDS :

Anisotropic NMR  
Spectral enantiodetection  
Polypeptide Oriented media  
Stereochemistry  
Analytical applications

**CORRESPONDING AUTHOR : Philippe Lesot**

**Mail :** [philippe.lesot@universite-paris-saclay](mailto:philippe.lesot@universite-paris-saclay) / [philippe.lesot@u-psud.fr](mailto:philippe.lesot@u-psud.fr)

**Tel :** 33(1) 69 15 47 59

 : <http://orcid.org/000-0002-5811-7530>

## Content

### 1. General introduction

### 2. Basic considerations of NMR in chiral liquid crystals

- 2.1. Orientational order *versus* random motions
- 2.2. Chirality of the environment
- 2.3. A wealth of order-dependent NMR interactions
  - 2.3.1. The residual chemical shift anisotropy (RCSA)
  - 2.3.2. The residual dipolar coupling (RDC)
  - 2.3.3. The residual quadrupolar coupling (RQC)
- 2.4. Combination of two anisotropic interactions
  - 2.4.1.  $^{13}\text{C}$ -RCSA and  $^{13}\text{C}$ -X RDC
  - 2.4.2.  $^2\text{H}$ -RQC and  $^2\text{H}$ -X RDC

### 3. Weakly-orienting liquid crystals

- 3.1. Polypeptide-based LCs *versus* thermotropics
- 3.2. The polypeptide family
  - 3.2.1. Neat helical polymers (PBLG, PELG, PCBLL, PBMLG)
  - 3.2.2. Analysis of highly polar compounds
  - 3.2.3. Achiral oriented systems by compensation
  - 3.2.4. Mixtures of two homopolypeptides
- 3.3. Possible alternatives to polypeptide systems
- 3.4. The stretched/compressed gels

### 4. Simplifying anisotropic $^1\text{H}$ NMR spectra in weakly orienting phases

- 4.1. Measurement of homonuclear total couplings
- 4.2. Extraction of  $^1\text{H}$  homonuclear RDCs by selective refocusing based methods
  - 4.2.1. The SERF 2D experiment
  - 4.2.2. Improvements to the original SERF pulse sequence
- 4.3. Simplification of  $^1\text{H}$  lineshapes
  - 4.3.1. Pure-shift techniques applied along the direct spectral domain
  - 4.3.2. Multiple quantum correlation spectroscopy
  - 4.3.3. Other applications of spin state selection correlation spectroscopy
- 4.4. Determination of enantiomeric excesses (ee's) using  $^1\text{H}$  NMR

### 5. Exploiting the $^{13}\text{C}$ NMR spectroscopy

- 5.1. 1D experiments
  - 5.1.1. Proton-coupled  $^{13}\text{C}$  NMR
  - 5.1.2. Potential of  $^{13}\text{C}$ - $\{^1\text{H}\}$  NMR
- 5.2. **Variants** of  $^{13}\text{C}$ -detected 2D experiments
  - 5.2.1. The  $T_{\text{CH}}$ -resolved 2D experiments
  - 5.2.2. The concept of down-scaled  $T_{\text{CH}}$ -resolved sequences
  - 5.2.3. HETSERF
  - 5.2.4. HETCOR

5.2.5. INADEQUATE: exploiting the DQ coherences

5.3. Inverse  $^{13}\text{C}$ - $^1\text{H}$  correlation 2D experiments

5.4. Examples of applications in asymmetric synthesis

## 6. The potentialities of $^2\text{H}$ NMR spectroscopy

6.1. 1D-NMR analyses of deuterated chiral analytes

6.1.1. Illustrative 1D NMR examples of classical chirality

6.1.2. Exploring "atypical" chiralities

6.1.3. Derivatizing chiral molecules with achiral deuterated derivative agents

6.1.4. Discrimination by exchangeable deuterons

6.1.5. Isotopic chirality and spectral discrimination

6.2. Development of  $^2\text{H}$  multidimensional NMR: homonuclear QUOSY

6.2.1. Homonuclear 2D/3D tools for analysing complex  $^2\text{H}$  or natural abundance deuterium (NAD) spectra

6.2.2. The z-filter for obtaining pure-phased spectra

6.2.3. Methods involving  $^2\text{H}$  double quantum transitions

6.2.4. Non-uniform sampling and special processing

6.2.5. Anisotropic deuterium ultrafast (ADUF) NMR: Recording sub-second  $^2\text{H}$  2D experiments

6.3. Analytical applications involving isotopically enriched molecules

6.3.1. Investigation of intramolecular dynamic processes

6.3.2. Enantiopurity in asymmetric synthesis involving deuterated materials

6.3.3. Understanding the stereochemistry of enzymatic reactions

6.3.4. "On-the-fly" monitoring of enzymatic reactions

6.4. Deuterium NMR at natural abundance (NAD NMR)

6.4.1. From binary to ternary mixtures

6.4.2. NAD NMR and highly-abundant, magnetically active heteroatoms

6.4.3. Determination of enantioselectivity in asymmetric synthesis

6.4.4. Analysis of chiral hydrocarbons

6.5. Contribution of anisotropic natural abundance deuterium NMR (ANAD NMR<sup>®</sup>) to isotopic fractionation studies

6.5.1. Alternatives to the site-specific isotopic fractionation NMR (SNIF-NMR<sup>®</sup>) protocol

6.5.2. Revisiting the fatty acid family

6.5.3. Miliacine and vaniline

## 7. Pushing the limits: combining $^{13}\text{C}$ and $^2\text{H}$ anisotropic information

7.1. Correlating  $^2\text{H}$  with  $^{13}\text{C}$  nuclei: the carbon-deuterium correlation in oriented media (CDCOM) 2D experiment

7.1.1. Examples of weakly-aligned deuterated molecules

7.1.2. Analysis of the perdeuterated *cis*-decalin

7.2. The deuterium-carbon-deuterium (DCD) double-transfer based experiments

7.3. First natural abundance spectroscopy deuterium and carbon (NASDAC) 2D experiments: The ultimate frontier?

8. Exploring various magnetically-active nuclei

8.1. Mono- and trifluorinated probes

8.2. Phosphorous-31

8.3. Highly abundant exotic quadrupolar nuclei

## 9. From chirality to prochirality

9.1. Discrimination of enantiotopic elements in prochiral rigid compounds using NMR in chiral liquid crystals

9.2 Principles of symmetric and antisymmetric matrix decomposition

9.3. Enantiotopic discrimination investigated by  $^2\text{H}$  or natural abundance deuterium NAD NMR

9.4. Discrimination of enantiotopic elements in prochiral flexible compounds

9.5. Differentiation between enantiotopic  $\text{H}\cdots\text{H}$  directions in  $\text{C}_s$  molecules

9.6. Differentiation between enantiotopic C-H directions in  $\text{C}_{2v}$  molecules containing no prostereogenic tetrahedral center

## 10. Anisotropic NMR and structure determination

10.1. Using ( $^{13}\text{C}$ - $^1\text{H}$ )-RDCs and  $^{13}\text{C}$ -RCSAs

10.2. Contributions of  $^2\text{H}$ -RQCs to structural analysis

10.2.1. Structural assignment of RQCs

10.2.2. A hyphenated computational  $^2\text{H}$  protocol

10.2.3. Absolute configuration: a  $^2\text{H}$ -NMR-based empirical approach

## 11. Conclusion and prospects

## 12. Acknowledgments

## 13. Special dedications

## 14. References

## 1. General introduction

The term chirality is derived from the Ancient Greek word meaning hand, “ $\chi\epsilon\iota\rho$ ”. The mirror images of chiral molecules (like human hands) are non superimposable. This property has numerous consequences in Chemistry [1], so distinguishing the signature of chiral molecular objects is an important task. Naturally, the determination of the enantiomeric excess (*ee*) of chiral mixtures has been fostered by the development of enantioselective synthesis, an important field of modern Chemistry [1, 2, 3, 4, 5]. The reliable evaluation of enantiomeric purity is especially crucial for the pharmaceutical industry since enantiomers have different biological activities, including pharmacokinetics, toxicity, immune response, etc. In this context, much effort has been devoted to proposing effective analytical methodologies.

Chiroptical techniques (based on the optical rotatory power) as well as chiral gas chromatography (GC) or high-pressure liquid chromatography (HPLC) are generally employed as routine tools for robust and rapid determinations of *ee*. Chiroptical techniques are sensitive to numerous factors, such as concentration of the analyte, pH, wavelength, etc. and the measurement of enantiomeric purity using this technique can be skewed by the presence of chiral impurities. Chromatographical methods are not always successful while chiral columns can be rather expensive as well as very compound specific. More sophisticated optical spectroscopy methods exist such as Raman optical activity (ROA), optical rotatory dispersion (ORD) or vibrational circular dichroism (VCD) spectroscopy. However, those tools, which have to be combined with density functional theory (DFT) computations, are not really considered for routine analyses [2, 6, 7].

Methods based on Nuclear Magnetic Resonance (NMR) spectroscopy [8] have also been explored for the determination of enantiomeric purity, since this technique provides unique insights into the atomic-level structure and dynamics of gases, liquids and solids [8, 9, 10, 11, 12, 13, 14, 15]. In a strong magnetic field, precessing nuclear spins in chiral molecules in an isotropic liquid induce a rotating electric polarization of opposite signs for enantiomers [16, 17, 18]. Alternatively, an applied electric field should also induce distinct NMR signals for enantiomers in an isotropic liquid [19]. However, these effects have not yet been observed. Conversely, differences in the intensity of  $^1\text{H}\rightarrow^{13}\text{C}$  cross-polarization under magic-angle spinning (CPMAS) in solid-state NMR (SSNMR) between pure enantiomers of crystalline aminoacids have been reported [20]. Such a difference has been ascribed to distinct electron spin polarizations for the enantiomers because of a chirally-induced spin selectivity (CISS) effect. To the best of our knowledge, no other example of distinct NMR spectra between pure enantiomers has been reported at present time.

It has also been experimentally shown that the enantiomeric purity of chiral molecules can be determined using solid-state NMR. This determination can only be made to the extent that a racemate can form a racemic compound crystalline phase. In this case, the unit cell of such a phase contains an equal

amount of each enantiomer in a well-defined arrangement [1, 20, 21, 22, 23, 24]. The packing of molecules and symmetries in the crystals of enantiomers and racemic compounds differ, which can result in distinct NMR parameters, such as isotropic chemical shifts [21, 22] or dipolar couplings [22, 23, 24]. Nevertheless, this technique is not applicable for conglomerates, *i.e.* mechanical mixtures of pure enantiomer crystals, and pseudo-racemates, *i.e.* solid solutions of enantiomers which coexist in an unordered manner in the crystal lattice. Furthermore, it requires the crystallization of the investigated compound [1]. Finally, solid-state NMR is often less sensitive than NMR of liquids or NMR using mesophases (alignment media).

The enantiomeric purity of chiral compounds has also been determined using NMR spectroscopy in isotropic liquids or in mesophases. These approaches require the use of an enantiopure agent (a chiral partner). For NMR in isotropic liquids, three classes of enantiopure agent are commonly employed: i) chiral derivatizing agents (**CDAs**) which form covalent bonds with enantiomers and convert them into stable diastereoisomers; ii) chiral lanthanide-induced shift reagents (**CLSRs**) such as chiral europium (III) complexes, which are coordinated by the enantiomers and lead to the formation of diastereoisomeric complexes and iii) chiral solvating agents (**CSA**) (which should not be confused with chemical shift anisotropy, see the first list of acronyms) including chiral cyclodextrins [3, 26, 27, 28]. Obviously, each of these tools possesses analytical advantages and specific drawbacks in terms of practicability and application ranges. In particular, the enantiopure agent must often be carefully chosen as a function of the (specific) chemical functionalities (hydroxyl group, carboxylic acid, amine, ...) of the investigated chiral compound. With the exception of cyclodextrins (chiral macrocycles), these agents are often not suitable for apolar chiral compounds [29].

Another powerful approach to discriminating enantiomers relies on NMR spectroscopy using chiral ordering agents (**COAs**) as solvent, such as enantiopure liquid crystals (**LCs**). Due to the chirality of the system, enantiomers dissolved in these aligning media adopt distinct orientations on average, thus leading to two NMR spectra, one for each enantiomer. This approach was first demonstrated by Snyder *et al.* in 1968 using cholesteric systems and  $^1\text{H}$  NMR [30], and then was later revisited in 1989 [31]. The difference in orientations between enantiomers in a chiral oriented solvent can be observed *via* residual intramolecular anisotropic interactions, such as: i) residual chemical shift anisotropy (**RCSA**); ii) residual dipolar coupling (**RDC**); and iii) residual quadrupolar coupling (**RQC**) for nuclei with a spin  $I > \frac{1}{2}$  [32, 33, 34, 35].

Historically, NMR in LC began in 1963 with the famous work of Saupe and Englert [36, 37, 38, 39], which opened a new and successful branch of NMR spectroscopy, and which is still in progress. By definition, anisotropic NMR arises when host/guest molecules are, on average, oriented [32, 33, 34]. Indeed, in isotropic liquids, random molecular motion averages most anisotropic (order-dependent) NMR

interactions to zero, and hence, the NMR resonance frequencies are only determined by the isotropic chemical shift and the isotropic  $J$ -couplings. In contrast, in oriented liquids, the molecules are partially ordered with respect to the static magnetic field and the intramolecular anisotropic interactions remain [32, 33, 34]. Note, however, that diffusion and rotation of molecules in LC averages most intermolecular anisotropic interactions to zero, as in an isotropic liquid. Hence, the NMR spectra of oriented liquids can be modelled by considering spin systems of isolated molecules.

Interestingly, in weakly ordering solvents, such as polypeptide-based liquid crystals, the degree of solute orientation is low and the magnitude of residual anisotropic NMR interactions (such as RCSA or RDC) is comparable to or lower than that of isotropic NMR interactions (such as isotropic electronic shielding or the  $J$  coupling). Solutes dissolved in such media generally exhibit high-resolution spectra with linewidths at half of maximum (FWHM) of few Hertz, which are often easier to analyse and assign than NMR spectra recorded in strongly ordering solvents, such as thermotropic liquid crystals [32, 33, 34]. Thus, the introduction by Courtieu *et al.* of weakly-ordering chiral ordering agents in 1992 [40], such as chiral liquid-crystalline systems made of polypeptides and conventional organic solvents, has been a groundbreaking development, and has considerably expanded the application range of these agents [35, 41]. In particular, these types of chiral mesophases can accommodate high concentrations of (organo-soluble or water-compatible) solutes incorporating various chemical functionalities.

After three decades of fertile developments involving polypeptide-based chiral systems, we present here an overview of the state-of-the-art for this technique. In this review, we describe the theoretical framework to interpret the anisotropic NMR data ( $^1\text{H}$ ,  $^{13}\text{C}$ ,  $^2\text{H}$ ,  $^{19}\text{F}$ ,  $^{31}\text{P}$ ). We detail the main NMR methods that have been developed and employed, so far. Finally, we present and discuss the most important applications of this approach.

## 2. Basic considerations of NMR in chiral liquid crystals

Serendipitously discovered by Reinitzer in 1886 [42], the liquid-crystalline state is an important state of soft matter which has properties between those of solid crystals and conventional liquids [43] (see Fig. 1). From the NMR point of view, liquid crystals (LCs) used as solvents combine two important advantages: i) the partial alignment (named also orientational ordering) of guest molecules (solute compounds) with the static magnetic field,  $B_0$ , which allows the detection of anisotropic intramolecular interactions in the NMR spectra [32, 34, 44]; ii) the averaging out of most intermolecular anisotropic interactions.

The first high-resolution  $^1\text{H}$  NMR spectra in a LC were obtained using thermotropic systems (strongly aligning media) in 1963 [36]. The particular property of liquid-crystalline systems is that the molecules of the phase and the analytes dissolved in them rotate and diffuse as in normal liquids, but are partially



ordered with respect to the direction of an applied magnetic field, as in NMR experiment. Under these conditions, it becomes possible to access three (significant) intramolecular anisotropic interactions of various magnitudes (RCSA, RDC and RQC for nuclei with a spin  $I > \frac{1}{2}$ ) [32, 33, 34]. Due to the presence of order-dependent NMR interactions, the anisotropic NMR spectra of a given nucleus recorded in LCs contain more analytically useful information than those recorded in isotropic solvents. However, this wealth of information content has a “cost” in terms of spectral complexity that needs to be overcome by the development of suitable NMR methodologies.

Another powerful property of LC phases is their ability to orient differently pairs of enantiomers of chiral molecules [1] or pairs of enantiotopic elements (atoms, groups of atoms, internuclear directions) in prochiral compounds on the NMR timescale [1], when dissolved in a chiral anisotropic environment [35, 41]. Besides, when the degree of alignment of the mesophase is rather weak as in the case of polypeptide-based CLCs (and compared to nematic thermotropics), anisotropic interactions ( $\sigma^{\text{aniso}}$  and  $D$ ) are smaller than or equal to the isotropic ones ( $\sigma^{\text{iso}}$  and  $J$ ), and hence high-resolution NMR spectra can be acquired.

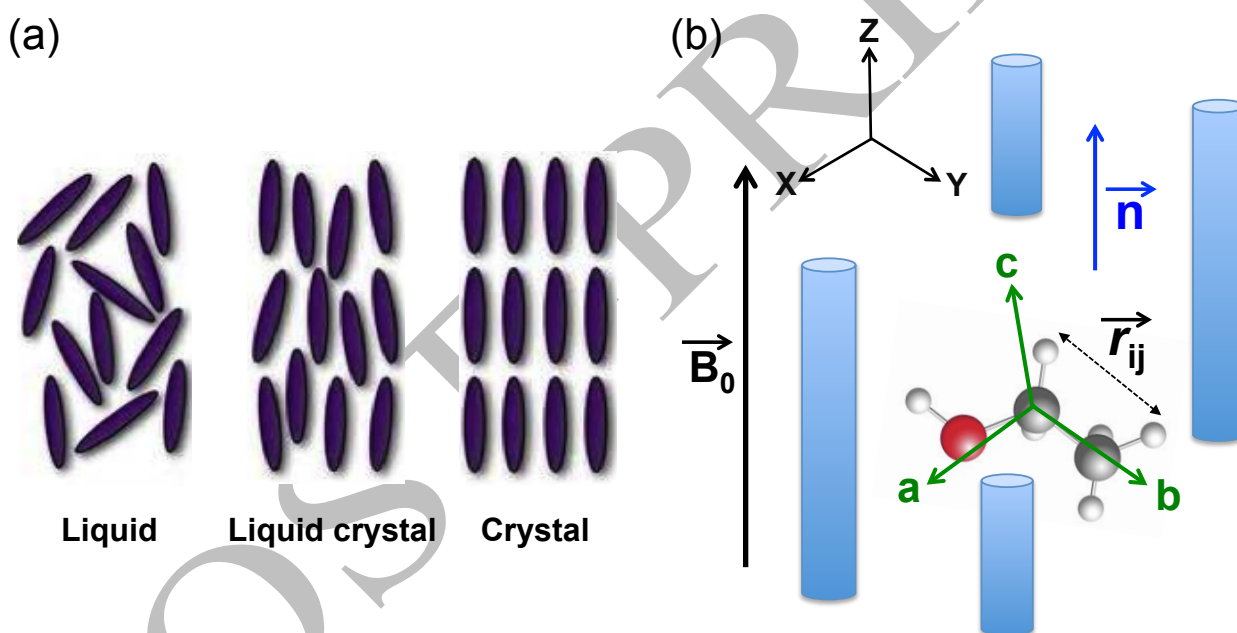


**Fig. 1.** (a) Schematic orientational order in isotropic liquid, liquid crystal (nematic type) and (crystalline solid). The black ellipsoids represent mesogenic molecules, helical polymers or micelles in lyotropic systems). (b) Example of a molecular reference axis system (a, b and c) attached to a molecule dissolved in a nematic phase with a positive molecular magnetic susceptibility anisotropy,  $\Delta\chi_m > 0$ . The axes of the laboratory frame are denoted X, Y and Z. In this case, the director of the mesophase,  $\vec{n}$ , aligns parallel with the  $\vec{B}_0$  axis. When  $\Delta\chi_m < 0$ , the director aligns perpendicular to  $\vec{B}_0$ .

## 2.1. Orientational order versus random motions

Molecules in isotropic liquids exhibit a fast-moving random motion. On average, a given molecule adopts all orientations relative to the magnetic field  $\vec{B}_0$  with the same probability on the NMR timescale, *i.e.* it does not possess any orientational order. Such isotropic motions average out to zero all order-dependent NMR interactions (see below).

In contrast, in LC, solute molecules are partially oriented in the static field  $\mathbf{B}_0$ , *i.e.* each of their orientations does not possess the same probability. For the sake of simplicity, we limit ourselves in this section to the case of a rigid molecule. The orientational behavior of this rigid molecule is described by a molecular orientational probability function,  $P(\theta)$  [32, 45, 46]. However, the dependence on the molecular orientation of most NMR interactions, which affect the NMR spectra, can be described by a second-rank tensor, which is much easier to work with. Furthermore, under (i) the high-field approximation, *i.e.* the Zeeman interaction is assumed to be much larger than the internal spin interactions, and for (ii) a uniaxial nematic phase, the orientation of molecules can be described by five independent order parameters,  $S_{aa}$ ,  $S_{bb} - S_{cc}$ ,  $S_{ab}$ ,  $S_{ac}$  and  $S_{bc}$ , which are defined as [32, 44, 45]:

$$S_{\alpha\beta} = \frac{1}{2} \langle 3 \cos \theta_Z^\alpha \cos \theta_Z^\beta - \delta_{\alpha\beta} \rangle \quad (1)$$

where the indices  $\alpha$  and  $\beta$  denote the axes a, b or c, of a molecular-fixed reference frame (see Fig. 1b), arbitrarily defined by the user and generally called the reference axis system (RAS).  $\theta_Z^{\alpha,\beta}$  represents the angle between the RAS and the  $B_0$  axis, parallel to the nematic director,  $\mathbf{n}$  ( $B_0$  is aligned to the Z axis of the laboratory frame, X,Y,Z).  $\delta_{\alpha\beta}$  is the Kronecker symbol (unity if  $\alpha = \beta$ , and zero otherwise). The angular brackets denote a statistical average over all orientations of the molecule as well as over all intramolecular motions. These five order parameters form the Saupe order matrix, which is a real, symmetric ( $S_{\alpha\beta} = S_{\beta\alpha}$ ), and traceless ( $S_{aa} + S_{bb} + S_{cc} = 0$ ) matrix. This  $3 \times 3$  matrix can be diagonalized, leading to only two non-zero, independent order parameters, among  $S_{a'a'}$ ,  $S_{b'b'}$  and  $S_{c'c'}$ , ( $S_{a'a'} + S_{b'b'} = -S_{c'c'}$ ) expressed in the principal axis system (PAS) where the axes a', b' and c' are the eigenvectors of the matrix. Three Euler angles (at maximum) can be used to convert the RAS into the PAS. In practice, the number of non-zero, independent order parameters in the RAS depends of the molecular group symmetry and the chirality of the LC. The number of non-zero, independent order parameters for a given symmetry in achiral and chiral phases, as well as the location of the axes in PAS is reported in Table 1 [47, 48]. For instance, for a molecule of  $C_1$  and  $C_s$  symmetry point group, the number of order parameters in an achiral liquid crystal (ALC) is equal to five and three, respectively, while five parameters are required for both symmetries in a chiral liquid crystal (CLC).

**Table 1.** Location of the a, b and c axes of the Saupe matrix for molecules of different point group symmetries dissolved in a uniaxial, achiral or chiral mesophase

	Achiral mesophase			Chiral mesophase		
Molecular point group symmetry	Effective molecular point group	Indep. order parameters (Saupe elements)	Location of a,b,c axes	Effective molecular point group	Indep. order parameters (Saupe elements)	Location of a,b,c axes
$C_1, C_i$	$C_1, C_i$	$S_{aa}, S_{bb} - S_{cc}$ $S_{ac}, S_{ab}, S_{bc}$	arbitrary	$C_1$	$S_{aa}, S_{bb} - S_{cc}$ $S_{ac}, S_{ab}, S_{bc}$	arbitrary
<b><math>C_s^a</math></b>	$C_s$	$S_{ab}, S_{bb} - S_{cc}$ $S_{bc}$	a $\perp$ to the plane or // to the 2-fold axis	<b><math>C_1</math></b>	$S_{aa}, S_{bb} - S_{cc}$ $S_{ac}, S_{ab}, S_{bc}$	arbitrary
$C_2, C_{2h}$	$C_2, C_{2h}$	$S_{ab}, S_{bb} - S_{cc}$ $S_{bc}$	a // to the 2-fold axis, b $\perp$ to the mirror plane	$C_2$	$S_{ab}, S_{bb} - S_{cc}$ $S_{bc}$	a // to the 2-fold axis
<b><math>C_{2v}^a</math></b>	$C_{2v}$	$S_{aa}, S_{bb} - S_{cc}$	a // to the 2-fold axis, b $\perp$ to the mirror plane	<b><math>C_2</math></b>	$S_{ab}, S_{bb} - S_{cc}$ $S_{bc}$	a // to the 2-fold axis
<b><math>S_4^a</math></b>	$S_4$	$S_{aa}$	a // p-fold axis or intersection of mirror planes	<b><math>C_2</math></b>	$S_{ab}, S_{bb} - S_{cc}$	a // to the 2-fold axis
$D_2, D_{2h}$	$D_2, D_{2h}$	$S_{aa}$ $S_{bb} - S_{cc}$	a,b,c // to the 2-fold axes	$D_2$	$S_{aa}, S_{bb} - S_{cc}$	a,b,c // to 2-fold axes
<b><math>D_{2d}^a</math></b>	$D_{2d}$	$S_{aa}$	a // p-fold axis or intersection of mirror planes	<b><math>D_2</math></b>	$S_{aa}, S_{bb} - S_{cc}$	a,b,c // to 2-fold axes
$C_n, C_{nv}, C_{nh}$ $D_n, D_{nh}, D_{nd}$ (with n = 3, 4, 6) $S_6$ $C_{\infty}, C_{\infty v}$ $C_{\infty h}, D_{\infty h}$	$C_n, C_{nv}, C_{nh}$ $D_n, D_{nh}, D_{nd}$ (with n = 3, 4, 6) $S_6$ $C_{\infty}, C_{\infty v}$ $C_{\infty h}, D_{\infty h}$	$S_{aa}$	a // p-fold axis or intersection of mirror planes	$C_n$ or $D_n$ with n > 3	$S_{aa}$	// n-fold axis

<sup>a</sup> Compounds with these point groups (shown in bold) have a lower effective symmetry and a change in the location of PAS of the order matrix.

## 2.2. Chirality of the environment

In a CLC, the distinct interactions of enantiomers with the enantiopure molecules of the phase (diastereomorphous interactions) results in different average orientations of enantiomers with respect to the  $\mathbf{B}_0$  field, *i.e.* two distinct Saupe's order matrix,  $S_{\alpha\beta}^S$  and  $S_{\alpha\beta}^R$ , whose elements can be expressed as [32, 35, 49, 50]:

$$S_{\alpha\beta}^{S \text{ or } R} = \frac{1}{2} \langle 3 \cos \theta_{\alpha z}^{S \text{ or } R} \cos \theta_{\beta z}^{S \text{ or } R} - \delta_{\alpha\beta} \rangle \quad (2)$$

From the matrix elements of  $S_{\alpha\beta}^{S \text{ or } R}$ , we can derive the order parameter,  $S_{ij}^{S \text{ or } R}$ , of any direction along an

internuclear  $ij$  vector ( $r_{ij}$ ) in the molecular axis system (a, b, c)<sup>S or R</sup> [32, 35, 50]:

$$\begin{aligned}
 S_{ij}^{S \text{ or } R} &= \sum_{\alpha\beta=a,b,c} \cos \theta_{\alpha ij}^{S \text{ or } R} \cos \theta_{\beta ij}^{S \text{ or } R} S_{\alpha\beta}^{S \text{ or } R} \\
 &= \frac{1}{2} \left( 3 \cos^2 \theta_{a ij}^{S \text{ or } R} - 1 \right) S_{aa}^{S \text{ or } R} \\
 &\quad + \frac{1}{2} \left( \cos^2 \theta_{b ij}^{S \text{ or } R} - \cos^2 \theta_{c ij}^{S \text{ or } R} \right) \left( S_{bb}^{S \text{ or } R} - S_{cc}^{S \text{ or } R} \right) \\
 &\quad + 2 \left( \cos \theta_{a ij}^{S \text{ or } R} \cos \theta_{b ij}^{S \text{ or } R} \right) \left( S_{ab}^{S \text{ or } R} \right) \\
 &\quad + 2 \left( \cos \theta_{a ij}^{S \text{ or } R} \cos \theta_{c ij}^{S \text{ or } R} \right) \left( S_{ac}^{S \text{ or } R} \right) \\
 &\quad + 2 \left( \cos \theta_{b ij}^{S \text{ or } R} \cos \theta_{c ij}^{S \text{ or } R} \right) \left( S_{bc}^{S \text{ or } R} \right)
 \end{aligned} \tag{3}$$

where the terms,  $\cos \theta_{\beta ij}^{S \text{ or } R}$ , are the director cosines of the internuclear vector,  $r_{ij}$ , in the molecular IAS. All anisotropic NMR interactions are related to these order parameters, as we will see in the next sections. As in an ALC, the number of non-zero, independent parameters expressed in the (RAS)<sup>ALC</sup> depends on the point group symmetry of the molecule as listed in Table 1.

### 2.3. A wealth of order-dependent NMR interactions

As the order parameters of enantiomers in CLC differ, they are subject to distinct anisotropic NMR interactions and the total static spin Hamiltonian,  $\mathcal{H}_{\text{tot}}$ , can be written as [32, 35]:

$$\begin{aligned}
 \mathcal{H}_{\text{tot}}(S \text{ or } R) &= \sum_i \mathcal{H}_i^Z + \sum_i \mathcal{H}_i^{CS} (S \text{ or } R) \\
 &\quad + \sum_{i<j} \mathcal{H}_{ij}^J (S \text{ or } R) + \sum_{i<j} \mathcal{H}_{ij}^D (S \text{ or } R) + \sum_i \mathcal{H}_i^Q (S \text{ or } R)
 \end{aligned} \tag{4}$$

where  $\mathcal{H}_i^Z$  is the Zeeman term,  $\mathcal{H}_i^{CS}$  is the electronic shielding contribution,  $\mathcal{H}_{ij}^J$  and  $\mathcal{H}_{ij}^D$  are the indirect electron-coupled and direct through-space spin-spin interactions respectively, and  $\mathcal{H}_i^Q$  is the quadrupolar interaction between the electric field gradients and the electric quadrupolar moment of nuclei with  $I > 1/2$ .

#### 2.3.1 The residual chemical shift anisotropy (RCSA)

In a CLC, the shielding constant of a nucleus  $i$  contains both an isotropic,  $\sigma_i^{\text{iso}}$ , and an anisotropic contribution,  $\sigma_i^{\text{aniso}^{S \text{ or } R}}$ , (denoted also RCSA) to the electronic shielding. For a pair of enantiomers, their respective resonance frequencies (in Hz),  $\nu_i^S$  and  $\nu_i^R$ , can be written as [32, 35, 50]:

$$\nu_i^{S \text{ or } R} = \frac{\gamma}{2\pi} \left( 1 - \sigma_i^{\text{iso}} - \sigma_i^{\text{aniso}^{S \text{ or } R}} \right) B_0 \tag{5}$$

Expressed in a molecular frame (a, b, c axes), the terms  $\sigma_i^{\text{iso}}$  and  $\sigma_i^{\text{aniso}^{S \text{ or } R}}$  are defined as:

$$\sigma_i^{\text{iso}} = \frac{1}{3}(\sigma_{aa_i}^{\text{iso}} + \sigma_{bb_i}^{\text{iso}} + \sigma_{cc_i}^{\text{iso}}) \text{ and } \sigma_i^{\text{aniso}^{S \text{ or } R}} = \frac{2}{3} \sum_{\alpha, \beta = a, b, c} \sigma_{\alpha\beta_i}^{S \text{ or } R} S_{\alpha, \beta}^{S \text{ or } R} \quad (6)$$

Eq. (5) indicates clearly that spectral enantiodiscrimination is detected as depicted in Fig. 2 when  $\sigma_i^{\text{aniso}^S}$  significantly differs from  $\sigma_i^{\text{aniso}^R}$ . However, the term,  $\sigma_i^{\text{aniso}}$ , is not trivial to analyze because it depends on both the elements,  $\sigma_{\alpha\beta_i}^{S \text{ or } R}$ , of the shielding tensor and the orientational order parameters,  $S_{\alpha, \beta}^{S \text{ or } R}$ , in the same RAS. In order to take into account the various factors governing this term, the previous equation can be reformulated as follows [35, 50]:

$$\begin{aligned} \sigma_i^{\text{aniso}^{S \text{ or } R}} &= \frac{2}{3} \left[ \sigma_{aa_i} - \frac{1}{2}(\sigma_{bb_i} + \sigma_{cc_i}) \right] S_{aa_i}^{S \text{ or } R} \\ &+ \frac{1}{3} [(\sigma_{bb_i} - \sigma_{cc_i})(S_{bb_i}^{S \text{ or } R} - S_{cc_i}^{S \text{ or } R})] \\ &+ \frac{4}{3} [\sigma_{ab_i} S_{ab_i}^{S \text{ or } R} + \sigma_{bc_i} S_{bc_i}^{S \text{ or } R} + \sigma_{ac_i} S_{ac_i}^{S \text{ or } R}] \end{aligned} \quad (7)$$

For each nucleus  $i$  of both enantiomers, there exists a PAS ( $a'_i, b'_i, c'_i$ ) <sup>$S \text{ or } R$</sup>  in which the chemical shift tensor is diagonal. Consequently, Eq. (7) can be rewritten as [35, 50]:

$$\begin{aligned} \sigma_i^{\text{aniso}(S \text{ or } R)} &= \frac{2}{3} \left[ \sigma_{a'a'_i} - \frac{1}{2}(\sigma_{b'b'_i} + \sigma_{c'c'_i}) \right] S_{a'a'_i}^{S \text{ or } R} \\ &+ \frac{1}{3} [(\sigma_{b'b'_i} - \sigma_{c'c'_i})(S_{b'b'_i}^{S \text{ or } R} - S_{c'c'_i}^{S \text{ or } R})] \end{aligned} \quad (8)$$

with:

$$S_{\alpha'\alpha'_i}^{S \text{ or } R} = \sum_{\alpha, \beta = a, b, c} \cos\theta_{\alpha'\alpha_i}^{S \text{ or } R} \cos\theta_{\alpha'\beta_i}^{S \text{ or } R} S_{\alpha, \beta}^{S \text{ or } R}. \quad (9)$$

In Eq. (9),  $\theta_{\alpha'\alpha_i}$  are the angles between the  $\alpha'$  axis of RAS and the  $\alpha$  axis of PAS for the chemical shift tensor associated to a nucleus  $i$ .

Interestingly, in Eq. (8), the first quantity,  $\sigma_{a'a'_i} - (\sigma_{b'b'_i} + \sigma_{c'c'_i})/2$ , corresponds to the anisotropy of the electronic shielding of the atom  $i$ , while the second term  $(\sigma_{b'b'_i} - \sigma_{c'c'_i})$  is proportional to the asymmetry of the electronic shielding. Spectral separation originates from the order parameter differences,  $[S_{a'a'_i}^S - S_{a'a'_i}^R]$ , as well as  $[(S_{b'b'_i}^S - S_{c'c'_i}^S) - (S_{b'b'_i}^R - S_{c'c'_i}^R)]$ . Hence, all the factors that can increase either the difference in order parameters between enantiomers or the electronic shielding anisotropy of nuclei  $i$  (such as the hybridization state of carbon atom and the nature of the bound

substituents or the adjacent nucleus) will increase the magnitude of  $\sigma_i^{\text{aniso}}$ . The magnitude of shielding anisotropy is rather small for proton ( $^1\text{H}$ ), deuterium ( $^2\text{H}$ ), and  $\text{sp}^3$  carbon-13 nuclei ( $^{13}\text{C}$ ), whereas significant RCSAs can be measured for fluorine atoms ( $^{19}\text{F}$ ) or  $\text{sp}$  and  $\text{sp}^2$   $^{13}\text{C}$  nuclei [35, 50, 51]. In practice,  $^{13}\text{C}\{-^1\text{H}\}$  1D NMR is a robust tool, relatively easy to implement on any routine NMR spectrometer for the spectral discrimination of enantiomers.

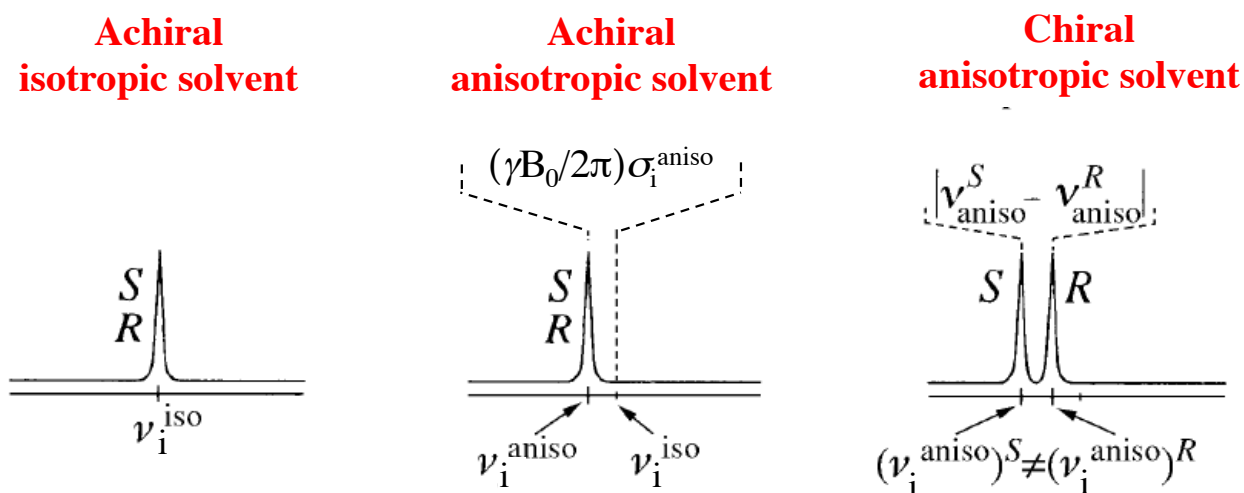


**Fig. 2.** Schematic principle of the enantiodiscrimination in CLCs based on an absolute difference of RCSAs (spin  $I = 1/2$ ),  $|\nu_i^{\text{aniso}} - \nu_i^{\text{iso}}|$ . Disregarding any solvent effects (associated with the nature of the phase, isotropic or anisotropic), the frequency difference,  $|\nu_i^{\text{aniso}} - \nu_i^{\text{iso}}|$  is equal to the quantity  $(\gamma_i B_0 / 2\pi) \sigma_i^{\text{aniso}}$ . The various 1D spectra are not plotted to scale and the S and R assignments are arbitrary. Figure partly adapted from Ref. [35] with permission.

### 2.3.2 The residual dipolar coupling (RDC)

In spectra of enantiomers dissolved in CLCs, internuclear dipolar interactions are not averaged to zero [32, 51, 52]. In this case, each pair of interacting nuclei  $i$  and  $j$  for both isomers produces a RDC defined in Hz as [35, 53]:

$$D_{ij}^{S \text{ or } R} = -k_{ij} \left\langle \frac{S_{ij}^{S \text{ or } R}}{r_{ij}^3} \right\rangle \quad \text{with} \quad k_{ij} = \left( \frac{\mu_0}{4\pi} \right) \left( \frac{h\gamma_i\gamma_j}{4\pi^2} \right) \quad (10)$$

In this equation,  $\gamma_i$  and  $\gamma_j$  are the gyromagnetic ratios of interacting nuclei  $i$  and  $j$ ,  $\mu_0$  is the magnetic permeability of free space,  $r_{ij}$  is the internuclear distance between  $i$  and  $j$  nuclei, and  $S_{ij}$  is the order parameter for the internuclear vector,  $r_{ij}$  (see Fig. 1b). The angular brackets denote an average over molecular tumbling and/or internal motions (vibrational motions, conformational changes, ...) on the NMR time scale. The magnitude and sign of  $k_{ij}$  depend on the isotopes involved and vary by one or two orders of magnitude. A few examples of  $k_{ij}$  values associated with interacting homo- and hetero-nuclear pairs are listed in Table 2.

Assuming that the mesophase induces no changes on the geometry between enantiomers, Eq. (10) shows that spectral enantiodiscriminations occur when the internuclear order parameters,  $S_{ij}$ , are different for the  $S$  and  $R$  isomers leading to a doubling of signals as seen in the case of a first-order (AX) spin

system (see Fig. 3c). In practice,  $S_{ij}$  can be simply calculated using Eq. (11) [35, 53].

$$S_{ij}^{S \text{ or } R} = \frac{1}{2} \langle 3 \cos^2 \theta_{ij}^{S \text{ or } R} - 1 \rangle. \quad (11)$$

Furthermore when the number of independent anisotropic NMR measurables is sufficient,  $S_{ij}$  values can be used to determine the molecular order matrix,  $S_{\alpha\beta}$ , using Eq. (3) [35, 53]. In Eq. (11),  $\theta_{ij}^{S \text{ or } R}$  is the angle between the internuclear vector,  $r_{ij}^{S \text{ or } R}$ , and the  $\mathbf{B}_0$  axis.

Internuclear dipolar interactions can strongly affect the NMR spectra or the spectral patterns. A significant difference between NMR in isotropic liquids and LCs is that, unlike scalar couplings, dipolar couplings are observable between magnetically equivalent nuclei. For instance, in an anisotropic solvent, the protons of an isolated methylene group produces a 1:1 doublet, while those of an isolated methyl group produce a 1:2:1 triplet. In both cases, the splittings between lines are equal to  $3D_{\text{HH}}$  (see Fig. 3b and c). Actually, in an anisotropic medium, the spectrum of any  $n$ -magnetically equivalent  $I = 1/2$  nuclei consists of a  $n$ -multiplet with line spacing  $3D$  and a binomial distribution of intensities. For a pair of anisochronous (homo- or heteronuclear) weakly coupled nuclei,  $i$  and  $j$ , the total splitting (denoted  $T_{ij}$ ) observed between the components of each doublet is equal to  $J_{ij} + 2D_{ij}$ . Here,  $J_{ij}$  is the isotropic part of the scalar coupling, since the anisotropic part of the scalar coupling is usually negligible (see Fig. 3c).  $T_{ij}$  is defined as the total spin-spin coupling. Depending on its magnitude,  $D_{ij}$  can be smaller, equal to, or larger than  $J_{ij}$ , as well as positive, null or negative (see Eq. (10)).

**Table 2.** Examples of  $k_{ij}$  values involving nuclei  $^1\text{H}$ ,  $^2\text{H}$ ,  $^{13}\text{C}$ ,  $^{19}\text{F}$  and  $^{31}\text{P}$ , and ranked in decreasing order

Pair of interacting nuclei	$k_{ij}$ values (kHz.A <sup>3</sup> )	Sign <sup>a</sup>
$^1\text{H}$ - $^1\text{H}$	120.07	> 0
$^1\text{H}$ - $^{19}\text{F}$	112.99	> 0
$^{19}\text{F}$ - $^{19}\text{F}$	106.30	> 0
$^1\text{H}$ - $^{31}\text{P}$	48.62	> 0
$^1\text{H}$ - $^{13}\text{C}$	30.20	> 0
$^{13}\text{C}$ - $^{19}\text{F}$	28.41	> 0
$^{31}\text{P}$ - $^{31}\text{P}$	19.68	> 0
$^1\text{H}$ - $^2\text{H}$	18.44	> 0
$^{13}\text{C}$ - $^{31}\text{P}$	12.23	> 0
$^{13}\text{C}$ - $^{13}\text{C}$	7.59	> 0
$^2\text{H}$ - $^{31}\text{P}$	7.46	> 0
$^2\text{H}$ - $^{13}\text{C}$	4.64	> 0
$^2\text{H}$ - $^2\text{H}$	2.83	> 0

<sup>a</sup>  $k_{ij}$  is negative when one of interacting atoms has negative gyromagnetic ratio (as  $^{15}\text{N}$ ).

Generally, for weakly ordered molecules, the value of  $2 \times D_{13\text{C-H}}$  for a one-bond  $^{13}\text{C-}^1\text{H}$  interatomic pair, is smaller than  $^1J_{13\text{C-H}}$ , but the opposite situation may also occur. As the sign of  $D_{ij}$  can be either negative or positive (see Eqs. (10) and (11)), the splitting between two non-equivalent nuclei becomes null when  $J_{ij} = -2D_{ij}$ . This latter situation may possibly be encountered for analytes oriented in highly concentrated solutions of polypeptide LCs, where dipolar and scalar couplings can be of the same order of magnitude.

From the enantiodiscrimination point of view, it must be emphasised that the residual dipolar coupling differences,  $\Delta D_{ij}$ , measured on spectra for two enantiomers vary with the relative position of the internuclear vectors,  $r_{ij}$ , with respect to  $B_0$ , as discussed in the Section 2.3.3.

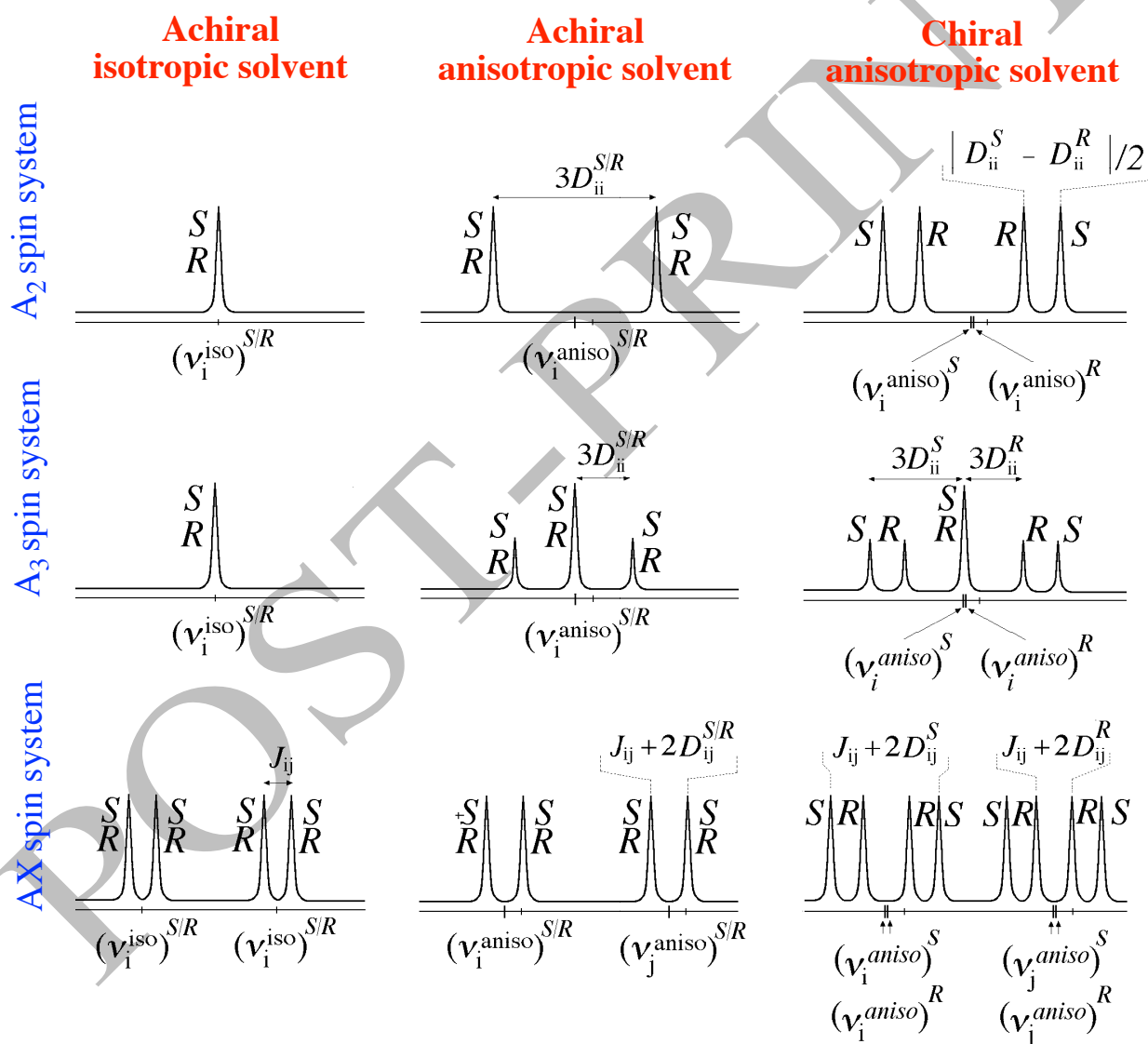


**Fig. 3.** Principle of the spectral enantiomeric discrimination in a CLC based on a difference of RDCs ( $l = 1/2$ ), in the case of: (a) two coupled equivalent nuclei (an isolated  $A_2$  spin system), (b) three coupled equivalent nuclei (an isolated  $A_3$  spin system), and (c) two coupled (at first order) non-equivalent nuclei (an AX spin system). In these schemes, the variation of RCSAs between S and R isomers,  $|\sigma_{i,j}^{\text{aniso}}(S) - \sigma_{i,j}^{\text{aniso}}(R)|$ , is assumed to be negligible. For (c),  $D_{ij}$  is assumed to be positive ( $T_{ij} > J_{ij}$  with  $J_{ij} > 0$ ). As in Fig. 2, the S and R assignments shown are arbitrary. The various 1D spectra are not plotted to scale and the S and R assignments are arbitrary. Figure partly adapted from Ref. [35] with permission.



### 2.3.3 The residual quadrupolar coupling (RQC)

In oriented solvents, the NMR spectra of quadrupolar nuclei (spin  $I > \frac{1}{2}$ ) are dominated by the interaction between a nuclear quadrupolar moment and an electric field gradient at the nucleus. Disregarding any spin-spin coupling, the signal of an isolated nucleus of spin  $I > \frac{1}{2}$  consists of a multiplet of  $2I$  equally-spaced components, corresponding to the transitions between  $m$  and  $m + 1$  energy levels. The separation between the lines is named the quadrupolar splitting (QS) and commonly noted,  $\Delta\nu_Q$ , as shown in Fig. 4b in the case of spin  $I = 1$  nucleus. For two enantiomers oriented differently in a CLC and assuming that the quadrupolar term is much smaller than the Zeeman term, the quadrupolar Hamiltonian can be written in frequency units as [32, 35, 54]:

$$\mathcal{H}_Q^{S \text{ or } R} = \frac{2}{3} \sum_i \frac{e^2 Q_i q_{zz_i}^{S \text{ or } R}}{4I_i(2I_i - 1)} [3I_{zi}I_{zi} - I(I_i + 1)] \quad (12)$$

where  $eQ_i$  is the nuclear electric quadrupole moment of nucleus  $i$ , and  $eq_{zz_i}^{S \text{ or } R}$  is the component of the electric field gradient (EFG) tensor along the magnetic field ( $z$  axis) at the position of nucleus  $i$  for each enantiomer. In this equation,  $eq_{zz_i}^{S \text{ or } R}$ , is related to the elements of the EFG tensor in the molecular frame,  $eq_{\alpha\beta_i}^{S \text{ or } R}$  by:

$$eq_{zz_i}^{S \text{ or } R} = \frac{2}{3} \sum_{\alpha, \beta=a,b,c} eq_{\alpha\beta_i}^{S \text{ or } R} S_{\alpha\beta}^{S \text{ or } R} \quad (13)$$

For most quadrupolar nuclei, the relaxation induced by the anisotropic quadrupolar interaction produces sufficient line broadening that the spectral discriminations between enantiomers cannot be detected. However, due to their small quadrupolar moment, the relaxation of some nuclei, like boron-10 ( $I = 3$ ), boron-11 ( $I = 3/2$ ) or deuterium ( $I = 1$ ), is slow enough to produce high-resolution NMR spectra, and hence observe these discriminations [32, 35, 54, 55]. Only the case of deuterium atoms will be discussed in this section. As deuterium is monovalent, the associated EFG in the case of weakly oriented LC is usually assumed to lie along the C-D bond direction (deuterium bound to carbon atom) and to be axially symmetric [54]. The quadrupolar splitting between the two lines can then be written as [35, 55, 56]:

$$\Delta\nu_{Q_i}^{S \text{ or } R} = \frac{3}{2} K_{C-D_i} S_{C-D_i}^{S \text{ or } R} \text{ with } K_{C-D_i} = \frac{e^2 Q_{D_i} q_{C-D_i}}{h} \quad (14)$$

where  $S_{C-D_i}$  is the order parameter of the C-D<sub>*i*</sub> axis for the *S* or *R* enantiomer (see Fig. 4c), and  $K_{C-D_i}$  is the <sup>2</sup>H quadrupolar coupling constant (QCC). Note that the  $K_{C-D_i}$  value varies depending on the hybridization state of the carbon atom bonded to a given deuterium, but also the electronegativity of close substituents.

Generally,  $K_{C-D_i}$  is approximately equal to  $170 \pm 5$  kHz,  $185 \pm 5$  kHz and  $210 \pm 5$  kHz, for  $sp^3$ ,  $sp^2$  and  $sp$  carbon atoms, respectively [32, 35, 57, 58].

Similarly to Eq. (11), the order parameter associated with the EFG for a given C-D bond for two enantiomers can be expressed relative to  $B_0$  as [35, 57]:

$$S_{C-D_i}^{S \text{ or } R} = \frac{1}{2} \langle 3 \cos^2 \theta_{C-D_i}^{S \text{ or } R} - 1 \rangle \quad (15)$$

As already described for the dipolar interaction, Eq. (14) shows that spectral enantiodifferentiations occur when  $S_{C-D_i}^S \neq S_{C-D_i}^R$ , assuming that  $K_{C-D_i}^S = K_{C-D_i}^R$ . Eq. (15) indicates, however, that local order

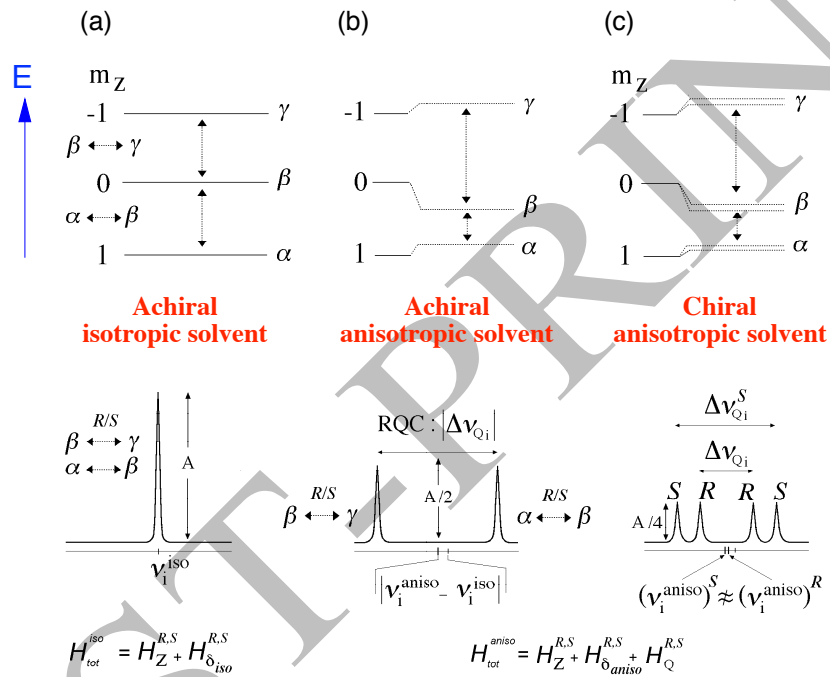


**Fig. 4.** (Top) Diagrams of energy levels of a single deuteron under the effect of  $H_Z$  and  $H_Q$  interactions in the case of two enantiomers. (Bottom) Schematic  $^2H\{-^1H\}$  spectral patterns expected in (a) achiral liquids, (b) in achiral mesophases and (c) in CLCs. Each 1D spectrum is plotted at the same vertical scale. Figure adapted from Ref. [54] with permission.

parameters,  $S_{C-D_i}^{S \text{ or } R}$ , are composite quantities depending both on the trigonometric term,  $[3 \cos^2 \theta_{C-D_i} - 1]$ , and the motional averaging ( $\langle \dots \rangle$ ). Consequently, establishing that a difference of  $S_{ij}$  for enantiomers originates from a purely geometrical reason,  $\theta_{C-D}$ , or from a difference involving motional averaging, or both is not easy. In practice, we can admit that the magnitude of the differentiation ( $\Delta \nu_{Q_i}$ ) should strongly depend on the difference of the relative position of the EFG of the C-D direction for both isomers with respect to  $B_0$ , assuming that the motional averaging for enantiomers is mainly the same (no significant difference in relaxation times has ever been measured so far), [59]. As an illustration, the dependence of  $\Delta \nu_{Q_i}^{S \text{ or } R}$  as function of  $\theta_{C-D}^{S \text{ or } R}$  with  $\theta_{C-D}^S = \theta_{C-D}^R + 10^\circ$  is graphically shown in Fig. 5. The

variation of  $\Delta\Delta\nu_Q$  vs.  $\theta_{C-D}$  occurs because the trigonometric function,  $[3\cos^2_{C-D_i} - 1]$ , is very steep for angles around the magic angle,  $\theta_m = 54.7^\circ$ , ( $S = 0$ ) and rather flat in the angular ranges of  $[-5^\circ, +5^\circ]$  and  $[+85^\circ, +95^\circ]$ . One can easily see that larger chiral discriminations are obtained in the interval  $\theta_m \pm 20^\circ$ , while producing the smaller quadrupolar splittings. Finally, several particular spectral situations exist corresponding to either the cancellation of QS for one of the enantiomers ( $\theta_{C-D}^S = \theta_m$  or  $\theta_{C-D}^R = \theta_m$ ) or the disappearance of the chiral discrimination  $\theta_{C-D}^S = \theta_{C-D}^R$ .

The great efficiency of  $^2\text{H}\{-^1\text{H}\}$  NMR in the discrimination of enantiomers in CLCs mainly originates from the relatively large magnitude of  $K_{C-D_i}$  compared with the term  $k_{ij}$ , involved in the dipolar interaction. Indeed, even when the DOE between enantiomers is rather small, the relatively large magnitude of the  $^2\text{H}$ -QCC allows the enantiomers to be spectrally discriminated. Interestingly,  $^2\text{H}$  spectra can be recorded on isotopically-enriched molecules or at natural abundance deuterium (NAD) level [54, 55].

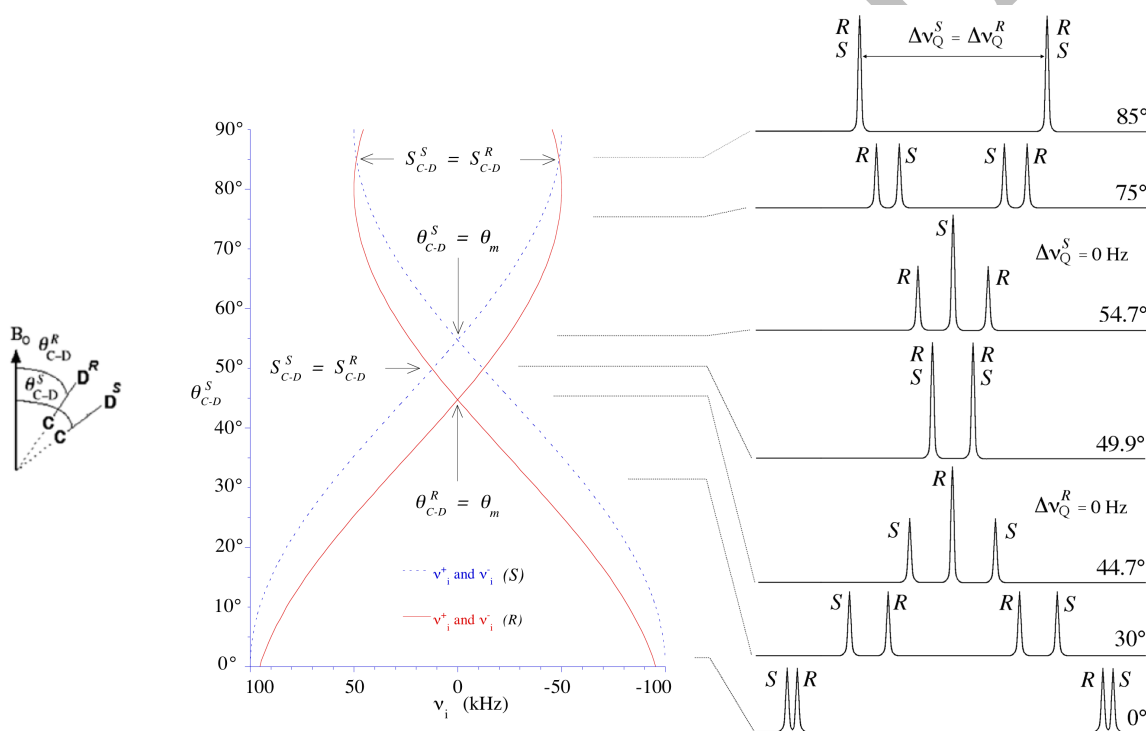


**Fig. 5.** Theoretical variation of the two components of a  $^2\text{H}$ -QD associated with *R*- and *S*-enantiomers versus the angle  $\theta_{C-D}^{S,R}$ , assuming that  $\theta_{C-D}^S = \theta_{C-D}^R + 10^\circ$ . Figure adapted from Ref. [35] with permission.

## 2.4. Combining two anisotropic interactions

### 2.4.1 $^{13}\text{C}$ -RCSA and $^{13}\text{C}$ -X RDC

The presence of a magnetically-active heteroatomic nucleus X at 100% abundance, such as phosphorus-31 or fluorine-19 atom, in a chiral compound induces the presence of short and/or long-range  $^{13}\text{C}$ -X scalar/dipolar couplings ( $J_{13\text{C-X}} / D_{13\text{C-X}}$ ) that can considerably complicate the analysis of  $^{13}\text{C}\{-^1\text{H}\}$  1D NMR spectra. The most straightforward solution to simplify such analysis consists of simultaneously

decoupling both the signal of protons and the X-nuclei. This type of NMR experiment is denoted  $^{13}\text{C}\{-^1\text{H}, \text{X}\}$  [35, 60]. This experimental procedure is, however, only possible when the NMR spectrometer possesses two X-channels and an adequate triple resonance NMR probe (*e.g.*  $^1\text{H}$ ,  $^{13}\text{C}$ , X/BB). An increasing number of NMR spectrometers are now equipped with such hardware. Nevertheless, the presence of an additional spin-1/2 heteronucleus X leads to  $^{13}\text{C}\text{-X}$  dipolar couplings, which can provide additional enantiodifferentiations, in particular for molecules devoid of  $\text{sp}^2$  carbon atoms.

The internuclear total coupling,  $T_{ij}^{R \text{ or } S}$ , defined in Hz unit between  $^{13}\text{C}$  and X nuclei of enantiomers in CLCs can be expressed as:

$$T_{^{13}\text{C-X}}^{S \text{ or } R} = J_{^{13}\text{C-X}} + 2D_{^{13}\text{C-X}}^{S \text{ or } R} \quad (16)$$

From a spectroscopic point of view, the analysis of proton-decoupled, X-coupled  $^{13}\text{C}$  spectra in oriented phases is very similar to that made in isotropic solvents, except that splittings are not equal to  $J_{ij}$  but  $T_{ij}$ . The spectral features of proton-decoupled, X-coupled  $^{13}\text{C}$  spectra are governed both by the magnitude of ( $^{13}\text{C}\text{-X}$ )-RDCs for each isomer as well as the difference in  $^{13}\text{C}\text{-RCSA}$  associated with a given carbon atom. As a consequence, various spectral enantiodifferentiation patterns depending on the relative magnitude of these two anisotropic interactions can be observed for a pair of interacting  $^{13}\text{C}\text{-X}$  nuclei. Fig. 6 schematically depicts the different possible spectral patterns (as a function of the magnitude of  $T_{ij}$  and  $\sigma_i^{\text{aniso}}$ ) that can be encountered in the  $^{13}\text{C}\{-^1\text{H}\}$  and  $^{13}\text{C}\{-^1\text{H}, \text{X}\}$  NMR spectra of a racemic mixture of enantiomers (*R/S*) having a single X nucleus with spin  $I = 1/2$ . The detailed description of each of these spectral situations was reported in the original paper [60].

#### 2.4.2 $^2\text{H}\text{-RQC}$ and $^2\text{H}\text{-X RDC}$

As we will see,  $^2\text{H}\{-^1\text{H}\}$  1D/2D NMR in CLCs is a powerful tool for discriminating between enriched and isotopically unmodified (NAD NMR) enantiomers, mainly on the basis of  $^2\text{H}\text{-RQC}$  differences since the difference of  $^2\text{H}\text{-RCSAs}$  for two enantiomers are generally negligible (see above). However, as in the case of  $^{13}\text{C}\{-^1\text{H}\}$  NMR, the presence of an abundant nucleus in the molecule, such as  $^{19}\text{F}$  or  $^{31}\text{P}$  atom, can lead to a further splitting of lines caused by heteronuclear ( $^2\text{H}\text{-X}$ )-RDCs. In practice, the low magnetogyric ratio of the deuteron has two consequences: i) the magnitude of short-range  $T_{\text{H-X}}$  remains small compared to the magnitude of  $^2\text{H}\text{-QDs}$ ; ii) long-range ( $^2\text{H}\text{-X}$ )-RDCs participate in line broadening of components of QDs [61]. However, when small, these heteronuclear couplings can significantly

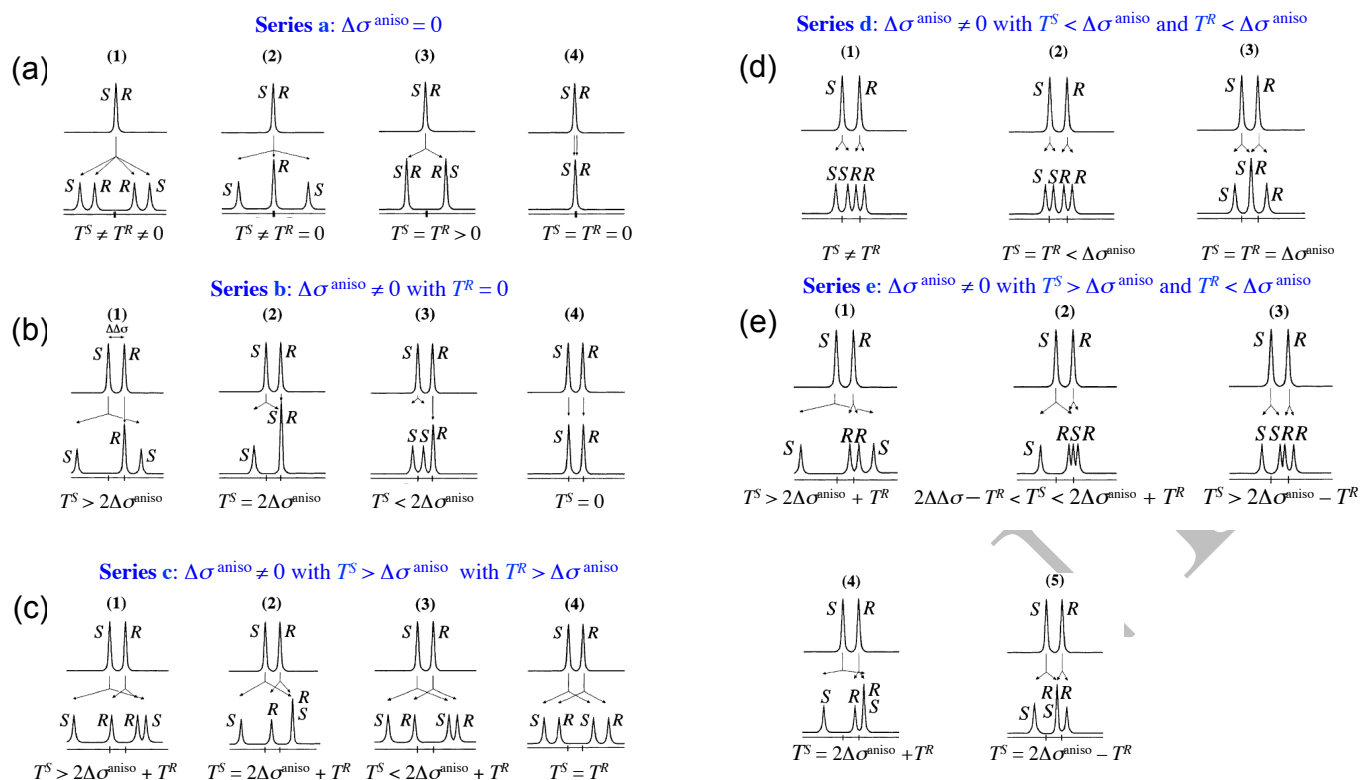


**Fig. 6.** (a to e) Possible spectral enantiodifferentiation patterns expected to be observed in the  $^{13}\text{C}\{-^1\text{H}, \text{X}\}$  NMR spectra (top row) and  $^{13}\text{C}\{-^1\text{H}\}$  NMR spectra (bottom row) of enantiomers (racemic mixture) having a single spin-1/2 heteroatomic nucleus (noted X) with spin  $I = 1/2$ , and embedded in a CLC. The chiral differentiation, if any exists, arises through differences of the chemical shift anisotropies ( $\sigma_i^{\text{aniso}}$ ) and/or of the  $^{13}\text{C}\text{-X}$  total couplings ( $T_{ij}$ ). Note that for all series, we have arbitrarily assumed that the carbon-13 signal of the S-enantiomer was deshielded relative to the R-enantiomer. Figure adapted from Ref. [60] with permission.

complicate the analysis of anisotropic NAD 1D spectra by superposition of signals [61]. The use of QUOSY 2D experiments then becomes necessary to extract and exploit all spectral information (see Section 7) [35, 61, 62].

### 3. Weakly-orienting liquid crystals

#### 3.1. Polypeptide-based LCs versus thermotropics

The analytical potential of NMR spectroscopy in thermotropic LCs was demonstrated in 1963 by Saupe and Englert who first used this type of LC as an alignment medium for dissolved molecules [36]. The possibility of distinguishing the NMR signals of enantiomers in CLCs was reported five years later [30, 63] using chiral cholesteric systems made of a complex mixture of ZLI 2806 (a thermotropic) doped by esters of cholesterol [63], and was then revisited later in 1989 by the Orsay group [31, 64]. From a practical point of view, both achiral and chiral thermotropic systems have several disadvantages, which reduce their application range and have undoubtedly limited the interest of chemists in anisotropic NMR: i) they are poor solvents for many compounds of interest; ii) they possess a rather low ability to dissolve a large amount of solute (1-2 % max), which limits the sensitivity of experiments in these media; iii) the uniform and homogeneous orientation of the samples in the magnet is rarely easily to obtain; and iv) the

large magnitude of anisotropic interactions, such as ( $^1\text{H}$ - $^1\text{H}$ )-RDCs, leads to second-order  $^1\text{H}$ -NMR spectra. As a consequence, during two decades, numerous practical approaches were developed to simplify the analysis of strongly oriented  $^1\text{H}$  NMR spectra, and subsequently also of  $^{13}\text{C}$ . Without being exhaustive, we can mention: i) the selective or partial deuteration [65, 66]; ii) the use of multiple quantum (MQ) 2D experiments [67, 68, 69, 70] or the combination of them [71]; iii) the reduction of anisotropic interactions by spin manipulation *via* appropriate multiple-pulse sequences [72, 73, 74, 75]; or iv) the variable angle spinning sample (VASS) technique [76, 77, 78, 79].

Besides conventional thermotropics, other orienting systems exist, such as lyotropic liquid crystals (LLC). Achiral or chiral lyotropic liquid crystals are mesophases formed by dissolving molecules (that do not possess intrinsic mesogenic properties as in case of thermotropics) in an appropriate solvent (water or organic solvents) under suitable conditions of concentration, temperature (T), and pressure [80, 81, 82]. While the adjective “lyotropic” was initially used to qualify LC phases, such as micellar, hexagonal or lamellar phases, formed by amphiphilic molecules [80, 81, 83], the term has also been applied to LC phases formed by rod-like macromolecules, such as helical polymers, mixed with suitable solvent under appropriate conditions [84, 85, 86].

Interestingly, polypeptide-based LLCs result in solute order parameters, ranging from  $10^{-3}$  to  $10^{-6}$ , which are much smaller than those of solutes in thermotropic solvents ( $10^{-1}$  to  $10^{-2}$ ). Many LLCs have been employed mainly for the investigation of large water-soluble biomolecules, such as proteins or DNA [87, 88, 89]. LLCs used for this application include i) bicelles [90, 91]; ii) micelles [92]; iii) bacteriophages [93]; iv) amphotropic ionic liquid crystals [94]; or v) non-ionic dilute liquid crystalline media [95]. Other systems such as polyacrylamide-based gels [96] or collagen-based gels [97] can be also mentioned. A good overview of the main types of aligning systems used with biomolecules is given in the review of Prestegard *et al.* [89]. However these systems are generally not well suited for the majority of small organic molecules due to the requirement of water as a co-solvent.

The use of weakly orienting media (LLCs, polymeric systems, or compressed/stretched gels) has created a change in paradigm and a fantastic interest from the 2000's onwards in the domain of the structural elucidation of biomolecules and water incompatible organic natural products. In both cases, RDCs (and not just nuclear Overhauser effects (NOE)) [87, 98, 99, 100, 101, 102], and more recently RCSAs [102, 103, 104, 105], have become key parameters to establish internuclear distances and information about relative angles between internuclear vectors, and hence to determine relative configurations (RC) or absolute configurations (AC) [104, 105].

The first description of enantiodiscrimination of small chiral molecules in water-based chiral LLC was reported by Tracey and Diehl in 1975 [106], but the number of efficient and very robust systems proposed remains rather limited. We can mention: a) the potassium *N*-dodecanoyl-L-alaninate based system [107];

b) glucoxon (a mixture mainly composed of alkyl (octyl and decyl)  $\alpha$ - and  $\beta$ -mono- and diglucosides)/hexanol/buffered water [108]; c) the alanine-based system [109]. More recently, the use of polynucleotide-based CLC made of short DNA-fragments was reported, and showed its enantiodiscrimination potential when combined with  $^2\text{H}$  NMR of labelled molecules [110, 111]. Those systems may provide convenient oriented media for NMR studies, but they are generally not commercially available and their preparation (control of pH, ionic balance, sample homogeneity, ...) is sometimes difficult.

In fact the renaissance of anisotropic NMR for analysing small organic (chiral or prochiral) molecules has really started from 1992, when Bayle and Courtieu after the wise advice of Loewenstein (see Fig. 72) reported the first enantiodiscrimination of deuterated chiral solutes using  $^2\text{H}$ - $\{^1\text{H}\}$  NMR in organic solutions of helically-chiral homopolymers, here the poly- $\gamma$ -benzyl-*L*-glutamate (**PBLG**) [40]. This paper again highlighted the advantages and the analytical potential of  $^2\text{H}$ - $\{^1\text{H}\}$  1D NMR, previously explored with a cholesteric solvent in 1989 [112]. From a practical viewpoint, oriented solutions of polypeptide are much more “flexible” systems than conventional thermotropics. They can accommodate a large amount of almost any type of organosoluble solute, while maintaining their liquid-crystalline properties. Also their degree of alignment, and in turn the magnitude of anisotropic interactions of analytes, can be controlled by adjusting the amount of polymer in the phase and its degree of polymerisation (DP).

## 3.2. The polypeptide family

### 3.2.1. Organic solutions of neat helical polymers (PBLG, PELG, PCBL, PMBLG, PBPMGL)

Among organo-compatible CLCs, a special attention was paid to systems based on  $\alpha$ -helical-chiral-polymers, such as polypeptide-based homopolymers with different achiral lateral chains (see Fig. 7) [113]. So far, the homopolymer most used as an enantiodiscriminating chiral liquid crystal is made of PBLG whose AC is of *L*-type. PBLG was one of the most investigated polypeptides, and a vast literature exists on its physical properties and areas of application [113, 114, 115, 116, 117]. However, other polymers, such as poly- $\epsilon$ -carbobenzyloxy-*L*-lysine (**PCBL**) [113], poly- $\gamma$ -ethyl-*L*-glutamate (**PELG**) [113, 118, 119] or mixtures of two of them [120, 121], can provide robust enantiodiscriminating systems. Cross-linked helically chiral poly- $\gamma$ -benzyl-*L*-glutamate has also been described as an enantiodiscriminating alignment system [122]. More recently, new variants of enantiodiscriminating polypeptide-based polymers have been reported. For instance, we can mention systems made of poly- $\beta$ -phenethyl-*L*-aspartate (**PPLA**) [123], of poly- $\beta$ -benzyl-*L*-aspartate (**PBLA**) [124], of poly- $\gamma$ -p-biphenylmethyl-*L*-glutamate (**PBPMGL**) [125] as well as a co-polymer of phenethyl and benzylpolyaspartate [126]. Interestingly, the alignment process of PPLA or PBPMGL systems, for instance, change drastically (reversal point) as function of the temperature, thus providing two sets of

**Table 3.** Main organosoluble helically-chiral polymers used as NMR solvents ranked by type of polymer with the year of the first reports

Helical polymer	Acronym <sup>a</sup>	Position of stereogenic center <sup>b</sup>	Main possible organic solvents <sup>c</sup>	Year	Ref.
<i>Poly(peptide)</i>	PB(L)G	BB	CHCl <sub>3</sub> , CH <sub>2</sub> Cl <sub>2</sub> , CHBr <sub>3</sub> , DMF, NMP, TCE, THF, TMU, benzene, dioxane, <i>m</i> -cresol, pyridine, toluene,	1992	[40]
	PCB(L)L	BB	CHCl <sub>3</sub> , DMF, dioxane,	2001	[113]
	PE(L)G	BB	CHCl <sub>3</sub> , CH <sub>2</sub> Cl <sub>2</sub>	2001	[113]
	PB(L)G (cross-linked)	BB	CHCl <sub>3</sub> , CH <sub>2</sub> Cl <sub>2</sub> , THF, benzene, dioxane	2013	[122]
	PP(L)A <sup>d</sup>	BB	CHCl <sub>3</sub> , TCE	2017	[123]
	PB(L)A	BB	CHCl <sub>3</sub> , CH <sub>2</sub> Cl <sub>2</sub> , TCE	2018	[124]
	PBPM(L)G <sup>d</sup>	BB	CHCl <sub>3</sub>	2018	[125]
	PSMB(L)G <sup>d</sup>	BB / SC	CHCl <sub>3</sub>	2017	[126]
<i>Poly(guanidine)</i>	( <i>R</i> )-PPEMG	SC	CHCl <sub>3</sub>	2010	[137]
<i>Poly(isocyanide)</i>	PPI-( <i>L</i> )-Ala	SC	CHCl <sub>3</sub> , CH <sub>2</sub> Cl <sub>2</sub> , THF	2012	[138]
<i>Poly(arylacetylene)</i>	PPA-( <i>L</i> )-Ala	SC	CHCl <sub>3</sub> , CH <sub>2</sub> Cl <sub>2</sub>	2012	[139]
	PPA-( <i>L</i> )-Phe	SC	CHCl <sub>3</sub>	2012	[140]
	PPA-( <i>L</i> )-Val	SC	CHCl <sub>3</sub>	2012	[141]
<i>Poly(isocyanopeptide)</i>	( <i>L,L</i> )-PIAF-OBn	SC	CHCl <sub>3</sub>	2017	[142]

<sup>a</sup>Acronym generally used. In parenthesis is given the AC of polymers. For some of them, *L* can be replaced by *D* (PBDG, PCBDL, PBDA, ...). <sup>b</sup>BB: The stereogenic center is located on the backbone, SC: The stereogenic center is located on the side chain. <sup>c</sup>The organic co-solvent can be deuterated or not. <sup>d</sup>Thermoresponsive aligning systems.

molecular alignments for the same sample. Finally, in 2017, a polypeptide with a chiral side-chain, poly- $\gamma$ -(*S*)-2-methylbutyl-*L*-glutamate (**PSMBLG**) has been reported; the idea being to reinforce the enantiodiscrimination efficiency in order to increase spectral enantio-separations [127]. Key data related to the cited polypeptides above are listed in Table 3.

Several reasons can explain the high level of interest in polypeptide systems and notably PBLG: i) their commercial availability with a large range of DP; ii) a vast choice of compatible organic co-solvents ranging from polar (DMF, TMU, NMP) to weakly polar (benzene, CH<sub>2</sub>Cl<sub>2</sub>, CHCl<sub>3</sub>); iii) simple preparation of samples and easy and rapid alignment of polymers with the B<sub>0</sub> field. Spectral enantiodiscriminations using PBLG-based mesophase were reported for almost all classes of organic chiral molecules, but also for other aspects of enantiomorphism, such as chirality by virtue of the isotopic H/D substitution, or the enantiotopy in prochiral molecules [41, 128].

Outside the magnetic field, microdomains of PBLG, PELG, and PCBL- based CLC samples behave as a cholesteric system (Ch) with a positive molecular anisotropic diamagnetic susceptibility ( $\Delta\chi_m > 0$ ) [129]. Under the effect of the magnetic field, the cholesteric helix of each microdomain unwinds, and a uniform chiral nematic system (N\*) where all polymer fibers are aligned along the B<sub>0</sub> axis is then



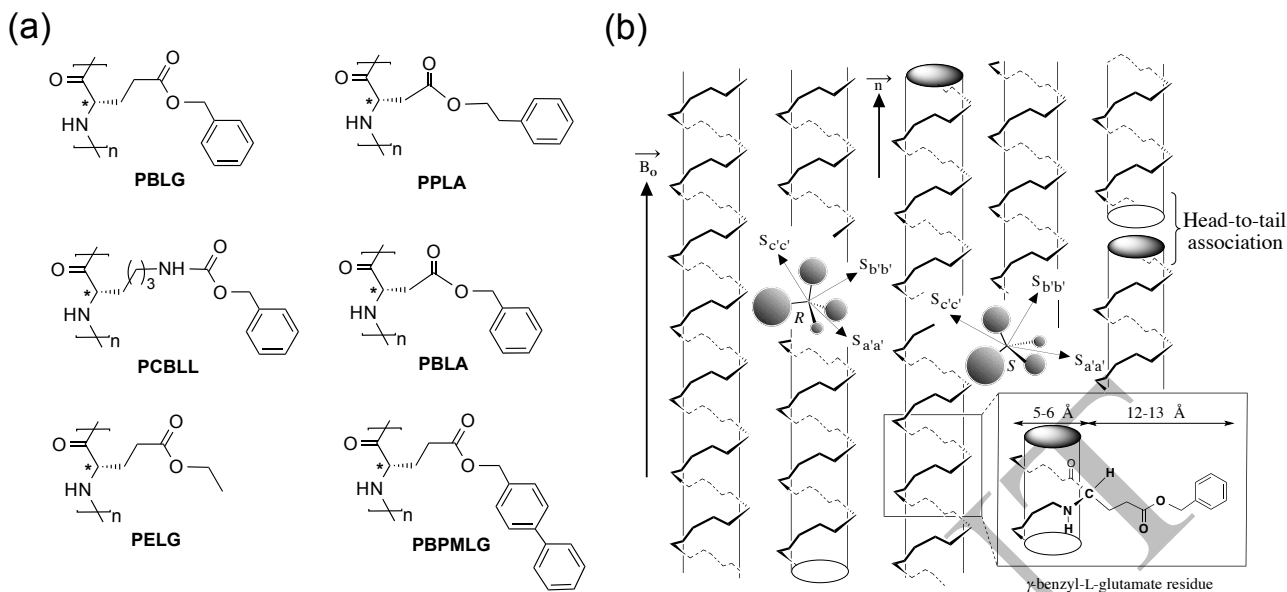


**Fig. 7.** (a) Structures of six homopolypeptide-based helical polymers: PBLG, PCBL, PELG, PPLA, PBLA, and PBPMGL (see Table 3). (b) Schematic illustration of the differential ordering effect for two enantiomers dissolved in the PBLG phase. To clarify the drawing, the glutamate side chains of the polypeptide and the co-solvent molecules are not displayed. The spatial representation of the orientational principal axis system ( $a'$ ,  $b'$ ,  $c'$ ) of enantiomers should be regarded as arbitrary. The PBLG fibers and chiral solutes are not plotted to scale. Note the head-to-tail associations between two PBLG fibers. Figure partially adapted from Ref. [35] with permission.

obtained, as depicted in Fig. 7b [129, 130, 131]. At high magnetic field, the Ch-N\* conversion is fast and the degree of disorder in these polymeric helical systems is generally low for homogenous and uniform samples. In practice, the quality of orientation of PBLG fibers in the sample can be evaluated: i) rapidly on the basis of the linewidth and the asymmetry of the components of  $^2\text{H}$ -QD (in particular of co-solvent); and ii) more rigorously by measuring the spatial variation of  $^2\text{H}$ -RQC using  $^2\text{H}$  NMR imaging [132]. This latter approach allows magnetic field and alignment inhomogeneities to be distinguished.

### 3.2.2. Analysis of highly polar compounds

One limitation of homopolypeptide-based CLC is their difficulty/inability to dissolve highly polar molecules or water-compatible analytes. To overcome this drawback, two approaches have been proposed. The first consists of the addition of a small proportion (1% w/w) of polar additives, such as DMSO, in the organic solution in order to (slightly) increase the amount of analyte in solution in the mesophase [133]. However, this approach does not ensure exploitable results. Another more drastic option is to record spectra in  $\beta$ -peptide-based helical systems in the presence of water [134].

### 3.2.3. Achiral oriented systems by compensation

While organic solutions of a single chiral polypeptide lead to enantiodiscriminating oriented environments, mixtures prepared by mixing equal amounts by weight of polypeptides of the same type but with opposite absolute configuration (e.g. PBLG and its enantiomer PBDG) lead to achiral environments where enantiodiscrimination mechanisms are inactive. In these achiral mesophases, noted "PBG", both enantiomers -hereafter denoted for the sake of simplicity  $l$  and  $d$ , and without any link to

absolute stereodescriptor- exchange rapidly, between the *L*- and *D*- helical vicinities of each polypeptide on the NMR time scale. This results in identical average magnetic interactions for enantiomers, and no difference between their NMR spectra is therefore expected [135].

The disappearance of enantiodiscrimination mechanisms can be conceptually described as follows. At molecular level, the physical interactions are invariant by symmetry, and so the homochiral (resp. heterochiral) diastereoisomeric interaction potentials in the PBDG and PBLG phases, denoted “ $d_{\text{solute...Dpolypeptide}}$ ” and “ $l_{\text{solute...Lpolypeptide}}$ ”, (resp. “ $l_{\text{solute...Dpolypeptide}}$ ” and “ $d_{\text{solute...Lpolypeptide}}$ ”), are symmetrical to each other as depicted in Fig. 8a.

Thus from the  $^2\text{H}$  NMR point of view, the strict inversion of interaction potentials in PBLG and PBDG leads to simply an interchange of the spectrum of each enantiomer (see Fig. 8b). In a racemic mixture of enantiomeric polypeptides, the overall interactions undergone by the *d* solute (“ $d_{\text{solute...Dpolypeptide}}$ ” + “ $d_{\text{solute...Lpolypeptide}}$ ”) and the *l* solute (“ $l_{\text{solute...Lpolypeptide}}$ ” + “ $l_{\text{solute...Dpolypeptide}}$ ”) become equal. Hence in the fast exchange regime, any enantiodiscrimination vanishes on the NMR time scale [135].

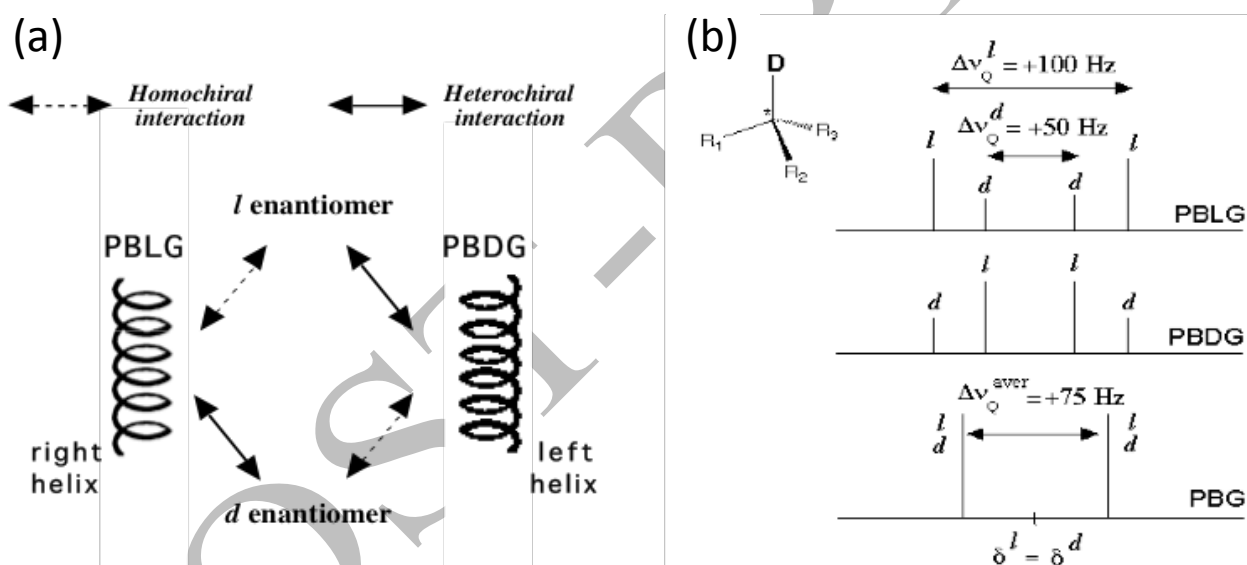


**Fig. 8.** (a) Definition of homo- and heterochiral interactions involved between *l* levogyre (*l*) and dextrogyre (*d*) enantiomers and the PBLG or PBDG helices in a racemic mixture of both polypeptides (PBG mixture). (b) Variation of  $^2\text{H}\{-^1\text{H}\}$  spectra associated with a monodeuterated chiral molecule (enriched in *l* isomer) dissolved in (top) the PBLG phase, (middle) the PBDG phase and (bottom) PBG phases. The strict inversion of interaction potentials in PBLG and PBDG leads to interchange the spectrum of each enantiomer. Here we assumed that the sign of the  $\Delta\nu_{\text{Q}}$ 's were identical. Opposite sign would lead to a value for  $\Delta\nu_{\text{Q}}$  equal to  $\pm 25$  Hz. Note that the  $\Delta\nu_{\text{Q}}$  values and the *d* and *l* assignment are arbitrary. In Fig. 8b, we assume  $\delta^l = \delta^d$ . Figure reproduced from the SI of Ref. [121] with permission.

Analytically, the comparison of NMR spectra recorded in the achiral phase against those obtained in the chiral phases readily allows one to understand the latter, because in the achiral phase, the spectral enantiodiscriminations have disappeared while the spectral diastereodiscriminations are still active. In addition, for  $^2\text{H}$  spectra, it is possible to determine the relative sign of  $\Delta\nu_{\text{Q}_i}$  (see Fig. 8b) associated with enantiomeric or enantiotopic direction pairs (see Section 9.1). Indeed, the  $\Delta\nu_{\text{Q}}$  values measured in the

achiral mesophase (denoted  $\Delta v_{Q_i}^{\text{aver}}$ ) are equal to the average of values obtained in the PBLG or PBDG chiral mesophases (denoted  $\Delta v_{Q_i}^{\text{aver}}$ ). This equality can be easily demonstrated. For instance, in the PBLG phase, we can write:

$$\Delta v_{Q_i}^{\text{aver}} = \left( \frac{\Delta v_{Q_i}^l(L) + \Delta v_{Q_i}^d(L)}{2} \right) = \frac{3}{2} K_{C-D_i} \times \left( \frac{S^l(L) + S^d(L)}{2} \right) \quad (17)$$

In this equation,  $S^l(L)$  and  $S^d(L)$  are the order parameters of the C-D bond that derive from interactions between the  $l$  and  $d$  enantiomers, respectively, with the polypeptide of  $L$  configuration. The same kind of average can be defined in the PBDG phase, except that the  $L$  stereodescriptor is replaced by the  $D$  stereodescriptor. In the achiral PBG mesophase, the order parameter for a given C-D bond results from the average of order parameters of the  $l$  (resp.  $d$ ) enantiomer interacting with the  $L$  and  $D$  helices if we assume that the residence times of  $l$  and  $d$  stereoisomers in the vicinity of PBLG and PBDG are identical. Experimentally, Eq. (17) should be valid if two polymers have similar DP [135]. Thus we can write:

$$S^l(L + D) = \left( \frac{S^l(L) + S^l(D)}{2} \right) \text{ and } S^d(L + D) = \left( \frac{S^d(L) + S^d(D)}{2} \right) \quad (18)$$

From symmetry considerations, the term  $S^l(D)$  (resp.  $S^l(L)$ ) is identical to the term  $S^d(L)$  (resp.  $S^d(D)$ ), and so, we can write this series of equalities:

$$\begin{aligned} S^l(L + D) &= \left( \frac{S^l(L) + S^l(D)}{2} \right) \\ &= \left( \frac{S^l(L) + S^d(L)}{2} \right) = S^{\text{aver}}(L) \\ &= \left( \frac{S^d(D) + S^l(D)}{2} \right) = S^{\text{aver}}(D) \\ &= \left( \frac{S^d(D) + S^d(L)}{2} \right) = S^d(L + D) \end{aligned} \quad (19)$$

From Eqs. (14), (18) and (19), we conclude that  $\Delta v_Q^{\text{aver}} = \Delta v_Q^{l \text{ or } d}(L + D)$ . Experimentally, the enantiodiscrimination exactly disappears when the DP of  $L$ - and  $D$ -polypeptide are as close as possible [135]. Note that the same phenomenon arises for enantiotopic directions in prochiral molecules dissolved in ALCs made of stereochemically-inverted polymer mixture.

### 3.2.4. Mixtures of two homopolypeptides

When compatible, mixtures of two polypeptides with different types of side chains, such as PBLG and PCBL (same AC), may be used and they allow the discrimination of both enantiomers and enantiotopic directions in prochiral molecules. Interestingly in such systems, enantiodiscrimination magnitudes and resolution can be adjusted by varying the relative proportion of the two polypeptides. Therefore, these

enantiodiscriminating media can be appealing alternatives to single-polypeptide mesophases for stereochemical applications [136].

Using a “mean-field” model derived from that proposed for mixtures of thermotropic nematics [120], and based on the separation of intermolecular interactions between the solute and both polypeptides, it was pointed out that solute distribution in the vicinity of each polypeptide partly governs enantiodiscrimination magnitude and NMR relaxation rates. From the analysis of experimental NMR observables of solute ( $\Delta\nu_Q$ ,  $T_1$ ) versus the fraction of peptide units, it is possible to determine the relative solute-fiber affinities [121, 136].

In order to understand the interaction process of a solute toward two chemically-different homopolypeptides, a model involving two boxes has been proposed: the first one contains a fragment of a polypeptide a (“a-box”) and the second one contains a fragment of the polypeptide b (“b-box”). This model assumes that a solute molecule interacts with a single polypeptide fiber and we disregard the interactions with the end of the polypeptide fiber. Under these assumptions, the mean value,  $\langle A \rangle$ , of any NMR observable noted “A” (e.g.  $^2\text{H}$ -RQC or  $(^1\text{H}\text{-}^1\text{H}/\text{}^{13}\text{C}\text{-}^1\text{H})$ - RDC) can be defined for a molecule (denoted by 1) as [121]:

$$\langle A \rangle_{\text{mix}} = P_{\text{solute}}^a \int_{a,\text{box}} Af_{a,\text{box}}(X_1) dX_1 + P_{\text{solute}}^b \int_{b,\text{box}} Af_{b,\text{box}}(X_1) dX_1 \quad (20)$$

In this equation,  $P_{\text{solute}}^a$  and  $P_{\text{solute}}^b$  are the probabilities to find the solute in the environment of polypeptides a and b, respectively. Eq. (20) can be recast as:

$$\langle A \rangle_{\text{mix}} = \frac{k_a x_a^{\text{pu}}}{(k_a x_a^{\text{pu}} + k_b x_b^{\text{pu}})} \langle A \rangle_a + \frac{k_b x_b^{\text{pu}}}{(k_a x_a^{\text{pu}} + k_b x_b^{\text{pu}})} \langle A \rangle_b \quad (21)$$

where  $k_i = c_{i,\text{box}}^{\text{solute}} / (c_{a,\text{box}}^{\text{solute}} + c_{b,\text{box}}^{\text{solute}})$  with  $i = a$  or  $b$  are the molar fractions of solute in the boxes a and b, respectively,  $c_{i,\text{box}}^{\text{solute}}$  with  $i = a$  or  $b$  are the concentrations of solute in boxes a and b,  $x_i^{\text{pu}} = n_i^{\text{pu}} / (n_a^{\text{pu}} + n_b^{\text{pu}})$  with  $i = a$  or  $b$  are the molar fractions of peptide unit and  $n_i^{\text{pu}}$  with  $i = a$  or  $b$  are the amounts of peptide units a or b.

By introducing  $K = k_a / k_b$  and using  $x_b^{\text{pu}} = 1 - x_a^{\text{pu}}$ , Eq. (21) can be simplified into:

$$\langle A \rangle_{\text{mix}} = \frac{x_a^{\text{pu}} (K \langle A \rangle_a - K \langle A \rangle_b) + \langle A \rangle_b}{(K - 1) x_a^{\text{pu}} + 1} \quad (22)$$

The constant  $K$  can be considered as the distribution coefficient of a solute between the polypeptide fibers in the mixture. As the sum  $k_a + k_b = 1$ , it is possible to recalculate the constants  $k_a$  and  $k_b$  from the parameter  $K$ , using the following relations:  $k_a = K / (K + 1)$  and  $k_b = 1 / (K + 1)$ . According to Eq. (22), the average value of any solute property,  $\langle A \rangle$ , follows a hyperbolic evolution where the maximal deviation

compared to a linear evolution (see Eq. (23)) is observed when  $x_a^{\text{pu}} = 1/(1 + \sqrt{K})$ . Note here that if  $K = 1$ , Eq. (22) is simplified into:

$$\langle A \rangle_{\text{mix}} = x_a^{\text{pu}}(\langle A \rangle_a - \langle A \rangle_b) + \langle A \rangle_b = x_a^{\text{pu}} \langle A \rangle_a + x_b^{\text{pu}} \langle A \rangle_b \quad (23)$$

This particular case corresponds to the “random mixing” as defined by Emsley *et al.* [120], and then leads to a linear variation of  $\langle A \rangle$  versus  $x_a^{\text{pu}}$  or  $x_b^{\text{pu}}$  [121].

The fast exchange regime of solutes towards the two chemically-different polypeptides in the chiral mixtures (“PBLG-PCBLL”) is comparable to that observed in the “PBG” or “PCBL” achiral oriented systems (see above). However, in those systems, the inversion of the chirality of polypeptide (*L* and *D*) leads to an achiral oriented medium without enantiomeric or enantiotopic discrimination. Consequently, the racemic mixture of two pairs of homopolypeptides (chemically different and with inverted AC), for instance the “PBLG/PBDG” pair added to the “PCBLL/PCBDL” pair, in the same sample provide again an achiral oriented medium that prevents any enantiodiscrimination. In this case, the residual anisotropic interactions measured in the four-homopolypeptide-based achiral system is equal to the average of those measured in the two-polypeptide chiral oriented systems. This situation has been experimentally evidenced first in the case of norbornene dissolved in a four-polypeptide achiral mixture [136].

### 3.3. Possible alternatives to polypeptide systems

From 2010, various new chiral mesophases made of helically chiral polymers have been synthesised and described as enantiodiscriminating oriented systems by various groups (for example, those of Berger, Luy, Reggelin and Thiele). Chronologically, we can cite systems made of: i) poly(guanidine) in 2010 (see Fig. 9a) [137]; ii) poly(arylisocyanide) in 2012 (see Fig. 9b) [138]; iii) poly(arylacetylene) containing chiral side chains in 2012 [139, 140, 141] (see Fig. 9c); iv) poly(isocyanopeptide) in 2017 [142]; v) poly(arylisocyanide) [143] in 2017. Table 3 also summarizes the main organosoluble helically chiral polymers other than polypeptide systems.

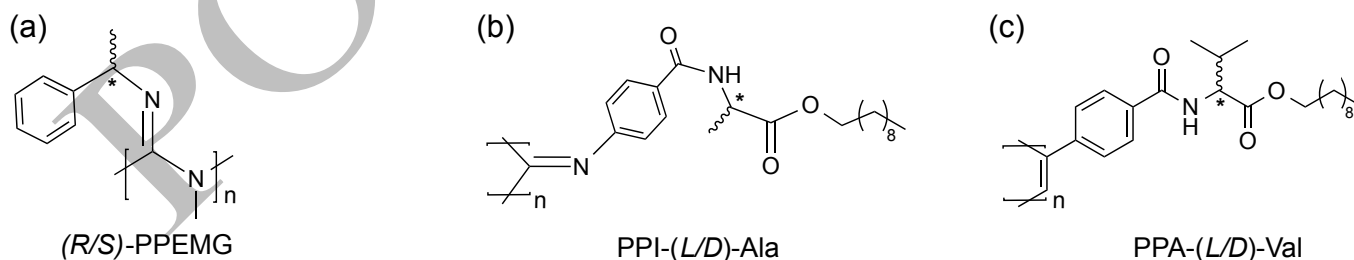


Fig. 9. Three examples of organosoluble, helically-chiral polymers, which are not polypeptides: (a)  $(R/S)$ -PPEMG [137], (b)  $(L/D)$ -Ala-based PPI [138], (c)  $(L/D)$ -Val-based PPA [139]. In these structures, the stereogenic center is located on the side-chain.

Among all these different systems, polyacetylene-based polymers appear as an interesting alternative to PBLG mesophase [139, 144]. They are easier to synthesize compared to polyisocyanides and give homogeneous liquid-crystalline phases. A recent extended investigation of the analytical potential of an *L*-

valine-derived polyacetylene chiral mesophase (see Fig. 9c) has shown it has a strong ability to discriminate enantiomers or enantiotopic directions of a large collection of (pro)chiral model compounds (including examples from rigid to flexible and polar to apolar). They cover various important aspects of enantiomorphism (*e.g.* chirality, isotopic chirality by virtue of the isotopic (D/H) substitution, prochirality) [144]. Promising NAD NMR results were also obtained, in particular the enantiodiscrimination of a chiral alkane.

### 3.4 The stretched/compressed gels

The determination of anisotropic observables requires the creation of an anisotropic environment through an alignment medium. This can be obtained using weakly-orienting systems as presented above, but also by the use of compressed or stretched polymeric gels. The analytical potential of both equivalent methods for introducing anisotropy in the sample have been demonstrated from the mid-2000's by various groups such as those of Luy [145, 146, 147], Torres [148], Kuchel [149], or Gil [150, 151]. These work proposed suitable protocols and/or dedicated apparatus to adjust the degree of stretching or compression of the polymer gel in the NMR tube, thus controlling the amount of cross-linking of the polymer, and in consequence the magnitude of all anisotropic NMR interactions (RCSA, RDC, RQC). Most stretched/compressed chiral gels are compatible with water or highly polar solvents (DMSO). Typically, these include gelatin- and *e*-gelatin-based gels [149, 152, 153], collagen-based gels [154] or polyacrylamide-based gels [155].

## 4. Simplifying the anisotropic $^1\text{H}$ NMR spectra in weakly orienting phases

The analytical potential of polypeptide-based CLCs for deciphering NMR spectra of enantiomeric mixtures was firstly explored through the analysis of  $^1\text{H}$  resonances. However, using  $^1\text{H}$  NMR was considered by chemists as too complex for two reasons: i) the high natural abundance (99.985%) of  $^1\text{H}$  nuclei generates a dense homonuclear network of  $^1\text{H}$ - $^1\text{H}$  residual dipolar interactions, which results in poorly resolved and intricate spectra; the analysis of such data being a time-consuming process (see Section 3); ii) the presence of two enantiomers as well as the important number of short- and long-range intramolecular ( $^1\text{H}$ - $^1\text{H}$ )-RDCs further complicates the multiplets for each non-equivalent  $^1\text{H}$  site [35]. Moreover, the inhomogeneity of the sample, which is due to the distribution of the orientation of the molecules throughout the weakly orienting medium, also leads to a broadening of the observed lines [155, 156]. An illustrative example of a  $^1\text{H}$  1D spectrum of a small chiral molecule recorded in PBLG phase is shown in Fig. 10.

Several approaches have been explored to improve the resolution of  $^1\text{H}$  NMR spectra of enantiomeric mixtures in CLCs, and to extract the structural information related to the numerous anisotropic

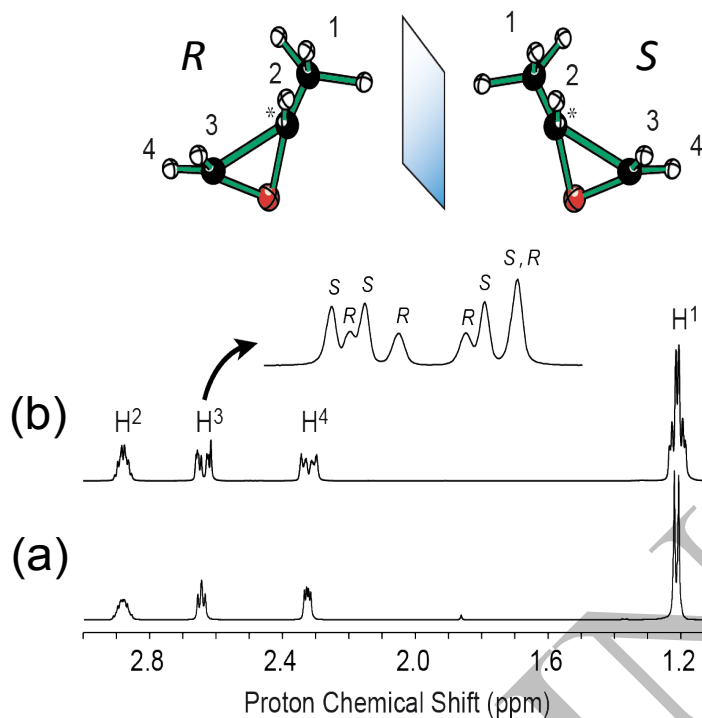


**Fig. 10.** (a) 400.1 MHz  $^1\text{H}$  spectrum recorded at 295 K of (*R*)-1,2-epoxypropane (25% ee) dissolved in (a)  $\text{CDCl}_3$  and (b) in PBLG/ $\text{CHCl}_3$ . An assignment of the lines belonging to each enantiomer is shown for the site  $\text{H}^3$ . In this example, each non-equivalent  $^1\text{H}$  site is observed.

interactions. Most of these methods rely on the ability of some pulse sequences to separate the evolution of chemical shifts and spin-spin coupling interactions [157].

#### 4.1. Measurement of homonuclear total couplings

As mentioned above (Section 2), the splitting of  $^1\text{H}$  multiplets in molecules dissolved in a weakly orienting medium is dominated by the total coupling,  $T_{\text{HH}} = J_{\text{HH}} + 2D_{\text{HH}}$ , where  $J_{\text{HH}}$  is the isotropic part of the scalar coupling and  $D_{\text{HH}}$  is dipolar coupling, for anisochronous coupled proton spins, and the total coupling,  $T_{\text{HH}} = 3D_{\text{HH}}$ , for isochronous nuclei. Although these RDCs are very informative probes of both the structure of the solute and its orientation in the anisotropic phase, extracting the value of these anisotropic interactions from strongly overlapping signals raises a major resolution issue, as can be seen in the case of 1,2-epoxypropane (see Fig. 10). To overcome this difficulty, high-resolution methods based on the implementation of selective spin echoes in 2D experiments have been shown to be particularly well-adapted, though challenging.

Several original methods have been developed to address this problem and applied in the field of the chiral analysis. They are based on the SElective ReFocusing (SERF) experiments first introduced by Facke and Berger in 1995 [158]. The following sections will present a brief overview of the most successful developments of this selective refocusing approach, in the particular case of *T*-resolved spectroscopy. For a more general discussion of progress achieved in the whole field of SERF pulse sequences, readers may consult the complete and thorough review published in 2018 [159].

## 4.2 Extraction of $^1\text{H}$ homonuclear RDCs by selective refocusing based methods

### 4.2.1. The SERF 2D experiment

SERF experiments are built on the well-known  $J$ -resolved pulse sequence, whose key element is the spin echo evolution block [160]. The key idea of the approach consists in selectively inverting the coherences of two coupled nuclear spins, so that only their spin-spin interaction is allowed to evolve during the selective spin echo, whereas all other spin interactions (chemical shifts and couplings with other spin nuclei) are refocused (see Fig. 11). This pulse sequence was originally conceived for addressing weakly coupled protons in molecules dissolved in isotropic solvents, but its suitability for enantiomeric mixtures interacting weakly with orienting CLCs has also been successfully demonstrated [161]. The efficiency of the SERF experiment is nicely illustrated for ( $\pm$ )-1,2-dibromopropane dissolved in PBLG/ $\text{CHCl}_3$ . In the example shown in Fig. 12, the offset of the selective pulses was set to the resonance frequency of the methyl protons, allowing for editing highly resolved multiplets ( $A_3$  spin system) with splittings between lines corresponding to the methyl total couplings ( $3D_{A_3}$ ) for each enantiomer [161].

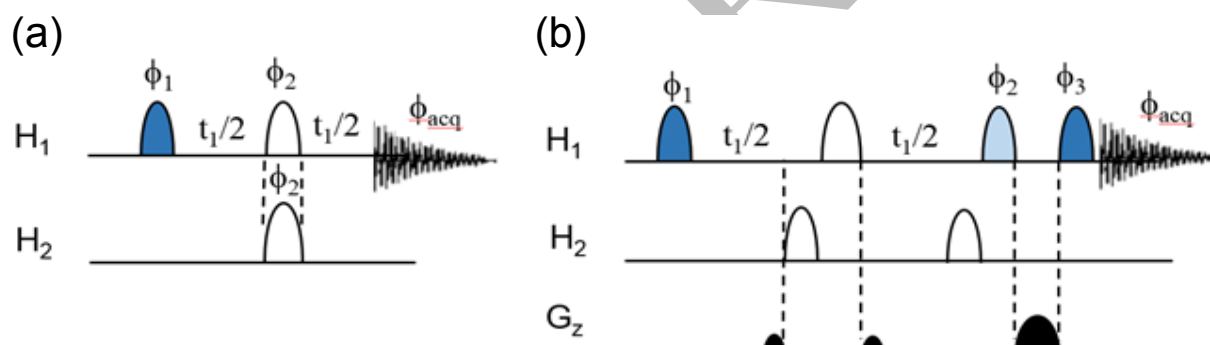


**Fig. 11.** Pulse schemes of (a) the basic SERF experiment and (b) the phasable (in pure absorption mode) SERF (SERFph) experiments. Dark blue, light blue and white ellipsoids shapes correspond to 90°, 90° flip back, and 180° semi-selective shaped pulses, respectively. Black ellipsoid shapes on the gradient channel are the sine-shaped z gradients for insuring clean refocussing during  $t_1$  and coherence selection within the z-filter block. Phase cycles are  $\phi_1 = \phi_{acq} = x, -x, -x, x$ ;  $\phi_2 = x, x, x, x$ ; for the 2D SERF and :  $\phi_1 = x, -x, x, -x$ ;  $\phi_{acq} = x, -x, -x, x$ ;  $\phi_2 = x, x, x, x$ ;  $\phi_3 = x, x, -x, -x$  for the SERFph. Phase cycles are x for non-specified phases. Figure partially adapted from Ref. [157] with permission.

As it was recently discussed in detail by Berger [159], the original SERF pulse sequence, which is a straightforward implementation of selective irradiations in the original  $J$ -Resolved experiment, has been further improved in order to increase the quality of the analytical content of the resulting spectra. In the field of chiral analysis, four issues were raised by the nature of the samples studied: i) the size of the residual dipolar interactions that are re-introduced in proton spectra by the anisotropic medium needs to be controlled so that strong coupling and/or pulse selectivity issues can be avoided; ii) pure absorption 2D maps are needed to optimize the separation between sub-spectra arising from each enantiomer; iii) it is helpful to separate the coupling information that is made available for each enantiomer from SERF



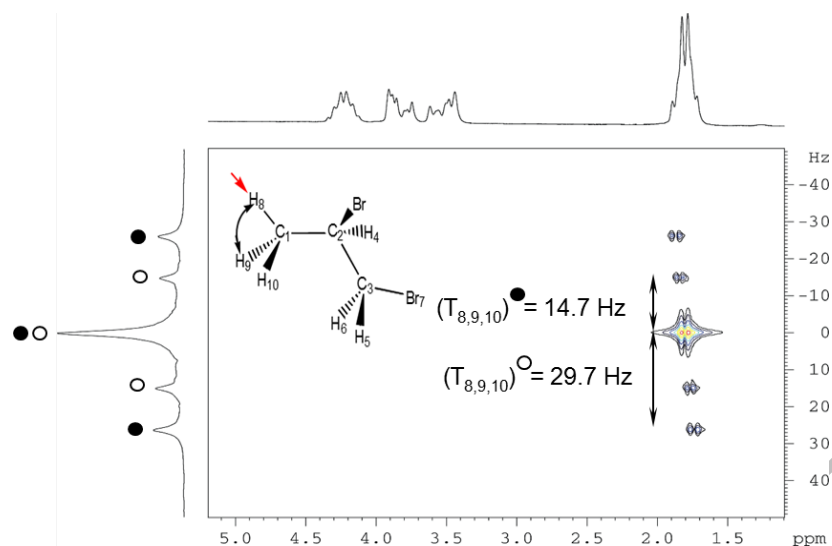


**Fig. 12.** 400.1 MHz  $^1\text{H}$ -SERF 2D spectrum (magnitude mode) of the racemic mixture of ( $\pm$ )-1,2-dibromopropane in PBLG/ $\text{CDCl}_3$ . All selective pulses have been applied at the resonance frequency of the methyl protons. Open and black circles correspond to the lines of the two triplets that were assigned to the *S* and *R* enantiomers respectively. Figure partially adapted from Ref. [161] with permission.

spectra into two different data sets, in order to facilitate their analysis; iv) and a generalization of the selective refocusing approach would allow for editing the whole coupling network within a single dataset.

#### 4.2.2 Improvements to the original SERF pulse sequence

Significant efforts were also made to select adequate coherence pathways during of the SERF experiment that are capable of providing pure absorption 2D spectra. On the one hand, since the selective pulses in the middle of the spin echo cannot be applied simultaneously, it was demonstrated that it is necessary to add a third selective refocusing pulse at the end of this block in order to symmetrize this selective spin echo, hence to fully refocus chemical shift and coupling evolution that may arise during the selective irradiation whose duration can reach several tenths of milliseconds. On the other hand, it was also shown that implementing a z-filter at the end of the SERF pulse sequence allows removal of anti-phase coherences that are generated during the spin echo, thereby leading to pure absorption 2D spectra (see Fig. 11b) [162].

Another improvement of the SERF technique in the field of chiral analysis was achieved by rotating the sample around an axis tilted from the static magnetic field by an angle close to the magic angle ( $\theta_m = 54.7^\circ$ ). The principle of this approach is illustrated in Fig. 13a [76, 77]. The sample rotation, which is in general relatively slow, induces an alignment of the director of the nematic phase,  $n$ , along the rotation axis. Under these conditions,  $^1\text{H}$ - $^1\text{H}$  dipolar interactions are almost fully averaged to zero, thus leading to a spectral simplification as well as a reduction of the signal broadening (due to the long-range couplings) that would otherwise be detrimental to the spectral resolution for samples interacting with an orienting medium. The combination of the so-called VASS method with phased SERF 2D (SERFph) experiments has been successfully demonstrated on the model compound propylene oxide dissolved in a phase

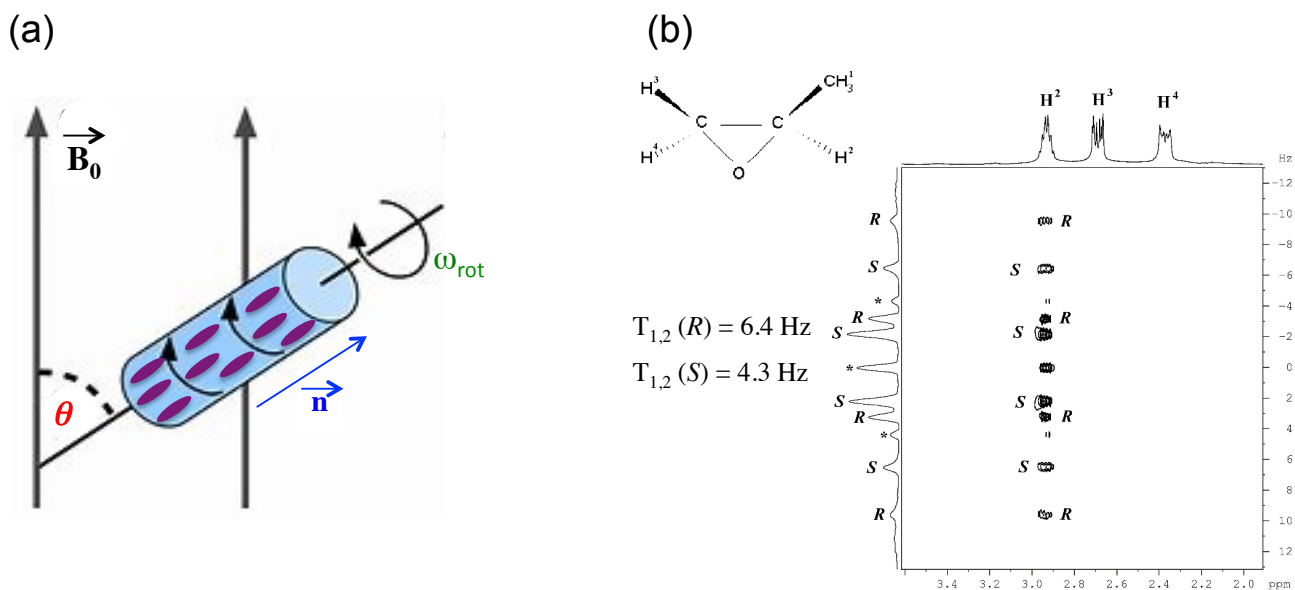


**Fig. 13.** (a) Illustration of the VASS technique where the director,  $\mathbf{n}$ , is aligned along the axis of rotation of the sample inclined by an angle  $\theta$ . At  $\theta = \theta_m = 54.7^\circ$  (the magic angle), all order-dependent NMR interactions are cancelled. (b) 400.1 MHz  $^1\text{H}$  SERFph 2D spectrum of ( $\pm$ )-1,2-epoxypropane dissolved in PBLG/ $\text{CDCl}_3$ . The sample was spun at 660 Hz around an axis ( $\theta$ ) tilted at  $40^\circ$  with respect to  $\mathbf{B}_0$ . Figure partially adapted from Ref. [162] with permission.

composed of PBLG/ $\text{CDCl}_3$  (see Fig. 13b), leading to the selective observation of multiplets with fully tailored total coupling magnitudes and the separation of the lines belonging to each enantiomer [163, 164].

Capitalizing on the unique ability to control spin evolutions in a reliable manner in weakly oriented media, a SERF-filtered pulse sequence has also been developed, which allows for filtering out of the correlations from one enantiomer by exploiting one passive coupling from the proton network of the studied chiral compound that is different in each enantiomer. Fig. 14 shows how this approach can be exploited to record separately, and thus to assign each measured coupling to the right enantiomer, which is a challenging task when standard methods are implemented [164].

Another significant enhancement of the selective refocusing approach in the field of chiral analysis was the implementation of spatially-encoded selective spin echoes in order to visualize the whole total coupling network involving a given proton site in a single  $T$ -edited 2D spectrum. The schematic principle is described in Fig. 15 [165]. The G-SERF 2D experiment fulfills this goal by triggering simultaneously the whole series of SERF experiments related to a given proton nucleus in the chiral molecule. The resulting 2D spectrum shows a series of multiplets which are often reduced to doublets and appear for each enantiomer at the resonance frequency of each coupling partner of the probed proton site, hence allowing for a straightforward assignment and measurement of the total couplings, as it is illustrated in Figs. 15b,c,d [165]. Different approaches have been developed to produce such edition of the spin-spin interaction network. Among them, only the one based on the Zangger-Sterk method [166], which involves selective pulses whose resonance offset is spatially encoded by a weak pulsed field gradient (PFG),

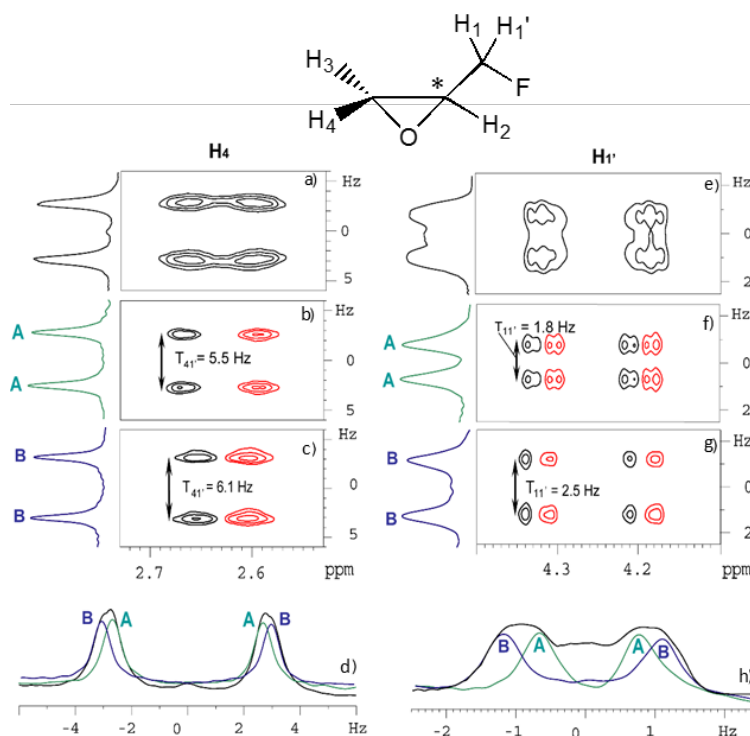


**Fig. 14.** 400.1 MHz  $^1\text{H}$  SERFph 2D experiments applied on ( $\pm$ )-epifluorhydrin in PBLG/ $\text{CHCl}_3$ : (a-c) SERFph between  $\text{H}_4$  and  $\text{H}_{1'}$ , with (b,c) an additional SERF filter between  $\text{H}_3$  and  $\text{H}_4$  optimized to select the signals of enantiomers (b) A and (c) B. (d) Overlay between  $F_1$  positive projections of (a) and (b) and (c) 2D spectra. (e-g) SERFph between  $\text{H}_{1'}$  and  $\text{H}_1$  with (f,g) an additional SERF filter between  $\text{H}_2$  and  $\text{H}_{1'}$  optimized to select the signals of enantiomers (f) A and (g) B. (h) Overlay between  $F_1$  positive projections of (e), (f), and (g) (in black) 2D spectra. Figure partially adapted from Ref. [164] with permission.

revealed to be robust enough to address enantiomeric mixtures dissolved in CLC to date [167]. Further details about these developments can be found in Ref. [157]. More recently, some improvements of the G-SERF technique allowed the removal of unwanted axial peaks in the  $F_1$  dimension of 2D maps that generally hinder and therefore bias the measurement of  $T_{\text{HH}}/J_{\text{HH}}$  homonuclear couplings. Implementing prior to spatially encoded selective refocusing, a selective COSY [168] or a selective TOCSY [169] is a good alternative for selecting overlapped signals and obtaining cleaner and simpler spectra to analyse.

### 4.3 Simplification of $^1\text{H}$ lineshapes

It should be remembered here that the complexity of  $^1\text{H}$  spectra recorded on enantiomeric mixtures dissolved in CLCs arises from two sources. First, as it was described above, the presence of several homonuclear RDCs between protons broadens each signal. Second, although these interactions are different for each enantiomer for the same  $^1\text{H}$  site, the effect of  $^1\text{H}$ -RCSA (even if small) leads to an overlap of these signals. In addition, the presence of these dense homonuclear RDC networks yields correlations that are composed of a large number of lines. Two approaches were more specifically explored to address this issue: i) performing homonuclear decoupling to reduce proton multiplets to singlets [170]; ii) implementing spin state selection techniques to simplify the analytical content of correlation spectra [171].

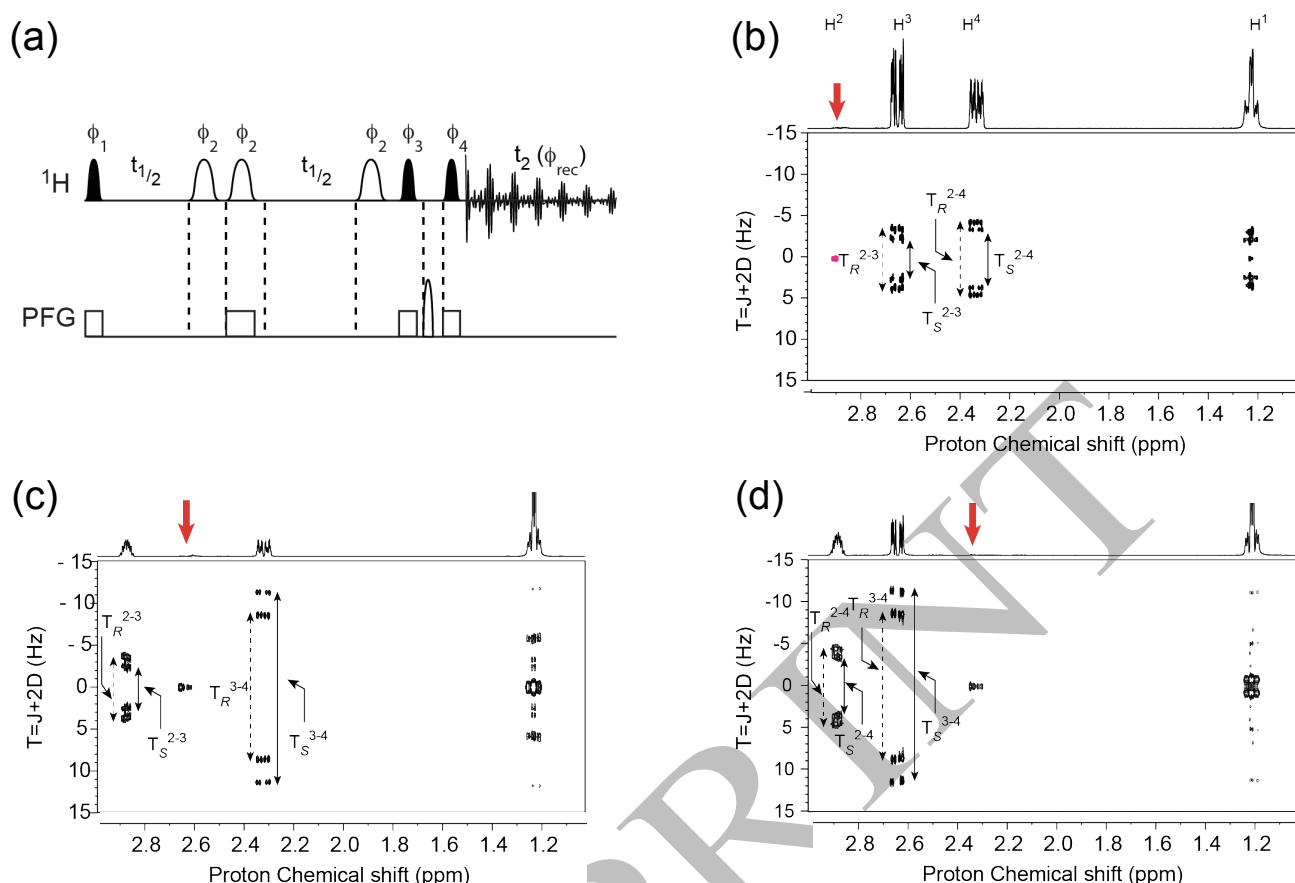


**Fig. 15.** (a) Schematic pulse diagram of the G-SERF 2D experiment. (b to c) Examples of G-SERF spectra applied on ( $\pm$ )-1,2-epoxypropane (see Fig. 13) dissolved in PBLG/ $\text{CDCl}_3$  for an easier measurement of total couplings involving proton sites  $\text{H}^2$  (b)  $\text{H}^3$  (c) and  $\text{H}^4$  (d). See Fig. 13 for the labeling of proton nuclei). For the signals generated at the chemical shift of methyl protons  $\text{H}^1$ , distortions from strong coupling effects are observed. For this reason, total couplings cannot be simply read from the splitting of these multiplets, but can be evaluated by an analysis based on the simulation of the observed lineshapes. Figure partially adapted from Ref. [165] with permission.

#### 4.3.1. Pure-shift techniques applied along the direct spectral domain

Several achievements have been made in performing broadband homonuclear decoupling over the last decades, which have set the foundations for the field of so-called “pure shift” NMR. Most of these methods are based on a generalization of the spin evolutions that can be triggered during a spin echo in the middle of which the spin state of a coupling partner is inverted in order to refocus the evolution of spin-spin interactions [170, 171]. The analysis of enantiomers interacting with a chiral oriented medium is a true challenge for these methods, in particular since the difference of RCSA between enantiomers is expected to be very small. This means that the chosen decoupling method must be very efficient. However, it should be noted that most of the methods reported to date are known to work better on weakly-coupled spin systems, which is not always the case in orienting media where homonuclear RDCs yield strongly-coupled spin networks. In this context, it was surprisingly reported that the Zangger-Sterk method was robust enough to provide an enantiomeric discrimination when it is implemented in a 2D delta-resolved experiment [166]. The robustness of this approach was demonstrated on second-order dipolar coupled model spin systems in which variations of RCSA of  $\sim 20$  Hz could be detected [172].

#### 4.3.2. Multiple quantum correlation spectroscopy

Many attempts have been made to reduce the number of lines that are present in each correlation in multi-dimensional spectra, in order to simplify their analysis. In this area, multiple quantum (MQ) spectroscopy has been shown to be particularly convenient for the purpose of chiral analysis. One interesting approach consists in creating MQ coherences, letting them evolve, and finally converting them to single quantum coherences (SQ) prior to the detection of signal. In the resulting correlation spectrum, the order  $n$  of these MQ coherences determines the level of simplification that is achieved through an appropriate setting of the chosen coherence transfer pathway. This approach, developed by Suryaprakash and co-workers, was successfully used to assign the lines to each enantiomer, and/or to measure the total couplings ( $J_{ij} + 2D_{ij}$ ) with a high accuracy in enantiomeric mixtures dissolved in CLCs based on PBLG [173, 174, 175]. MQ spectroscopy was also used to generate coherences of order  $N$  evolving at the sum of the chemical shifts of  $N$  coupled protons and enantiomeric discriminations were reported based on differences in RCSA of these protons [176].

#### 4.3.3. Other applications of spin state selection correlation spectroscopy

In a slightly different spirit, the need for simplifying the number of lines in correlation spectra arising from the interaction of enantiomeric mixtures with an anisotropic medium has led to original developments arising in the COSY experiment. The BASE- $\beta$ -COSY pulse sequence combines for instance, selective pulses with small flip angles to simplify spectral analysis. This pulse sequence takes benefit of selective pulses combined with small flip angles. It provides homonuclear correlation 2D spectra with reduced spectral width in the indirect dimension, and a small number of lines contributing to each correlation, thereby allowing for the acquisition of data with better resolution than in standard COSY spectra, within a shorter amount of time [177]. Furthermore, the resolution of these experiments has been improved by the implementation of a  $z$ -filter to produce pure absorption spectra [178]). BASE- $z$ -COSY pulse sequence combines the use of selective irradiation with dipolar-coupling-mediated single-quantum transfers to obtain enantiopure correlation 2D spectra [119]. With the same idea, in 2012, the combination of selective pulses and DQ quantum coherence (the “DQ-SERF-COSY” 2D experiment) was reported [180].

An extension of spin state selection techniques to heteronuclear correlation spectroscopy is the XHRES TOCSY experiment, which allows for editing one-bond, as well as long-range heteronuclear couplings  $T_{C-H}$  along the direct and indirect dimensions of the 2D spectrum, respectively (see Fig. 16). All the spectroscopic features of these interactions, namely the amplitude and the sign of the  $^1\text{H}$ - $^{13}\text{C}$  total couplings, are made accessible through the analysis of spin-state selective  $^{13}\text{C}\alpha/\beta$  satellite transitions. The properties of this experiment were notably demonstrated on an enantiomeric mixture of propylene carbonate dissolved in PBLG/ $\text{CDCl}_3$  [181].

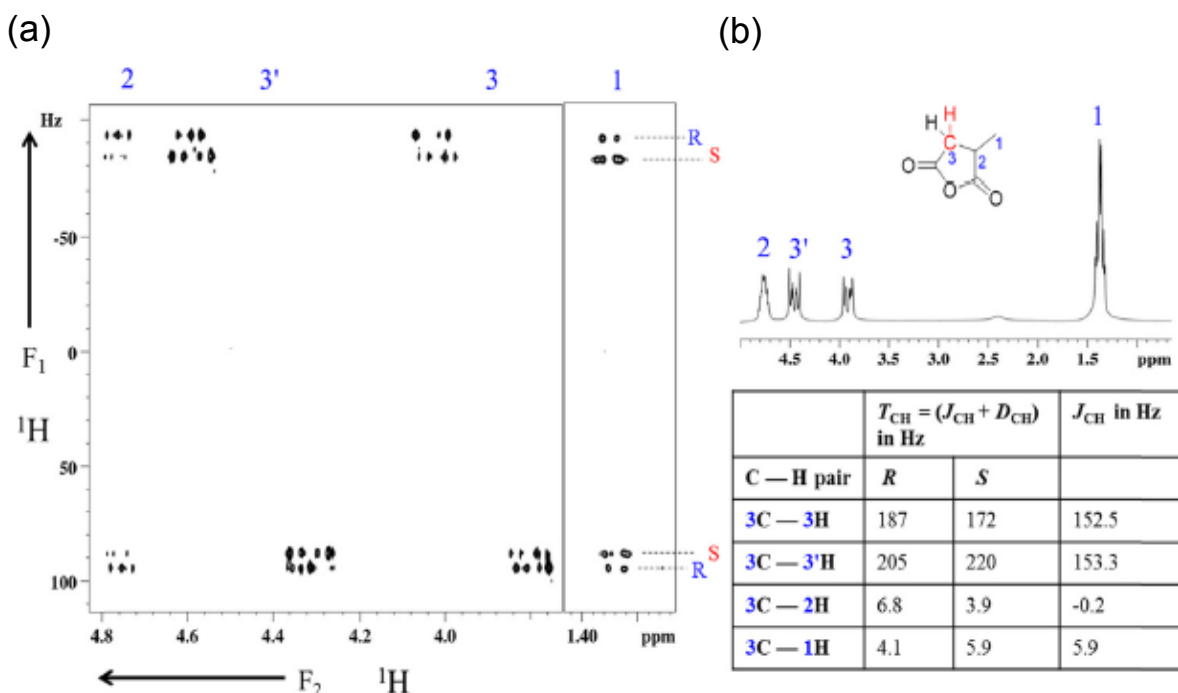


**Fig. 16.** (a) 100.3 MHz  $^{13}\text{C}$ - $^1\text{H}$ -RES-TOCSY spectra of ( $\pm$ )-propylene carbonate. The  $^{13}\text{C}_3$ -bonded proton was selectively excited.  $^1T_{\text{CH}}$  and  $^nT_{\text{CH}}$  could be extracted from the spectrum for each enantiomer. (b) Experimental values of  $T_{\text{CH}}$  extracted from the 2D spectrum. Figure partially adapted from Ref. [181] with permission.

A **SAPS-HSQC** 2D experiment has also been proposed to provide enantio-separation based on the visualization of  $^1\text{H}$  and  $^{13}\text{C}$  chemical shift differences [182]. It is based on the well-known HSQC pulse 2D sequence, which is implemented with BIRD homonuclear decoupling [183] to refocus  $^1\text{H}$  chemical shifts along the direct time domain, while spectral aliasing [184] together with non-uniform sampling (NUS) [185] allows optimization of both the resolution along the indirect  $^{13}\text{C}$  dimension and the acquisition time. The principle of spectral aliasing has also been applied successfully to the HSQMBC experiment, in order to probe enantiomeric discrimination through the measurement of long-range  $^1\text{H}$ - $^{13}\text{C}$  correlations [182].

#### 4.4 Determination of enantiomeric excesses (ee's) using $^1\text{H}$ NMR

$^1\text{H}$  NMR spectroscopy has rarely been used to determine enantiomeric excesses, because the overcrowded spectra obtained using CLC solvents have not allowed quantitative analyses to be carried out with the required accuracy. For this reason, most of the quantitative studies of enantiomeric mixtures were performed using  $^{13}\text{C}$  or  $^2\text{H}$  based NMR analyses. It should be noted, however, that very similar values of the  $T_1$  and  $T_2$  relaxation times have been measured for protons from each enantiomer in most of the chiral compounds investigated to date, which suggests that a sensitive and quantitative measurement using  $^1\text{H}$  NMR is perfectly possible provided a sufficient spectral resolution can be achieved.

Among the first approaches that have opened the way to fully resolved  $^1\text{H}$  correlation spectra, the SERF experiment has been shown to give access to the determination of enantiomeric excesses with a 1-5% accuracy [161-162].

Other variants of the SERF experiment, such as the  $\omega_1$ -het-CH-SERF or the DQ-SERF sequences, have also led to the measurement of  $ee$ 's with 1 to 5 or 6% error. These latter developments require, however, that the integrals measured on each correlation are corrected to account for differences in spin evolution between enantiomers [186]. Similar performance was also reported for a series of pulse sequences derived from the COSY experiment, both in 1D [177] and 2D [178].

More recently, the suitability of experiments based on editing using total spin-spin couplings ( $T_{ij}$ -edited experiments) for determining accurately  $ee$ 's has been demonstrated in the case of the G-SERF pulse sequence. In this latter case, one major issue is the contribution of: i) the selectivity of the different pulses; ii) the spatial selection process, and iii) the strong coupling effects to the observed lineshape of each NMR signal, which has been shown to lead in several cases to a bias when  $ee$ 's are estimated directly from integrated intensities. Thus, it was shown that an accuracy of a few percent can be reached if experimental G-SERF 2D spectra are fitted to simulated data, which can account for the spin dynamics occurring during the spatial selection process (see Fig. 17) [156].

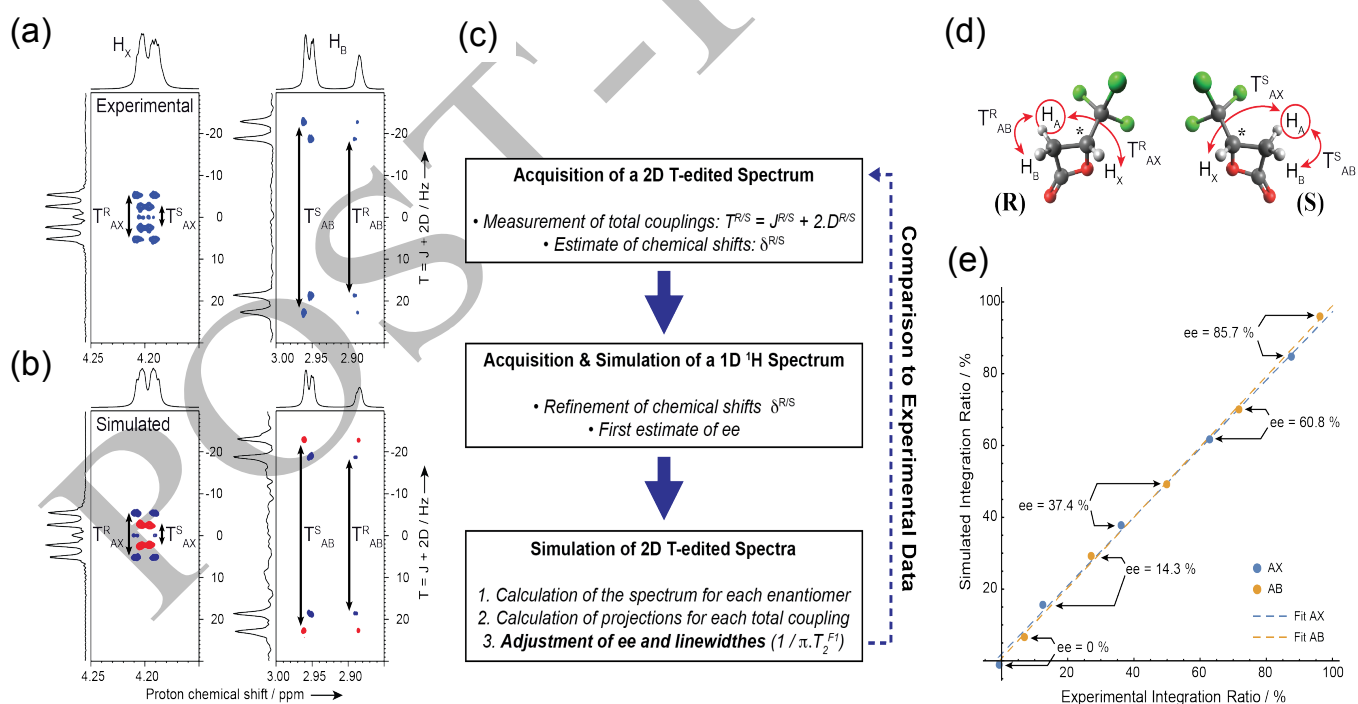


**Fig. 17.** (a and b) Experimental and simulated regions of interest of G-SERF spectra recorded on  $(\pm)$ -3-hydroxy-4,4,4-trichlorobutyric  $\beta$ -lactone (structure shown in (d)) dissolved in PBLG/ $\text{CDCl}_3$  for the editing of the total couplings involving the proton site  $H_A$ . (c) Flowchart describing the steps for determining enantiomeric excesses from a combination of experimental and simulated T-edited spectra. (e) Correlation between the simulated and experimental integration ratios for five different samples of the analyte. Dashed lines correspond to the linear regressions performed on the integration ratios calculated for the total couplings  $T_{AX}$  and  $T_{AB}$ , respectively. The prepared  $ee$  is indicated for each point. Figure partially adapted from Ref. [156] with permission.

## 5. Exploiting $^{13}\text{C}$ NMR spectroscopy

As in the case of protons,  $^{13}\text{C}$  nuclei constitute another important and informative probe for the chiral differentiation process [35, 50, 187].  $^{13}\text{C}$ -RCSAs and ( $^{13}\text{C}$ - $^1\text{H}$ )-RDCs can also be measured on standard  $^{13}\text{C}$  1D-NMR spectra [50,53]. On the one hand, RCSA is in general larger for  $^{13}\text{C}$  than for  $^1\text{H}$  nuclei (see Section 2), which suggests that higher differences in RCSA can be expected between enantiomers. On the other hand, since  $^{13}\text{C}$  are in general surrounded by  $^1\text{H}$  nuclei, several ( $^{13}\text{C}$ - $^1\text{H}$ )-RDCs may also be used to probe the local structure as well as the orientation of the molecule. By extension, when other heteronuclei X are present in the molecule, ( $^{13}\text{C}$ -X)-RDCs can also be expected to constitute useful probes for chiral analysis (see Section 2). However, to fully exploit such  $^{13}\text{C}$  NMR resources, two methodological issues have to be addressed. The first is related to the high number of short and long-range ( $^{13}\text{C}$ - $^1\text{H}$ )-RDCs for medium-sized molecules that rapidly obscure standard  $^{13}\text{C}$  1D-NMR spectra, and in turn hinder simple extraction of heteronuclear dipolar data, as well as the measurement of  $^{13}\text{C}$ -RCSA [50,53]. Such effects are clearly visible in Fig. 18 where two examples of spectral patterns of a methyl group are compared. In Fig. 18a, all ( $^{13}\text{C}$ - $^1\text{H}$ )-RDCs for each isomer can be measured, whereas in Fig. 18b, excessive signal overlap prevents such measurements [53, 188].

The second issue is related to the low sensitivity of  $^{13}\text{C}$ -detected NMR experiments compared to  $^1\text{H}$ , mainly due to the low natural abundance of  $^{13}\text{C}$  nuclei (1.1%). Hence, the detection of  $^{13}\text{C}$  NMR signals can be difficult for analytes with high molecular weights (MW) for which only low amounts are available. This lack of sensitivity can often be overcome by the use of commercially available cryogenic NMR probes [189].

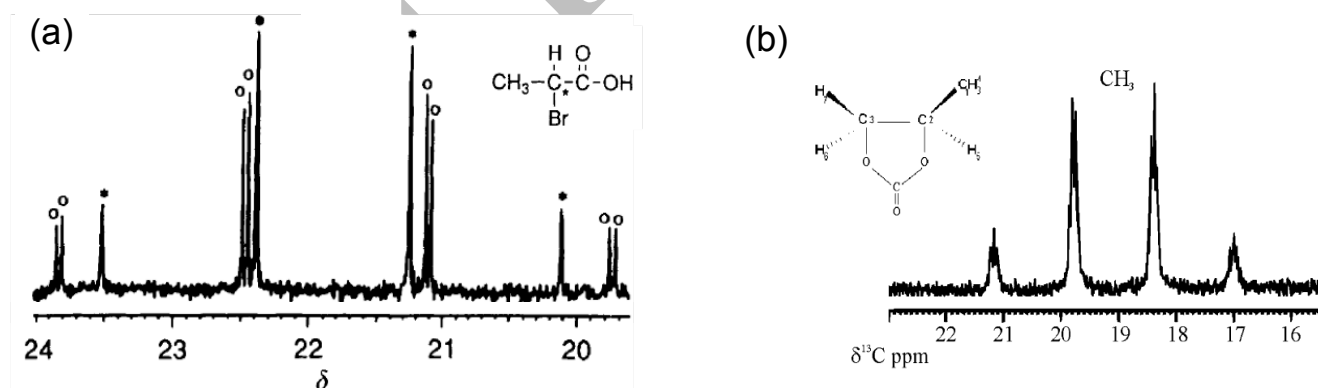


**Fig. 18.** Two typical examples of  $^1\text{H}$  coupled  $^{13}\text{C}$  spectral patterns (100.3 MHz) observed for the methyl group of (±)-2-bromopropionic acid and (±)-propylene carbonate recorded in PBLG CLC. Note the complexity in (b) arising from superimposition of lines due to three  $^1\text{H}$ - $^1\text{H}$  long-range couplings. Figure partially adapted from Refs. [53] and [193] with permission.

### 5.1 1D experiments

#### 5.1.1 Proton-coupled $^{13}\text{C}$ 1D-NMR

The first enantiomeric visualizations of chiral compounds dissolved in an optically active liquid crystal by  $^{13}\text{C}$ -detected NMR were reported for the analysis of 1D spectra recorded at natural abundance [50, 53]. It



was reported that differences of  $^{13}\text{C}$ -RCSA can be measured on proton-decoupled  $^{13}\text{C}$  spectra, whereas the multiplet structures obtained in proton-coupled  $^{13}\text{C}$  experiments give access to both the RCSA and RDC interactions. It should be noted that for these enantiomeric analyses, the complex lineshapes observed in  $^{13}\text{C}$  spectra need to be fitted by a simulation of the expected spectrum in order to extract every interaction, which can be a time-consuming process. It was also established in 1995 that the combination of homonuclear  $^1\text{H}$ - $^1\text{H}$  and heteronuclear  $^{13}\text{C}$ - $^1\text{H}$  RDCs made available in  $^1\text{H}$  and  $^{13}\text{C}$  1D spectra paved the way to the calculation of the molecular ordering parameters of two enantiomers. This has led to the first numerical quantification of the difference in orientation through the Euler angles. Such a quantification was first exemplified in the case of 3-hydroxy-4,4,4-trichlorobutyric  $\beta$ -lactone [49], and then followed by the study on the ( $\pm$ )-3-butyn-2-ol, both dissolved in a PBLG mesophase [190] (see Fig. 19).

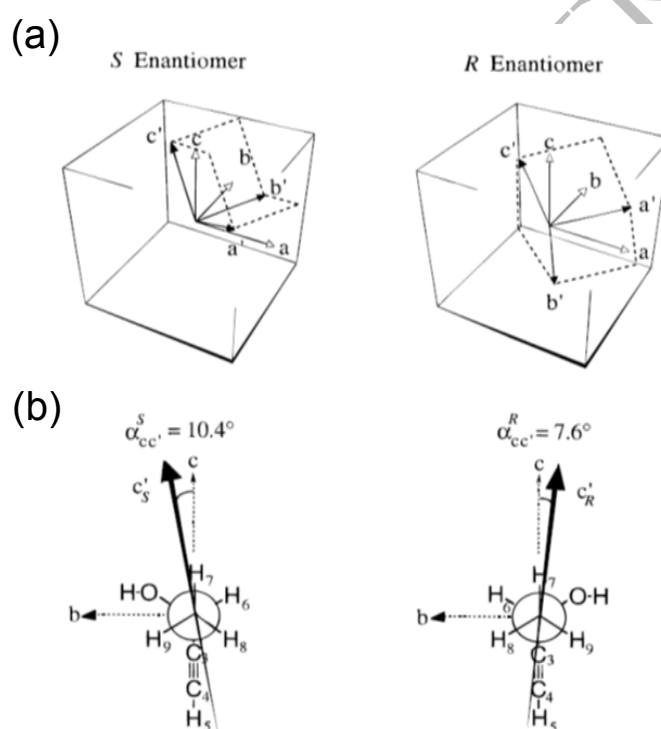


**Fig. 19.** (a) Spatial representation of each principal axis system associated with enantiomers of the ( $\pm$ )-3-butyn-2-ol. The eigenvectors associated with the eigenvalues of the diagonal are orthonormal. (b) Representation of the major orientation axis  $c'$ , relative to the  $ac$  plane. The  $\alpha$  angle between the  $ac$  plane and the  $c'$  axis is  $7.6^\circ$  for the  $R$  and  $10.4^\circ$  for the  $S$  enantiomer. Figure adapted from Ref. [190] with permission.

### 5.1.2 Potential of $^{13}\text{C}$ - $\{^1\text{H}\}$ NMR

Natural abundance proton decoupled  $^{13}\text{C}$  1D-NMR was first shown to be a general and quantitative method for the analysis of enantiomers dissolved in CLCs. In this method, all  $^{13}\text{C}$ - $^1\text{H}$  interactions are cancelled by the application of classical low-power heteronuclear composite pulse decoupling sequences (CPD) (0.5 to 1W), such as WALTZ-16 or WALTZ-64 [191], or more recent adiabatic sequences [192]. These decoupled  $^{13}\text{C}$  spectra are composed only of independent singlets associated with each inequivalent  $^{13}\text{C}$  site of the analyte. In the field of chiral analysis, this method offers an efficient way to separate the

$^{13}\text{C}$  signals of enantiomers by observing the variations in  $^{13}\text{C}$ -RCSA for each of their  $^{13}\text{C}$  sites. Besides, the comparison with the isotropic  $^{13}\text{C}$ - $\{^1\text{H}\}$  1D spectrum generally allows a direct and rapid identification of  $^{13}\text{C}$  resonances that are doubled in the spectrum recorded in the CLC. As illustrated in Fig. 20a, only simplified singlets are observed on the  $^{13}\text{C}$ - $\{^1\text{H}\}$  spectrum of ( $\pm$ )-oct-1-yn-3-ol dissolved in PBLG/ $\text{CDCl}_3$ , which allows for monitoring the doubling of signals resulting from the chiral differentiation process for the different atoms along the carbon chain.

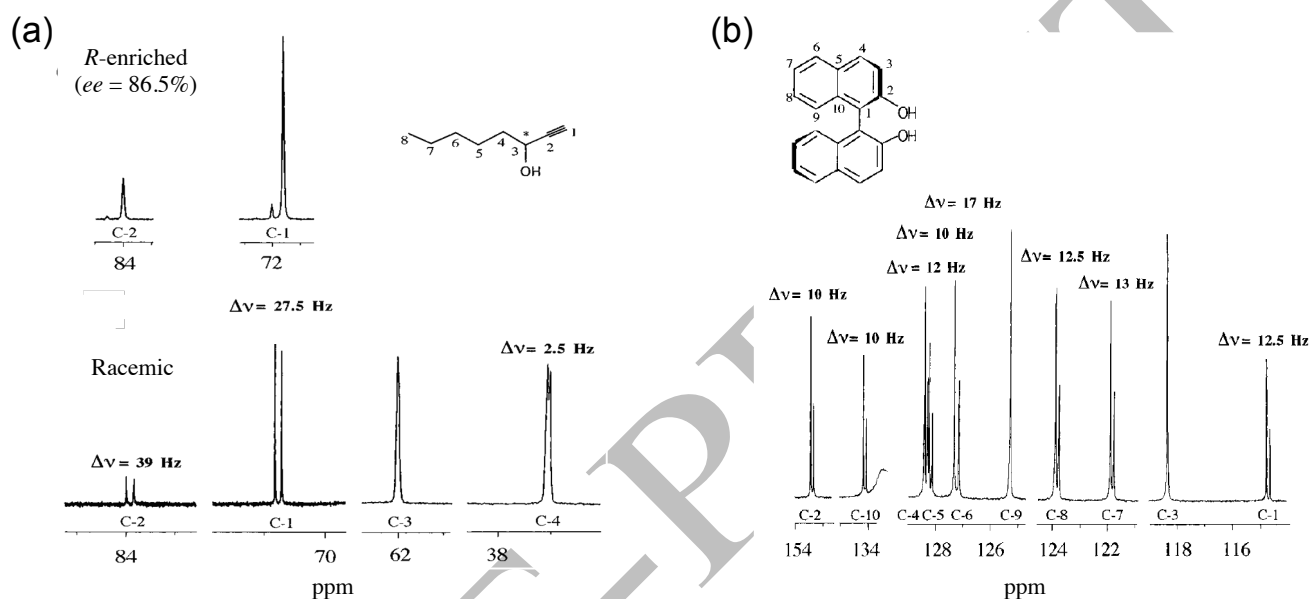


**Fig. 20.** 100.3 MHz  $^{13}\text{C}$ - $\{^1\text{H}\}$  1D NMR spectra of (a) oct-1-yn-3-ol in PBLG/ $\text{CDCl}_3$ , for a racemic (bottom) and enantio-enriched (top) sample and (b) (*R*)-1,1'-bi-2-naphthol (31% ee) in PBLG/ $\text{DMF-d}_7$ . Figure adapted from Ref. [50] with permission.

For a given carbon nucleus, the magnitude of the splitting into two distinct  $^{13}\text{C}$  singlets is related to the magnitude of its  $^{13}\text{C}$ -RCSA. This magnitude has been shown to depend on the hybridization of the  $^{13}\text{C}$  atom in the following order:  $\text{RCSA}(\text{sp}) > \text{RCSA}(\text{sp}^2) > \text{RCSA}(\text{sp}^3)$ . It is also modulated by the electronegativity of neighbouring substituents (see Section 2) [50]. This trend was clearly observed for oct-1-yn-3-ol, where only alkyne carbons, C-1 and C-2, exhibit the enantiomeric differentiation [50]. It should be highlighted that when the differentiation process yields sufficiently resolved lines, and the assignment of each enantiomer is known,  $^{13}\text{C}$ - $\{^1\text{H}\}$  spectra of enantiomeric mixtures provide an accurate way to determine *ee*'s. As the magnitude of RCSA is proportional to the strength of  $\mathbf{B}_0$  (see Eq. (5)), a greater number of enantiodiscriminations with very high magnetic fields are expected.

The potential and robustness of the method has been demonstrated on a wide range of chiral analytes [50, 190, 193], either rigid or flexible, weakly polar to polar, as well as with or without stereogenic center, as illustrated by the atropoisomer compounds (such as the binaphthol, and latter the case of 2,2'-dimethyl-1,1'-binaphthyl in 2003) (see Fig. 20b) [50]. In 2010, the first experimental enantiodetections and evaluations of enantiopurity of chiral mixtures dissolved in PBLG, combined with using inverse

gated  $^{13}\text{C}\{-^1\text{H}\}$  1D experiments and a NMR cryogenic probe technology were reported. As expected, a substantial advantage in experimental time and/or sensitivity were obtained [194].

In  $^1\text{H}$  decoupled  $^{13}\text{C}$  spectra, RDCs between  $^{13}\text{C}$  and other heteronuclei, such as  $^{19}\text{F}$  or  $^{31}\text{P}$ , provide an additional means to discriminate the NMR signals of each enantiomer. For instance,  $^{13}\text{C}\text{-}^{19}\text{F}$  total couplings could be extracted successfully from  $^{13}\text{C}\{-^1\text{H}\}$  1D spectra recorded for a series of racemic mixtures of mono or trifluorinated compounds dissolved in PBLG. Two examples are reported in Fig. 21 [50, 195 200].

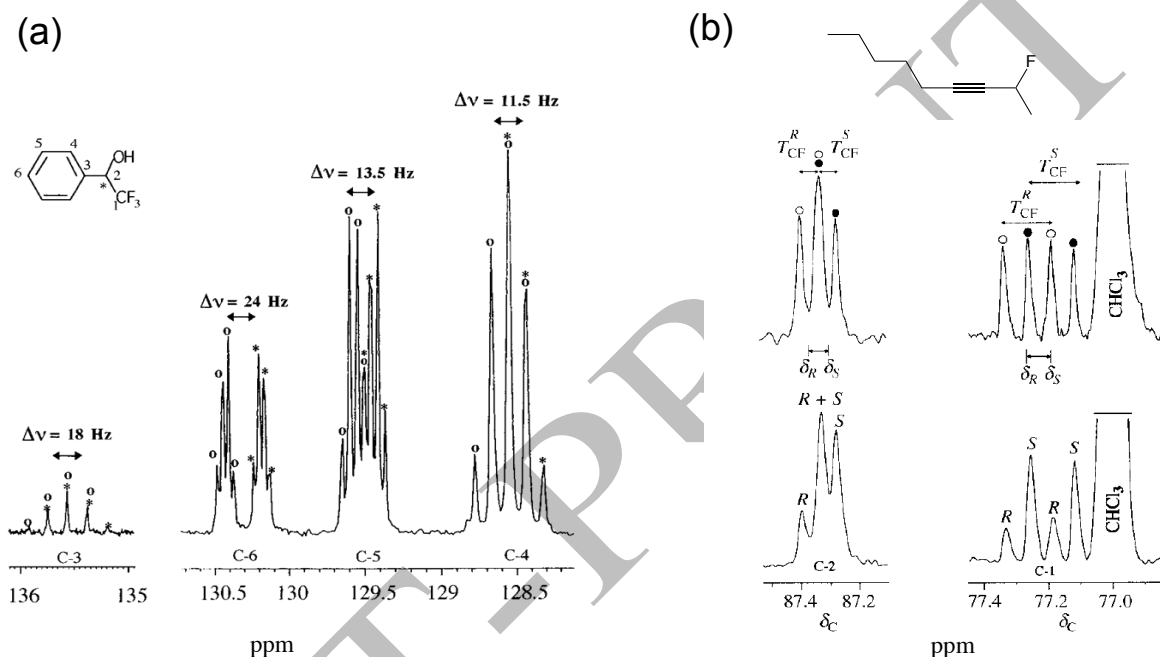


**Fig. 21.** Expansion of a  $^{13}\text{C}\{-^1\text{H}\}$  NMR spectrum of (a)  $(\pm)$ -1-deutero-1-phenyl-2,2,2-trifluoroethanol and (b) the ethynyl carbons of 2-fluoro-3-nonyne in racemic (top) and enantiomerically enriched (bottom) series. Both 1D spectra were recorded at 100.3 MHz for  $^{13}\text{C}$  of the PBLG/ $\text{CHCl}_3$  system. Figure adapted from Refs. [50] and [195], with permission.

Similarly, the presence of a phosphorus atom has, for instance, been exploited to monitor the enantiomeric differentiation process for monophosphine oxides dissolved in a PCBLG-based mesophase [60]. In fact both  $^{13}\text{C}\text{-RCSA}$  and  $^{13}\text{C}\text{-}^{31}\text{P}$  total couplings contribute to the discrimination of the enantiomeric NMR signals in such  $^{13}\text{C}\{-^1\text{H}\}$  spectra (see Fig. 22).

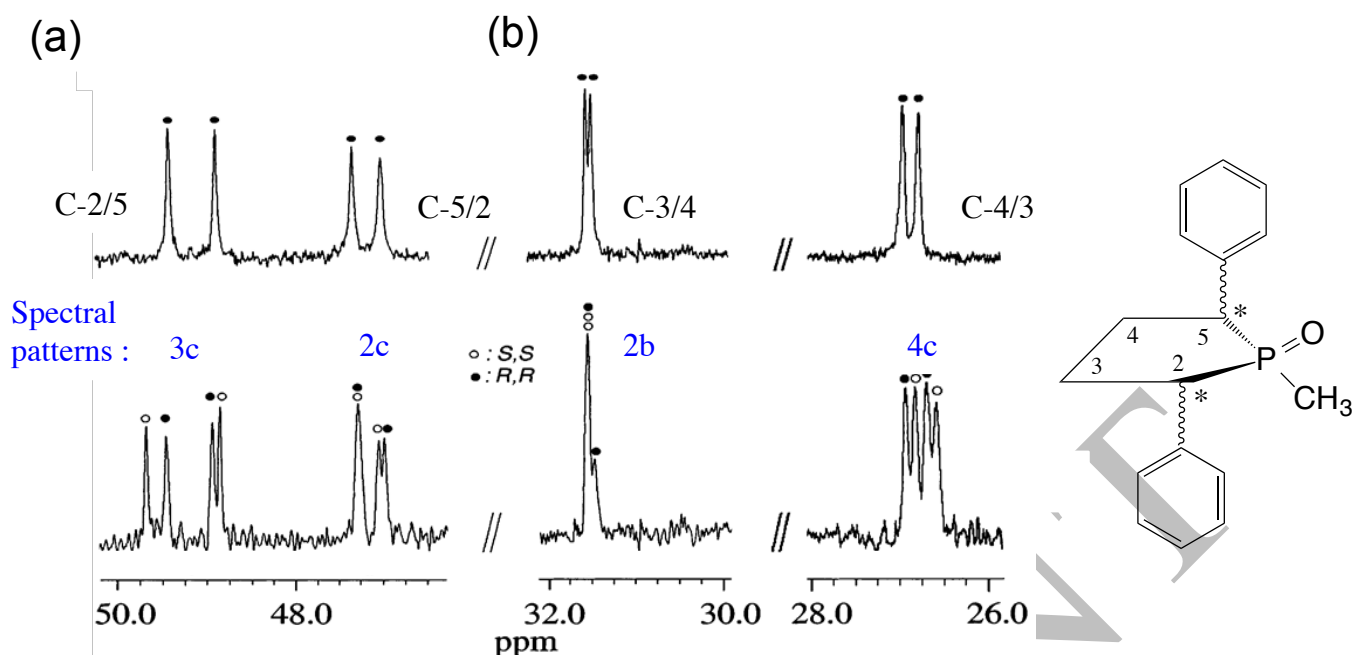


**Fig. 22.** 100.3 MHz  $^{13}\text{C}\{-^1\text{H}\}$  1D NMR signals of the phospholane ring ( $\text{sp}^3$  carbon atoms) of 1-methyl-1-*r*-oxo-2-*cis*-5-*trans*-diphenyl-phospholane recorded in PCBL/CHCl<sub>3</sub> and showing a chiral discrimination on the basis of a difference of  $^{13}\text{C}\text{-}^{31}\text{P}$  total couplings,  $T_{\text{CP}}$ : (top) (-)-enantiomer and (bottom) racemate. For each carbon site, the type of spectral enantiodiscrimination patterns is given (see Fig. 6). Figure adapted from Ref. [60] with permission.

## 5.2 Variants of $^{13}\text{C}$ -detected 2D experiments

### 5.2.1 The $T_{\text{CH}}$ -resolved experiments

In order to simplify the analysis of  $^{13}\text{C}$  spectra in CLCs, different 2D experiments have been designed. The resolution can be increased by: i) spreading correlations throughout 2D spectra, and ii) separating different spin interactions along different spectral dimensions. A straightforward application of this well-known concept of acquiring multi-dimensional data has been the  $^{13}\text{C}$ -detected  $T$ -resolved pulse sequence (also named “ $JD$ -resolved”) (see Fig. 23a). In the resulting correlation 2D spectrum, the  $^{13}\text{C}$  chemical shift dispersion available in the direct dimension ( $F_2$ ) allows for a separation of the  $T_{\text{CH}}$ -resolved multiplets of each enantiomer along the indirect domain ( $F_1$ ) [196]. Formally, the maps obtained are similar to a homonuclear  $J$ -resolved map, with the advantage that they show fewer artefacts due to second-order effects of  $^1\text{H}$  spin systems.

From a practical point of view, this kind of 2D experiment has been used to discriminate spectrally enantiomers of compounds showing antifungal and plant growth regulating activities [197] and also to extract ( $^{13}\text{C}\text{-}^1\text{H}$ )-RDCs for each carbon site of racemates of chiral trisubstituted biaryl compounds (see Fig. 23a) [198].

Another field of application for such resolved ( $^{13}\text{C}\text{-}^1\text{H}$ )-RDCs measurements is their combination with other anisotropic NMR interactions extracted from  $^1\text{H}$  and/or  $^2\text{H}$  analyses (at natural abundance) to model

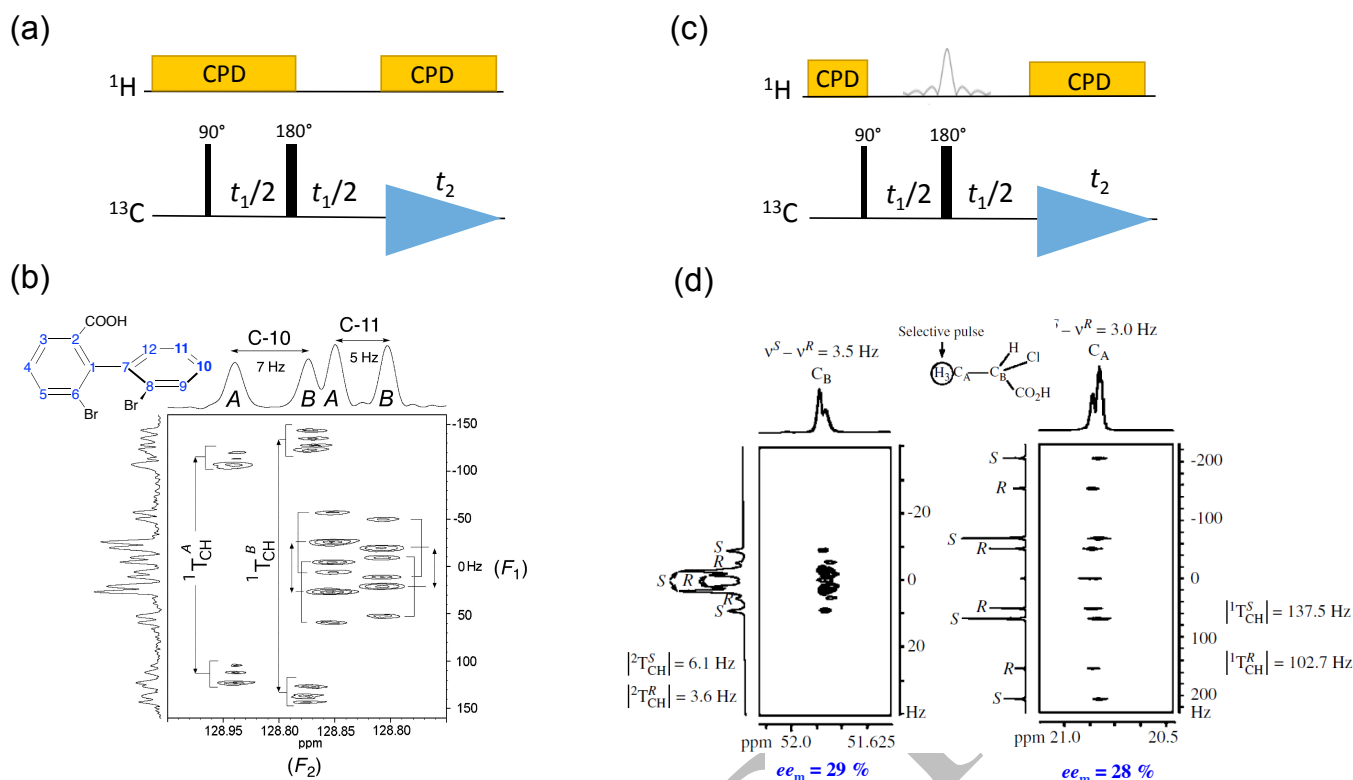


**Fig. 23.** (a and c) Pulse diagrams of the basic  $T$ -resolved and  $(^{13}\text{C}-^1\text{H})$ -HETSERF sequences. (b) Part of a  $T_{\text{CH}}$ -resolved spectrum of  $(\pm)$ -2,2'-dibromobiphenyl-6-carboxylic acid (sites C-10 and C-11), an ortho trisubstituted axially chiral biphenyl. (d) Part of a  $^{13}\text{C}$  HETSERF spectrum of  $(\pm)$ -2-bromopropionic acid with selection of the methyl signal. Both anisotropic 2D spectra (magnitude mode for the  $T_{\text{CH}}$ -resolved) were recorded 100.3 MHz in PBLG systems.  $A/B$  (or  $R/S$ ) stands for the chiral stereodescriptors of each enantiomer. Figure adapted from Refs. [198] and [200], with permission.

the orientational order and the conformational distributions of chiral and flexible molecules dissolved in PBLG mesophases [199].

### 5.2.2. The concept of down-scaled $T_{\text{CH}}$ -resolved sequences

A further variant of the phased  $T_{\text{CH}}$ -resolved pulse sequence can be obtained by desymetrization of the delays during which the proton decoupling is applied during the  $^{13}\text{C}$  echo period in  $t_1$  time domain. This scheme leads to a formal reduction of magnitude of heteronuclear couplings in the  $F_1$  dimension by a controlled scaling factor (for instance, a reduction factor of 4 in the case of the sequence presented in Fig. 24a). As a result, all  $T_{\text{CH}}$  couplings are reduced, importantly including the smaller ones that generally contribute to the linewidths of  $^{13}\text{C}$  peaks, thus allowing a more accurate measurement of  $^1T_{\text{CH}}$  couplings, as shown in Fig. 24b [201].

This type of down-scaled  $T_{ij}$ -resolved sequence was applied to analyze the molecule of dehydroepiandrosterone (**DHEA**) dissolved in a PBLG-based medium.

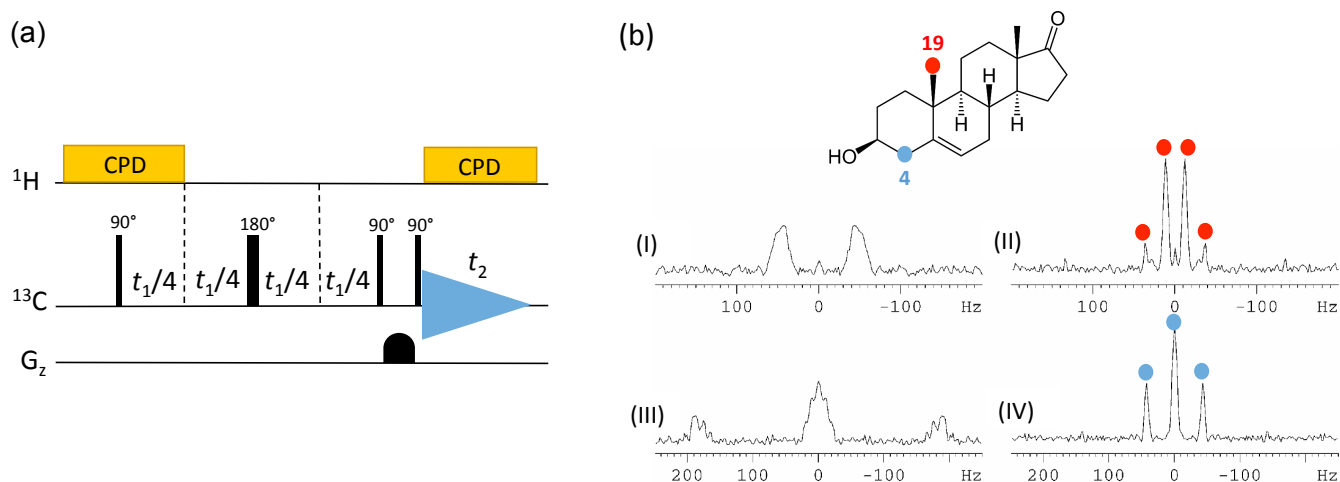


**Fig. 24.** (a) Modified phased  $T_{CH}$ -resolved 2D sequence with a scaling factor of 4 for  $T_{CH}$  ( $T_{CH}/4$ -resolved 2D experiment). A z-filter is used. (b)  $F_1$  columns extracted from the conventional (100.3 MHz)  $T_{CH}$ -resolved experiments (I and III) and the  $T_{CH}/4$  resolved experiment (II and IV) and associated to the methyl site 19 and methylene site 4 of DHEA dissolved in PBLG/ $CD_2Cl_2$ , respectively. Note the narrower linewidth of the peaks (spectra II and IV) leading to a very accurate determination of the  $^1T_{CH}$  value. Figure adapted from Ref. [201] with permission.

### 5.2.3 HETSERF

In 2004, a conceptual improvement of the  $T$ -resolved experiment, named HETSERF, was introduced to extract in a simplified manner the ( $^{13}C$ - $^1H$ )-RDCs. In the HETSERF experiment, a selective  $\pi$  pulse is added on the proton channel in the middle of the indirect evolution delay, which allows for selective evolution of only the heteronuclear couplings involving the proton selected by the refocusing pulse (see Fig. 23b). In the resulting 2D spectrum, a correlation is obtained at the chemical shift of each  $^{13}C$  nucleus coupled to the proton of interest with a splitting along the indirect dimension equal to their total coupling. The simplification of the lineshape in each dimension allows the sub-spectra to be separated, and thus the  $^{13}C$ -RCSA and ( $^{13}C$ - $^1H$ )-RDC differences can be correlated for each enantiomer as illustrated on Fig. 23d [200, 205].

### 5.2.4 HETCOR

The determination of five non-zero order parameters of the Saupe order matrix (see Section 2) for each  $C_1$ -symmetry enantiomer in a mixture requires a coherent set of spectral data with at least six homo- and/or heteronuclear RDCs [49, 190].

When the number of ( $^1H$ - $^1H$ )-RDCs and/or ( $^{13}C$ - $^1H$ )-RDCs is not sufficient, a combination of both types of RDCs is needed for each isomer. This combination can easily be achieved when working with a scalemic mixture ( $0\% < ee < 100\%$ ), due to the observed difference in peak intensities between enantiomers. In contrast for a racemic mixture of enantiomers, this combination is only possible if  $^{13}C$  and  $^1H$  resonances can be spectrally correlated for each isomer, which then allows the full set of anisotropic interactions to be extracted together for each enantiomer. For this purpose, the  $^{13}C$ - $^1H$  heteronuclear correlation 2D experiment (**HETCOR**) with no proton decoupling during acquisition can be successfully

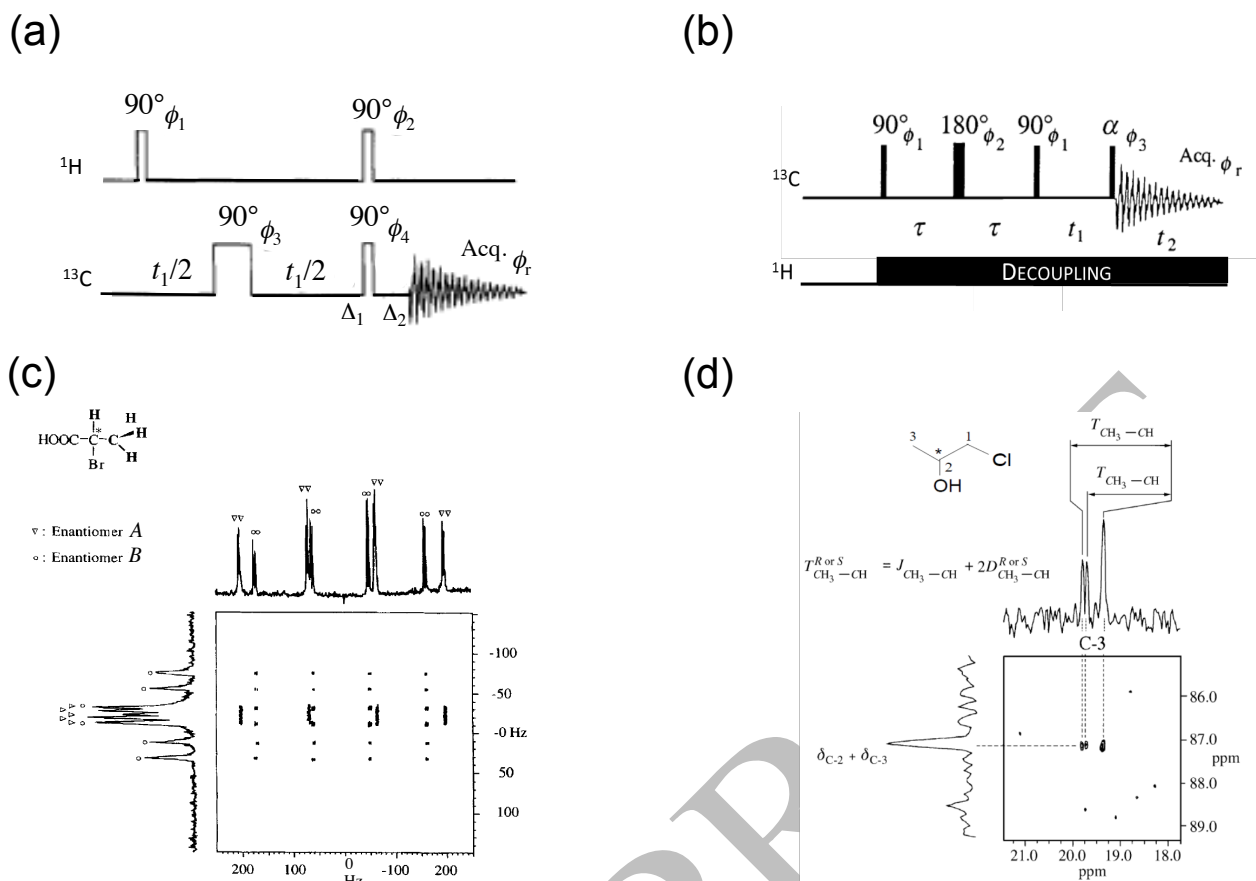


**Fig. 25.** (a and b) Pulse diagrams of the basic  $^{13}\text{C}$ - $^1\text{H}$  HETCOR and  $^{13}\text{C}$ - $^{13}\text{C}$  INADEQUATE 2D sequences, respectively. (c) Zoom on the regions of the methyl group of the  $^1\text{H}$ - $^{13}\text{C}$  HETCOR 2D spectrum of (±)-2-bromopropionic acid. (d) Zoom on the region of the methylene group (C-3 site) of  $^{13}\text{C}$ - $^{13}\text{C}$  INADEQUATE spectrum of (±)-1-chloropropan-2-ol. Both anisotropic 2D spectra (magnitude mode) were recorded at 9.4 T in PBLG systems. Figure adapted from Refs. [35] and [207], 70 with permission.

exploited as was first demonstrated in the case of (±)-2-bromopropionic acid oriented in the PBLG/ $\text{CD}_2\text{Cl}_2$  system (see Fig. 25a,c) [70].

### 5.2.5 INADEQUATE: exploiting the DQ coherences

Another alternative approach to increase the quality of spectral separation for enantiomeric mixtures is to use double quantum (DQ) spectroscopy. In this spirit, the 2D  $^{13}\text{C}$ - $^{13}\text{C}$  INADEQUATE (Incredible Natural Abundance Double QUAntum Transfer Experiment) has proved its potential for the purpose of chiral analysis. Although the abundance  $^{13}\text{C}$ - $^{13}\text{C}$  isotopomers is only 0.01%, it has been shown that the visualization of enantiomers with the help of homonuclear total couplings,  $^1T_{\text{CC}}$ , is possible (see Fig. 25b,d) [202, 203, 204, 205]. In this case, the spectral separation is expected to arise on the one hand from the combination of the classical dispersion yielded in the direct domain by single-quantum chemical shifts and total couplings, and on the other hand from the specific simplification provided in the  $F_1$  dimension by the evolution of DQ coherences at the sum of the chemical shifts of the considered pair of coupled carbons. Compared to other tools involving pairs of atoms, detection of ( $^{13}\text{C}$ - $^{13}\text{C}$ )-DQ for the purpose of

enantiodiscrimination is not trivial for three reasons: i) the natural abundance of isotopomers with two  $^{13}\text{C}$  carbons ( $1.1\% \times 1.1\%$ ) is weak; ii) the  $k_{\text{CC}}$  parameter for two interacting  $^{13}\text{C}$  nuclei is small with respect to that of  $^1\text{H}$ - $^{13}\text{C}$  dipolar couplings ( $\gamma_{\text{C}}\gamma_{\text{C}}/\gamma_{\text{C}}\gamma_{\text{H}} \approx 0.25$ ) (see Eq. (10) and Table 2); iii) the larger internuclear distances between adjacent carbon-13 atoms (1.20 - 1.54 Å versus with 1.09 Å for a  $^{13}\text{C}$ - $^1\text{H}$  bond) significantly reduces the sensitivity of ( $^{13}\text{C}$ - $^{13}\text{C}$ )-RDCs to the DOE compared with that of the ( $^{13}\text{C}$ - $^1\text{H}$ )-RDCs. Although the sensitivity problem can be partly circumvented by the use of a cryogenic probe, INADEQUATE experiments (but also HETCOR or any XH correlations experiments) do not allow the simultaneous optimisation of refocusing delays for two enantiomers, thus possibly limiting their potential for an accurate determination of  $ee$ 's. Applying adiabatic polarization transfer methods should limit this effect and lead to acceptable measurements of  $ee$  [206]. So far such  $T_{\text{CC}}$ -based enantiodifferentiation has successfully been performed on ( $\pm$ )-1-chloropropan-2-ol embedded in the PBLG/ $\text{CHCl}_3$  phase (see Fig. 25d) [35].

### 5.3 Inverse $^{13}\text{C}$ - $^1\text{H}$ correlation 2D experiments

Many 2D correlation experiments involving  $^{13}\text{C}$  nuclei have been designed to improve enantiomeric visualization. A major improvement was obtained by inserting a BIRD module in the middle of the indirect evolution delay of  $^{13}\text{C}$ - $^1\text{H}$  correlation experiments in order to filter out long range heteronuclear couplings, leading to 2D spectra showing only one-bond heteronuclear correlation. Several experiments have been derived from this selection of anisotropic interactions evolving during the indirect evolution period. The resulting spectra show simplified multiplets with splittings corresponding either to the  $^1T_{\text{C-H}}$  total coupling, or the contribution of both  $^1T_{\text{C-H}}$  and  $T_{\text{H-H}}$  couplings. It should be noted here that all these experiments are  $^1\text{H}$ -detected, which means that they offer a significant gain in sensitivity compared to the  $^{13}\text{C}$ -detected sequences described in the previous section. Among these sequences, the  $^1\text{H}$ - $J$ -HSQC-BIRD sequence has been shown to be particularly suitable for chiral analysis since it allows the  $^{13}\text{C}$ - $^1\text{H}$  couplings in a  $\text{CH}_2$  group with diastereotopic protons to be separately measured, as well as the heteronuclear couplings among  $\text{CH}$ ,  $\text{CH}_2$  and  $\text{CH}_3$  groups, and the  $^1\text{H}$ - $^1\text{H}$  geminal couplings among the  $\text{CH}_2$  and  $\text{CH}_3$  groups [188]. An example of  $^1\text{H}$ - $J$ -HSQC-BIRD 2D spectra is presented in Fig. 26 [188]. As reported in 2010 by Nath and Suryaprakash, a notable achievement of this method was the highly-resolved measurement of all  $^2T_{\text{HH}}$  and  $^1T_{\text{CH}}$  total couplings in propylene carbonate dissolved in PBLG/ $\text{CDCl}_3$  [207].

In the field of inverse  $^1\text{H}$  detected techniques, Thiele and coworkers have recently applied a CLIP/CLAP HSQC 2D experiment [208, 209], originally developed by Luy et al., [210] to monitor the influence of the composition of the chiral liquid-crystalline phase on the value of RDCs. It was shown that this 2D experiment yields heteronuclear correlation spectra without phase distortion, which allows the total couplings  $^1T_{\text{CH}}$  to be extracted with high resolution from the indirect domain. Moreover,



Suryaprakash *et al.* have also proposed sequences designed in the spirit of  $^1\text{H}$  MQ-SQ correlation spectroscopy, in which  $^{13}\text{C}$  spin states are used to generate and select a limited number of multiple quantum coherences. After being converted to single quantum, these coherences allow correlation patterns to be simplified, so that heteronuclear  $^{13}\text{C}$ - $^1\text{H}$  as well as homonuclear  $^1\text{H}$ - $^1\text{H}$  couplings can be extracted for each enantiomer. It should be noted that for this class of experiments, selective pulses can be applied to excite a reduced set of protons in order to further simplify the number of signals and thus facilitate their analysis [186, 210, 211, 212].

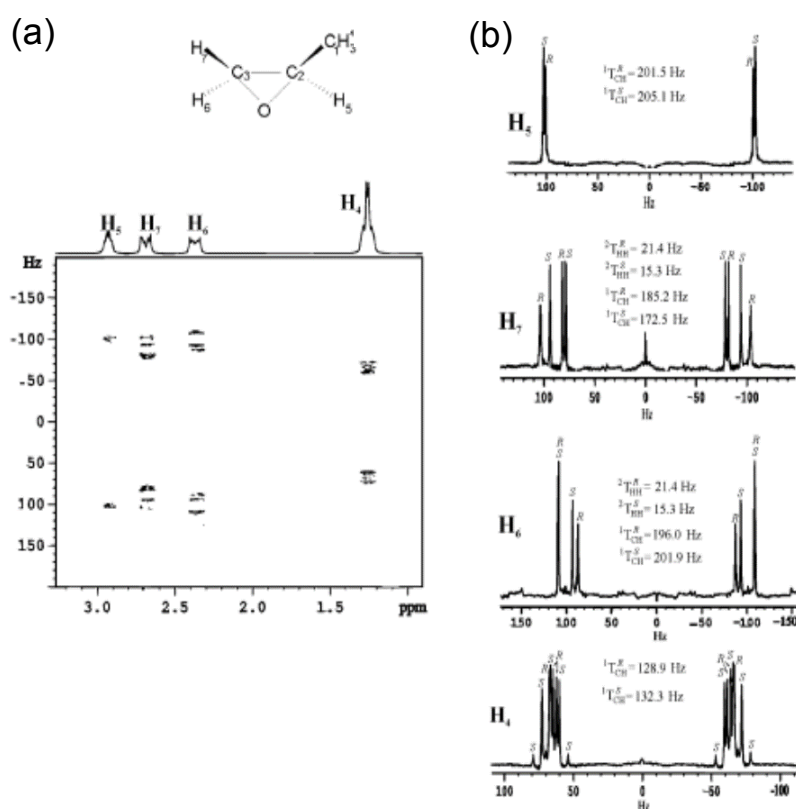


**Fig. 26.** (a)  $^1\text{H}$ -J-HSQC-BIRD 2D spectra of an enantiomeric mixture of ( $\pm$ )-propylene oxide in PBLG/ $\text{CDCl}_3$ . (b) Four projections are calculated, one for each proton site, to extract the different homonuclear and heteronuclear total couplings. Figure adapted from Ref. [188] with permission.

#### 5.4 Examples of applications in asymmetric synthesis

In agreement with the initial analytical aim,  $^{13}\text{C}$ - $\{^1\text{H}\}$  1D NMR in CLCs was rapidly applied to investigate the enantioselectivity of various asymmetric syntheses. Such cases included the double diastereoselection in [2+3] cycloaddition reactions of chiral oxazoline *n*-oxides and their application to the kinetic resolution of a racemic  $\alpha,\beta$ -unsaturated  $\delta$ -lactone [213], the intramolecular hydroamination catalysed by neutral rare-earth catalytic or ate complexes [214, 215], or the aza-Michael additions of *O*-benzylhydroxylamine to *N*-alkenoyloxazolidinones catalysed by samarium iodobinaphtholate [216].

The method has been also used to establish the enantioselectivity of monofluorination reactions of propargylic compounds [219] nor asymmetric reactions leading to chiral monophosphine oxides and boranes [60]. This approach has been also successively applied to investigate new asymmetric reactions leading to enantiopure complexes, such as chiral ( $\eta^6$ -arene) chromium tricarbonyl complexes [217] (see Fig. 27a) or cationic planar chiral ( $\eta^6$ -arene) $\text{Mn}(\text{CO})_3^+$  complexes [218].

More recently, the synthesis of enantiopure atropisomers (ortho, ortho'-dibromobiphenyls bearing an additional substituent in the 6-position) has been experimentally examined (see Fig. 27b) [198]. Finally in 2010, in the course of a methodological study,  $^{13}\text{C}$ - $\{^1\text{H}\}$  1D NMR in CLCs was used to address the dynamic kinetic resolution (DKR) of racemic  $\alpha$ -chloro- $\beta$ -ketoesters and  $\alpha$ -chloro- $\beta$ -ketophosphonates through ruthenium-mediated asymmetric hydrogenation [219].

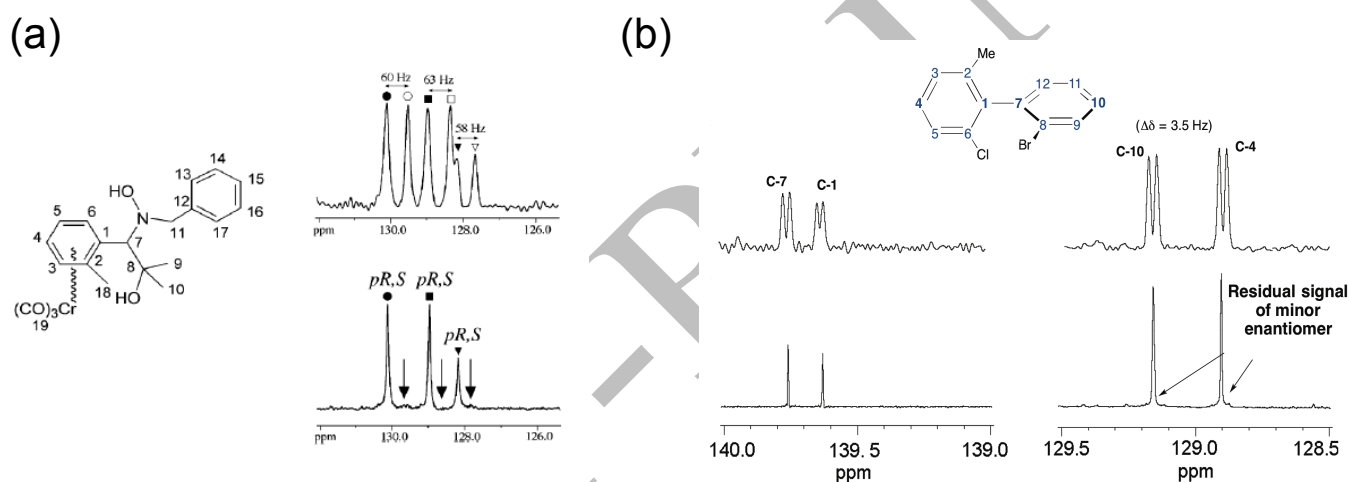


**Fig. 27.** (a) Comparison of  $^{13}\text{C}$ - $\{^1\text{H}\}$  1D signals in racemic (top) and enantiopure series (bottom) of  $^{13}\text{C}$  signals of sites C-13/17, C-14/16 and C-15 of the N-(2-methyl-2-hydroxy-1-((2-methylphenyl)chromium tricarbonyl)propyl)-N-benzyl-hydroxylamine, a chiral ( $\eta^6$ -arene) chromium tricarbonyl complex ( $ee(R) > 95\%$ ) in PBLG. (b)  $^{13}\text{C}$  signals of sites C-1, C-4, C-7 and C-10 of ( $\pm$ )-2,2'-dibromo-6-methyl biphenyl, a tri-ortho-substituted biphenyl ( $ee(R) > 95\%$ ). Spectra are recorded at 100.3 MHz. Figure adapted from Refs. [198] and [217] with permission.

## 6. The power of $^2\text{H}$ NMR spectroscopy

### 6.1. 1D-NMR analyses of deuterated chiral analytes

#### 6.1.1 Illustrative 1D NMR examples of classical chirality

In the field of chiral analysis, the enantiodiscrimination potential of polypeptide mesophases was first explored with deuterium-labelled compounds in 1992 using  $^2\text{H}$ - $\{^1\text{H}\}$  1D NMR. Even if the deuteration step of the analytes is not always straightforward, the use of selectively deuterated chiral compounds benefits from: i) the simplicity of the spectral analysis (see Section 2.3.3) due to the absence of total couplings  $^1\text{H}$ - $^2\text{H}$  because of  $^1\text{H}$  decoupling leading to two QDs observed when discrimination occurs, one for each enantiomer (for a given labelled position), and ii) and the sensitivity of quadrupolar interactions

to a difference of local order parameters,  $S_{C-D}$  (see Eq. (14)). Based on this idea, several series of  $^2\text{H}$  NMR studies carried out on many deuterated materials showed that the method is very general. Thus, an exploratory, systematic study of almost all classes of organic chiral compounds was performed, and enantiomers with a large variety of structures and functional groups, such as alcohol, amines, carboxylic acids, esters, ethers, epoxides, tosylates, chlorides, bromides, amongst others, and even cyclic hydrocarbons could be spectrally discriminated [220, 221, 222, 223, 224]. The method proved also to be efficient whatever the molecular structure: rigid, semi-rigid or flexible, although there were significant variations in the magnitude of enantiodiscriminations ( $|\Delta\Delta\nu_Q|$ ), which generally decrease for increasing distance of deuterated site to the stereogenic center in flexible compounds [220]. Three typical examples of  $^2\text{H}$ - $\{^1\text{H}\}$  1D spectra of monodeuterated flexible and rigid enantiomers, and one example of perdeuterated (semi-rigid) molecules are reported in Fig. 28a,b,c and Fig. 28d respectively; all these cases employed organic solutions of PBLG ( $\text{CH}_2\text{Cl}_2$  or  $\text{CHCl}_3$ ). Among flexible chiral molecules difficult to enantiodiscriminate by NMR or by other methods, enantiomers of chiral deuterofluoroalkanes with generic formula  $\text{C}_m\text{H}_{2m+1}\text{C}^*\text{D}(\text{F})\text{C}_n\text{H}_{2n+1}$  were also discriminated both in PBLG/ $\text{CHCl}_3$  or PCBL/DMF chiral systems (see Fig. 28b) [222].

In this example, the spectral enantiodifferences, though smaller, are observed both in a difference of  $^2\text{H}$ -RQCs as well as in the total  $^2\text{H}$ - $^{19}\text{F}$  spin-spin couplings, leading *in fine* to a doubling of QDs, namely eight resonances visible on the spectra (see Section 2.4.2).

The analysis of these four selected examples illustrates the versatility of the method in terms of magnitude of enantiodiscriminations and some specificities of COAs. First the enantiodifferentiation mechanisms in CLCs does not require a specific functional group in the analyte (OH, NH, ...), and second the choice of the deuteration position (on the stereogenic center or not) is not necessarily crucial [220]. Thus using polydeuterated compounds (and then NAD NMR), it has been shown that the relationship of the deuterium position to the asymmetric centre is important but not an absolute determinant, and thus a good discrimination between the  $^2\text{H}$ - $\{^1\text{H}\}$  spectra of enantiomers does not necessitate that the deuterons are bound to the chiral centre (see Fig. 28d). Furthermore, it was demonstrated that, for a homologous series of chiral aliphatic alcohols of comparable molecular order, enantiodiscrimination increases with molecular dissymmetry [221].

In fact, by the examination of various series of molecules, it has been pointed out several times that molecular recognition mechanisms play an important role in chiral discrimination phenomena by polypeptides [198, 225, 226]. Indeed, due to the high sensitivity of  $^2\text{H}$ -RQCs to differences of molecular ordering,  $^2\text{H}$  NMR is a powerful tool for studying several molecular-properties, such as molecular shape, symmetry, and conformational motions [226].

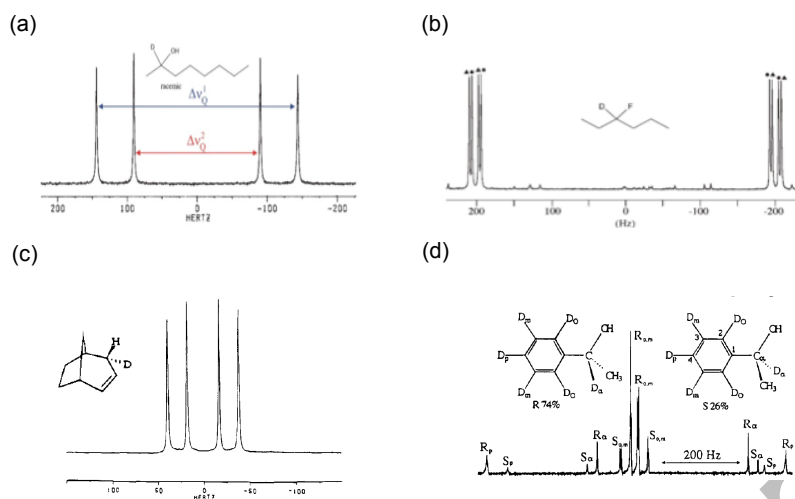


**Fig. 28.** 38.4 MHz  $^2\text{H}\{-^1\text{H}\}$  1D NMR spectra of: (a)  $(\pm)$ -2-deuterio-octan-2-ol in PBLG/ $\text{CH}_2\text{Cl}_2$ , (b)  $(\pm)$ -3-deuterio-3-fluorohexane in PBLG/ $\text{CHCl}_3$ , (c)  $(\pm)$ -3-deuterio-bicyclo[3.2.1]oct-2-ene, and (d)  $(R)$ -1-perdeuterio-phenyl-1-deutero-ethanol (48% ee). Extra splittings seen in (b) are due to  $^2\text{H}\text{-}^{19}\text{F}$  total couplings. Peaks marked with  $\blacktriangle$  belong to one enantiomer and those marked with  $\bullet$  are due to the other enantiomer. Figure adapted from Refs. [220], [221] and [222], with permission.

### 6.1.2. Exploring “atypical” chiralities

The concept of chirality covers many fascinating aspects of enantiomorphisms in molecules with or without a stereogenic center (atropisomerism, axial chirality, planar chirality, helical chirality, chirality by isotopic (H/D) substitution, etc) [1]. Therefore, chiral discrimination in CLC made of PBLG is not limited to one kind of chirality, such as chiral compounds bearing an asymmetric atomic centre (carbon, sulfur, phosphorus, etc). Thus, enantioseparations have also been observed by  $^2\text{H}\{-^1\text{H}\}$  NMR for labelled chiral compounds exhibiting axial chirality with  $C_1$  symmetry (see Fig. 29a) [227] or cone-shaped chiral compounds with  $C_3$  symmetry (see Fig. 29b) [228]. The spectral discrimination of enantiomers ( $\Lambda$  and  $\Delta$ ) of deuterated metallic complexes that are chiral by virtue of helical chirality has been also reported (see Fig. 29c) [229, 230, 231].

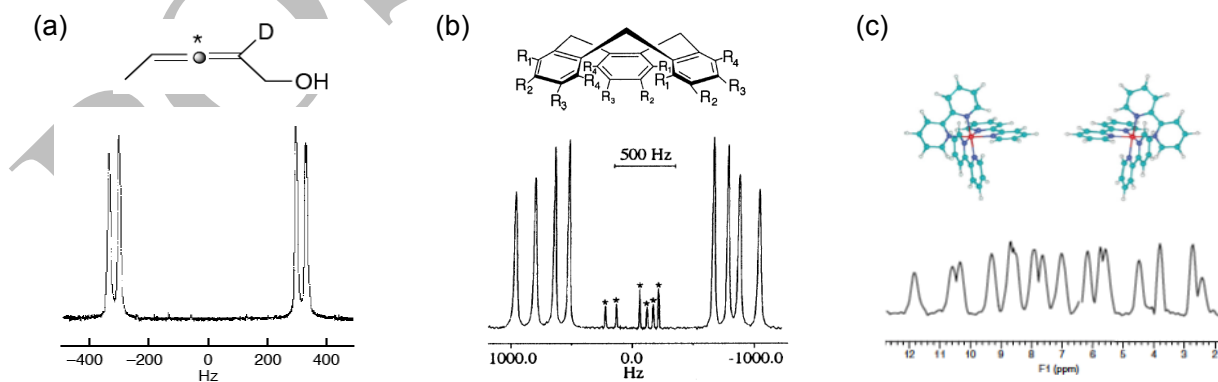


**Fig. 29.** Three examples of atypical chirality:  $^2\text{H}\{-^1\text{H}\}$  spectra of (a)  $(R/S)$ -2-deutero-2,3-pentadiene-1-ol (61.4 MHz), (b)  $(M/P)$ -hexadeuterated cyclotrimeratrylene (on two diastereotopic sites of methylene groups) (61.4 MHz for  $^2\text{H}$ ), and (c)  $(\Lambda/\Delta)$ -perdeuterated tris(diimine)ruthenium(II) complexes (46.0 MHz for  $^2\text{H}$ ). For (c), the 1D spectrum corresponds to the projection of a  $^2\text{H}$  Q-COSY 2D experiment. Spectra were recorded for PBLG/ $\text{CH}_2\text{Cl}_2$ , PBLG/DMF and PBLG/dioxane, respectively. Figure adapted from Refs. [227], [228] and [231], with permission.

### 6.1.3. Derivatizing chiral molecules with achiral deuterated derivative agents

While it is often possible to introduce a deuterium atom into a target molecule during a multi-step synthesis [232], the need to deuterate a compound may be complex, and can therefore be considered mainly as a severe limitation on the use of  $^2\text{H}$ -NMR as a routine tool. As we will see below, NAD NMR allows this synthetic step to be overcome. However, in order to open the technique to organic chemists, achiral deuterated derivatizing agents (ADDAs) that are either commercially available or easy to prepare, have been proposed for use with certain classes of molecules in order to determine enantiomeric excesses [233, 234, 235]. The chiral discrimination is thus realised by a CLC and observed through the deuterium nuclei of the resulting adducts. Interestingly, this approach excludes any kinetic resolution in the course of the derivatization, and therefore the reaction does not need to be complete.

The first successful illustration of this methodology was achieved in the 1990's, by esterification of aminoacids with perdeuteromethanol ( $\text{CD}_3\text{OD}$ ), and subsequent protection of the amino group using benzophenone imine giving (diphenylmethylene)amino esters [232]. The  $^2\text{H}$  NMR spectra obtained with these derivatives in PBLG-methylene chloride liquid crystal allowed the enantiodiscrimination of all the compounds under study. The presence of the minor isomer was detected in the spectrum even at the 1% level. In a similar manner, acetyl- $\text{d}_3$  chloride was proposed as an ADDA for amines through their amide derivatives [234]. The method proved to be efficient with primary amines but was of limited efficiency for amides derived from secondary amines. For the latter, the presence of amide rotamers leads to linewidth broadening and requires a study at different temperatures in order to find the optimum conditions to obtain exploitable spectra. Even then, the linewidths observed prevent the accurate measurement of  $ee$ 's.

The use of ADDAs bearing magnetically different  $^2\text{H}$  atoms provides the possibility to measure  $ee$ 's on different sites in a molecule. This feature prevents the fortuitous situation where the NMR signals of enantiomers are not well resolved for a given deuterium. Thus, the use of the perdeuterobenzoyl fragment ( $\text{C}_6\text{D}_5\text{-CO-}$ ), added by reaction with perdeuterobenzoyl chloride, is a powerful way to determine  $ee$ 's of alcohols, primary amines and aminoacids derivatives (see Fig. 30a) [233]. Similarly, perdeuterobenzyl alcohol ( $\text{C}_6\text{D}_5\text{-CD}_2\text{-OH}$ ) is another very efficient ADDA with which to perform enantiomeric analysis of carboxylic acids through their ester derivatives (see Fig. 30b) [235].

The enantiomeric analysis of isotopically labelled chiral amines by  $^2\text{H}\text{-}\{^1\text{H}\}$  NMR in PBLG when a weakly polar, chlorinated solvent ( $\text{CH}_2\text{Cl}_2$ ,  $\text{CHCl}_3$ ) is used is somehow problematic. The spectra obtained in such CLC exhibit anomalously wide lines, with linewidths up to 150-200 Hz, and chiral discrimination has seldom been observed. In some cases, unexplained extra lines were even seen [220, 224]. This behaviour cannot be attributed to any exchange phenomenon, as when heating or cooling samples, no

coalescence process is detected. Provided that DMF is used as the polar organic co-solvent, these problems vanish. In these conditions, perdeuterobenzylchlorid ( $C_6D_5-CD_2-Cl$ ) appears as an excellent ADDA for enantiomeric analysis of chiral primary and also secondary amines [224].

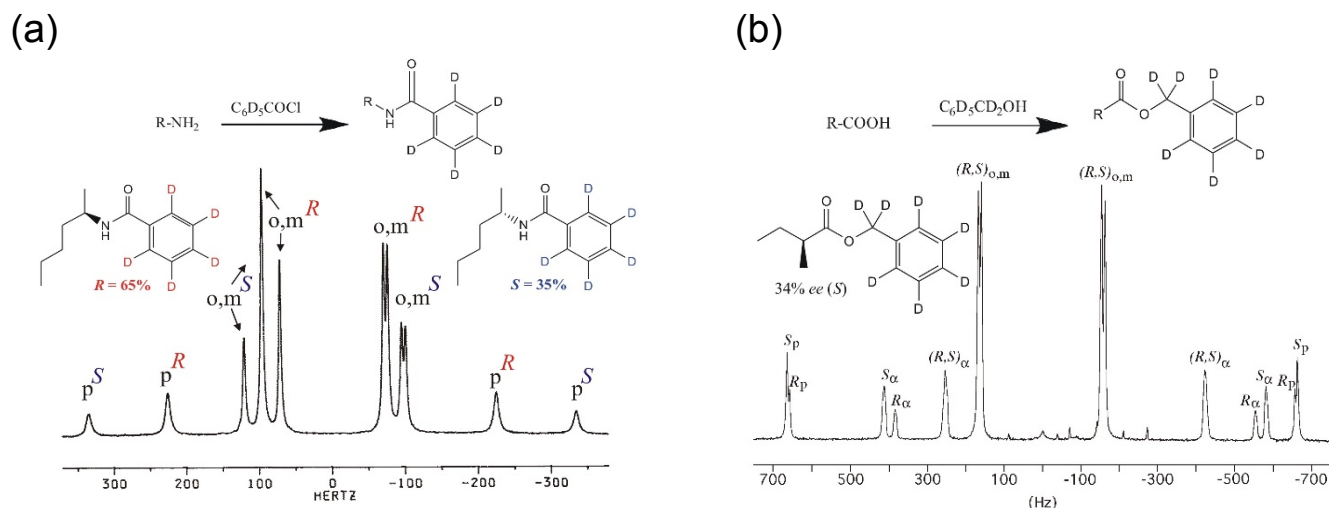


**Fig. 30.** 38.4 MHz  $^2H\{-^1H\}$  NMR spectra of (a) (*R*)-*N*-(1-methyl-butyl)-perdeuterobenzamide (30% *ee*) in PBLG/ $CH_2Cl_2$  and (b) (*S*)-2-methylbutyric acid perdeuterobenzyl ester (34% *ee*) in PBLG/DMF. Enantiomeric discrimination is mainly observed for the deuterons in *para* and  $\alpha$  positions. Figure adapted from Refs. [235] and [236], with permission.

#### 6.1.4. Discrimination by exchangeable deuterons

The use of an ADDA simplifies greatly the synthetic step of deuteration. Nevertheless, in the case of molecules bearing labile protons, the isotopic labelling can be achieved by a simple exchange using  $D_2O$  or MeOD. On this basis, Philipps and Sharman, replaced hydrogen by deuterium on the NH group of amides and amines of drug candidates [237]. They observed their enantiomers by  $^2H\{-^1H\}$  NMR in PBLG CLC at room temperature (RT), under which conditions the labile deuterium is in a slow exchange regime. However, with the spectra obtained for deuterated amines, the large linewidths relative to peak separation does not allow a precise measurement of *ee*.

In the case of alcohols, the labile deuterons in -OD are generally in the fast exchange regime. As they jump rapidly from one enantiomer to the other, the chiral discrimination vanishes at around room temperature. It is, however, possible to slow down the exchange rate on the NMR time scale, and thus visualize the enantiodiscrimination by decreasing the temperature. Thus satisfactory enantio-separations are obtained at 260 K with PBLG system (see Fig. 31, where the spectrum of racemic  $[O\text{-}^2H]$ -1-phenylethanol is presented at different temperatures) [238].

The residual deuterium signal of water, although systematically observed, does not interfere that much with that of the analyte signals. The linewidth, typically 50-90 Hz, is far larger than that observed for CD substrates. Nevertheless, such enantioseparations allow a robust measurement of *ee* whether by direct integration of the signals or by using lineshape deconvolution.

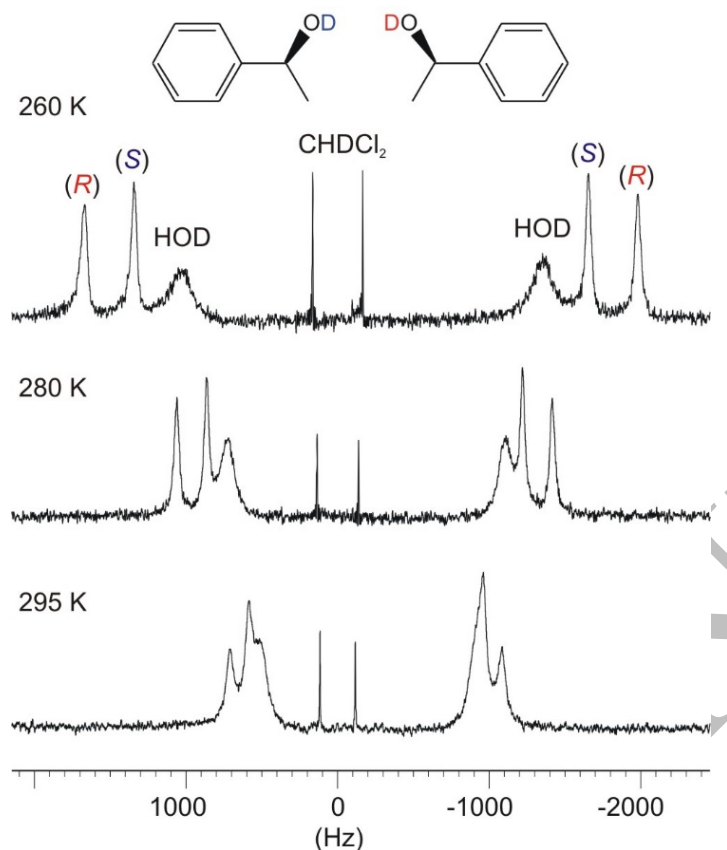


**Fig. 31.** 61.4 MHz  $^2\text{H}\{-^1\text{H}\}$  NMR spectra of  $(\pm)$ -[O- $^2\text{H}$ ]-1-phenylethanol in PBLG/ $\text{CH}_2\text{Cl}_2$  recorded at different temperatures. Assignments of  $R$  and  $S$  stereodescriptors were deduced from the spectrum of  $(S)$ -[O, $^2\text{H}_2$ ]-1-phenylethanol (49% ee). Fig. adapted from Ref. [238] with permission.

In practice, the H-D exchange procedures can be further simplified. Indeed it can be directly made in the NMR tube containing the anisotropic phase and the analyte by adding MeOD (or  $\text{D}_2\text{O}$ ). The liquid-crystalline mixture is then centrifuged again in order to achieve the H/D exchange process. This avoids product loss and allows working with very small quantities of substrate, without the need for any kind of preliminary preparation step. Nevertheless, one should keep in mind that as methanol or water may induce the precipitation of PBLG, only small amounts (a few microliters) should be added to the CLC with an appropriate syringe). Provided this precaution is taken,  $^2\text{H}\{-^1\text{H}\}$  NMR spectra obtained in this manner are very similar to those where the H/D exchange is made prior to the anisotropic NMR sample preparation, but additionally to the HOD signals, the quadrupolar doublet of MeOD is also visible when the latter is used. [238].

### 6.1.5. Isotopic chirality and spectral discrimination

Deuterium labelling is widely used by chemists and biochemists in order to elucidate the mechanism of chemical or enzymatic reactions or to assess their stereospecificity. In the case where the labelling comprises the introduction of a deuterium at a pro- $R$  or a pro- $S$  position, leading to a -CHD- pattern, the stereochemical analysis of such compounds becomes problematic, in particular when the analyte possesses no asymmetric centre close to the CHD group position. The problem becomes even more

challenging if the pro-*R* and the pro-*S* deuterons are incorporated in enantiotopic positions (of prochiral molecules) [1].

Here again  $^2\text{H}\{-^1\text{H}\}$  NMR in PBLG liquid crystals has proved to provide an analytical solution to this issue. Indeed, in 1994 it was demonstrated that this tool allows the discrimination of enantiomers of compounds whose chirality is due to an isotopic substitution of a proton (or a group) by a deuterium (or a group) such as  $\text{R-C}^*\text{HD-R}'$  or  $\text{CH}_3\text{-C}^*\text{R(R}')\text{-CD}_3$  (see Fig. 32a,b) [128]. For such compounds, the technique is very general and the spectral separations generally observed are comparable to those measured for analytes of “classical” chirality, as illustrated on the example of the Fig. 32a ( $|\Delta\Delta\nu_{\text{Q}}| = 100$  Hz). It should be noted that isotopic enantiomers have also been spectrally discriminated on the basis of differences of  $^{13}\text{C}\text{-RCSAs}$  using  $^{13}\text{C}\{-^1\text{H}\}$  NMR [239].

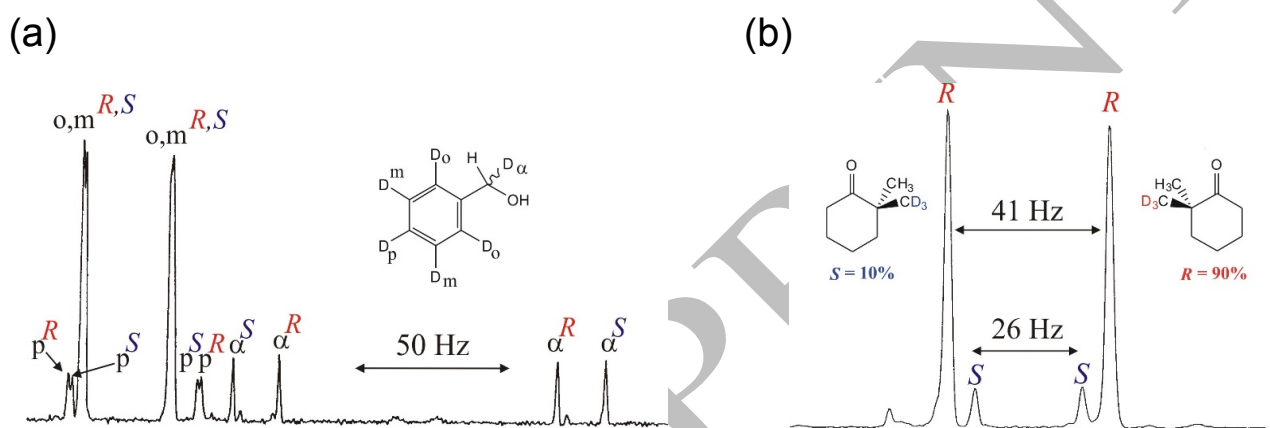


**Fig. 32.**  $^2\text{H}\{-^1\text{H}\}$  NMR spectra of (a)  $(\pm)\text{-C}_6\text{D}_5\text{-CHD-OH}$  in PBLG (the R and S signals were deduced from the spectrum of a (*R*)-enriched sample) and (b) (*R*)-2-(methyl- $\text{d}_3$ )-2-methylcyclohexanone (80% ee) dissolved in PBLG/ $\text{CH}_2\text{Cl}_2$ . Figure adapted from Ref. [128] with permission.

Undoubtedly, the small difference in the geometry of  $^1\text{H}$  and  $^2\text{H}$  nuclei cannot explain the noticeable difference in the orientation leading to the discrimination of isotopic (H/D) enantiomers. In fact, it was shown that the origin of the discrimination of isotopic enantiomers in CLCs is possible because enantiotopic deuterium nuclei (in a parent prochiral molecule interacting with CLCs) intrinsically lead to distinct  $^2\text{H}\text{-QD}$  signals [128]. This is because the order parameters of the two C-D bonds in a di-deuterated methylene group are different. Thus, for perdeuterated-1-octanol ( $\text{CD}_3\text{-(CD}_2)_7\text{-OD}$ ), 14 QDs were observed for the methylene groups, *i.e.* one doublet for each enantiotopic deuterium [128].

In Section 9, we will examine the analytical potential originating from enantiotopic discrimination in CLCs, and the possible applications when using NAD 2D-NMR spectroscopy [35].

## 6.2 Development of $^2\text{H}$ multidimensional NMR: homonuclear QUOSY

### 6.2.1. Homonuclear 2D/3D tools for analysing complex $^2\text{H}$ or natural abundance deuterium spectra

Although various procedures for regioselective  $^2\text{H}$  isotopic enrichment of molecules are described in



the literature (see above), this step is neither always possible nor easy to do (under simple conditions), and in general can be considered as too time-consuming to be attractive. Besides, the enantiodiscrimination can only be observed for the isotopically enriched site(s) of a chiral solute, thus decreasing the probability of differentiating the relevant spectral signatures.

As the perdeuteration of analytes under study is generally not feasible, then it becomes preferable to detect the  $^2\text{H}$  nuclei at the natural abundance level. A proof of concept for the first experimental detections of NAD 1D- and 2D-NMR spectra in PBLG was first reported in 1998 [240, 241].

Interestingly from a NMR point of view, while disregarding all contributions of  $^2\text{H}$ - $^2\text{H}$  couplings, the complexity of  $^2\text{H}$ - $\{^1\text{H}\}$  1D/2D spectra of enriched (perdeuterated) and isotopically normal solutes are identical. In the first case, the  $^2\text{H}$  spectrum originates from a single polydeuterated molecule (100%), while for the second, a sum of monodeuterated isotopomers is detected.

Even for rather structurally-simple chiral molecules (whether fully isotopically enriched or not), the  $^2\text{H}$ - $\{^1\text{H}\}$  spectra in weakly orienting CLC can become overcrowded and complex mainly due to the small range of  $^2\text{H}$ -RQCs (generally below 500-600 Hz) compared to the range of  $\delta^{\text{aniso}}(^2\text{H})$ . Spectral analysis is therefore not trivial, in particular when the spectral discrimination occurs on all  $^2\text{H}$  sites of a molecule ( $2n$   $^2\text{H}$ -QDs in a CLC are expected for  $n$  inequivalent sites), several QDs are interlaced or several peaks overlap. This complexity of analyzing congested  $^2\text{H}$  NMR spectra obviously grows with the number of inequivalent  $^2\text{H}$  (diastereo-isotopomers, enantio-isotopomers) present in the molecule [62].

To facilitate the analysis of overcrowded anisotropic  $^2\text{H}$ - $\{^1\text{H}\}$  1D spectra (in NAD or poly- and perdeuterated molecules), several types of homonuclear  $^2\text{H}$ - $\{^1\text{H}\}$  2D/3D-NMR experiments referred to under the generic name “QUadrupole Ordered SpectroscopY” (QUOSY) have been designed [62, 242, 243, 244].

Fig. 33 shows a schematic representation of homonuclear 2D QUOSY experiments. Their common aim is to correlate the two components of each doublet on maps, though the data in the  $F_1$  and  $F_2$  dimensions (and their post-acquisition processing) differs for the various types of experiments. For instance, the  $^2\text{H}$  signal in **Q-COSY** 2D experiments evolves under the effect of  $\delta^{\text{aniso}}(^2\text{H})$ 's and  $\Delta\nu_{\text{Q}}(^2\text{H})$ 's in both  $t_1$  and  $t_2$  dimensions, while  $\delta(^2\text{H})$ 's and  $\Delta\nu_{\text{Q}}(^2\text{H})$ 's are refocused in the  $t_1$  dimension in the **Q-resolved** and  **$\delta$ -resolved** 2D experiments, respectively. Depending on the pulse sequence, tilting as well as symmetrization processing of spectral data may be used after the double Fourier transformation (FT). While symmetrization can be cautiously used to eliminate some artefacts ( $t_1$  lines), the tilt procedure applied on **Q-COSY** and **Q-resolved** 2D spectra removes the  $^2\text{H}$ -QDs in  $F_2$  dimension, and the  $F_2$  projection formally resembles the isotropic NAD NMR spectra [62].

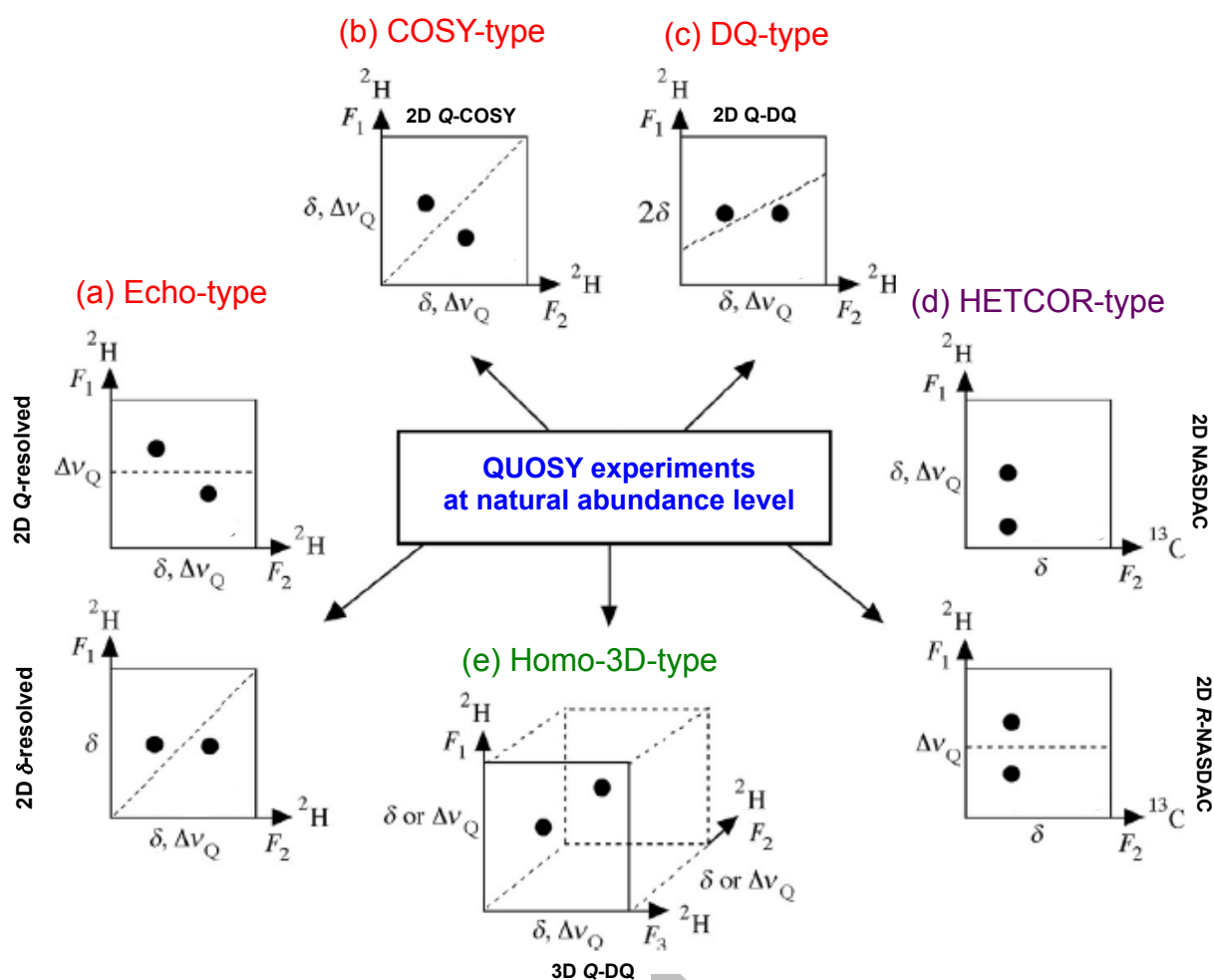


**Fig. 33.** Homo- and hetero-nuclear 2D/3D QUOSY experiments: (a) echo-type schemes, such as 2D Q-resolved sequences and  $\delta$ -resolved, which refocus  $\delta(^2\text{H})$ , and  $\Delta v_Q(^2\text{H})$ , respectively, during the  $t_1$  period, (b) COSY-type scheme, such as 2D Q-COSY, (c) Double quantum-type scheme, also denoted 2D Q-DQ, (d) heteronuclear HETCOR-type sequence, such as 2D NASDAC or 2D Refocussed-NASDAC, and (e) homonuclear 3D-type sequence, such as 3D Q-DQ. Figure adapted from Ref. [55] with permission.

The QUOSY concept was then interestingly extended to the case of homonuclear 3D experiments [243, 244] as well as to the case of heteronuclear approaches involving the detection of  $^{13}\text{C}$  signals of molecules such as those shown in Fig. 33e [245, 246, 247]. Description and details of all NMR sequences can be found in the associated references (see also below), while the tailored formalism involving Cartesian spin-operators that allows these experiments to be easily understood was described in Ref. [242].

Although QUOSY experiments are important tools for simplifying anisotropic overcrowded  $^2\text{H}$  1D spectra of isotopically normal or enriched solutes recorded in polypeptide CLCs and then measuring  $^2\text{H}$ -RQC, the determination of the sign of RQCs is impossible. In 2015, an extension of the E.COSY principle (the “Q.E.COSY” 2D experiment) applied to spin systems consisting of a spin-1 ( $^2\text{H}$ ) coupled to a spin- $\frac{1}{2}$  ( $^1\text{H}$  or  $^{13}\text{C}$ ) nucleus (using a stretched Poly(dimethylsiloxane) (PDMS) gel instead of PBLG), was introduced to determine of the sign of  $^2\text{H}$ -RQC relative to the  $^2\text{H}$ - $^1\text{H}$  /  $^2\text{H}$ - $^{13}\text{C}$  heteronuclear coupling between the same two spins [248].

### 6.2.2. The z-filter for obtaining pure-phase spectra

The generation of phase-twisted signals by the basic sequences (*Q*-COSY, *Q*-resolved,  $\delta$ -resolved or *Q*-DQ) makes it necessary to display the 2D map in magnitude mode. This drawback can be eliminated by inserting a modified z-gradient filter before signal acquisition (see Fig. 34a), leading to new sequences renamed ***Q*-COSY-Fz** and ***Q*-resolved-Fz** sequences (see Figs. 34b,c) [249]. Note here that the TPPI, States or States-TPPI methods can be used to perform quadrature detection in  $F_1$  dimension.

The choice of pulse angle ( $\alpha$ ) in the z-gradient filter is not trivial and requires an analysis of amplitude variations of autocorrelation and diagonal peaks of QUOSY to optimize the sensitivity of the experiments while removing the undesired  $^2\text{H}$  signals. Thus for the *Q*-COSY-Fz pulse sequence, the analysis of the evolution of the density operator for a spin  $I = 1$  indicates that the optimal  $\alpha$  angle is equal to the magic angle value of  $54.7^\circ$  well-known from SS-NMR (see Fig. 34d) [249].

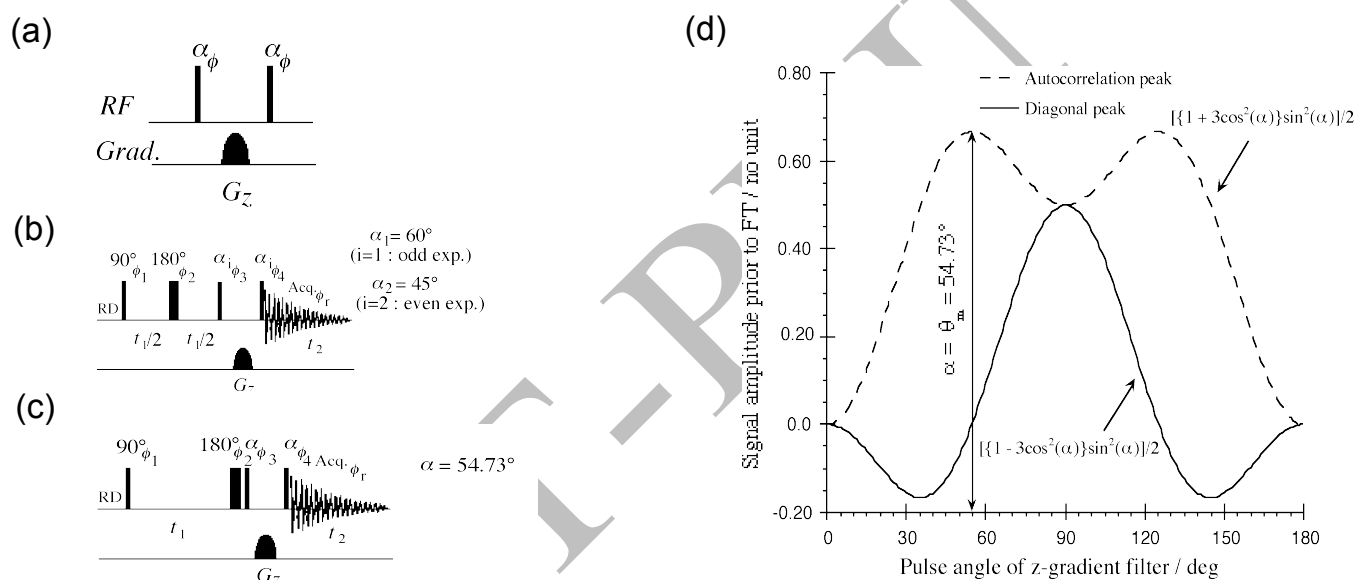


**Fig. 34.** (a) Principle of the Z-filter block. The gradient pulse,  $G_z$ , suppresses all the coherences except the spin polarization,  $I_z$ , and quadrupolar order,  $(3I_z^2 - I^2)$ , terms. (b-c) Diagram of the *Q*-COSY Fz and *Q*-resolved Fz 2D pulse sequences, respectively. (d) Variation of signal amplitude of autocorrelation and diagonal peaks vs. the pulse angles of the z-gradient filter for the 2D *Q*-COSY Fz sequence. At  $\alpha = \theta_m = 54.73^\circ$ , the autocorrelation signal is maximum while the diagonal signal is eliminated. Figure adapted from Ref. [249] with permission.

In terms of spectral resolution, these modified sequences give phased spectra in pure absorption in the  $F_1/F_2$  dimensions, thus substantially reducing the linewidths of components of DQs. These tools are therefore well-suited for analyzing congested NAD spectra of large chiral molecules, even if they are less sensitive than the corresponding basic *Q*-COSY and *Q*-resolved 2D sequences (by factors of -33% and -25%, respectively). However, this loss in sensitivity can be more than compensated by using  $^2\text{H}$  cryogenic probes [189].

### 6.2.3. Methods involving $^2\text{H}$ double quantum transitions

Due to the spin value of  $I = 1$  for the deuterium nucleus, and unlike  $\frac{1}{2}$ -spin nuclei, it is possible to excite the double quantum (DQ) coherence of any (isolated) single  $^2\text{H}$  nucleus in order to correlate the two components of a QD. This approach can be advantageous because these DQ coherences precess at twice the rate of a SQ coherence, thus potentially increasing the resolution of spectra in the indirect dimension of 2D spectra. In practice, the  $^2\text{H}$  Q-DQ 2D experiment uses the same pulse sequence as the well-known  $^{13}\text{C}$ - $^{13}\text{C}$  INADEQUATE experiment (see Section 4.3.2). Here,  $^2\text{H}$ -DQ coherence is classically excited by two  $90^\circ$  pulses) (see Fig. 35a), and hence the  $^2\text{H}$  signal evolves at twice  $\delta(^2\text{H})$  during  $t_1$  [62].

An example of a Q-DQ 2D NMR spectrum of a perdeuterated molecule is presented in Fig. 35c.

The optimization of SQ to DQ transfer for all  $^2\text{H}$  sites is basically impossible because it depends on the magnitude of each QD. To overcome this problem, the fixed defocusing delay  $\tau$  in the sequence can be converted into a variable time period,  $t_1$ , in order to maximize the build-up of DQC's during the  $t_2$  time in Fig. 35c [243, 244].

After a four-step phase cycle and disregarding all phase terms, the expression of the signal in the three time domains,  $S(t_1, t_2, t_3)$ , for a single deuteron is given by:

$$S(t_1, t_2, t_3) \propto \sin[\omega_Q t_1] \exp\left[-\frac{t_1}{T_2^{SQ}}\right] \times \sin[2\omega_D t_2] \exp\left[-\frac{t_2}{T_2^{DQ}}\right] \times \sin[\omega_Q t_3] \exp\left[-\frac{t_3}{T_2}\right] \quad (24)$$

where  $\omega_D = 2\pi\nu_D$  and  $\omega_Q = \pi\Delta\nu_Q$  denote the deuterium offset frequency and quadrupolar splittings, respectively.  $T_2^{SQ}$  and  $T_2^{DQ}$  are the transverse relaxation times of respectively single- and double-quantum coherences.

Thus, in contrast with the Q-DQ 2D version, the peak intensities of Q-DQ 3D spectrum do not depend anymore on the magnitude of  $^2\text{H}$ -RQCs. Consequently Q-DQ 3D experiments can be applied, in principle, for quantitative measurement of  $ee$ 's. Interestingly after a triple FT, pure absorption resonances are obtained. Fig. 35d shows the Q-DQ 3D spectrum of *n*-butanol- $d_{10}$ , where the  $F_2$  dimension corresponds to the evolution of the DQ coherence of each inequivalent  $^2\text{H}$  nucleus during  $t_2$ . The 3D cube and associated 2D projections allow for a simplified analysis of the QD network. In 2008, the first NAD Q-DQ 3D experiment of a chiral solute (( $\pm$ )-hept-3-yn-2-ol) in PBLG/ $\text{CHCl}_3$  was reported [244]. The usefulness of 3D-NMR approaches is to split spectral information between three dimensions, in order to obtain information that is not accessible using separate 2D experiments, and/or to improve the resolving power of the 2D experiments.

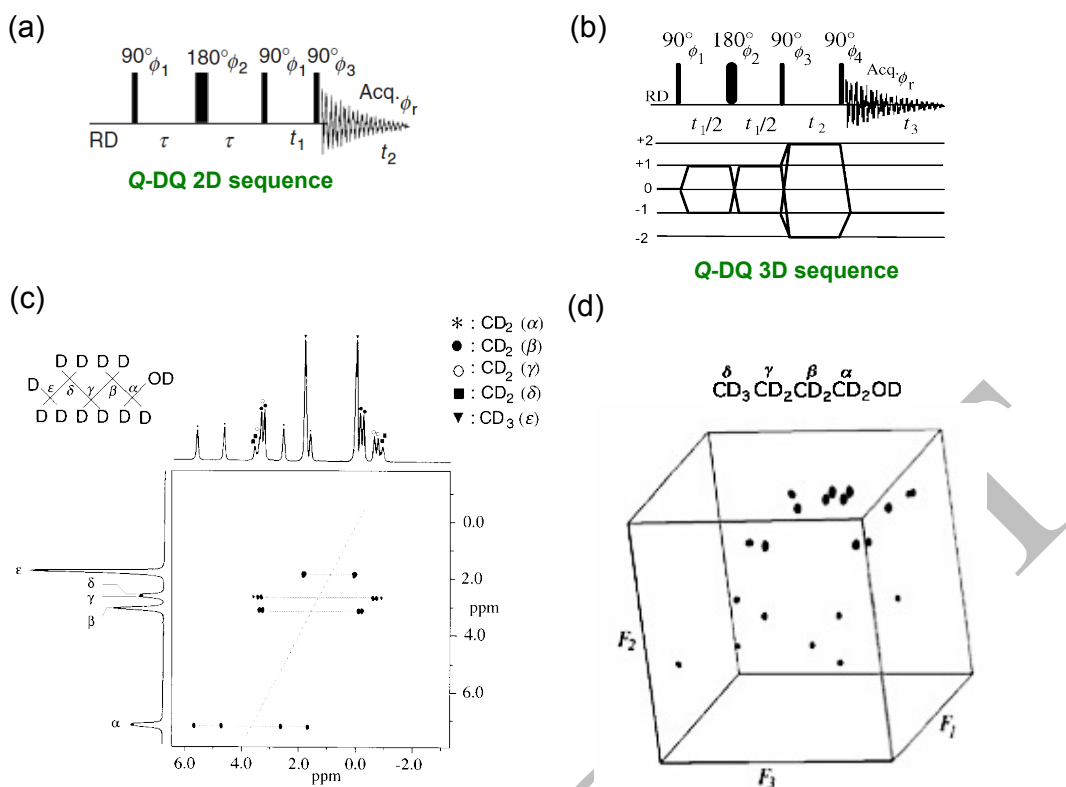


**Fig. 35.** (a and b) Q-DQ 2D and Q-DQ 3D pulse sequences. Phase cycles are reported in the original papers. (c) 61.4 MHz  $^2\text{H}$  Q-DQ spectrum (magnitude mode) of *n*-pentanol- $\text{d}_{12}$ . (d) 92.1 MHz NAD- $\{^1\text{H}\}$  Q-DQ 3D spectrum of *n*-butanol- $\text{d}_{10}$  (absorption-mode). Diagonal and correlation peaks have opposite phases. Both prochiral solutes are dissolved in PBLG/ $\text{CHCl}_3$  phase. Figure adapted from Refs. [250] and [62 243], with permission.

#### 6.2.4. Non-uniform sampling and special processing

The acquisition of multidimensional NMR spectra of solutes in isotropic samples can be accelerated by various strategies. Among them, we can include for instance: i) the enhancement of the population difference across the excited transition using high magnetic field, DNP [250], low and ultralow temperatures [251]; or polarization transfer methods [9, 10, 15]; ii) the use of more sensitive detection schemes through the indirect detection of abundant nuclei ( $^1\text{H}$ ,  $^{19}\text{F}$ ); iii) the minimization of the recycling delay ( $T_R$ ), by using band-selective  $^1\text{H}$  or  $^{13}\text{C}$  excitation and/or optimized flip angles (well-known as Ernst angle), such as the SOFAST and BEST approaches [252] (see below); iv) and the reduction of the number of increments in the indirect evolution periods by a non-uniform sampling (NUS) [253]

This latter combined with the reconstruction methods provides alternative to classical schemes based on a uniform sampling (US) of the free induction decay (FID) followed by a conventional FT [253, 254, 255].

Considering the practical interest in reducing the experimental time ( $T_{\text{exp}}$ ) of anisotropic QUOSY 2D experiments (see below), data acquisition using NUS in  $t_1$  combined with an adapted reconstruction such as the covariance (Cov) method or compressed sensing (CS) processing have been explored. Thus the gain in acquisition time of anisotropic NAD QUOSY-type experiments was investigated while the effect

on spectral resolution and sensitivity was examined [256, 257, 258].

The choice of the data reconstruction method depends on the type of QUOSY experiment used, *i.e.* whether the 2D spectral map is symmetrical or not. Thus, the Cov method has been efficiently used for the reconstruction of NUS  $Q$ -COSY (Fz) experiments [256], where spectral information ( $\delta$  and  $\Delta\nu_Q$ ) are identical in the  $F_1$  and  $F_2$  spectral dimensions. In contrast, CS processing is more general and is suitable for a symmetrical spectrum as well as for an asymmetrical one such as with  $Q$ -resolved (Fz) experiments where the spectral information content differs between the  $F_1$  and  $F_2$  dimensions due to refocusing of the quadrupolar interaction during  $t_1$  [257, 266].

The effects of time reduction on sensitivity and resolution when using NUS-Cov with  $Q$ -COSY Fz, and NUS-CS with  $Q$ -resolved Fz experiments are illustrated in Figs. 36a,b, respectively. In short, the analysis of these results has shown that: i) the combination of NUS-Cov allows spectral resolution to be enhanced and measurement time to be reduced by a factor of 4 with respect to US-FT and by a factor of 2 with respect to US-Cov techniques [256]; ii) for the NUS-CS schedule, it was shown that the highest spectral fidelity is obtained for  $T_S \approx 0.5-0.6 \times T_2^*$  in the case of exponentially decaying NUS [257], and this sampling scheme enhances the sensitivity and resolution of anisotropic NAD 2D-NMR experiments compared to US-FT classical combination [258].

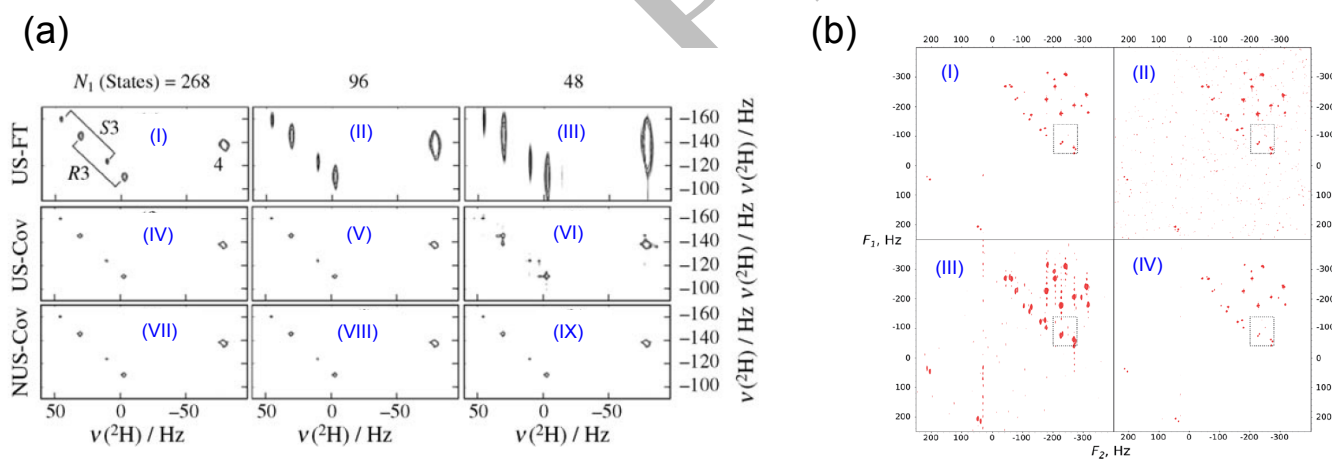


**Fig. 36.** (a) Same selected region of the 61.4 MHz NAD  $Q$ -COSY Fz 2D spectra of ethyloxirane ( $ee(R) = 50\%$ ) in PBLG solvent obtained by different sampling and processing methods: (I-III) US-FT, (IV-VI) and (VII-IX) US-Cov and NUS-Cov with  $N_1$  varying from 256 to 64 and  $NS = 72$ , for each case. (b) Four full 61.4 MHz NAD  $Q$ -resolved Fz 2D spectra of  $\alpha$ -pinene ( $ee(S,S) = 30\%$ ) in PBLG/ $CHCl_3$  acquired with different sampling schedules and reconstruction methods: (I) FT-US ( $N_1 = 256$ ,  $NS = 64$ ), (II) FT-US FID ( $N_1 = 256$ ,  $NS = 16$ ), (III) FT of US FID ( $N_1 = 64$ ,  $NS = 64$ ), (IV) NUS-CS ( $N_1 = 64$ ,  $NS = 64$ ). Figure adapted from Refs. [256] and [257], with permission.

### 6.2.5. Anisotropic deuterium ultrafast (ADUF) NMR: Recording sub-second $^2H$ 2D experiments

In 2013, the possibility of following chiral enzymatic transformations by  $^2H$ -NMR in DNA-based CLCs was demonstrated, allowing various information about the chemical process to be extracted (see Section 6.3.4). The main drawback of this strategy is the experimental time needed to record spectral data for

suitably monitoring the time-dependent variations of all compounds in the mixture, in particular for extremely fast and/or multiple (cascade) chemical transformations, for which rapid identification and reliable quantification of  $^2\text{H}$  signals of chiral (or not) products (reactants, (un)stable intermediates, products, etc) require 2D-NMR experiments with sub-minute time resolution or less. Although NUS can reduce the experiment times of anisotropic NAD (**ANAD**) 2D-NMR experiments (see above), the gain in time is not enough to reach sub-second durations. A modern alternative is to apply the ultrafast (**UF**) 2D NMR concept, which is capable of yielding homo- or hetero-nuclear 2D correlations within a single scan when sensitivity allows it [259, 260]. In 2012, the first measurement of ( $^{13}\text{C}$ - $^1\text{H}$ )-RDCs of chiral molecules in PBLG phase from an ultrafast HSQC 2D NMR experiment (recorded as little as 60 sec) was presented [261]. Application of this approach to anisotropic  $^2\text{H}$  NMR was explored successfully three years later, in 2015 [262].

The variant of UF experiments in liquids involving  $^2\text{H}$  nuclei was named anisotropic deuterium ultra fast (**ADUF**) NMR. A proof of concept was demonstrated by recording an ultrafast  $^2\text{H}$ - $\{^1\text{H}\}$   $\delta$ -resolved constant-time pulse 2D NMR spectrum of a perdeuterated prochiral molecule (*n*-pentanol- $\text{d}_{12}$ ) dissolved in PBLG using the UF NMR pulse sequence displayed in Fig. 37a within a duration of one second [262].

The ADUF 2D pulse sequence shown follows the basic scheme of homonuclear 2D UF experiments, where the usual time encoding is replaced by a spatial encoding, formed by two chirp pulses applied together with a pair of opposite gradients [263]. This spatial encoding block is followed by a conventional mixing period and a detection block based on echo planar spectroscopic imaging (**EPSI**) [264].

Although the  $^2\text{H}$  hard-pulse scheme ( $90_x^\circ$  pulse followed by a  $180_x^\circ$  pulse) is identical to the conventional *Q*-COSY sequence leading to magnitude-mode spectra [62], this UF scheme is a constant-time experiment, leading to the refocusing of all coupling patterns ( $^2\text{H}$ - $^2\text{H}$  dipolar and  $^2\text{H}$  quadrupolar coupling) in the  $F_2$  dimension (see Fig. 37b). Consequently the associated  $^2\text{H}$ - $\{^1\text{H}\}$  UF 2D map is formally identical to that obtained for the conventional  $^2\text{H}$   $\delta$ -resolved experiments [242], except that the spectral content of  $F_1$  and  $F_2$  are inverted compared to conventional 2D spectra. Interestingly, the  $F_2$  dimension is therefore a “pure  $\delta(^2\text{H})^{\text{aniso}}$  shift” dimension, which limits the spectral information to  $\delta(^2\text{H})^{\text{aniso}}$  only. While the original ADUF experiments were recorded using deuterated molecules, we may already anticipate the recording of the first ADUF 2D spectra at natural abundance is likely in the near future.

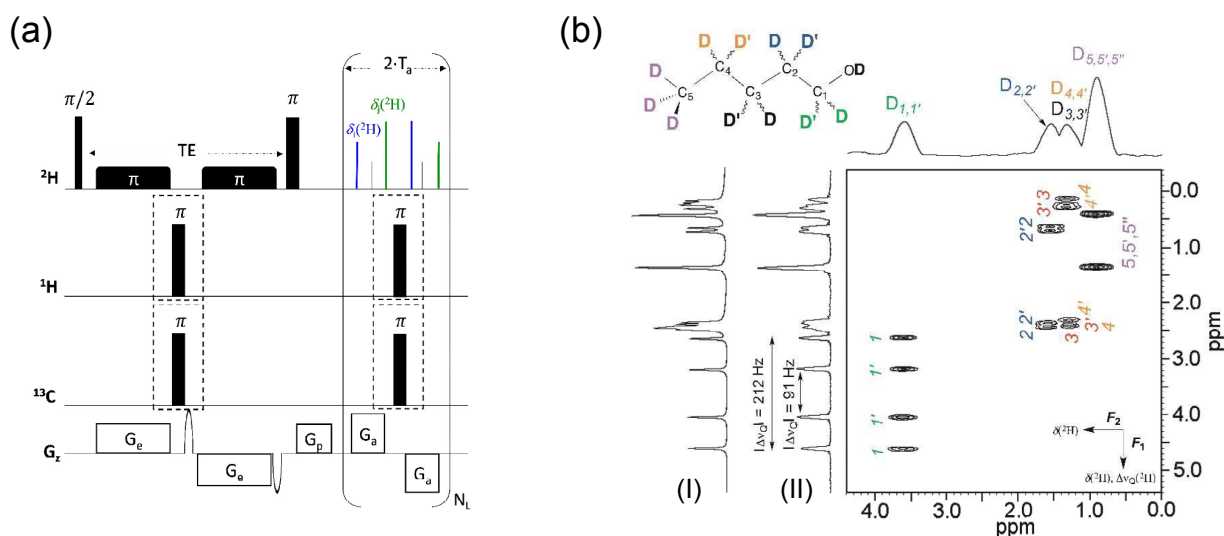


**Fig. 37.** (a) Pulse scheme of the  $^2\text{H}\{-^1\text{H}\}$  ultrafast  $\delta$ -resolved constant-time pulse NMR sequence. The blocks for  $^1\text{H}$  decoupling during the spatial encoding and acquisition periods are shown in dashed boxes.  $G_e$  and  $G_a$  correspond to the gradients applied during the same periods, respectively. (b) 107.5 MHz Single-scan ADUF- $\{^1\text{H}\}$  2D spectra (magnitude mode) of *n*-pentanol- $\text{d}_{12}$  in PBLG/ $\text{CHCl}_3$  recorded in ca. 400 ms. Vertical spectra (I) and (II) correspond to the real 1D spectra and the projections of columns of the map, respectively. Figure adapted from Ref. [262] with permission.

### 6.3. Analytical applications involving isotopically enriched molecules

#### 6.3.1. Investigation of intramolecular dynamic processes

The analysis of conformational dynamic processes is of great interest for understanding molecular internal motions and accessing experimentally exchange or interconversion rate constants, which themselves depend on the magnitude of the barrier to interconversion,  $\Delta H^\ddagger$ , and the sample temperature,  $T$ . For such investigations,  $^2\text{H}\{-^1\text{H}\}$  NMR studies with molecules dissolved in CLCs possess three advantages: i) simple high-resolution spectra dominated by the  $^2\text{H}$  quadrupolar interaction are obtained; ii) the coalescence phenomenon can be clearly identified; iii) spectral separations between exchanging  $^2\text{H}$  anisotropic signals can be much larger than those observed in isotropic  $^2\text{H}$  or  $^{13}\text{C}$  NMR, thus allowing a much wider dynamic process range to be studied. When the oriented medium is chiral, then it becomes possible to study various conformational dynamic phenomena (as intramolecular interconversion or exchange processes) involving enantiomeric molecular forms or enantiotopic elements in prochiral molecules [265, 266, 267, 268]. These exchange processes are invisible in achiral media. The dependence of the exchange/interconversion rate constant,  $k$ , on temperature is described by Eyring's equation as [265, 266]:

$$k = \frac{RT}{N_A h} \exp\left(-\frac{\Delta G^\ddagger}{RT}\right) \text{ with } \Delta G^\ddagger = \Delta H^\ddagger - T\Delta S^\ddagger. \quad (25)$$

where  $R = 8.32 \text{ J}\cdot\text{K}^{-1}\cdot\text{mol}^{-1}$ ,  $N_A = 6.02 \times 10^{23} \text{ mol}^{-1}$  and  $h = 6.62 \times 10^{-34} \text{ J}\cdot\text{s}$ , and  $T$  is expressed in K. Thus, from data measured in simulated NMR spectra and the analysis of the Eyring plot, namely the natural logarithm of  $kN_A h/RT$  against  $1/T$  above and below the coalescence temperature [265, 266], the activation



parameters  $\Delta H^\ddagger$ ,  $\Delta S^\ddagger$ , and subsequently  $\Delta G^\ddagger(T)$ , can be extracted; the slope and the y-intercept of plot are equal to the ratio  $(-\Delta H^\ddagger/R)$  and  $(\Delta S^\ddagger/R)$ , respectively. Interestingly, the rate constant,  $k$ , and the free energy of activation,  $\Delta G^\ddagger$ , at the coalescence temperature,  $T_c$ , (denoted hereafter  $\Delta G^\ddagger(T_c)$ ) can easily be deduced from the measurement of the half-difference of quadrupolar splittings,  $|\Delta\nu_Q| = |\Delta\nu_Q^A/2 - \Delta\nu_Q^B/2|$ , in the  $^2\text{H}$  spectrum below  $T_c$  [267]. Indeed, at this particular temperature, assuming identical time constant ( $T_2^*$ ) for the FID decay of both exchanging deuterons, we can write:

$$k = \pi \times \left| \frac{\Delta\nu_Q^A}{2} - \frac{\Delta\nu_Q^B}{2} \right| \quad (26)$$

and

$$\Delta G^\ddagger(T_c) = RT_c \times \ln \left( \frac{RT_c}{N_A h} \times \frac{2\sqrt{2}}{|\Delta\nu_Q^A - \Delta\nu_Q^B|} \right) \quad (27)$$

In practice, the anisotropic  $^2\text{H}\{-^1\text{H}\}$  / NAD- $\{^1\text{H}\}$  spectra measured at  $T_c$  can be very different depending on the signs of  $\Delta\nu_Q$  for deuterons  $A$  and  $B$  as well as the magnitude of  $|\Delta\nu_Q^A - \Delta\nu_Q^B|$  compared to  $\Delta\nu_Q^A$  and  $\Delta\nu_Q^B$  [267].

As typical illustrative case, Fig. 38 shows the case of  $(\pm)$ -1-bromo-2-methyl-3-deuterio-5-(1'-naphthyl)benzene, a chiral atropoisomer orthosubstituted biaryl investigated by  $^2\text{H}\{-^1\text{H}\}$  1D NMR in PBLG/ $\text{CHCl}_3$  as a function of temperature. In this example of a weakly sterically crowded compound, the coalescence effect is reached at  $T = 250$  K, thus corresponding to a value of  $k$  equal to  $3.2 \times 10^2 \text{ s}^{-1}$ .

The activation parameters of Eq. (25) derived from the Eyring plot analysis (not shown) were found to be equal to  $\Delta H^\ddagger = 44.7 \pm 0.5 \text{ kJ.mol}^{-1}$ ,  $\Delta S^\ddagger = -18 \pm 2 \text{ J.mol}^{-1}.\text{K}^{-1}$  and  $\Delta G^\ddagger(T_c) = 49.0 \pm 0.5 \text{ kJ.mol}^{-1}$ . As the bulkiness of substituents mainly determines the height of barrier to the rotation about the  $\text{sp}^2\text{-sp}^2$  bond between enantiomeric atropoisomers, the activation barrier can be correlated with the bulkiness of substituents in this molecular series.

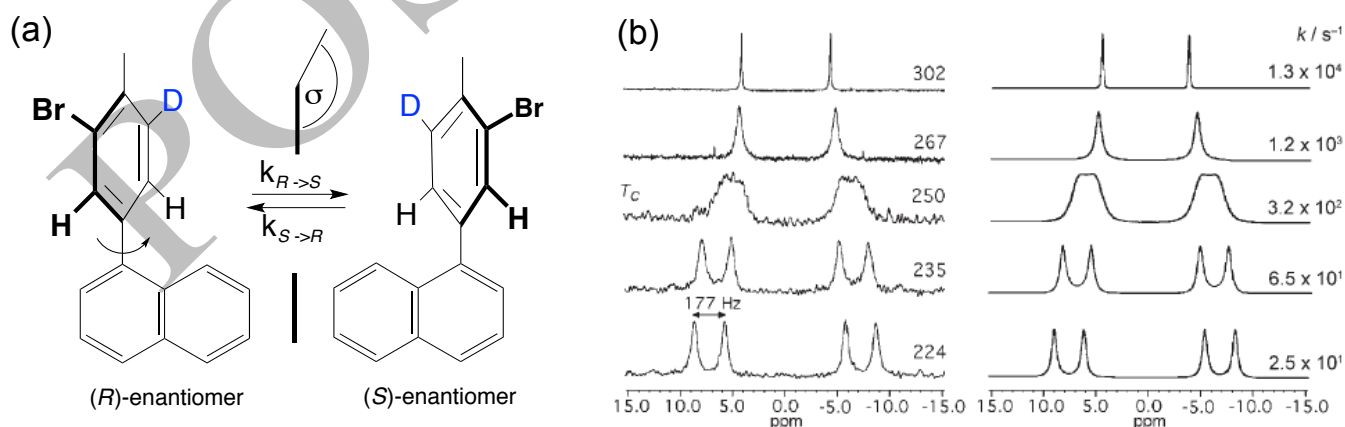


**Fig. 38.** (a) Enantiomeric conformers associated with the  $(\pm)$ -1-bromo-2-methyl-3-deuterio-5-(1'-naphthyl)benzene. (b) Associated experimental (left) and simulated (right) 61.4 MHz  $^2\text{H}\{-^1\text{H}\}$  1D-NMR spectra in PBLG versus five temperatures. Figure adapted from Ref. [267] with permission.

The same approach has been used to investigate the case of prochiral (D/D) and chiral (H/D) diaryl derivatives due to the isotopic substitution of hydrogen by deuterium in the same molecular family, the 1-(2',6'-dideutero-4'-methylphenyl)naphthalene and the 1-(2'-deutero-4'-methylphenyl)naphthalene, respectively (see Fig. 38a) [267, 268]. For the former, it has been pointed out that at sufficiently high temperature (267 K), it behaves as an achiral molecule on average and exhibits homotopic pairs of C-D directions (free rotation), while below  $T_c$ , the molecule adopts an averaged  $C_s$  symmetry with enantiotopic C-D directions [268]. At very low temperature, the rotation around the  $sp^2$ - $sp^2$  bond will be slow on the NMR time scale and the spectral separation of two enantiomers should be possible, since the C-D directions become diastereotopic. However, this third case was not observed experimentally since the oriented sample freezes below 200 K. From the analysis of spectral data, it has been concluded that the activation parameters calculated for chiral or prochiral molecules were identical, thus confirming that both types of solutes behave similarly from a conformational dynamic viewpoint.

Among other studies of dynamic conformational enantio-processes by  $^2\text{H}$  NMR in CLC, we can mention the case of *cis*-decalin (CDC) which exists as a pair of chiral invertomers at low temperature (see Sections 7.1.2 and 9.1), as well as the case of an 18-membered hexathiametacyclophanes, dodecamethoxyhexathiametacyclophane- $d_4$  (HTMC), which exhibits a two-step racemization as function of temperature [41, 269, 270], associated with the following changes in the molecular symmetry  $C_2 \rightarrow C_{2v}$  (at 170-210 K) and  $C_{2v} \rightarrow D_{2h}$  (at 290-320 K). Due to the temperature ranges of both processes, only the second process (that is compatible with the mesophase properties) could be experimentally monitored and characterized by  $^2\text{H}$  NMR in polypeptide CLCs.

### 6.3.2. Enantiopurity in asymmetric synthesis involving deuterated materials

Using deuterium labelled compounds,  $^2\text{H}\{-^1\text{H}\}$  NMR in CLCs allows enantiomeric purity determination but also mechanistic studies. It should be pointed out that for monodeuterated substrates, it is necessary to prepare racemic compounds in order to check that enatio-separation is achieved. Fig. 39 summarizes the structure of all molecules discussed in this section.

In a multistep asymmetric synthesis, it is necessary to assess the enantiomeric purity of each intermediate compound. If deuterium is introduced in an early step of the synthesis, such chiral analysis can be realised using deuterium NMR in CLCs. Fadel *et al.* used this strategy for the asymmetric synthesis of sesquiterpene precursors [271]. The enantiomeric purities of intermediates **1**, **2**, **3**, and **4**, were established by deuterium NMR in PBLG-methylene chloride. In the case of cyclopentanones **6** and **7**, the presence of minor diastereoisomers did not interfere with *ee* measurements. Notably, no spectral separation was observed between enantiomers of **5**, possibly due to the comparable van der Waals volumes for  $\text{CH}_2=\text{C}(\text{D})$ - and  $\text{O}=\text{C}(\text{H})$ - groups.

Spectral discrimination using deuterium NMR in CLCs is not specific to enantiomers of organic compounds. It is also applicable to chiral organometallic compounds as exemplified by the cationic planar chiral manganese complex derivative **8** [218].

In the case of compounds bearing more than one stereogenic centre, stereochemical analysis implies the determination of both diastereomeric and enantiomeric excesses. Thus, for such mixtures, deuterium NMR in chiral CLCs allow direct measurement of the *ee* of each diastereoisomer as well the proportions between all the diastereoisomers, as shown for cyclopentanones **6** and **7** [271] and cyclohexane derivatives **9** and **10** [272].

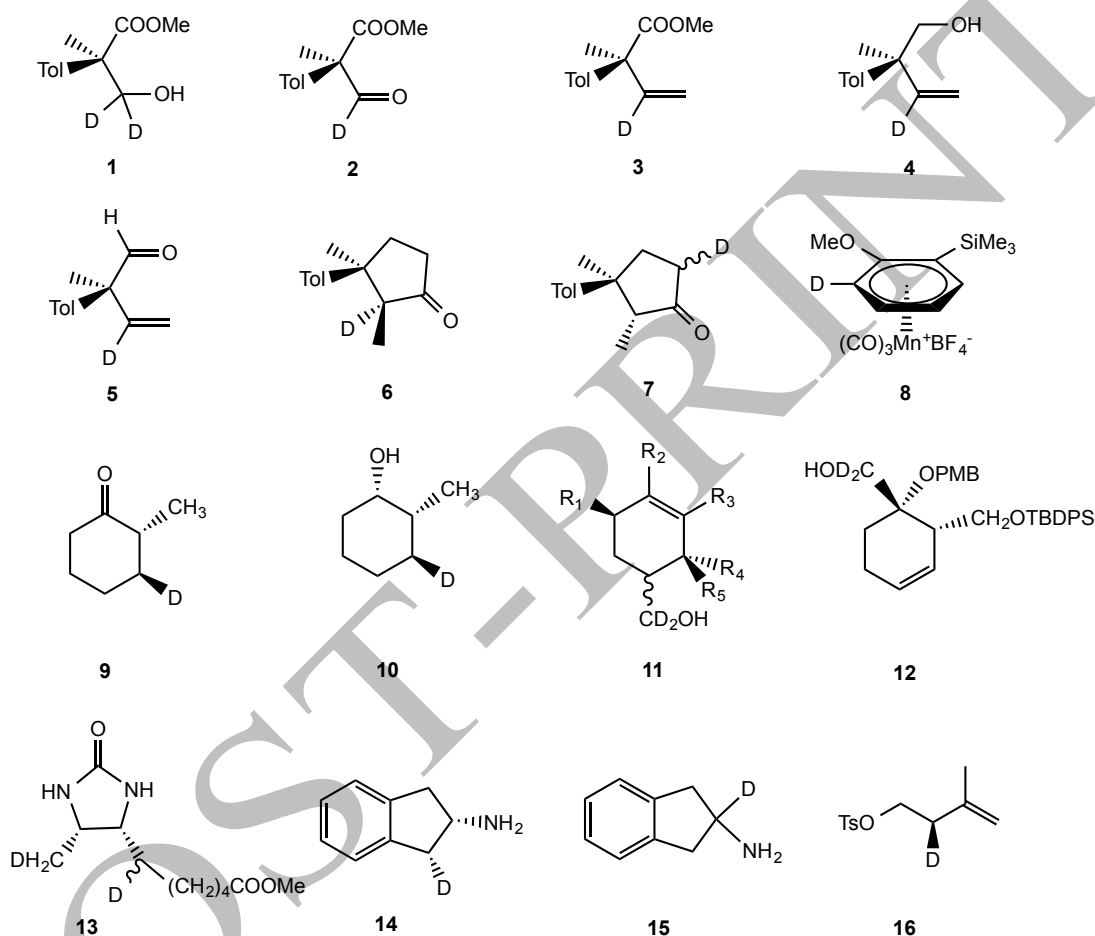


**Fig. 39.** Fifteen examples of various structures of mono- or dideuterated chiral molecules investigated.

When the stereoselectivity of a new reaction cannot be established straightforwardly by analysing the resulting products directly, a chemical transformation, such as the reduction of an ester group using lithium aluminium deuteride ( $\text{LiAlD}_4$ ), can provide a simple way to introduce a deuterium allowing a chiral analysis by deuterium NMR in chiral CLC. Based on this idea, the stereoselectivities in an asymmetric Diels-Alder cycloaddition of 2-alkoxy-2-vinyl-1,3-dioxolanes produced from chiral 1,2 diols [273] and in a Claisen-Ireland rearrangement followed by a ring closing metathesis have been established [274] for compounds with general structures **11** and **12** respectively. Small to moderate stereoselectivities were observed in the former reaction while the later turned out to be highly enantioselective.

Even in the case of reactions whose stereoselectivity is known, it may be important to check their selectivities towards substrates whose use has not previously been described. For chemical transformations implying a reduction step using lithium aluminium hydrides or sodium borohydrides, it becomes easy to obtain deuterium labelled substrates by the simple use of deuterated reducing reagents, such as  $\text{LiAlD}_4$  or  $\text{NaBD}_4$ . Using such an approach, the stereoselectivity of hydrogenolysis of a carbon-sulfur bond in the dialkylsulfoxide of biotin using nickel chloride and sodium borodeuteride was confirmed for the resulting ester derivative **13** using deuterium NMR in PBLG/DMF [275].

Similarly, it was shown that the reduction of *trans*-2-azido-1-bromoindane using  $\text{LiAlD}_4$  proceeds according to a  $\text{S}_{\text{N}}2$  mechanism and leads to aminoindane **14** as confirmed through its *N*-trifluoroacetamide derivative by deuterium NMR in PBLG- $\text{CH}_2\text{Cl}_2$  liquid crystal. In contrast, for *cis*-2-azido-1-bromoindane, a [1,2] hydride shift rearrangement emerges as the main reaction pathway leading to the non-chiral aminoindane **15** [276]. The mechanistic elucidation of transition metal catalysed asymmetric reactions is challenging as they can proceed through competitive pathways, which may provide the same mixture of products. Deuterium labelled compounds associated with NMR in CLC can be used successfully for this purpose.

The stereochemical course of the asymmetric allylic substitution of cinnamyl (linear) and isocinnamyl (branched) carbonates with malonates catalyzed by  $\text{C}_1$ -symmetrical complexes of molybdenum was assessed using deuterium labelled substrate analysis by  $^2\text{H}$ - $\{^1\text{H}\}$  NMR in CLC in combination with chiral HPLC data. For all the components of the anticipated products, isotopically labelled analogues were stereospecifically synthesised and their signals assigned in the deuterium NMR spectrum obtained in PBLG methylene chloride. The analysis of the products arising in the Mo-catalyzed allylic substitution could therefore be achieved [277].

Similarly, deuterium NMR in CLC turned out to be successful for the mechanistic investigation of the chiral palladium-DUPHOS catalysed benzylic alkylation of 1-naphthylethyl acetates with malonates. In such conditions, elimination products are obtained along with substitution products. Performing the reaction using a mixture of quasi-enantiomeric substrates (one enantiomer bearing a  $\text{CD}_3$  group while the other has  $\text{CH}_3$ ) showed that for a given enantiomer of the catalyst, one enantiomer of the substrate affords mainly the substitution product whereas the other enantiomer undergoes elimination [278].

Finally, as an important example of the use of deuterium labelling, we can mention the work of Leyes and Poulter on the synthesis of isopentenyl diphosphate, a universal precursor of more than 23 000 isoprenoid metabolites [288]. In this study, the enantiopurity of (*R*)-[2- $^2\text{H}$ ]-isopentenyl diphosphate used for this purpose, was established on its penultimate precursor, the [2- $^2\text{H}$ ]-isopentenyl tosylate (a nice case of isotopic chirality) **16**, by  $^2\text{H}$ - $\{^1\text{H}\}$  NMR in PBLG/ $\text{CH}_2\text{Cl}_2$  phase. Interestingly, the analysis has been performed at  $-50^\circ\text{C}$ .

### 6.3.3. Understanding the stereochemistry of enzymatic reactions

A very elegant illustration of the use of  $^2\text{H}\{-^1\text{H}\}$  NMR in CLCs based on labelled compounds is provided by studies carried out by O'Hagan *et al.* on the elucidation of the mechanism of the biosynthesis of fluorometabolites in *S. cattleya* [280, 281]. For this purpose, a non-racemic mixture of  $[2\text{-}^2\text{H}]$ -fluoroacetate derivative of known configuration has been synthesised in order to assign the signals of (*R*) and (*S*)-enantiomers in the  $^2\text{H}$  NMR spectrum in PBLG CLC (see Fig. 40a). Thereafter, experiments in which isotopically labelled  $[2,3\text{-}^2\text{H}_4]$ -succinate, (*1S*, *2R*) and (*1R*, *2R*)- $[1\text{-}^2\text{H}_1]$ -glycerol were fed to *S. cattleya* gave rise to samples of enantiomerically enriched  $[2\text{-}^2\text{H}_1]$ -fluoroacetates. The predominant enantiomer resulting from each experiment suggests that the stereochemical course of biological fluorination takes place with an overall retention of configuration between a glycolytic intermediate and fluoroacetate (see Figs. 40b,c,d, respectively), and consequently that enzymatic fluorination takes place with an inversion of configuration consistent with an  $\text{S}_{\text{N}}2$  reaction mechanism [280, 281].

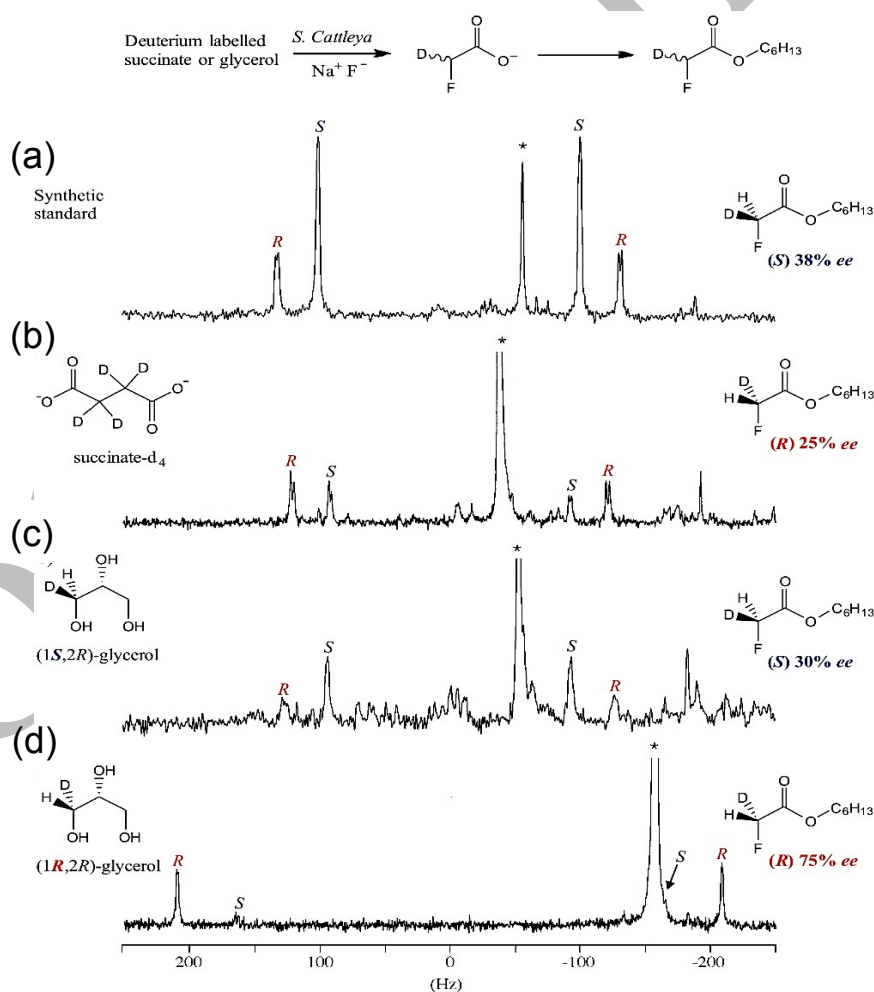


**Fig. 40.** 61.4  $^2\text{H}\{-^1\text{H}\}$  1D NMR spectra of hexyl  $[1\text{-}^2\text{H}_1]$ -fluoroacetates in PBLG/ $\text{CHCl}_3$  (11.0-14.4 wt% PBLG) of (a) a synthetic (*S*)-compound (38% ee) used as a reference for the assignment of absolute configuration; (b) (*R*)-compound (25% ee) after a feeding experiment to *S. cattleya* cells with  $[^2\text{H}_4]$ -succinate; (c) (*S*)-compound (30-40% ee) after a feeding experiment to *S. cattleya* cells with (*1S*,*2R*)-glycerol; (d) (*R*)-compound (75% ee) after a feeding experiment to *S. cattleya* cells with (*1R*,*2R*)-glycerol. The natural abundance signals from chloroform are labeled with an asterisk. Figure adapted from Ref. [280] with permission.

### 6.3.4. "On-the-fly" monitoring of enzymatic reactions

Understanding the enzymatic racemization mechanism is a crucial step for designing new enzyme inhibitors [282]. This task requires techniques able to distinguish between enantiomer signals, and hence to follow their concentrations *versus* time, in order to determine kinetic parameters and to study the effect of inhibitors. To provide alternative analytical methods to well-established methods (circular dichroism (CD) or UV spectroscopy) or more advanced tools (chiral capillary electrophoresis), a change of paradigm was proposed in 2013 by using  $^2\text{H}\{-^1\text{H}\}$  NMR in CLC [283].

The basic idea is to follow simultaneously, *in situ* and in real-time, the distinct  $^2\text{H}$  NMR signals of two (deuterated) enantiomers dissolved in a chiral mesophase in the presence of an active enzyme, and then to calculate the turnover numbers ( $k_{\text{catL}}$  and  $k_{\text{catD}}$ ) of the enzyme without the requirement of any chemical transformations of the substrate (as some for current tools), other than its prior deuteration (see Fig. 41). The proof of principle was explored in the case of the alanine racemase (AR) which recognizes a chiral substrate, such as L-Alanine (L-ALA) and reversibly converts it into its enantiomer, *i.e.* D-Alanine (D-ALA) or vice versa.

As AR is only water-compatible, chiral oriented solutions of DNA fragments in water have been used as a discriminating aligning medium [111, 283], while (D/L)-alanine was selectively deuterated on the methyl group in order to minimize the acquisition time of  $^2\text{H}$  spectra. Fig. 41a presents the variation of the  $^2\text{H}\{-^1\text{H}\}$  1D signals of L- and D-Alanine- $\text{d}_3$  at different intervals after the introduction of the enzyme. The time-dependent concentrations (see Fig. 41b) permit evaluation of  $k_{\text{catL}}$  and  $k_{\text{catD}}$  for a reversible

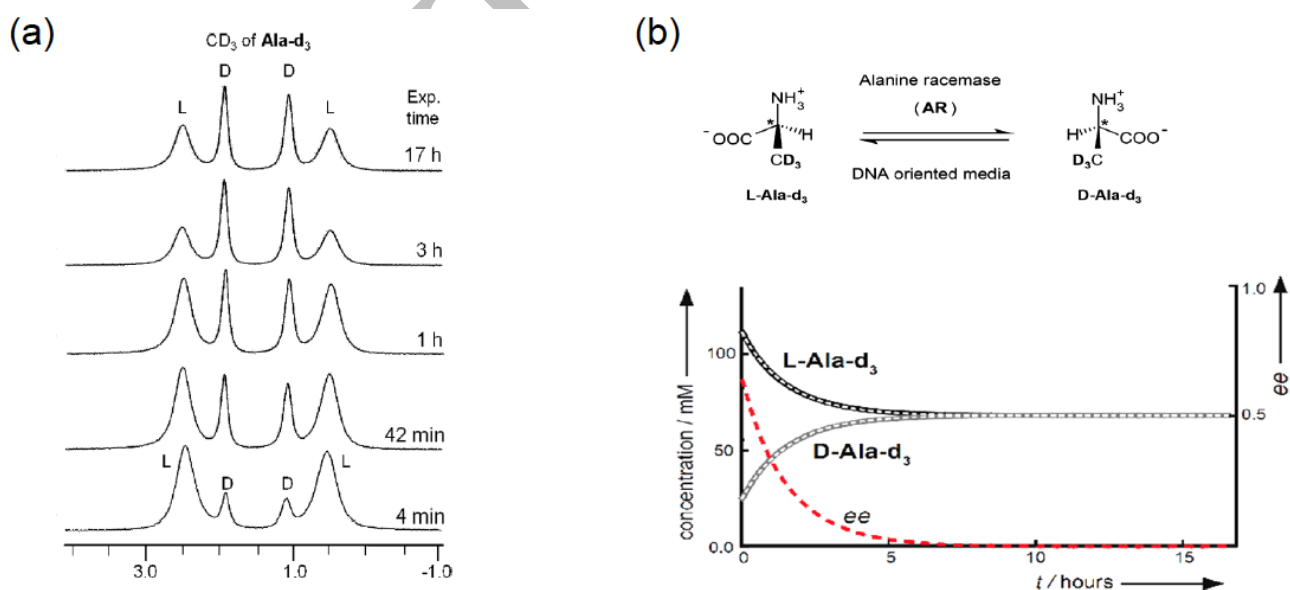


**Fig. 41.** (a) Examples of  $^2\text{H}\{-^1\text{H}\}$  1D signals (same vertical scale) of L- and D-Ala- $\text{d}_3$  recorded at different intervals after the introduction of AR in the mesophase. (b) (top) Principle of racemisation of alanine- $\text{d}_3$  by AR in DNA-based oriented media. (bottom) Variation of ee (red dashed line) and experimental (black and grey continuous lines) and fitted (white dashed lines) concentrations (in mM) of L- and D-Ala- $\text{d}_3$  as a function of time (in hours). The larger linewidth for the L-isomer originates from internal  $^2\text{H}\text{-}^2\text{H}$  total couplings that are not equal to zero as for the D-isomer. Figure adapted from Ref. [283] with permission.

Michaelis-Menten model, the Michaelis constants  $K_M$  and  $K_{M'}$  being determined independently. The values of  $k_{catL}$  and  $k_{catD}$  determined at pH = 7.5 are consistent with previous values obtained at pH = 6.9 and 8.9 using CD, thus showing the potential and robustness of the method proposed [292]

Also, the real-time variation of  $ee$  is a further key to provide new insights and a better understanding of enzymatic mechanisms, in particular through its ability to discriminate enantiomeric products of enzymes in the presence of inhibitors.

#### 6.4. Deuterium NMR at natural abundance level (NAD NMR)

Due to the absence of chemical modifications of analytes, NAD NMR in CLCs is a powerful tool for investigating and establishing the ability of polypeptide mesophases to discriminate spectrally between enantiomers of a large range of chiral compounds (monodeuterated diastereo-isotopomers), including rigid and flexible compounds as well as chiral analytes with or without stereogenic atomic centers [111, 269].

It also allows the discrimination of enantiomers of molecules that are chiral by virtue of the isotopic substitution D/H. The discrimination of these enantio-isotopomers is related to that of the enantiotopic elements in prochiral molecules [41]. All these examples investigated in the past will not be reviewed here, however, we will discuss two unusual classes of analytes: chiral molecules having highly-abundant active nuclei such as  $^{19}\text{F}$ , and the case of chiral hydrocarbons.

##### 6.4.1. From binary to ternary mixtures

The relative abundance of  $^2\text{H}$  relative to  $^1\text{H}$  is defined equal to 0.0155 % according to the “Vienna Standard Means Ocean Water” value (V-SMOW). Despite this low abundance, the NMR detection of natural abundance deuterium (NAD) (yields the signal of all inequivalent deuterium sites in analytes, as well as the nature of their stereochemical relationships (homotopic, enantiotopic and diastereotopic sites with respect to molecular symmetry elements) [1]. Note here that such an analytical approach is highly attractive, because in a single experiment, we combine the advantage of rare spins (lack of  $^2\text{H}$ - $^2\text{H}$  couplings detected, simplifying spectral analysis), the probing of all inequivalent  $^2\text{H}$  sites of the analyte and the sensitivity of the  $^2\text{H}$  quadrupolar interaction to the orientation.

The first pioneering results of proton-decoupled NAD (NAD- $\{^1\text{H}\}$ ) 1D NMR were recorded at 5.8 T in 1998 (with an old “AM 250” Bruker NMR spectrometer) using binary polypeptide oriented systems made of PBLG and a large amount of analyte (such as benzyl alcohol or ( $\pm$ )- $\alpha$ -methylbenzyl alcohol) able to dissolve the polymer and provide a homogeneous chiral mesophase (see Fig. 42a) [240].

The use of higher magnetic fields ( $> 9.4$  T) and selective  $^2\text{H}$  probes (standard probe or, better, a cryogenic probe) is a simple way to increase the sensitivity of NAD 1D/2D experiments, and hence to apply this technique to oriented samples of ternary polypeptide systems [225, 269, 270, 284].

Fig. 42b shows the NAD- $\{^1\text{H}\}$  1D-NMR spectrum of ( $\pm$ )-hept-3-yn-2-ol dissolved in the PBLG/ $\text{CHCl}_3$

CLC and recorded at 14.1 T with a selective  $^2\text{H}$  cryogenic probe [189], within 30 minutes [244].

Here again the signals of all inequivalent  $^2\text{H}$  sites in the CLC are observed; the difference of peak intensities originating from the number of hydrogenated sites giving rise to signal, the  $^2\text{H}$  linewidths and finally the site-specific isotopic (D/H) ratio of each site (that can differ from V-SMOW value up to 50%) (see Section 6.4.5). Compared to Fig. 42a, the NAD signal of co-solvent appears on the NAD spectrum (one doublet in case of chloroform) and the gain in sensitivity resulting from the use of a cryoprobe significantly increased the value of SNR. As mentioned above, simplification of the spectral analysis of ANAD spectra and assignment of  $^2\text{H}$ -QDs can be performed successfully using QUOSY-type experiments (see above) [54].

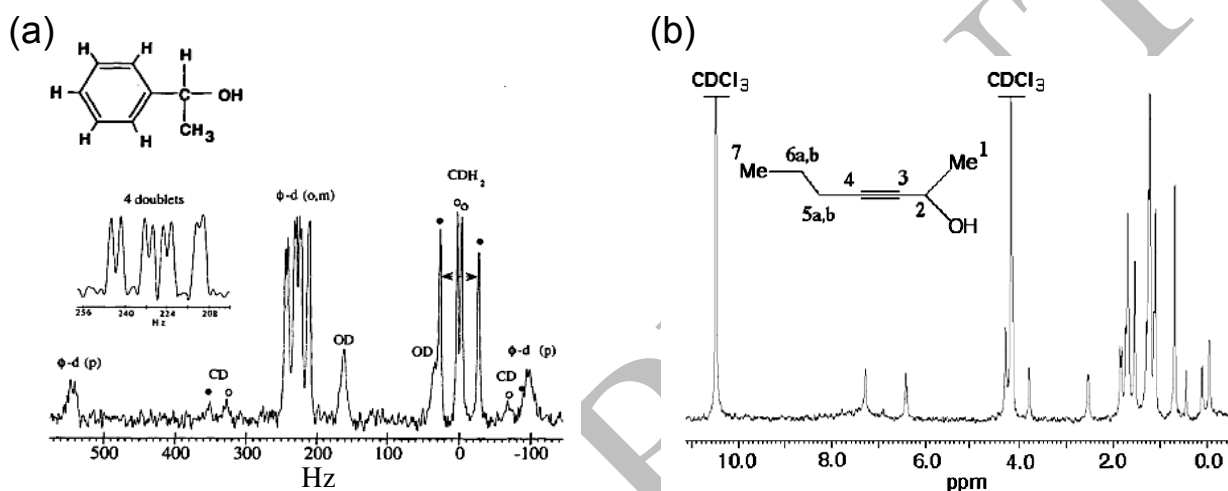


**Fig. 42.** (a) First NAD- $\{^1\text{H}\}$  1D NMR spectrum ( $(\pm)$ - $\alpha$ -methylbenzyl alcohol;  $m = 600$  mg) published in 1998 and using the binary system (solite/PBLG) recorded at 38.4 MHz (standard inverse probe). (b) Typical example of NAD- $\{^1\text{H}\}$  1D NMR spectrum ( $(\pm)$ -hept-3-yn-2-ol;  $m = 100$  mg) using a ternary system (solite/PBLG/ $\text{CHCl}_3$ ). Note the presence of NAD QD of chloroform. Figure adapted from Refs. [240] and [244], with permission.

#### 6.4.2. NAD NMR and highly-abundant, magnetically active heteroatoms

Numerous chiral molecules possess highly naturally-abundant (100%) and magnetically active heteroatoms, denoted hereafter as X, such as fluorine-19 or phosphorous-31 atoms ( $I = 1/2$ ). These X nuclei are likely to provide further patterns in the NAD- $\{^1\text{H}\}$  2D QUOSY spectrum through mutual " $^2\text{H}$ -X" scalar and residual dipolar couplings. The magnitude of such couplings is 6.5 fold less than for a corresponding  $^1\text{H}$ -X atomic pair. Due to this extra  $^1\text{H}$ -X coupling, the signal of coupled deuterons is now distributed on a larger number of components (thus decreasing inherently the S/N ratio). However, the sensitivity of  $^2\text{H}$  cryogenic probes still allows such spectra to be detected with an exploitable SNR.

This type of  $^2\text{H}$ -X heteronuclear coupling was first experimentally observed with ( $\pm$ )-2-(fluoromethyl) oxirane dissolved in PCBL/DMF (see Fig. 43a) [54, 285].

In this example, the analysis of the spectrum shows that the diastereotopic deuterium atoms (of methylene 1,1') are coupled to the fluorine atom and are characterized by four  $^2\text{H}$ -QD (two *per* enantiomer and diastereotopic site), and these components are further doubled by the  $^2\text{H}$ - $^{19}\text{F}$  coupling.



This further splitting appears parallel to the main diagonal of the NAD  $Q$ -COSY Fz 2D map (the dotted line). This separation of spectral information allows a direct reading of  $^2\text{H}$ - $^{19}\text{F}$  heteronuclear total coupling ( $T_{\text{DF}} = J_{\text{DF}} + 2D_{\text{DF}}$ ) at natural abundance. From the analytical aspect, these structures intrinsically possess much chirality-related information that can be useful for calculating the molecular orientational parameters of each enantiomer.

### 6.4.3. Determination of enantioselectivity in asymmetric synthesis

Similarly to  $^2\text{H}$ - $\{^1\text{H}\}$  NMR of deuterated molecules, ANAD- $\{^1\text{H}\}$  NMR is an original tool for understanding unusual asymmetric synthesis, such as the enantioselective mono-lithiation reaction in asymmetric halogen-lithium exchange, which leads to the desymmetrization of prochiral aromatic dihalides, such as the diiodide ferrocene, a prochiral molecule, in which the enantiotopic sites  $\text{H}_b$  and  $\text{H}_{b'}$  are spectrally discriminated (see Fig. 43b) [286]. One of the major challenges in the synthesis of large-size bioactive substances is the control of  $ee$ 's (see above) of various small chiral building blocks leading to the final molecular target. For such small precursors, NAD NMR in polypeptide CLC can play an important analytical role for two reasons: i) chiral precursors have rather low MW (100 to 200  $\text{g}\cdot\text{mol}^{-1}$ ); ii) large amounts of analytes are available during the initial stages of a total synthesis, allowing preparation of anisotropic samples in rather large quantities. This can be an advantage when using NMR spectrometers that lack a  $^2\text{H}$  cryogenic probe.

An illustrative example of interest of ANAD- $\{^1\text{H}\}$  2D NMR is afforded by the enantioselective synthesis of hept-6-yn-2-ol, a possible chiral building block for preparing the dolatrienoic acid used to

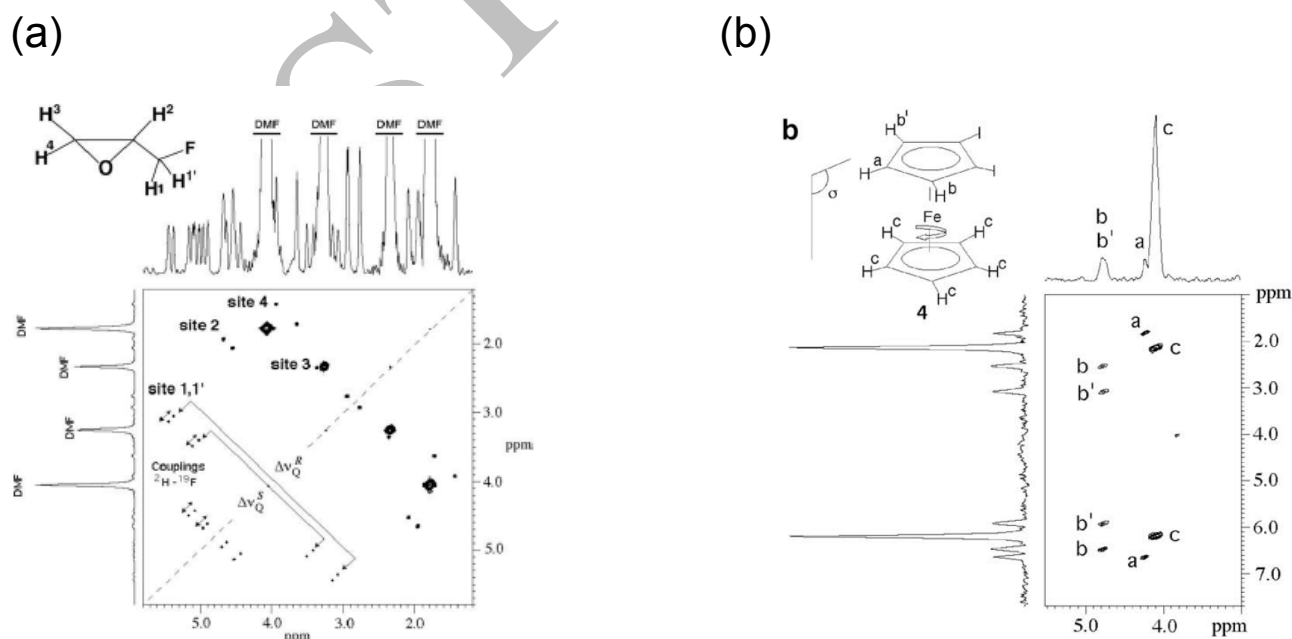


**Fig. 43.** Two examples of ANAD- $\{^1\text{H}\}$  Q-COSY Fz 2D experiments recorded at 92.1 MHz (cryogenic probe). (a) 2D spectrum of  $(\pm)$ -2-(fluoromethyl)-oxirane in PCBL/DMF where  $^{19}\text{F}$ - $^1\text{H}$  total couplings are observed. Note that the  $^2\text{H}$ - $^{19}\text{F}$  total couplings are slightly different for each enantiomer. (b) 2D spectrum of ferrocene diiodide where enantiotopic sites ( $b$  and  $b'$ ) are discriminated. Figure adapted from Refs. [285] and [286], with permission.

build the south fragment of dolastatine-14, a cyclic macromolecule with potential anticancer activities (see Fig. 44a) [287]. The specific question addressed by organic chemists in this case was the control of enantioselectivity of the alkyne zipper reaction leading to hept-6-yn-2-ol from the hept-3-yn-2-ol. The analysis of NAD signals of the precursor and final product established unambiguously that the reaction was a racemisation-free process. In this example, the absence of any NAD doublet emerging from spectral noise for (*S*)-(+)-hept-6-yn-2-ol implies a large *ee* value, over 95% (see Fig. 44b).

In another context, NAD 2D NMR in CLC was also successfully used for the preparation of an analogue of *Mycobacterium tuberculosis* tetra-O-acylated sulfolipid, in particular, the determination of enantiopurity of mono-methylated chiral fatty acids, prepared by a zinc-mediated cross-coupling, prior to its incorporation into the trehalose core [288].

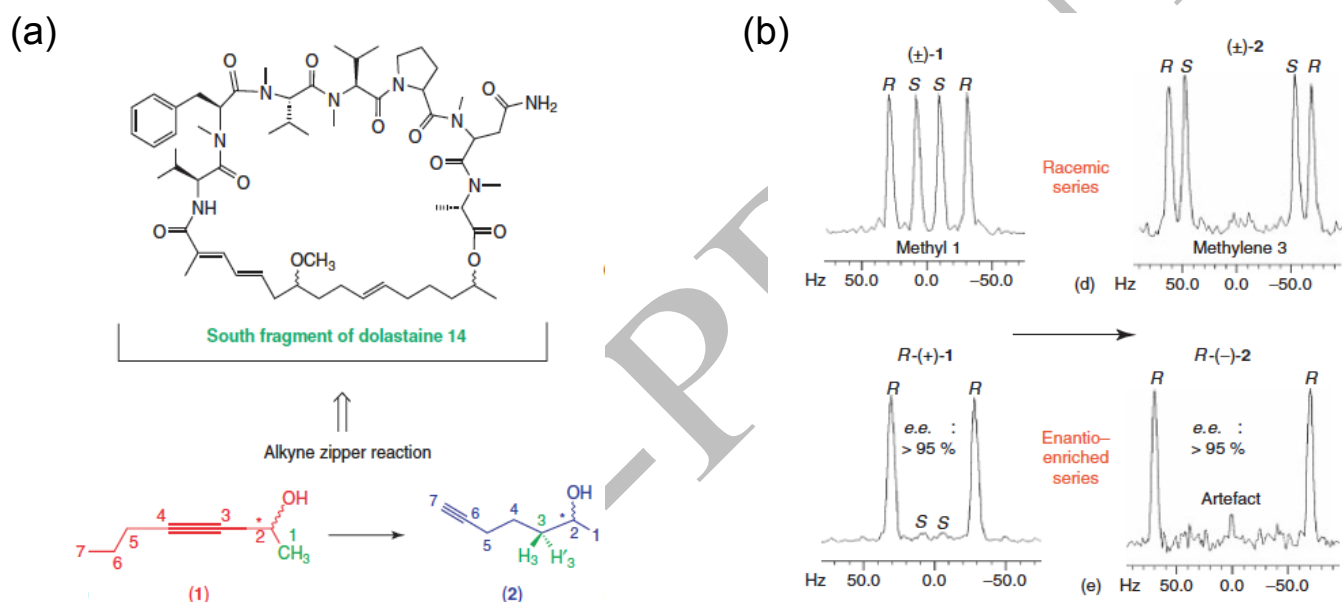


**Fig. 44.** (a) Structure of dolastatine-14 (top) and synthetic principle of the alkyne zipper reaction (bottom). (b) 61.4 MHz NAD- $\{^1\text{H}\}$  signals extracted from Q-COSY spectrum recorded in PBLG/ $\text{CHCl}_3$ . NAD signals of (left side) methyl group 1) of hept-3-yn-2-ol and (right side) of one of two monodeuterated diastereoisotopomers associated with the methylene group 3 of hept-6-yn-2-ol in (top) racemic mixture and (bottom) enantioenriched series. Figure adapted from Ref. [288] with permission

#### 6.4.4. Analysis of chiral hydrocarbons

The main reason that routine isotropic NMR methods used to differentiate enantiomers lack generality stems from the need for specific chemical functions on the analyte and adapted chiral auxiliaries (derivatizing agent, lanthanide shift reagent or solvating agent) in order to form stable diastereoisomers or diastereomeric adducts (see Introduction) [288]. Consequently, the unsaturated and saturated chiral hydrocarbons, which do not possess any highly reactive, polar functions, are difficult to discriminate using these approaches. Some advanced NMR tools (often considered as exotic or too sophisticated to be used routinely) have been reported in the literature. In reference [225], a compilation of references describing the most important approaches can be found. Although these strategies have been successfully applied for specifically discriminating some allenic, olefinic or aromatic chiral hydrocarbons, they do not

always guarantee sufficiently large resonance separations in isotropic  $\delta^{\text{aniso}}(^1\text{H})$  shifts for a reliable enantiomeric purity determination. Clearly, none of them (including the cyclodextrine systems) provides a general technique.

As an alternative to such isotropic NMR tools, ANAD NMR has proved to be a widely applicable approach for efficiently analysing chiral hydrocarbons [288, 289]. Indeed as the shape recognition by the polypeptide plays an important role in the mechanism of orientation of the solute [290], and in the enantiodiscrimination phenomenon, the presence of polar atoms/groups (halogen, -OH, -NH, COOH, etc.) able to establish specific interactions with the polymer (*e.g.* Hydrogen bonding) is not mandatory [198, 289].

Besides, as the  $^2\text{H}$  quadrupolar interaction is the most sensitive anisotropic NMR interaction to an orientational ordering difference, even small differences in  $S_{\text{C-D}}$  can be detected in the NAD spectra through a visible difference of RQC (see Section 2.3.3).

The screening of various classes of chiral hydrocarbons has shown that this technique is able to differentiate the NAD signals of enantiomers for a large collection of apolar (rigid and flexible) hydrocarbons, such as bicyclic and acyclic alkenes, alkanes, alkynes, aromatics, including the cases of chiral molecules with no stereogenic carbon [198, 225], thus showing the huge analytical potential compared to isotropic NMR methods.

To illustrate this, Fig. 45 shows examples of a rigid (bicyclic) molecule, ( $\pm$ )- $\alpha$ -pinene, and a flexible (cyclic) compound, ( $\pm$ )-*trans*-1,3-dimethylcyclohexane, for which the NAD QUOSY 2D spectra recorded in PBLG systems show spectral enantiodiscriminations of a large number of  $^2\text{H}$  sites. In both cases, enantiodiscrimination is seen on various  $^2\text{H}$  sites and ranges from 10 to 28 Hz and 8 to 20 Hz, respectively. Remarkably, the efficiency of the method has permitted, for the first time, discrimination by NMR of enantiomers of 3-methylhexane, the most simple, flexible apolar chiral hydrocarbon [289].

This initial result was nicely confirmed in 2019 by replacing PBLG by a poly(arylacetylene) polymer (see Section 3) [144]. However, it should be noticed that the method fails to discriminate the hexadeuterated enantiomers of ( $\pm$ )-hexadeuterated neopentane ( $\text{C}(\text{CH}_3)(\text{CH}_2^2\text{H})(\text{CH}_2^2\text{H}_2)(\text{C}^2\text{H}_3)$ ), which is the smallest chiral compound possessing a quaternary carbon stereogenic center. For this “ultimate” chiral analyte, the overall shape recognition mechanisms involved in the chiral discrimination phenomenon are in the case of PBLG insufficient to differentiate the extremely small topological differences between the mono-, di-, and trideuterated methyl groups around the central, stereogenic carbon atom [391].

Compared to other chiral selectors, the exceptional enantio-recognition power and capacity of homopolypeptide helices to interact enantioselectively with rigid as well as flexible chiral apolar derivatives suggest that none of the other methods (chiroptical, chromatographic or other NMR techniques) currently available for hydrocarbons seems to be as general as the NAD NMR in CLC.

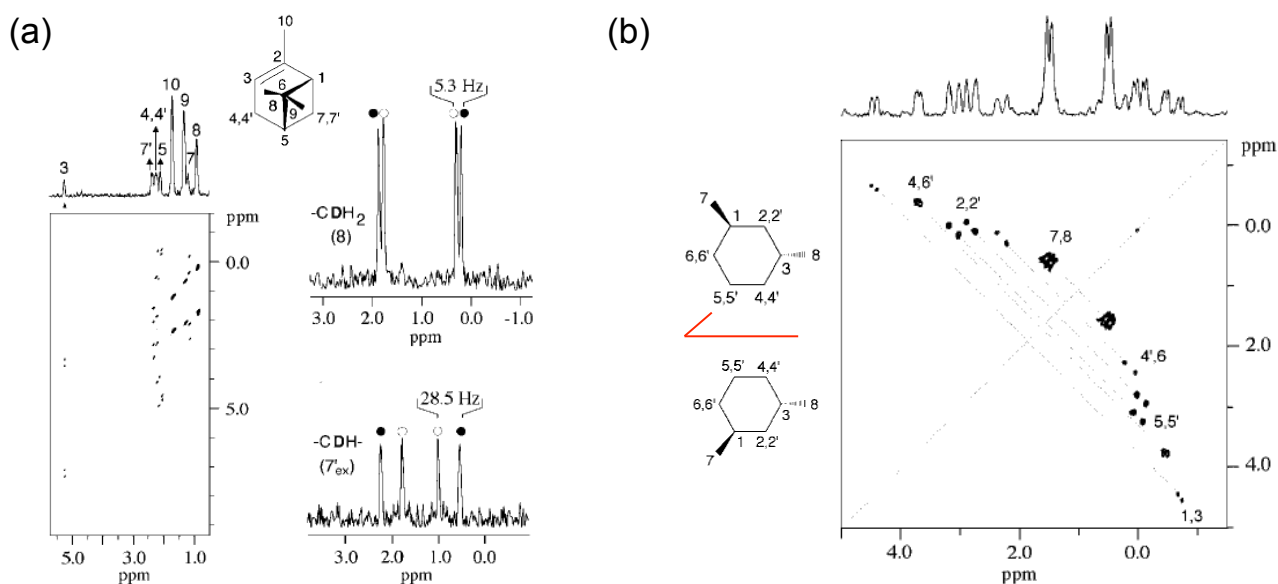


**Fig. 45.** (a) Tilted NAD- $\{^1\text{H}\}$  Q-COSY 2D spectrum of  $(\pm)\text{-}\alpha\text{-pinene}$  and two extracted columns from the map. (b) NAD- $\{^1\text{H}\}$  Q-COSY spectrum of  $(\pm)\text{-trans-1,3-dimethylcyclohexane}$ . Both 2D spectra are recorded in PBLG/ $\text{CHCl}_3$ . Figure adapted from Ref. [225] with permission.

## 6.5. Contribution of anisotropic natural abundance deuterium NMR (ANAD NMR<sup>®</sup>) to isotopic fractionation

### 6.5.1. Alternative to site-specific isotopic fractionation NMR (SNIF-NMR<sup>®</sup>) protocol

In nature, every organic compound can be seen as a mixture of various isotopomers that have the same chemical properties but whose physical behavior may differ. Two important analytical tools currently provide key molecular isotopic information: i) isotopic-ratio Mass Spectrometry (**irMS**) determines a global value for the amount of isotope in a molecule; ii) NMR spectroscopy leads to a measure of site-specific (named also position-specific) isotopic ratios ( $^2\text{H}/^1\text{H}$ )<sub>i</sub> in a molecule.

Historically, quantitative  $^2\text{H}\text{-}\{^1\text{H}\}$  1D-NMR in isotropic solvents was the first invaluable NMR approach for investigating the natural isotope  $^2\text{H}$  distribution (profile) in biosynthesized compounds (ethanol, fatty acids, vanilline, limonene, etc.) [292, 293, 294]

From the value of site-specific ( $^2\text{H}/^1\text{H}$ )<sub>i</sub> isotope ratios (expressed in ppm) measured by NMR, that can be different from one hydrogenated site to another and also different from the V-SMOW value (0.0155 %), it becomes possible to access crucial information concerning the geographical origin and/or botanical source of analytes. Developed and then patented by Martin and co-workers in the 1980's, this protocol is well-known as "Site-specific Natural Isotopic Fractionation NMR" (SNIF-NMR<sup>®</sup>) [292]

From an analytical viewpoint, the method affords robust solutions for: i) studying kinetic isotopic effects (KIEs) [294]; ii) determining the source of hydrogen atoms, elucidating biosynthesis pathways [295, 296]; iii) the fight against counterfeiting and adulteration of substances sold as "natural" (authenticity/traceability investigations), among others [297, 298, 299, 300].

According to the SNIF-NMR<sup>®</sup> protocol, isotropic NAD 1D-NMR spectra of analytes are recorded under quantitative conditions ( $T_R = 5 \times T_1$ ) with an internal isotopic reference whose ( $^2\text{H}/^1\text{H}$ ) ratio has been calibrated. If the mass of compounds (analyte and reference) are accurately known, the site-specific ( $^2\text{H}/^1\text{H}$ )<sub>i</sub> ratios (expressed in ppm) can be calculated from evaluation of peaks areas in NMR spectra as follows:

$$\left( ^2\text{H}/^1\text{H} \right)_i^{\text{anal}} = \left[ \frac{A_i^{\text{anal}}}{A_i^{\text{ref}}} \right] \times \left[ \frac{P_i^{\text{ref}} \times m^{\text{ref}} \times M^{\text{anal}}}{P_i^{\text{anal}} \times m^{\text{anal}} \times M^{\text{ref}}} \right] \times \left( ^2\text{H}/^1\text{H} \right)_i^{\text{ref}} \quad (28)$$

where  $A_i^{\text{anal}}$  and  $A_i^{\text{ref}}$  are the integrated intensity of the signals at site  $i$  for the analyte and the reference,  $P_i^{\text{anal}}$  and  $P_i^{\text{ref}}$  are the stoichiometric numbers of hydrogens at site  $i$  in analyte and reference respectively,  $M^{\text{anal}}$  and  $M^{\text{ref}}$  are the corresponding molecular weights,  $m^{\text{anal}}$  and  $m^{\text{ref}}$  are the masses of analyte and the reference present in the sample, respectively. Finally,  $\left( ^2\text{H}/^1\text{H} \right)_i^{\text{ref}}$  is the isotope ratio of the reference (at site  $i$ ). Generally, isotopically calibrated Tetramethylurea (TMU) is used as internal reference.

Although a wide range of applications has been explored by SNIF-NMR<sup>®</sup>, its analytical efficiency is limited by two factors: i) the small dispersion of  $\delta(^2\text{H})$  expressed in Hz; ii) the inability to measure ( $^2\text{H}/^1\text{H}$ ) ratios for enantiotopic hydrogen sites in isotropic achiral solvents. Recently, the toolkit for isotope ratio monitoring (**IRM** or **irm**) by NMR has been extended by the development of isotropic  $\text{irm-}^{13}\text{C}$  1D-NMR, which accesses the carbon skeleton of the molecule [301, 302].

Although this method provides additional isotopic information with respect to that obtained by  $^2\text{H}$  NMR,  $\text{irm-}^{13}\text{C}$  NMR does not give access to  $^2\text{H}$  isotopic information that is inaccessible by isotropic NMR. Clearly in the context of anisotropic NMR, these two limitations can be overcome through: i) accessing quadrupolar interactions of  $^2\text{H}$  nuclei; ii) using chiral orienting media to enable discrimination between enantio- or diastereo-isotopomers.

#### 6.4.2. Revisiting the fatty acid family

The application of  $\text{irm-}^2\text{H}$  NMR spectroscopy in combination with CLCs was experimentally pioneered from 2004 for the case of fatty acid methyl esters (**FAMEs**). The main challenge was obviously to access isotopic data on the enantiotopic positions of these prochiral flexible molecules of average symmetry  $C_s$ , which cannot be achieved by the SNIF-NMR<sup>®</sup> isotropic protocol (see Section 9). The real analytical interest was first demonstrated for the 1,1'-bis-(phenylthio)-hexane (**BPTH**), a prochiral fragment of the methyl linoleate (**ML**), an essential unsaturated fatty acid (**UFA**) (see Fig. 46) [303].

In this pioneering example, the analysis of the 61.4 MHz ANAD- $\{^1\text{H}\}$   $Q$ -COSY spectrum provided the first data on the intramolecular isotope ratios of each enantiotopic hydrogen site in each  $\text{CH}_2$  group of

the fragment. The assignment of  $^2\text{H}$ -QDs in the chiral ANAD spectrum showed that the proportion of (*R*)-enantio-isotopomers in both methylene sites of BPTH were higher than those of the (*S*)-enantio-isotopomers [304].

Taking advantage of NMR spectrometers operating at higher field (14.1 T, *i.e.* 92.1 MHz for  $^2\text{H}$ ) and equipped with a selective  $^2\text{H}$  cryogenic probe, the method was then successfully extended to the study of more complex prochiral FAMEs with longer chains, such as C-18 mono- or poly-unsaturated FAMEs as well as conjugated, unsaturated FAMEs (CUFAs), such as methyl oleate (MO), methyl linolenate (ML), methyl vernoleate (MV), methyl eleostearate (ME), methyl punicate (MP), etc. [305, 306, 307, 308].

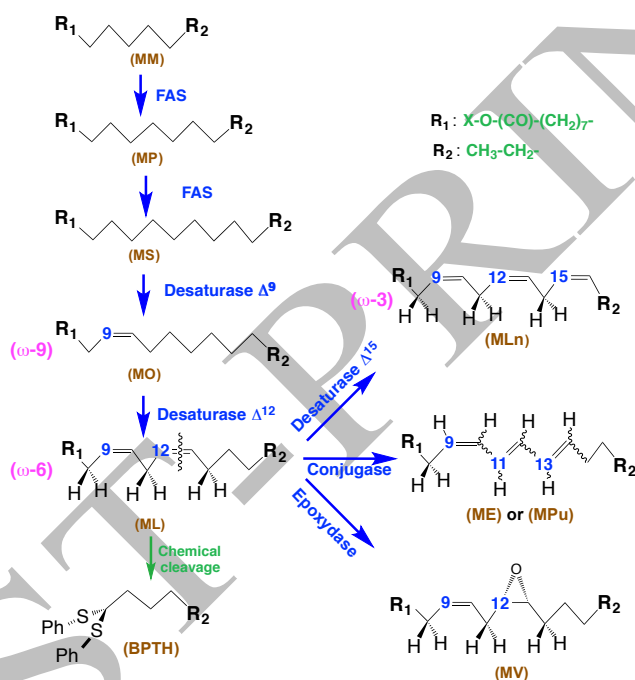


**Fig. 46.** Scheme of successive biochemical transformations of MM (SFA) leading successively to various UFAs, (9Z)-MO, (9Z, 12Z)-ML, (9Z, 12Z, 15Z)-MLn, (9Z, 12R, 13S)-MV or two CUFAs, (9Z, 11E, 13E)-ME and (9Z, 11E, 13Z)-MP. In plant or microorganism cells, X corresponds to coenzyme A (CoA) or carrier protein (ACP). For NAD NMR analysis, X is a methyl group. Figure adapted from Ref. [308] with permission.

The power of the method is nicely illustrated in Fig. 47b in the case of ML oriented in the PBLG/pyridine system. All inequivalent mono-deuterated and enantio-isotopomers are spectrally detected in a single experiment in CLC, whereas isotropic  $^2\text{H}$  1D-NMR spectra resolve only 30% of inequivalent  $^2\text{H}$  sites (see Fig. 47a) [306]. The determination of the AC associated with each  $^2\text{H}$ -QD has been explained in Ref. [306].

Combining quantitative isotropic/anisotropic  $\text{irm-}^2\text{H}$  NMR measurements, the evaluation of the isotopic fractionation of each enantio-isotopomer (*R* and *S*) was obtained with good accuracy (see Fig. 47c). Large variations of ( $^2\text{H}/^1\text{H}$ )<sub>*i*</sub> ratios exist between each enantioisotopomeric pair (for instance the

positions 15/15' and 17/17'), showing the variability of the sources of the hydrogens at these different positions. As new molecular information related to isotope fractionation, the discrimination of (*R/S*)-enantio-isotopomers in CLCs allows for the first time the determination of the bio enantio-isotopomeric excess, (**EIE**) (%) for each CH<sub>2</sub> group of the prochiral molecule, according to the equation [306].

$$eie(\%) = \frac{|(^2\text{H}/^1\text{H})_i^R - (^2\text{H}/^1\text{H})_i^S|}{(^2\text{H}/^1\text{H})_i^R + (^2\text{H}/^1\text{H})_i^S} \times 100 \quad (29)$$

Note here that using chiral solutes possessing CH<sub>2</sub> groups (as VM in the FAME family), the discrimination of diastereotopic positions in methylene groups allows the determination of the four bio diastereo-isotopomeric excesses, (**DIEs**) for each CH<sub>2</sub> group of the chiral molecule.

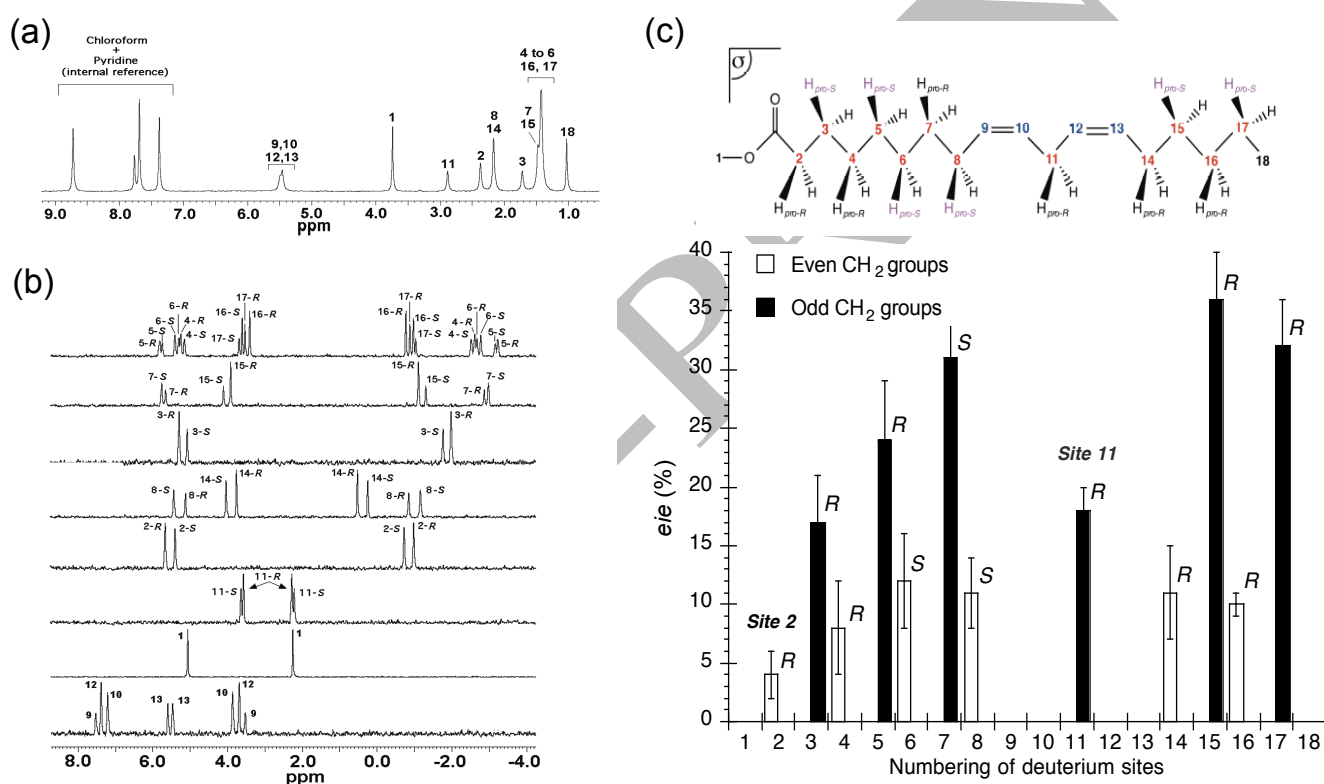


**Fig. 47.** (a) Isotropic NAD-<sup>2</sup>H 1D spectrum of methyl linoleate. (b) Series of NAD-<sup>2</sup>H 1D sub-spectra of ML in PBLG/pyridine extracted from the anisotropic tilted Q-COSY Fz map. The <sup>2</sup>H-QD of methyl group 18 is not shown. (c) Variation of *eie* % vs. the methylene groups. Figure adapted from Ref. [306] with permission.

In case of ML, it has been shown that *eie* at the odd-numbered CH<sub>2</sub> positions are larger than those measured at even-numbered CH<sub>2</sub> groups all along the chain (see Fig. 47c). This observation was explained by the different incorporation mechanisms of hydrogens into the chain during the elongation of fatty acids *via* the fatty acid synthetase (FAS) enzyme [309].

Except for sites 6 to 8, the AC of major enantio-isotopomers (at all other odd and even methylene sites) is *R*, similarly to what is expected all along the chain of the saturated precursor (MS) due to the mode of action of FAS enzymes in plant cells [305]. The inversion for methylene groups 6, 7 and 8 does

not represent a fundamental difference, but rather is just a consequence of the Cahn, Ingold and Prelog (CIP) priority rule for naming absolute configurations [1, 310].

Indeed, the presence of the double bond 9-10 in ML inverts the priority order of substituents around the stereogenic centers 6 to 8 induced by the isotopic chirality, but topologically the hydrogen positions (front or back relative to the symmetry plan of the average molecular structure) remain the same.

The first application studies of the anisotropic  $\text{irm-}^2\text{H}$  approach have enabled us to answer two specific biochemical questions concerning the unsaturated FAMES never previously solved. The first concerned aspects of stereoselectivity during the elongation (by FAS) and the desaturation steps (by the  $\Delta^9$  and  $\Delta^{12}$  desaturase) leading to the biosynthesis of the ML in *Fusarium Lateritium*, (a fungus species) [309].

The second concerned the possible difference of bioconversion processes of ML to MV involved in the case *Euphorbia lagascae* and *Vernonia galamensis*, plants that use different enzymatic systems [311]. In this second application, the relative variations in the natural site-specific isotopic fractionation ( $^2\text{H}/^1\text{H}$ )<sub>i</sub> were used to determine whether distinct characteristics at the reaction centre could be determined by comparing and analyzing the differences in the isotopic profile of the substrate, the ML, and the epoxidation product, the MV (see Fig. 48) [311].

Although *E. lagascae* and *V. galamensis* use different enzymes to achieve epoxidation of the ML in position 12 (a cytochrome P450 monooxygenase in the first case [312], and a di-iron dioxygenase in the second [313]), it has been demonstrated that the ML and MV isolated from the seeds of the two plants have remarkably similar isotopic profiles. Unexpectedly, analysis of these results indicated that the overall determinants of the final ( $^2\text{H}/^1\text{H}$ )<sub>i</sub> distribution in the final product are the encumbrance (steric accessibility) of the active site pocket and constraints to conformational readjustment during the linoleate to vernoleate transformation.

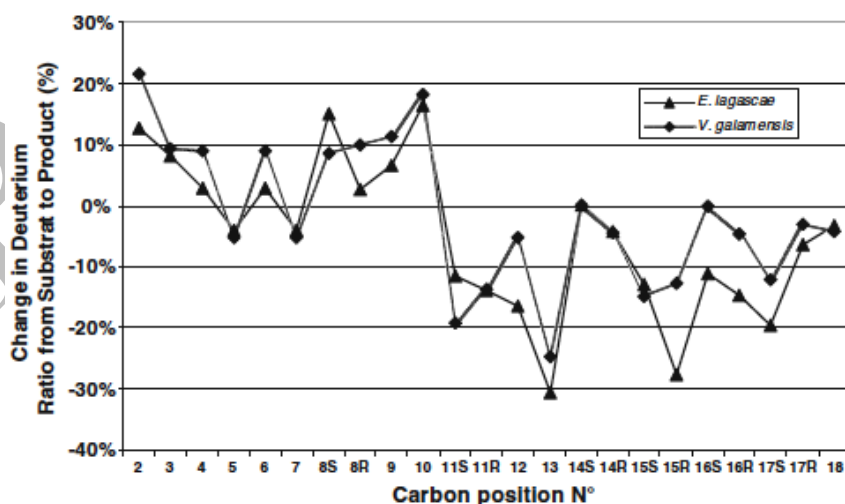


**Fig. 48.** Variations in isotope ratios (in percent) between substrate, the methyl linoleate and product, the methyl vernoleate observed when these UFAs are extracted from *V. galamensis* and *E. lagascae*. Note the enrichment and then the overall deuterium depletion on the C<sub>2</sub>-C<sub>10</sub> and C<sub>11</sub>-C<sub>17</sub> fragments, respectively. Figure adapted from Ref. [311] with permission.



In the same family of prochiral organic molecules, the more complex cases of C-14 to C-18 saturated FAMES (SFA), namely the methyl myristate (MM), methyl palmitate (MP) and methyl stearate (MS) were also successfully explored (see Fig. 46), thus demonstrating that ANAD NMR could provide a robust means of accessing a larger number of  $^2\text{H}$  sites (compared to isotropic NMR) [314]. In these long-chain SFAs, the spectral dispersion of methylene group  $\delta(^2\text{H})$  values is very limited due to absence of double bonds, and consequently the main obstacle to analysis of SFAs is the assignment of  $^2\text{H}$ -QDs of central methylene groups of the alkyl chain. This assignment of QDs was made from different sources of information [314]: i) the variation of chemical shift values, including previously known "even/odd" isotopic effects specific to FAs; ii) the variations in  $^2\text{H}$ -RQCs according to their position in the chain; iii) and the comparison of the various UFAs (mono- or polyunsaturated) between spectra. To confirm the assignments made, two further very different approaches were applied: i) the reductive and regioselective dideuteration of selected precursors; ii) the theoretical prediction of  $^2\text{H}$ -RQCs along the chain by computer modelling. The first of these provides key information on the magnitude of RQCs in the middle of the chain, the second made possible modeling of the orientational behavior of the chain in an achiral mesophase (PBG) (see Section 3.2.3), and comparison of the predicted RQC values with those from experiment (see Fig. 49a). As plotted in Fig. 49b, an excellent agreement was obtained between experimental and predicted values, based on an interaction model dominated by steric repulsion between the SFA and the helical polypeptide, modeled as an infinitely long cylinder solid [314].

As a last frontier to be crossed, chiral ANAD NMR was used to analyse the case of homogeneous triglycerides (TGs), the last class of lipids [315].

In accordance with Altmann's definition [316], homogeneous TGs are flexible molecules of  $C_s$  symmetry, on average containing a plane of symmetry  $\sigma$ . They have two enantiotopic side chains for which hydrogen atoms in a given methylene group are diastereotopic and a central chain (that is diastereotopic relative to the two side chains) for which hydrogen atoms in a given methylene group are enantiotopic. In Fig. 50a are reported all stereochemical relationships of tributyrin (TB), a short-chain TG. Its NAD 1D NMR spectrum in achiral isotropic medium exhibits seven resonances corresponding to all the diastereotopic sites of the molecule (50% of the molecule's inequivalent  $^2\text{H}$  sites). Therefore, chiral ANAD NMR is able to discriminate between the two lateral enantiotopic chains, a and c, chains as well as the enantiotopic C-H directions in the central chain b.

The analysis of the series of NAD signals extracted from subspectra from the  $Q$ -COSY Fz spectrum map of TB in PBLG/Py indicates that 95% of the unequivalent  $^2\text{H}$  sites (*i.e.* 19  $^2\text{H}$ -QDs out of 20) are spectrally discriminated (see Fig. 50c). In this example, the number of differentiated sites is in agreement with the theoretical number expected for a  $C_s$ -symmetry molecule (see Figs. 50a,b), which implies that the shape recognition phenomena involved in discrimination mechanisms differentiate the central chain

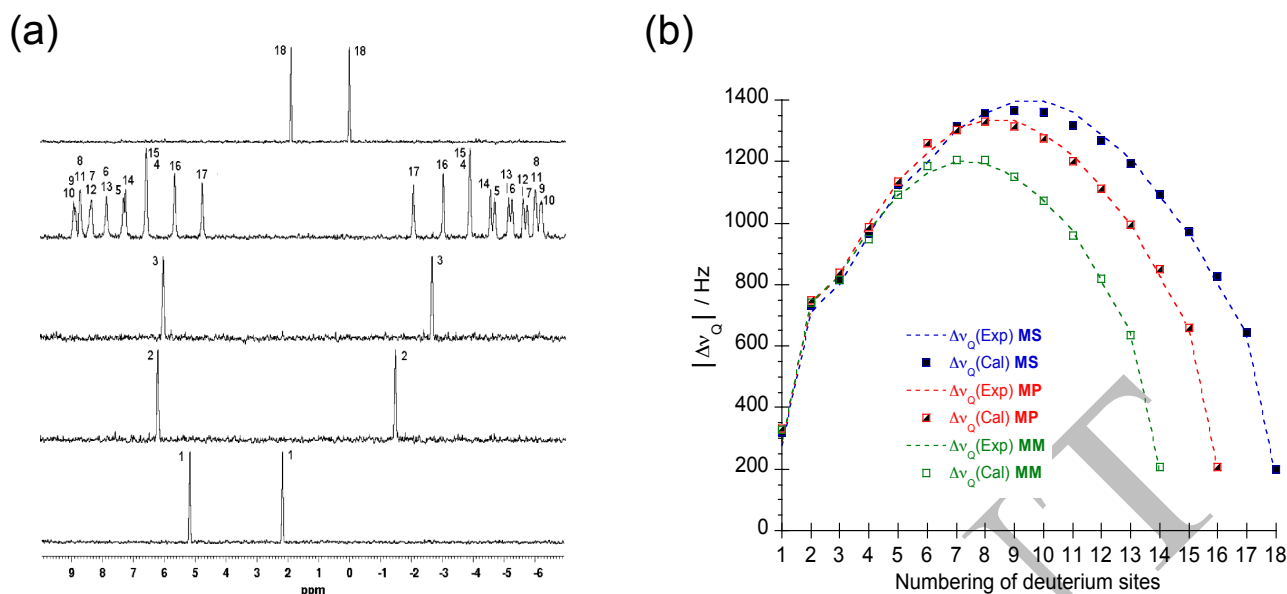


**Fig. 49.** (a) Series of NAD- $\{^1\text{H}\}$  1D subspectra extracted from the tilted 2D map of methyl stearate dissolved in the polypeptide achiral mesophase (PBG/Py). Experimental (dashed lines) and predicted (symbols) absolute values of  $\Delta\nu_{\text{Q}}$ 's as a function of the  $^2\text{H}$  site chain position, for methyl myristate (MM), methyl palmitate (MP) and methyl stearate (MS), all dissolved in PBG/Py. Figure adapted from Ref. [314] with permission.

from the two side chains. Such a favorable situation was unfortunately not the case for trimyristate (TM), since in that case only about twenty  $^2\text{H}$ -QDs out of the theoretically expected 80 were observed (no signal was detected for the glyceryl fragment sites). Deeper analysis of the results of TM have indicated that enantio-recognition mechanisms are no longer able to distinguish the side chains (a and c) from the central chain (b) as they did for TB. In other words, TM behaves more as a  $C_{3v}$ -symmetry molecule instead of a  $C_s$ -symmetry molecule on average. This situation occurs because the ratio ( $V_{a,c}/V_b$ ) of the persistent molecular volume of the side chain ( $V_{a,c}$ ) to the central chain ( $V_b$ ) tends strongly towards unity. Here  $V_{a,b,c}$  corresponds to the 3D space explored by the moving atoms of each chain [315].

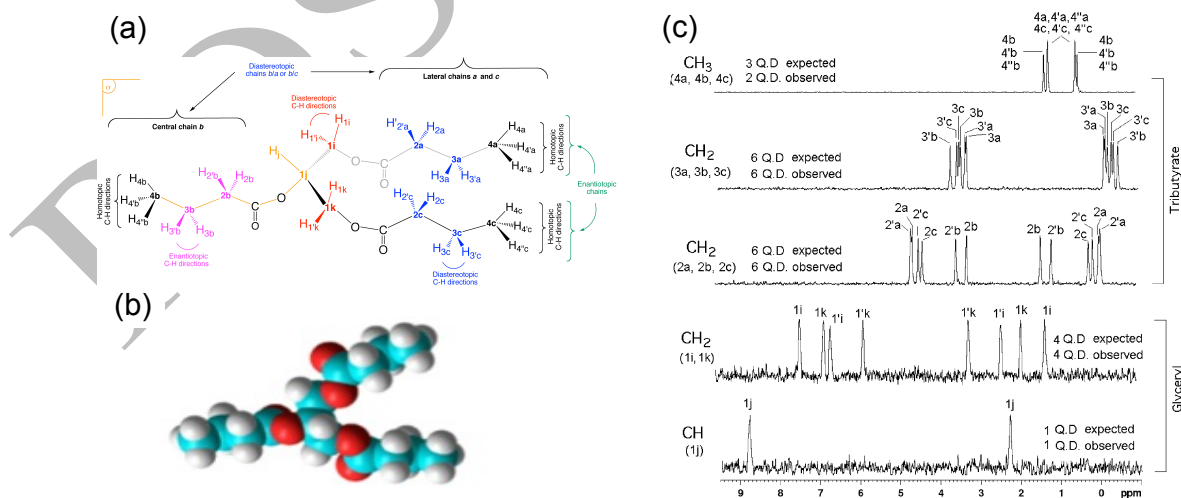


**Fig. 50.** (a) Atomic numbering and stereochemical relationships between the different hydrogenated sites of the glyceryl part (sites i, j, k) and methylene (2 and 3) and methyl (4) groups of the three hydrocarbon chains (a, b and c) of **TB**. (b) Computed 3D structure of the "all-trans" conformer of **TB**. (c) Series of 1D NAD subspectra extracted from the 92.1 MHz tilted Q-COSY Fz spectrum of **TB** in PBLG/Py. The assignment of QDs in relation to the various diastero- and enantiotopic positions is arbitrary. Figure adapted from Ref. [315] with permission.

### 6.4.3. Miliacin and vanilin

Although anisotropic  $\text{irm-}^2\text{H}$  2D-NMR can provide great help to biochemists in answering bioanalytical questions, other disciplines, such as geosciences, can also benefit, in particular because the determination of site-specific isotopic ratios in molecular biomarkers could provide: i) key paleoenvironmental information (analysis of past climatic conditions based on the variation in the isotopic composition of hydrogen (global and/or site-specific) of molecular biomarkers stored in sedimentary archives); ii) help to predict the impacts of diagenesis and to define the essential steps of the biosynthetic process.

So far, GC-irMS was only used by the geochemical community. In order to evaluate the potential of anisotropic  $\text{irm-}^2\text{H}$  NMR for them, the approach has been tested for studying the intramolecular hydrogen isotope profile of miliacin in 2016. Miliacin is a chiral enantiopure triterpene, extracted from broomcorn millet (*Panicum miliaceum* L) (see Fig. 51a) that can be used as a specific geological biomarker, and which is potentially preserved in sedimentary archives [317, 318].

In this new example, the analysis of spectral data extracted from an ANAD 2D map enabled, for the first time, the  $(^2\text{H}/^1\text{H})$  ratios at all methyl sites of this molecule to be determined (see Fig. 51a). From the analysis of variations in  $(^2\text{H}/^1\text{H})$  ratio values at endogenous methyl sites (23-30 sites) and tracking back of their origins in the various reaction steps leading to the miliacin, it has been experimentally determined that the key biosynthetic step is a tail-

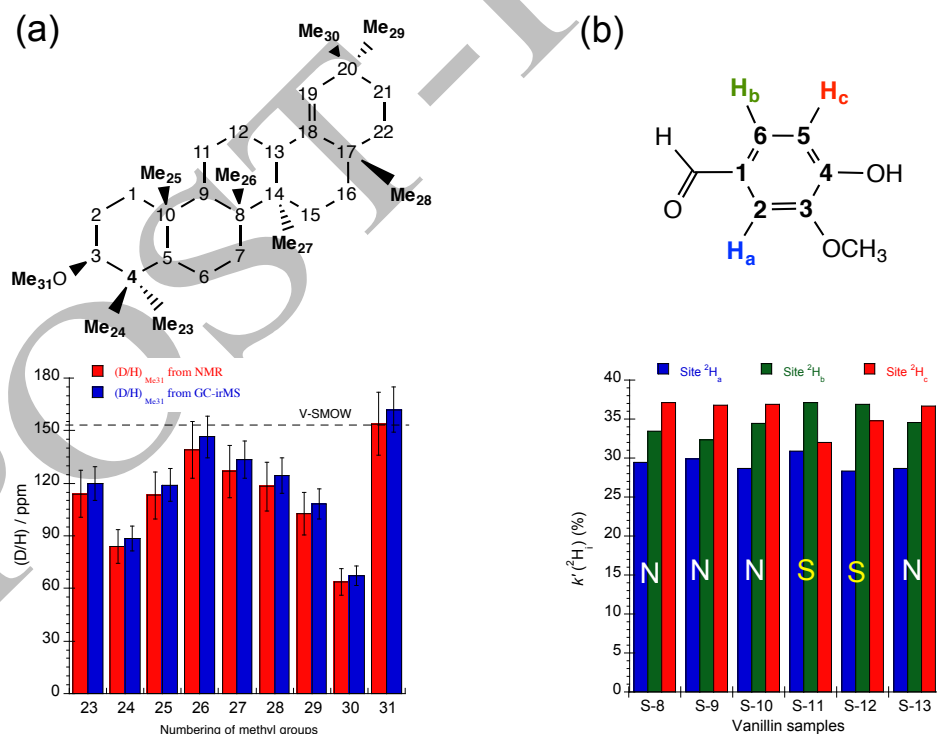


**Fig. 51.** Variations of the  $(^2\text{H}/^1\text{H})$  ratios for methyl groups of miliacin measured from a combination of anisotropic and isotropic  $\text{irm-}^2\text{H}$  NMR measurements (red) and anisotropic  $\text{irm-}^2\text{H}$  NMR / GC measurements (blue). (b) Variations of the relative distribution coefficients of deuterium for the three aromatic sites ( $\text{H}_a$ ,  $\text{H}_b$  and  $\text{H}_c$ ) for different vanillin samples with a natural aromatic core from lignin, ferulic, bean (noted N) and synthetic core from synthetic guaiacol and ferulic acid, (denoted S). Sample 13, of unknown origin (N or S), was identified as being of natural origin according to its relative distribution coefficients. Figure adapted from Refs. [318] and [321], with permission.

to-tail coupling of two farnesyl pyrophosphate units that are then cyclized. In addition, it appeared that this approach should also have the potential to permit the prediction of fractionations during the pentacyclic triterpene diagenesis [318].

More recently, in 2018, the anisotropic  $\text{irm-}^2\text{H}$  2D-NMR has been involved in new and challenging analytical applications associated with molecular authenticity/traceability investigations in food products [319, 320]. Among possible molecular targets, the case of the vanillin, the most widely-used aroma molecule and an important component of perfumery, has been examined, in particular because  $^2\text{H}$  isotopic composition of the aromatic core cannot be evaluated for sites  $\text{H}_a$  and  $\text{H}_b$  ( $\delta(^2\text{H}_a) = \delta(^2\text{H}_b) \neq \delta(^2\text{H}_c)$ ) by isotropic  $\text{irm-}^2\text{H}$  1D-NMR [320, 321]. Using an optimized polypeptide oriented phase (PBLG/ $\text{CHCl}_3/\text{CCl}_4$ ), the  $^2\text{H}$  signal of both sites has been separated on the basis of a difference of  $^2\text{H}$ -RQC magnitude ( $|\Delta\nu_Q(\text{C-}^2\text{H}_a)| \neq |\Delta\nu_Q(\text{C-}^2\text{H}_b)|$ ). Interestingly, the assignment for each  $^2\text{H}$ -QD was possible because the  $\text{C-}^2\text{H}_a$  and  $\text{C-}^2\text{H}_c$  bonds are collinear in the vanillin ( $S_{\text{C-H}_a} = S_{\text{C-H}_c}$ ), leading to equal RQCs for both sites ( $|\Delta\nu_Q(\text{C-}^2\text{H}_a)| = |\Delta\nu_Q(\text{C-}^2\text{H}_c)|$ ).

As seen in Fig. 51b, the variations of the relative distribution coefficients,  $k'(^2\text{H}_{a,b,c})$  of deuterium at three aromatic sites,  $\text{H}_a$ ,  $\text{H}_b$  and  $\text{H}_c$ , corresponding to a fraction of peak areas  $A$ , and defined as:

$$k'_{^2\text{H}_i (i=a,b,c)} (\%) = 100 \times \frac{A_{^2\text{H}_i}}{\sum_{i=a,b,c} A_{^2\text{H}_i}} \quad (30)$$

were found to be different between aromatic rings originating from natural and synthetic origin. In the series of vanillins analyzed, it appeared that the ratios vary as  $\text{H}_a < \text{H}_b < \text{H}_c$  for the samples of natural origin (bean or from natural precursor (ferulic acid or lignin)), whereas the two synthetic samples both show  $\text{H}_a < \text{H}_c < \text{H}_b$ . From these reference isotopic trends, it becomes possible to establish the origin of an unknown sample of vanillin by comparing the distribution coefficients of the three sites against reference data obtained for vanillin of known origin. From an applications viewpoint, these results show that the evaluation of intramolecular  $^2\text{H}$  isotopic composition of the aromatic ring should enable distinctions between materials of natural and synthetic origin, information that can be used in combination with isotopic data for non-aromatic sites of the molecule. From a theoretical point of view, it has been shown from the analysis of all aromatic isotopic data how the  $^2\text{H}$  distribution might relate to the biosynthesis of vanillin [319].

## 7. Pushing the limits: combining the $^{13}\text{C}$ and $^2\text{H}$ anisotropic information

### 7.1. Correlating $^2\text{H}$ with $^{13}\text{C}$ nuclei: the carbon-deuterium correlation in oriented media (CDCOM) 2D experiment

As demonstrated in Section 6, the analytical use of  $^2\text{H}$ -RQCs for isotopically normal or enriched molecules has proved to be a powerful approach in the field of chiral analysis for many applications. The

use of  $^2\text{H}$  homonuclear QUOSY 2D experiments greatly simplifies the analysis of overcrowded ANAD spectra, however assignment of  $^2\text{H}$ -QDs based on  $^2\text{H}$  chemical shifts is not always simple due to the rather low dispersion of  $^2\text{H}$  chemical shifts.

An interesting alternative approach to this particular issue is to acquire anisotropic  $^2\text{H}$ - $^{13}\text{C}$  heteronuclear correlation spectra using pulse sequences derived from the original  $^2\text{H}$ - $^{13}\text{C}$  HETCOR experiment [322, 233].

Using polypeptide CLCs and deuterated analytes, the experiment was renamed as Carbon-Deuterium Correlation in Oriented Media (**CDCOM**) (see Fig. 52a) [245, 324, 325]. In this experiment, the  $^2\text{H}$  magnetization is transferred to  $^{13}\text{C}$  so that one-bond  $^2\text{H}$ - $^{13}\text{C}$  correlations appear in the direct domain at the chemical shift of each carbon nucleus. The resulting spectra provide significant resolution enhancements in the direct domain ( $F_2$ ) as a result of the larger chemical shift dispersion of  $^{13}\text{C}$  nuclei (in ppm) compared to  $^2\text{H}$ . It has been demonstrated that the  $^2\text{H}$ - $^{13}\text{C}$  HETCOR sequence displays higher sensitivity than **HMQC** or **HSQC** sequences using the following expression of the sensitivity [326]:

$$\left(\frac{S}{N\sqrt{T_{\text{tot}}}}\right) \propto f\phi\gamma_{\text{exc}}\gamma_{\text{det}}^{3/2}\cdot\frac{1}{\sqrt{T_{\text{R}}}}\left[1 - \exp\left(-\frac{T_{\text{R}}}{T_1^{\text{exc}}}\right)\right] \quad (31)$$

where  $S/N$  is the signal-to-noise ratio,  $T_{\text{tot}}$  and  $T_1^{\text{exc}}$  are the total experiment time and longitudinal relaxation time of the initially excited nuclei, respectively,  $f$  is the efficiency of the magnetization transfer between the excitation and the detection,  $\phi = 1$  for 2D spectra displayed in phase mode and  $\phi = 1/\sqrt{2}$  for 2D spectra displayed in magnitude mode,  $\gamma_{\text{exc}}$  and  $\gamma_{\text{det}}$  are the gyromagnetic ratios of the excited and detected nuclear species, respectively. For instance, for  $T_1(^2\text{H}) = 0.25$  s, the optimal sensitivity for the  $^2\text{H}$ - $^{13}\text{C}$  HETCOR scheme is obtained for  $T_{\text{R}} \approx 0.3$  s.

After a two-step phase cycle and disregarding all relaxation terms and phase factors, the simplest expression of the NMR signal,  $S(t_1, t_2)$ , for a CDCOM signal from a coupled  $^2\text{H}$ - $^{13}\text{C}$  pair is:

$$\begin{aligned} S(t_1, t_2) \propto & \{ \cos[(2\pi\nu_D - \pi\Delta\nu_Q)(t_1 + \tau)] \\ & + \cos[(2\pi\nu_D + \pi\Delta\nu_Q)(t_1 + \tau)] \} \\ & + \{ \sin(\pi\ ^1T_{\text{C-D}}\tau) \times \sin(2\pi\ ^1T_{\text{C-D}}\tau') \times \exp[i2\pi\nu_{\text{C}}(t_2 + \tau')] \} \end{aligned} \quad (32)$$

An alternative  $^2\text{H}$ - $^{13}\text{C}$  correlation 2D-NMR experiment used in strongly oriented media, called DECOR, was described in 1997 for analyzing perdeuterated mesogenic molecules such as the 4-n-pentyl-4'-cyanobiphenyl (**5CB**), for which the magnitude of  $^2\text{H}$ -RQCs can vary up to a hundred kilohertz [327, 328]. As seen in Fig. 52b, the DECOR 2D experiment is based on a  $^2\text{H} \rightarrow ^{13}\text{C}$  cross-polarization (**CP**) transfer to correlate  $^2\text{H}$  and  $^{13}\text{C}$  signals.

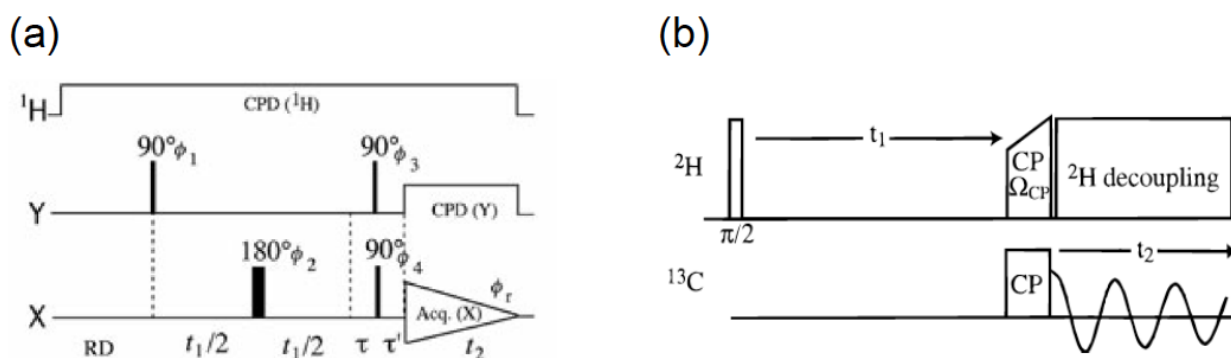


**Fig. 52.** Schematic pulse sequences of (a) CDCOM and (b) DECOR 2D experiments. Note the CP transfer block in the DECOR 2D experiment. Figure adapted from Refs. [245] and [327], with permission.

### 7.1.1. Examples of weakly-aligned deuterated molecules

CDCOM 2D experiments in weakly-orienting solvents were first applied successfully for polydeuterated organic compounds with  $^{13}\text{C}$  at natural abundance dissolved in PBLG/ $\text{CHCl}_3$ . The resulting correlation 2D spectra allow  $^2\text{H}$ -QDs centered at their respective  $^2\text{H}$  chemical shifts, to be linked to their associated  $^{13}\text{C}$  chemical shifts. Thus the CDCOM maps show simply how the magnitude of  $^2\text{H}$ -QDs is distributed with according to  $\delta(^{13}\text{C})$ . In the example of  $(\pm)\text{-}[^2\text{H}_{15}]\text{-2-ethyl-hexanoic acid}$  (see Fig. 53a), the deshielded  $^{13}\text{C}$  signal (C-2) corresponding to the stereogenic center is correlated to the largest  $^2\text{H}$ -RQC, for which the C-D direction is generally expected to be strongly oriented. In contrast, the most shielded  $^{13}\text{C}$  signals (C-6/8) are correlated to the smallest  $^2\text{H}$ -RQCs corresponding to the methyl groups; the weak magnitude of these RQCs results from their position relatively remote from the asymmetric center combined with the conformational dynamics of terminal methyls.

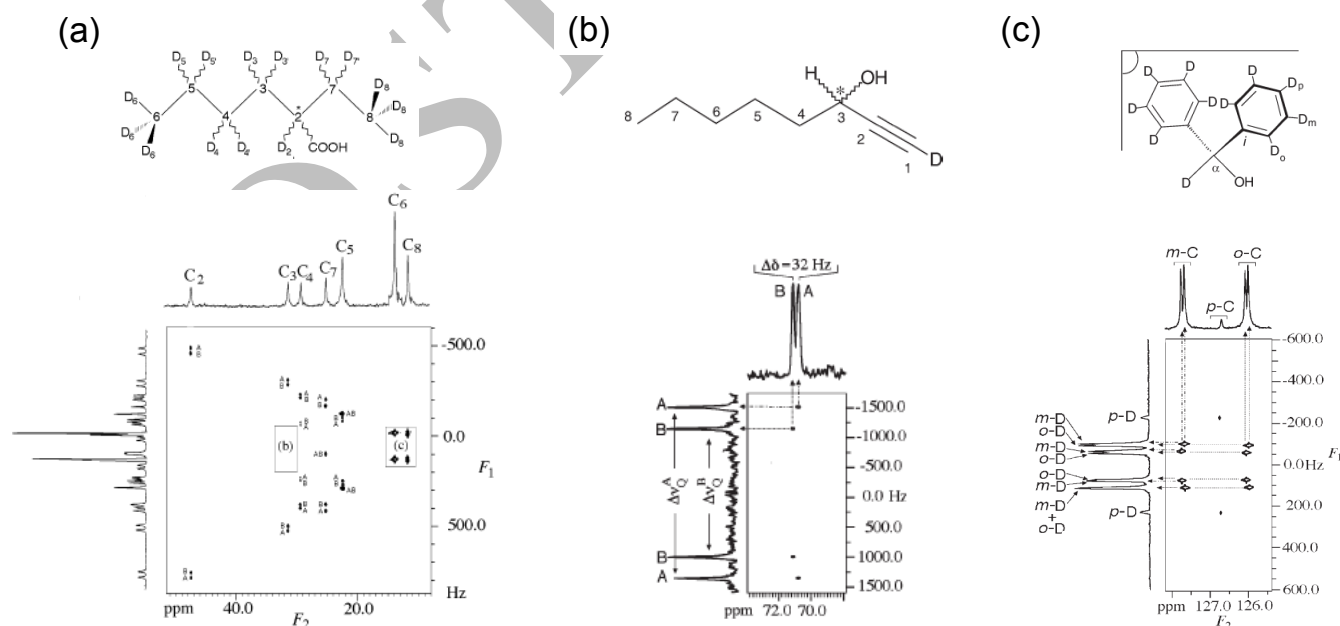


**Fig. 53.** Proton-decoupled CDCOM 2D map of (a)  $(\pm)\text{-}[^2\text{H}_{15}]\text{-2-ethyl-hexanoic acid}$ , (b)  $(\pm)\text{-}[1\text{-}^2\text{H}]\text{-1-octyn-3-ol}$  and (c)  $[^2\text{H}_{11}]\text{-dibenzylmethanol}$  recorded in PBLG phase and showing the simultaneous enantiodiscrimination for both  $^{13}\text{C}$  and  $^2\text{H}$  NMR signals. 2D spectra were recorded at 9.4 T, corresponding to Larmor frequencies for  $^{13}\text{C}$  and  $^2\text{H}$  of 400.1 and 61.4 MHz, respectively. Figure adapted from Refs. [245] and [334], with permission.

For all molecules that have deuterium(s) coupled with  $sp^2$  or  $sp$  carbon atoms, the CDCOM 2D experiments allow correlation of two order-dependent types of spectral information ( $^2\text{H}$ -RQC and  $^{13}\text{C}$ -RCSA), that can be used in complementary ways for the determination of the Saupe order matrix. This can be particularly interesting for the analysis of deuterated chiral molecules and prochiral molecules, for which the doubling of  $^2\text{H}$  and  $^{13}\text{C}$  signals due to enantiomers or enantiopic sites may significantly complicate the spectral analysis (see Figs. 53b and 53c) [324].

### 7.1.2. Analysis of perdeuterated *cis*-decalin

Analysis of *trans* and *cis*-decalin in polypeptide CLCs is an interesting analytical challenge, in particular from the point of view of conformational dynamics [223, 269, 329]. In 2001, the analysis of  $^2\text{H}$  NMR spectra of perdeuterated *cis*-decalin (CDC) in PBLG phase *versus* temperature was described using 1D and homonuclear QUOSY 2D experiments [269].

For this molecule, enantiomeric conformers (CDC-a and CDC-b) of  $C_2$  symmetry exist at low temperature and can be spectrally differentiated using NMR in CLCs. In contrast, at high temperature, CDC can be described as a prochiral structure (CDC-c) of  $C_{2v}$  symmetry (according to Altmann's definition, again [316]) in which enantiotopic elements can be spectrally differentiated using NMR in CLCs (see Fig. 54a). The change in molecular symmetry between low and high temperatures changes the number of resonances ( $^2\text{H}$ -QDs and  $^{13}\text{C}$  singlets) in the

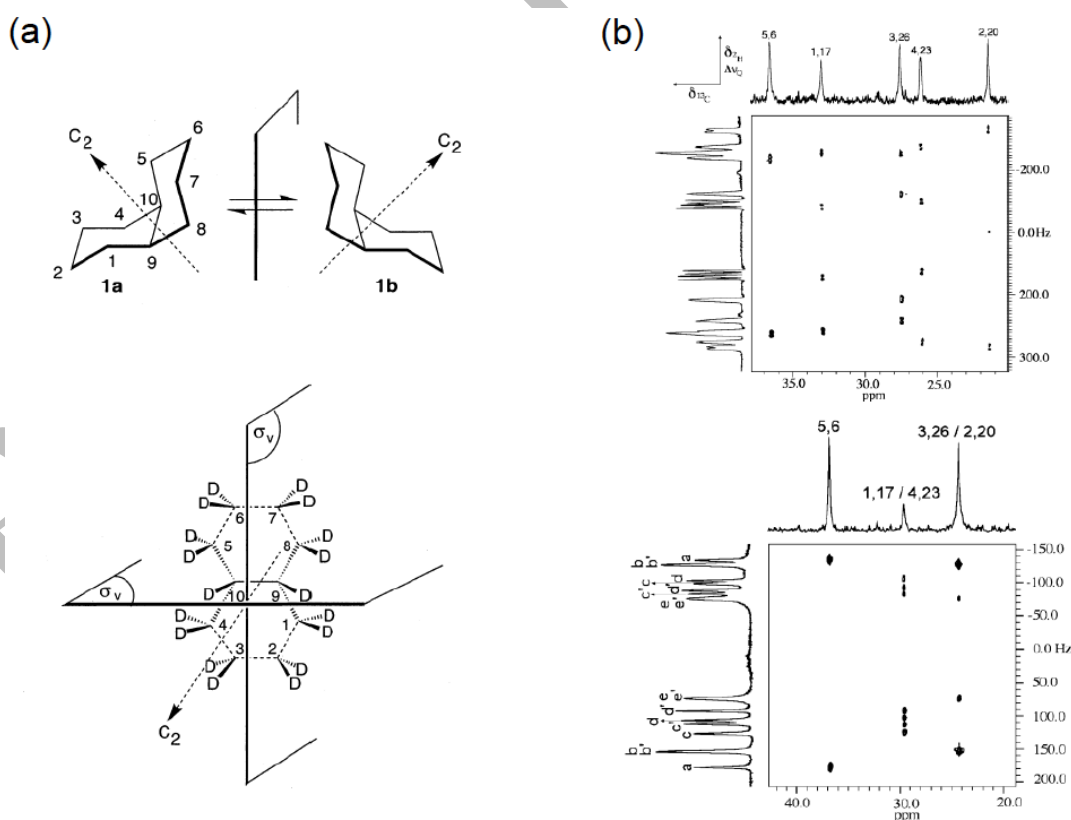


**Fig. 54.** (a) 3D structures of *cis*- $^2\text{H}_{18}$ -decaline along with the  $^{13}\text{C}$  atomic numbering and symmetry elements at (top) low and high temperature (bottom) (see Text). (b) 9.4-T CDCOM 2D spectra recorded in PBLG/ $\text{CHCl}_3$  at (top) low (243 K) and (bottom) high temperature (356 K) recorded in about 15 h. Figure adapted from Refs. [269] and [329], with permission.

anisotropic  $^2\text{H}\{-^1\text{H}\}$  and  $^{13}\text{C}\{-^1\text{H}\}$  1D spectra as can be seen in Fig. 54b [269, 329]. Due to the absence of  $\text{sp}^3$  carbon atoms, the enantiomers of CDC at low temperature are only observed on the basis of  $^2\text{H}$ -RQC differences. Interestingly, the CDCOM experiments allow a direct correlation between the two types of signals as well as a partial assignment of QD from the  $\delta(^{13}\text{C})$ , in particular because in organic solutions of PBLG, the relative positions of  $^{13}\text{C}$  peaks are mostly unchanged compared to isotropic solvents.

## 7.2. The deuterium-carbon-deuterium (DCD) double-transfer based experiments

Another class of  $^2\text{H}\text{-}^{13}\text{C}$  2D experiments has been developed to correlate deuterium and carbon atoms from remote stereogenic centers. This kind of multiple-transfer experiment was proposed in an experimental workframe to address the specific assignment issues for dideuterated *unlike/like* stereoisomers with two remote stereogenic centers of different stereochemistry for each asymmetric carbon [135, 330, 331, 332]. For this purpose,  $^2\text{H}\text{-}^{13}\text{C}$  heteronuclear polarization steps involving a carbon-13 relay were implemented to perform “D  $\rightarrow$  C  $\rightarrow$  D” polarization transfers, thereby generating long range  $^2\text{H}\text{-}^2\text{H}$  correlations through  $^{13}\text{C}$  atoms. Obviously, other multiple heteronuclear transfers can be designed to generate correlations as illustrated in Fig. 55a. In the case of “DCD” transfers, the experiment was named DEuterium CARbon DEuterium Nuclear Correlation spectroscopY), (**DECADENCY**) [331, 332]. They belong to the class of “X-relayed Y,Y-COSY” 2D experiments that was pioneered simultaneously by Lallemand and Wüthrich in 1984 in the case of  $^1\text{H}\text{-X}\text{-}^1\text{H}$  fragments [333, 334].

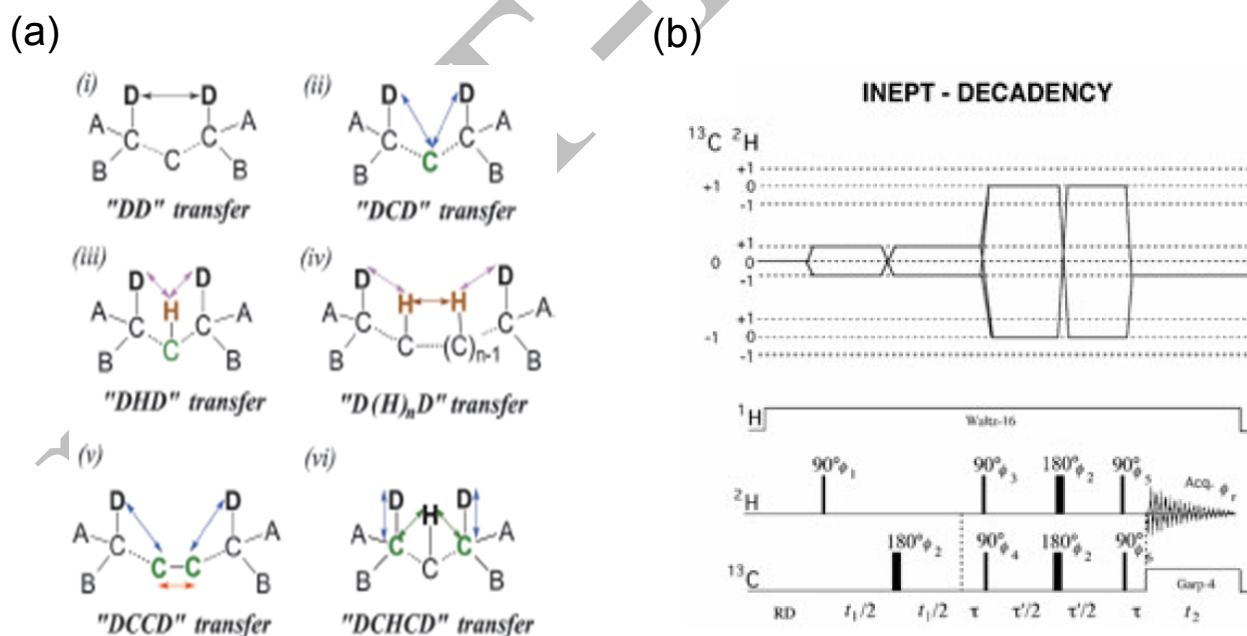


**Fig. 55.** (a) Examples of homonuclear NMR strategies (i to vi) to analyse the mixtures of dideuterated molecules, and involving none, two or four heteronuclear atom(s) as relays. (b) Pulse scheme of the DECADENCY-INEPT 2D sequence along with the coherence transfer pathway diagram. The basic four-step phase cycling is:  $\phi_1 = 2(x)$ ,  $2(x)$ ;  $\phi_2 = \phi_3 = \phi_5 = \phi_6 = 4(x)$ ;  $\phi_4 = 2(x, -x)$ ;  $\phi_r = x, -x, -x, x$ . The GARP-4 CPD sequence suppresses  $^{13}\text{C}\text{-D}$  couplings during the acquisition period. Figure adapted from Refs. [331] and [332], with permission.



To produce a double transfer, either an INEPT- or a DEPT-type transfer is possible. In Fig. 55a is shown the INEPT-DECADENCY pulse sequence, where INEPT transfers are employed. During the variable evolution period  $t_1$ ,  $^2\text{H}$  SQ coherences evolve under the influence of  $\delta(^2\text{H})$  and  $^2\text{H}$ -RQC interactions, while the  $^{13}\text{C}$ - $^2\text{H}$  total couplings,  $T_{\text{CD}}$ , are refocussed by the  $^{13}\text{C}$   $\pi$  pulse at the midpoint of  $t_1$ . In DECADENCY 2D experiments, only cross-correlation peaks provide the relevant information. Thus, during the  $\tau'$  period, only  $\delta(^{13}\text{C})$  are refocused by applying two simultaneous  $^2\text{H}$  and  $^{13}\text{C}$   $\pi$  pulses at the middle point. The antiphase  $^{13}\text{C}$  magnetization is then converted into antiphase  $^2\text{H}$  magnetization with respect to the  $^{13}\text{C}$ - $^2\text{H}$  coupling ( $\text{C} \rightarrow \text{D}^{\text{j,i}}$ ) by again applying two simultaneous  $^2\text{H}$  and  $^{13}\text{C}$   $\pi/2$  pulses.

For INEPT/DEPT-based experiments, the choice of values of the  $\tau$  and  $\tau'$  delays is important and affects the relative intensity of cross peaks (CP's) but also the autocorrelation peak (AP's) and diagonal peak (DP's). In practice, the defocusing and refocusing intervals  $\tau$  must be set as close as possible to  $1/(2|T_{\text{CD}}|)$ . In contrast, the evolution of intensities with  $\tau'$  significantly differs from that calculated for  $\tau$  before.

To illustrate its use, Fig. 56 shows the INEPT-DECADENCY map of phenyl[ $^2\text{H}_2$ ]methanol (**PM**) obtained by setting  $\tau$  and  $\tau'$  equal to  $1/(2T_{\text{CD}})$  and  $1/(4T_{\text{CD}})$ , respectively. Using these conditions, all types of peaks (the autocorrelation peaks (CP), the diagonal peaks (DP), and the (correlation peaks (CP)), are observed. In contrast, when setting  $\tau$  and  $\tau'$  equal to  $1/(2T_{\text{CD}})$  and  $1/(3T_{\text{CD}})$ , respectively, for the same sample, only the CPs are detected, thereby simplifying the spectral analysis.

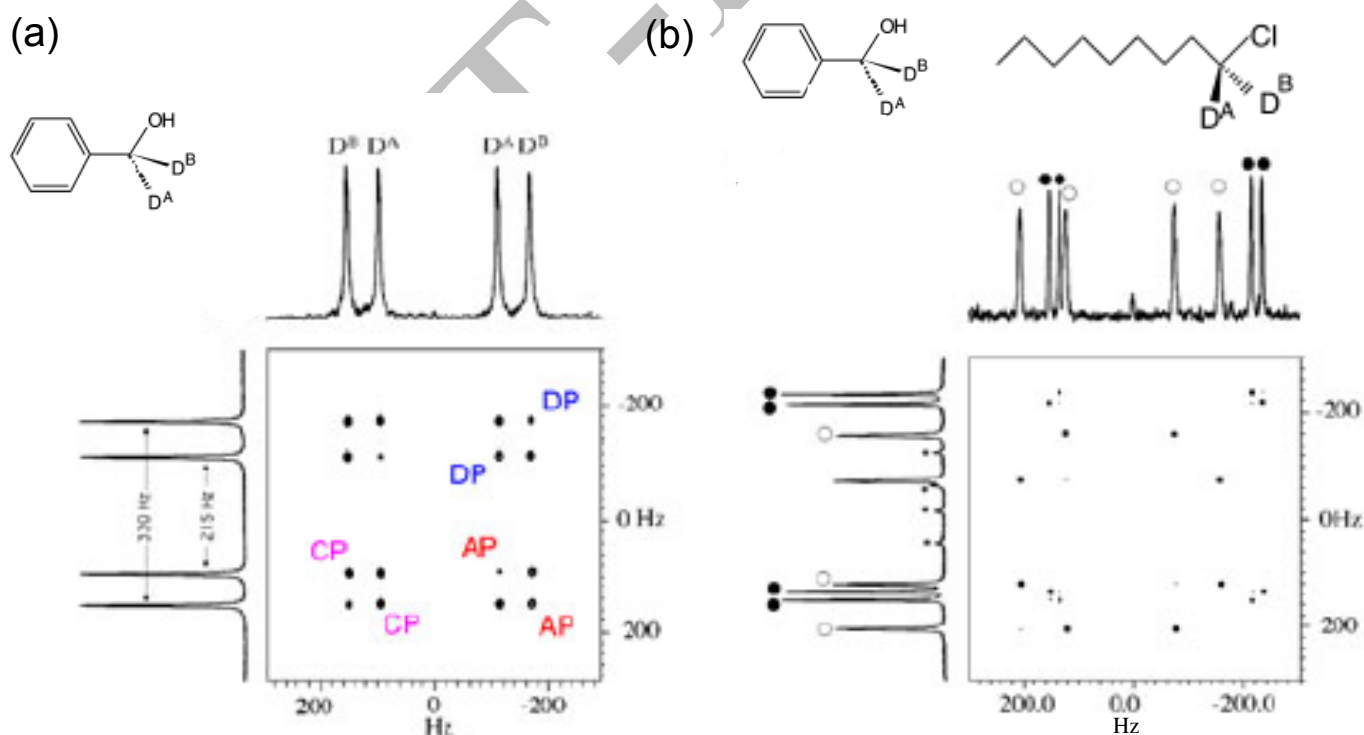


**Fig. 56.** (a) 61.4 MHz INEPT-DECADENCY 2D spectrum of phenylmethanol obtained when (a)  $\tau = 1/(2T_{\text{CD}})$  and  $\tau' = 1/(4T_{\text{CD}})$ . (b) 61.4 MHz INEPT-DECADENCY 2D spectrum of the equimolar mixture of two analytes (the phenylmethanol and the 2-chloro [ $^2\text{H}_2$ ] nonane) obtained when  $\tau = 1/(2T_{\text{CD}})$  and  $\tau' = 1/(3T_{\text{CD}})$ . Note the absence of DP and AP peaks in (b). Figure adapted from Ref. [331] with permission.

### 7.3. First natural abundance spectroscopy deuterium and carbon (NASDAC) 2D experiments: The ultimate frontier?

In the same spirit, natural abundance spectroscopy of deuterium and carbon experiments (NASDAC) were introduced to improve the resolution of QDs in isotopically natural compounds. As in case of the CDCOM sequence, the refocusing block was inserted during the indirect evolution delay, which refocuses only the  $^1T_{C-D}$  couplings (NASDAC) (see Fig. 57a) or both  $^1T_{C-D}$  and  $^2H$  chemical shifts (R-NASDAC) (see Fig. 57b) [326].  $^2H$  magnetization is then transferred to  $^{13}C$  so that one-bond  $^2H-^{13}C$  correlations appear in the indirect domain at the chemical shift of each carbon nucleus.

Compared to CDCOM, coherence pathway selection is ideally achieved by combining both pulsed  $B_0$  field gradients and a phase cycling of 128 steps. This combination is needed to eliminate more than 99.9825% of the signal from ( $^1H-^{13}C$ )-isotopomers, while retaining the desired signals from  $^2H$ ,  $^{13}C$  pairs that occur in only one molecule about 600,000 (using the  $^2H$  and  $^{13}C$ - PDB values).

Randomization pulses applied on the  $^{13}C$  channel before the first  $^2H$  pulse could also facilitate the suppression of signal from ( $^1H-^{13}C$ )-isotopomers, but this approach has not been explored [335]. We also used variants incorporating composite pulses for the first  $90^\circ$  and  $180^\circ$  pulses in order to compensate for offset as well as inhomogeneity and misadjustment of the radiofrequency field [336, 337].

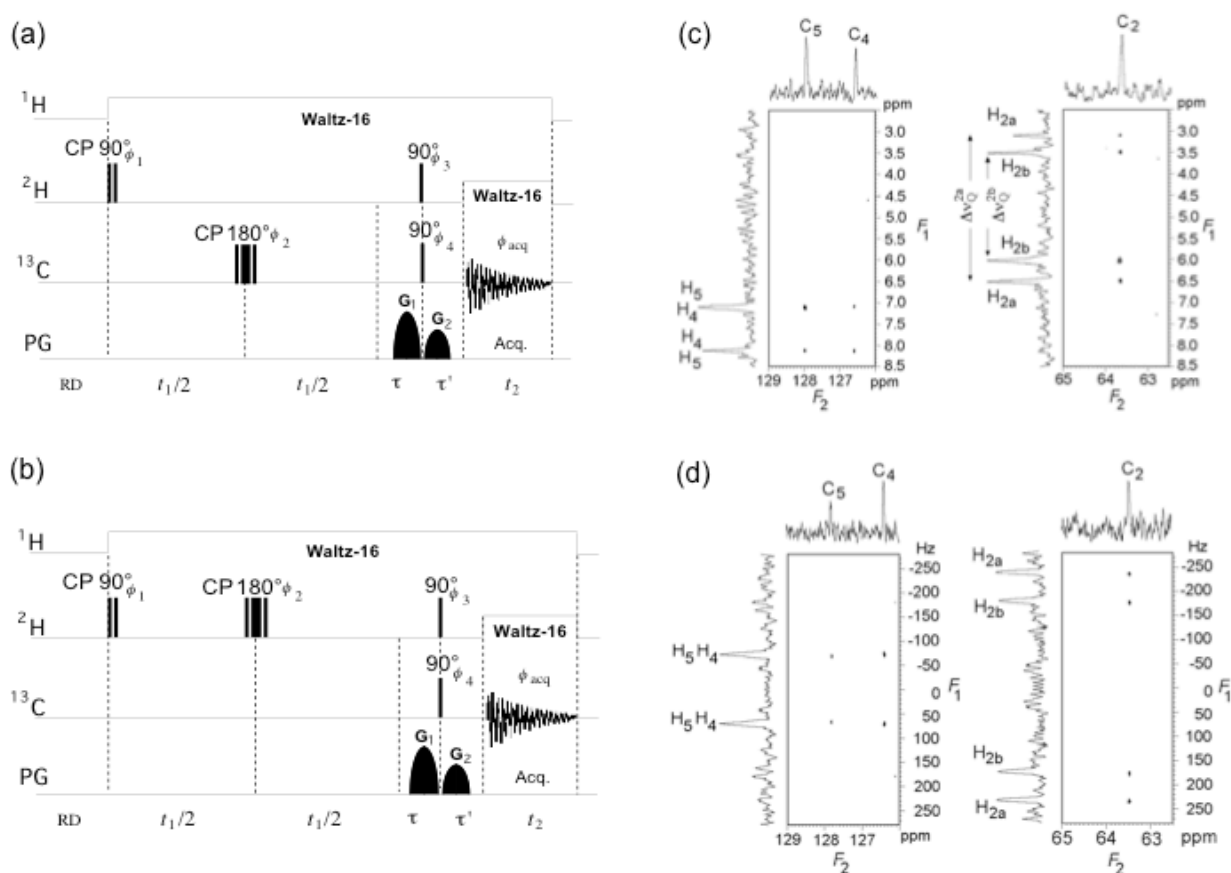


**Fig. 57.** Schematic pulse sequences of (a) the NASDAC and (b) R-NASDAC. (c and d) NASDAC and R-NASDAC (symmetrized map) 2D spectra of benzyl alcohol in PBLG. Maps are centred on the methylenic and aromatic region of the molecule. Figure adapted from Ref. [326] with permission.

These kinds of correlation experiments provided an efficient way of detecting  $^2\text{H}$ - $^{13}\text{C}$  enantiotopomers of benzyl alcohol dissolved in PBLG/ $\text{CHCl}_3$  (see Fig. 57c,d) [326]. Not surprisingly, a small but systematic isotopic shielding of  $^{13}\text{C}$  resonances was measured by comparing the  $F_2$  projection of the NASDAC spectrum with the  $^{13}\text{C}$ - $\{^1\text{H}\}$  1D spectrum both in isotropic and anisotropic solvents. This stems from the isotope effect of  $^1\text{H}/^2\text{H}$  substitution on the  $\delta(^{13}\text{C})$ s, and demonstrates the perfect elimination of  $^1\text{H}$ - $^{13}\text{C}$  and  $^2\text{H}$ - $^{12}\text{C}$  isotopomers [338].

## 8. Exploring other magnetically-active nuclei

Fluorine-19 and phosphorus-31 nuclei are among the most attractive heteronuclear spins  $I = 1/2$ , given their 100% natural abundance as well as their high gyromagnetic ratio. These spin-1/2 nuclei are very similar to proton from the NMR point of view. For both nuclei, their large RCSAs and long-range total spin-spin couplings with  $^1\text{H}$  or heteronuclei, such as  $^{13}\text{C}$ , can be exploited for spectral enantiomeric differentiation in chiral liquid-crystalline solutions. Therefore, they are good probes for determining enantiomeric excesses.

### 8.1. Mono- and trifluorinated probes

First attempts to observe spectral enantiodifferentiation using  $^{19}\text{F}$ - $\{^1\text{H}\}$  NMR were made with chiral compounds in which trifluoromethyl groups,  $\text{CF}_3$ , were deliberately introduced reversibly in order to benefit from: i) the detection of enantiodifferences based on the large values of  $^{19}\text{F}$ -RCSA, resulting in significant  $|\Delta\delta(^{19}\text{F})^{R/S}|$ ; ii) the difference in  $(^{19}\text{F}$ - $^{19}\text{F})$ -RDCs within each  $\text{CF}_3$  group for each enantiomer  $|T_{\text{FF}}^{R/S} = 3 \times D_{\text{FF}}^{R/S}|$  (see Section 2.3.2) [339]. Rapid chemical derivations of alcohols, amines and aminoacids can be performed, leading to demonstrations of the ability of  $^{19}\text{F}$  nuclei to be used in the quantification of enantiodifferentiation as illustrated in Fig. 58a.

Although the difference in ordering between enantiomers generally led to lower differences in the resonance doubling than in the case of quadrupolar nuclei such as  $^2\text{H}$  (see Section 6), the differences in  $^{19}\text{F}$ -RCSA were strong enough to be useful in most cases for  $\text{CF}_3$  probes (see Table 4), as well as for monofluorinated analytes (see Fig. 58b), for reasonable distances (3 to 4 bonds) to the asymmetric centers [195].  $^{19}\text{F}$ - $\{^1\text{H}\}$  NMR was also shown to be powerful for the spectral discrimination of the enantiomers of  $(\pm)$ -2,2,2-trifluoro- $(\alpha)$ -methylbenzylacetamide [237].

Although easy and reversible, the specific incorporation of a  $\text{CF}_3$  group may be seen as a limitation on the practicability of the method. However, it has clear analytical potential whenever fluorine atoms are already included in the solute backbone. This may be particularly appealing when a deuterated probe cannot be easily incorporated into the analyte or when a  $^2\text{H}/^1\text{H}$  isotopic measurement at natural abundance is required.

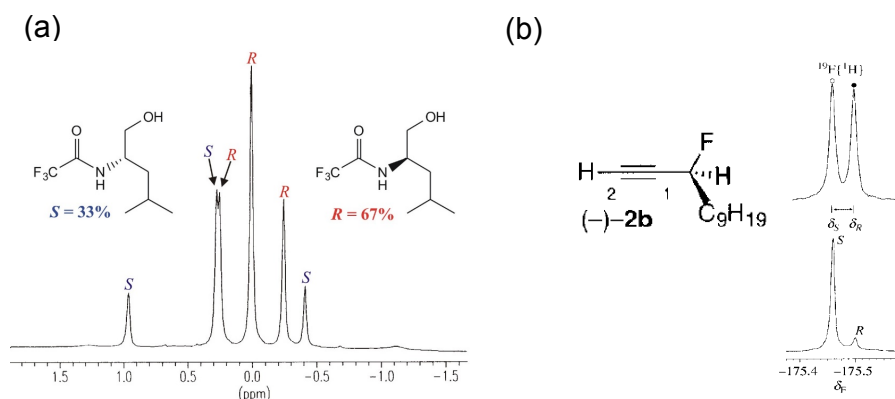


**Fig. 58.** Two examples of  $^{19}\text{F}\{-^1\text{H}\}$  spectra of two fluorinated chiral compounds in PBLG phase: (a) the  $(\pm)$ -2-trifluoroacetamido-4-methyl-1-pentanol and (b) the 3-fluoro-dodec-1-yn in racemic (top) and enantioenriched (bottom) mixtures. Note the spectral enantiodiscrimination on the basis of a difference of (a)  $^{19}\text{F}$ -RCSA and  $(^{19}\text{F}\text{-}^{19}\text{F})$ -RDC and (b)  $^{19}\text{F}$ -RCSA only. Figure adapted from Refs. [195] and [339], with permission.

In the field of biomolecules, substitution of hydrogen by fluorine atoms is quite frequently done to induce some specific biological activity owing to fluorine's high electronegativity [340, 341, 340] and its large van der Waals radius [343].

Recent studies demonstrate the potential of NMR in oriented media for determining the isotropic conformational distribution of fluorinated chiral molecules, such as diflunisal or flurbiprofen [344, 345, 346]. This approach is based on the AP method successfully developed by Emsley, Luckhurst and Stockley for solutes dissolved in thermotropic LCs, which has been applied to experimental residual dipolar couplings recorded in PBLG/co-solvent mesophases combined with *in vacuo* molecular modelling calculations for starting solvent mesophases and starting input conformational distributions [347, 348, 349].

**Table 4.** Differences (Hz) in  $^{19}\text{F}$ -RCSA and in  $^{19}\text{F}\text{-}^{19}\text{F}$  total spin-spin couplings between enantiomers for  $\text{CF}_3$  groups

Structure	$ \Delta\sigma^{R/S} $	$ T_{\text{FF}}^{R/S} = 3 \times D_{\text{FF}}^{R/S} $
	2.5	2.1
	2.5	2.4
	2.5	6.7
	5	7.3
	- <sup>a</sup>	1.4
	7.5	7.3

<sup>a</sup> - : No splitting measurable

In the course of these studies, G-SERF derived 2D-NMR sequences were designed, named gradient-encoded-heteronuclear SERF (**GET-SERF**), to efficiently and accurately extract  $^1\text{H}$ - $^{19}\text{F}$  spin-spin couplings [350]. In CLC, it has been shown that this method i) reveals spectral enantiodifferentiation; ii) determines values of *ee*'s or iii) can be used to extract ( $^{19}\text{F}$ - $^1\text{H}$ )-RDCs of non steroidal (AINS) drugs, such as diflunisal, a difluorinated equivalent to phenylsallylic acid [345].

The GET-SERF 2D experiment has also been successfully applied for analyzing chiral flexible solutes, such as flurbiprofen [346]. Although no tests have been carried out so far, it can also be expected that those experiments are potential tools to simplify the overcrowded  $^1\text{H}$  coupled  $^{31}\text{P}$ -NMR spectra.

## 8.2. Phosphorus-31 nuclei

Numerous organic compounds contain phosphorus-31 atom(s) that can be also used as a potential NMR tool to probe the chirality of molecules. As in case of fluorine-19 nuclei (see above), phosphorus-31 NMR enantiodiscrimination of chiral phosphorylated analytes in CLCs can be observed through a difference of  $^{31}\text{P}$ -RCSA and/or a difference in ( $^{13}\text{C}$ - $^{31}\text{P}$ )-RDCs (and therefore  $T_{\text{CP}}^{R/S}$ ) (see **Section 2**) [60]. The ( $^1\text{H}$ - $^{31}\text{P}$ )-total couplings can be also used, but generally the long-range  $^1\text{H}$ - $^{31}\text{P}$  scalar and dipolar couplings produce unresolved spectral patterns.

The first examples of organophosphorus chiral analytes to be examined in this way were chiral monophosphine oxides and boranes. In this work, the main target was to determine the *ee* of mixtures obtained through reaction pathways that could induce total or partial loss of chirality of the precursor. To ascertain the configurational integrity of the phospholane scaffold, NMR in weakly oriented chiral media was applied as an alternative to chromatographic and isotropic NMR methods (see **Section 1**), which failed to enantioresolve the signals of chiral phosphine oxides and boranes. For this purpose,  $^{31}\text{P}$ - $\{^1\text{H}\}$  NMR and  $^{31}\text{P}$  coupled  $^{13}\text{C}$ - $\{^1\text{H}\}$  NMR experiments in chiral oriented media were applied [60]. In fact, the optimal experiment would have been to record  $^{31}\text{P}$  /  $^1\text{H}$  doubly-decoupled  $^{13}\text{C}$  spectra ( $^{13}\text{C}$ - $\{^{31}\text{P}, ^1\text{H}\}$ ), but these experiments were not possible with the NMR equipment available to the authors at the time (no suitable probe and only a single X-nucleus channel). Examples of spectral enantiodiscrimination of chiral monophosphine boranes using  $^{31}\text{P}$  coupled  $^{13}\text{C}$ - $\{^1\text{H}\}$  NMR in PBLG system are presented in **Fig. 59a**.

On the basis of the spectral patterns observed and analysed (see **Section 2.4**), the enantiomeric composition was determined and it was possible to evaluate the relative magnitude of  $^{13}\text{C}$ -RCSA  $^{R/S}$  and  $|T_{\text{CP}}^{R/S}|$ . For the chiral phospholane-borane compounds investigated in the same study but using PBLG-based CLCs, the differences in  $^{13}\text{C}$ -RCSA between enantiomers were larger than those in ( $^{13}\text{C}$ - $^{31}\text{P}$ )-RDCs. Although the spectral separations are not very large, the deconvolution of signals enabled measurement of the *ee* with a good accuracy [60].

Enantiodifferentiation in weakly oriented mesophases can be improved by adjusting the composition of the solute/polymer/co-solvent mixture and the temperature. For the phosphine oxides, better discrimination was obtained by replacing PBLG by PCBL (see Section 3.2), another polypeptide known empirically to usually induce a stronger ordering for the solute and therefore potentially to increase the quantities  $|T_{C-P}^{R/S}|$  and  $|\sigma^{\text{aniso}R/S}|$ .

For the phosphine oxides, enantiodiscrimination is produced by differences in ( $^{13}\text{C}$ - $^{31}\text{P}$ )-RDCs, since  $\text{sp}^3$  type carbon atoms are investigated.

Finally, it should also be noted that in both classes of organophosphorus compounds,  $^1\text{H}$ -decoupled  $^{31}\text{P}$  or  $^{11}\text{B}$  1D spectra produce sufficient enantiodifferentiation on the basis of differences of  $^{31}\text{P}$ -RCSA or  $^{11}\text{B}$ -RCSA, as well as differences in ( $^1\text{H}$ - $^{31}\text{P}$ )-RDCs. The same spectral features are seen when dealing with cases of phosphonium salts using  $^{31}\text{P}$ - $\{^1\text{H}\}$  experiments [351].

Although these compounds could be reinvestigated using recently heteronuclear  $T_{ij}$ -resolved 2D sequences reported in previous sections, these earlier experimental results demonstrate how enantiodiscrimination can be observed using the X- $^{13}\text{C}$  couplings for X-containing organic analytes. However, the magnitude of these couplings strongly depends on the structure, shape anisotropy and electronic density profile of the solutes investigated. Thus the electronic shielding tensor anisotropy of phosphorous nuclei in a series of phosphorylated atropoisomers (tri-orthosubstituted biphenyls) are different enough between enantiomers to observe for the first time spectral discrimination based on

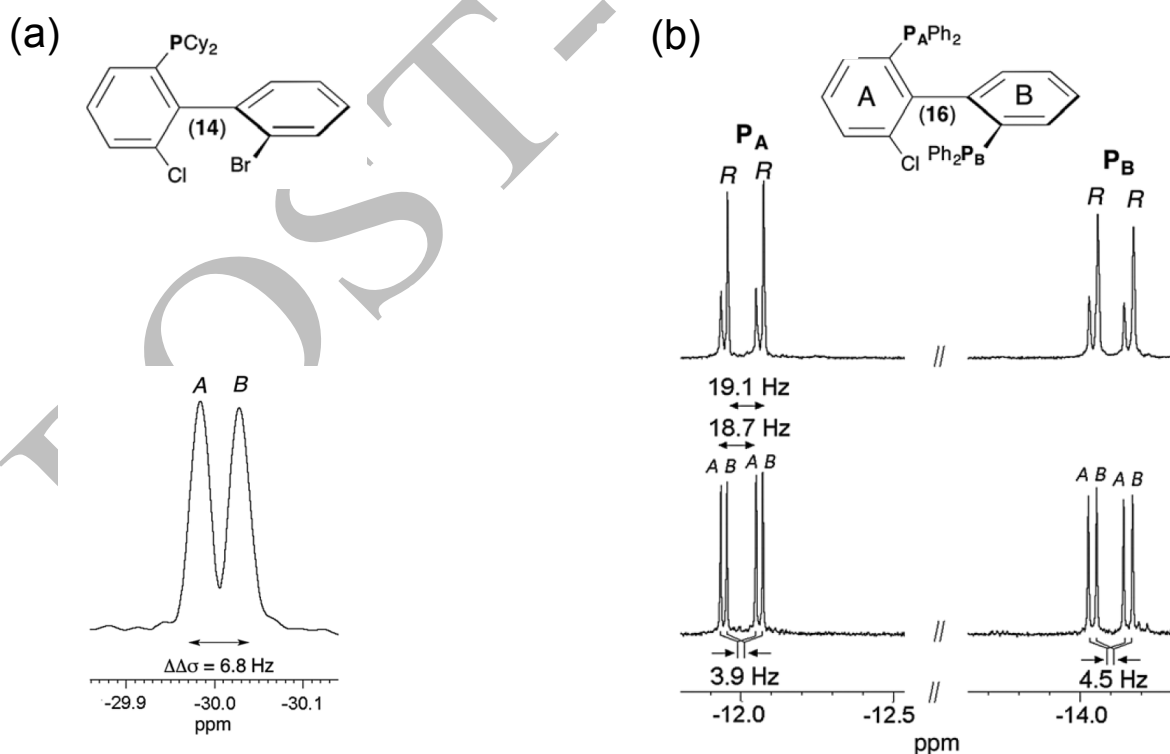


**Fig. 59.** 161.9 MHz  $^{31}\text{P}$ - $\{^1\text{H}\}$  NMR signals of (a) ( $\pm$ )- and (-)-2-diphenylphosphino-2-chloro-2'-bromo-1,1'-biphenyl and (b) of 2,2'-bis(diphenylphosphino)-2-chloro-1,1'-biphenyl in a racemic sample (bottom) and enantioenriched sample ( $ee(R) = 51\%$ ), each of them recorded in PBLG-based CLCs (Ref.  $\delta(80\%$  of  $\text{H}_3\text{PO}_4) = 0$  ppm). The italicized notations "A/B" stand for the chiral stereodescriptors of enantiomers A and B in a racemix mixture. Figure adapted from Ref. [198] with permission.

differences in  $^{31}\text{P}$ -RCSA (see Fig. 59b) [203]. The variability of these results illustrates the strong dependence of enantiodiscrimination mechanisms on molecular structure, shape anisotropy and electron density profile of the solutes studied.

### 8.3. Highly abundant exotic quadrupolar nuclei

Approximately 75%, of NMR-active isotopes possess a spin number greater than  $\frac{1}{2}$ , varying from 1 to 7. Thus only 36 of the 137 isotopes naturally present on the Earth have a spin  $I = \frac{1}{2}$ . While theoretically all quadrupolar nuclei can be detected by NMR, in practice a major limitation for their use originates from the magnitude of their quadrupole moment,  $Q$  [352] that governs the efficiency of quadrupolar relaxation mechanisms, and can lead, for some of them, to unresolved and very broad spectral lines [353].

Few of these isotopes are therefore efficient candidates as NMR probes of molecular entities in oriented media. Among those that are, we can mention the  $^6\text{Li}$ ,  $^{10}\text{B}$ ,  $^{11}\text{B}$ ,  $^{14}\text{N}$  and  $^{133}\text{Cs}$  (see Table 5) and the case of deuterium, a spin-1 isotope with a low natural abundance ( $1.5 \times 10^{-2}$  %), the analytical potentialities of which have been discussed in detail in Section 6 [352].

Second, natural abundance and receptivity are proportional to the cube of magnetogyric ratio and to the product  $I(I + 1)$ , so tentative evaluations can be made for the possibility of recording NMR signals of quadrupolar spins with reasonable signal-to-noise ratio (SNR), experimental time and spectral resolution. Among possible  $I > 1/2$  nuclei explored for enantiodifferentiation purpose in CLCs, Taulelle and co-workers elegantly demonstrated how NMR of quadrupolar nuclei of the ligand, such as  $^{10}\text{B}$ ,  $^{11}\text{B}$  or  $^{14}\text{N}$ , or the metal cation, such as  $^{133}\text{Cs}$ , can be detected to explore the chirality of chiral metal complexes (see Fig. 60) [56, 353, 354]. In their work, these authors were interested in describing the chirality observed at the alkaline cation site, which was induced by the spiroborate junction and mediated by the peristatic chirality of the cavity. Although in solid state it was established by X-rays diffraction studies that the complex  $\text{ML}^2$  exist as racemic mixture, where M is an alkaline metal [354], no experimental isotropic NMR observations confirm this result. To confirm the chiral structure of the cage, the molecular complex was therefore dissolved in PBLG/dichloromethane solvent, and  $^{133}\text{Cs}$  as well as  $^{10}\text{B}$  and  $^{11}\text{B}$  NMR spectra were recorded and presented for  $\text{CsL}^2$  (see Fig. 61a). Although not reported in this paper, the authors stated that complexes formed between the cryptand  $\text{L}^2$  and other cations, such as rubidium or potassium, should behave similarly.

Experimental results obtained using NMR of all quadrupolar nuclei available on  $[\text{CsL}^2]$  complexes (see Fig. 61a,d,g) show a superposition of two sets of signals that could be analysed, deconvoluted and quantified as a 1:1 ratio of both enantiomers as expected (see Fig. 61b,c,e,f,i). Note that neither absolute nor relative configurations are available from the experimental results, but these could have been derived from solid-state assignment.

**Table 5.** Data of main quadrupolar nuclei of interest

Nuclei	Spin $I$	Abundance level (%)	$Q$ (fm <sup>2</sup> )
<sup>2</sup> H	1	1.5 10 <sup>-2</sup>	0.286
<sup>6</sup> Li	1	7.5	-0.081
<sup>10</sup> B	3	19.9	8.459
<sup>11</sup> B	3/2	80.1	4.059
<sup>14</sup> N	1	99.6	2.044
<sup>133</sup> Cs	7/2	100.0	-0.343

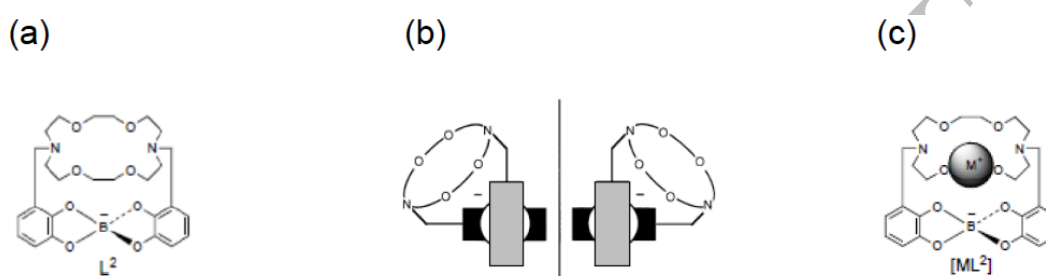


**Fig. 60.** (a) Chemical structure of the chiral ligand  $L^2$ . (b) The chirality of the cryptate is due to the spiroborate connection through the two aromatic rings as shown in the 3D schematic representation. (c)  $[ML^2]$  complexes, where  $M$  is an alkaline metallic cation such as  $K^+$ ,  $Cs^+$  or  $Rb^+$ , or an ammonium group. Figure adapted from Ref. [56] with permission.

Corresponding experiments using <sup>10</sup>B, <sup>11</sup>B and <sup>14</sup>N NMR gave similar results to these when an ammonium group was encapsulated by the  $L^2$  ligand. Here, we only describe the <sup>14</sup>N NMR spectra to exemplify the study (see Fig. 61a, I to III). Note that in all cases, no <sup>14</sup>N NMR signals associated with the ligand backbone are observed, since they have an unsymmetrical environment around the two bridgehead nitrogen atoms leading to quadrupolar interactions large enough that the signal is undetectable.

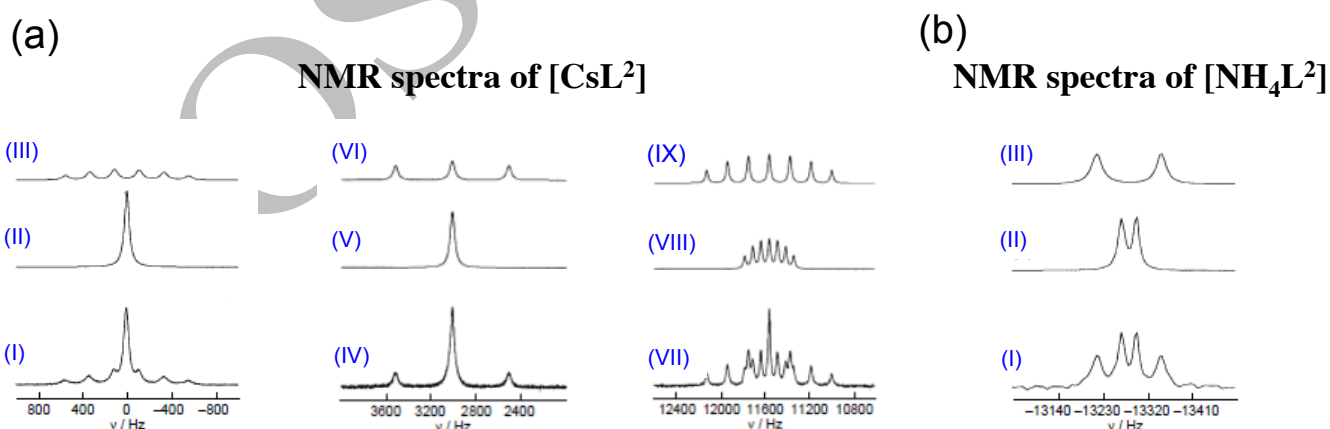


**Fig. 61.** (a) NMR spectra of  $[CsL^2]$ : 53.7 MHz <sup>10</sup>B experimental signals (I) and deconvoluted signals (II and III) of the enantiomers; 160.4 MHz <sup>11</sup>B experimental signals (IV) and deconvoluted signals (V and VI) of the enantiomers; 65.6 MHz <sup>133</sup>Cs experimental signals (VII) and deconvoluted signals (VIII and IX) of the enantiomers. (b) NMR spectra of  $[NH_4L^2]$ : 36.1 MHz <sup>14</sup>N experimental signals (I) and deconvoluted signals (II and III) of the enantiomers. <sup>10</sup>B, <sup>11</sup>B, <sup>133</sup>Cs and <sup>14</sup>N chemical shifts were calibrated with respect to  $BF_3 \cdot Et_2O$ , aqueous saturated  $CsNO_3$  solution and neat  $MeNO_2$ , respectively, as external standards. Figure adapted from Ref. [56] with permission.



## 9. From chirality to prochirality

Prochirality is another important form/geometric property of enantiomorphism with several consequences in chemistry [1]. Unlike chirality, which involves two constitutionally identical molecular 3D objects (enantiomers) that non-superimposable to their mirror images, prochirality involves intramolecular elements (enantiotopic) such as nuclei, groups of nuclei or internuclear directions, which are exchangeable by an improper symmetry operation [1, 41]. Proposing effective tools for spectrally discriminating enantiotopic elements therefore deserves special attention. In this Section, the potential of NMR in CLCs applied to the study of the (rigid or flexible) prochiral molecules and the possibility of discriminating their enantiotopic elements is examined and discussed.

So far isotropic NMR methodologies using chiral solvating agents or chiral lanthanide-induced shift reagents rarely succeeded in resolving signals of enantiotopic elements in prochiral molecules [355, 356, 357, 358]

The few reported examples include the use of cryptand ligands, leading to distinct isotropic chemical shifts for prochiral carboxylic acid groups [357]. Differences in interactions between the enantiopure agent and the enantiotopic elements are usually too small to produce significant difference in isotropic NMR interactions groups [41].

### 9.1. Discrimination of enantiotopic elements in rigid compounds using NMR in CLCs

As for enantiomers, the NMR discrimination of enantiotopic structural elements using NMR in CLCs stems from a difference in their order parameters, while the molecular geometry and magnetic interactions are assumed to be identical for both enantiotopic elements groups [41]. The first experimental enantiotopic discriminations of prochiral solute in polypeptide CLCs were demonstrated in 1996 by  $^2\text{H}$ - $\{^1\text{H}\}$  NMR of deuterated molecules [128]. In that work, it was proven that differentiation of ( $^2\text{H}/^1\text{H}$ ) isotopic enantiomers of  $C_1$ -symmetry chiral molecules was a consequence of the differentiation of enantiotopic elements in the parent  $C_s$ -symmetry prochiral molecules. Fig. 62 illustrates the relationship between dihydrogenated or dideuterated prochiral molecules and the chiral compound in virtue of the ( $^2\text{H}/^1\text{H}$ ) isotopic substitution in the simple case of ethanol. In all generic, achiral structures " $\text{R}_1\text{-CH}_2\text{-R}_2$ " with  $\text{R}_1 \neq \text{R}_2$ , the two methylene hydrogen atoms are enantiotopic, and hence, their corresponding monodeuterated compounds are *de facto* enantiomers. From the point of view of NAD NMR, these enantiomers are named enantio-isotopomers (see also Section 6.5.2).

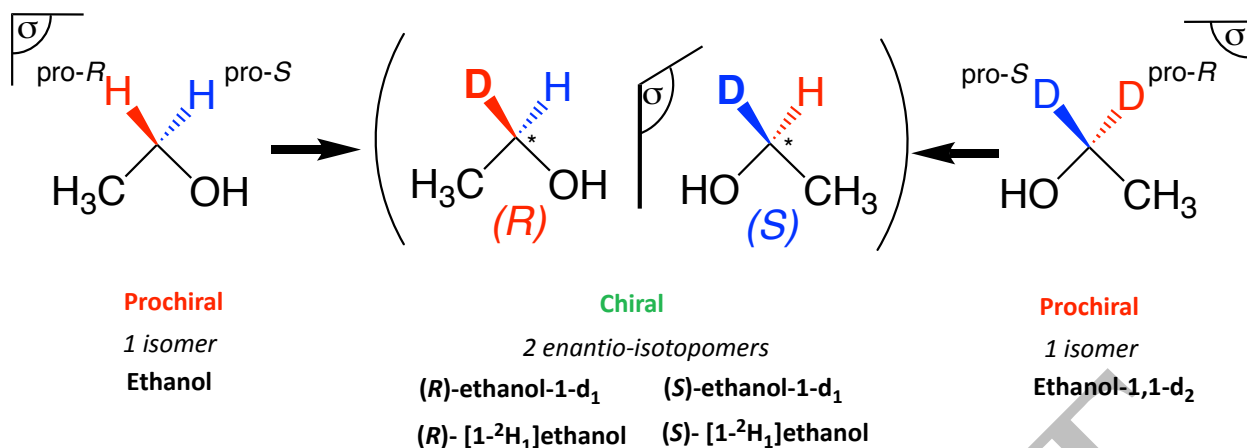


**Fig. 62.** Example of a pair of (D/H) isotopic enantiomers, *R/S*, (in a  $C_1$ -symmetry chiral molecule) detected by NAD NMR (monodeuterated enantio-isotopomers) associated to enantiotopic directions, *pro-R/pro-S*, ( $\text{CH}_2$  or  $\text{CD}_2$ ) of hydrogenated or deuterated prochiral analogous ( $C_s$  symmetry prochiral molecule). Figure adapted from Ref. [308] with permission.

In fact, using group theory, it has been demonstrated that for rigid molecules, the enantiotopic discrimination of prochiral solutes in CLCs for four molecular improper point groups, namely  $C_s$ ,  $C_{2v}$ ,  $S_4$  and  $D_{2d}$  originates from the reduction of their effective molecular symmetry when they interact with a chiral environment. In other words, these four symmetries correspond to rigid molecules having enantiotopic faces, groups of atoms, or internuclear directions, which can be discriminated using NMR in CLCs. This reduction of the effective symmetry increases the number of non-zero independent order parameters of  $S_{op}$  as well as changes in the location of the PAS of the orientational order matrices (see right column of Table 1 in Section 1). Interestingly, the changes in PAS take place on going from ALCs ( $\text{PAS}^{\text{ALC}}$ ) to CLCs ( $\text{PAS}^{\text{CLC}}$ ). For instance, the lowering of effective molecular point group from  $C_s$  to  $C_1$  entails the need to determine two additional order parameters. When the effective molecular point group  $C_{2v}$  is lowered to  $C_2$ , only one additional order parameter, corresponding to the angle  $\alpha$ , needs be defined, since the axis  $a$  parallel to  $C_2$  remains fixed. For  $D_{2d} \rightarrow D_2$  symmetry reduction, the loss of the  $\sigma_d$  planes in CLC renders the axes  $b$  and  $c$  nonequivalent leading to  $(S_{bb} - S_{cc}) \neq 0$ , but their orientation remains fixed. Finally, for  $S_4 \rightarrow C_2$  symmetry reduction, the equivalence of the  $b$  and  $c$  axes is lost and their orientation is changed [41, 363].

In Fig. 63 are portrayed the changes expected in the orientation and equivalence of the PAS of the Saupe order matrix for the four molecular point groups.

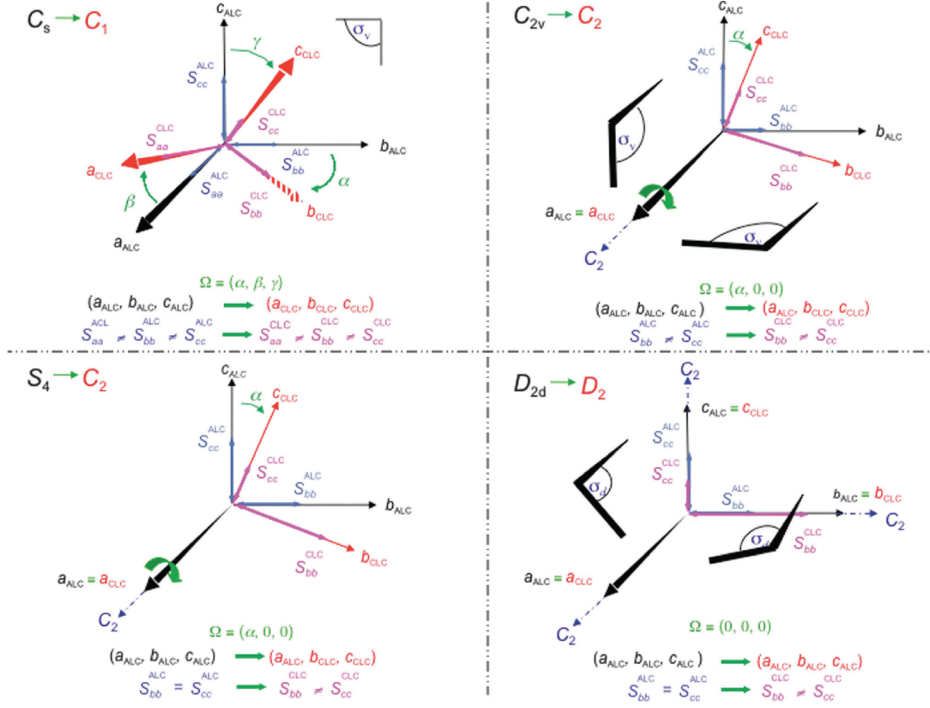


**Fig. 63.** Changes expected in the orientation and equivalence of the principal axes system (PAS) of the Saupe ordering tensor in the four allowed groups, on going from achiral to chiral liquid crystals. All panels follow the same color code. The variation of the length of the double arrows represents the change in the magnitude of the  $S_{ij}$ . Note that in the  $C_s$  group, the angle  $\alpha$  is dependent on angles  $\beta$  and  $\gamma$ . Figure adapted from Ref. [41] with permission.

## 9.2. Principles of symmetric and antisymmetric matrix decomposition

Each term of the total spin Hamiltonian (see Eq. (4)) can be decomposed into isotropic and/or anisotropic terms, and hence can be written as a dyadic of the form [41, 359]:

$$\begin{aligned} \mathcal{H}^k &= A^k \cdot (l^k \mathbf{1} + T^k) \cdot B^k = l^k \cdot A^k \cdot B^k + A^k \cdot T^k \cdot B^k \\ &= \mathcal{H}^k(\text{iso}) + \mathcal{H}^k(\text{aniso}) \end{aligned} \quad (33)$$

where  $A^k$ 's and  $B^k$ 's are (row and column) vector operators, the  $l^k$ 's are isotropic (scalar) interactions and the  $T^k$ 's are corresponding anisotropic (second rank tensor) interactions. To derive further expressions for the enantiotopic discrimination, it is possible to partition the  $T^k$  matrices into their symmetric,  $T^k(\text{sym})$ , and antisymmetric,  $T^k(\text{anti})$ , parts as well as the residue  $T^k(\text{res})$  [41, 359]:

$$T^k = T^k(\text{sym}) + T^k(\text{anti}) + T^k(\text{res}) \quad (34)$$

where  $T^k(\text{sym})$  is invariant by all symmetry operations of the molecular point group,  $T^k(\text{anti})$  is invariant under all proper symmetry operations of the molecular point group and is multiplied by  $-1$  under all improper symmetry operations, and  $T^k(\text{res})$  is neither symmetric nor antisymmetric. In an ALC, directions exchanged by an improper symmetry operation exhibit identical order parameters.

In other words, the  $S$  matrix is symmetric with respect to these operations:  $S = S(\text{sym})$ . The average anisotropic interaction,  $\Delta T^{ki}$ , of a general site  $i$  in a solute dissolved in ALC can be expressed as:

$$\Delta T^{ki}(\text{ALC}) = \frac{2}{3} \sum_{\alpha, \beta = a, b, c} S_{\alpha\beta}(\text{sym}) T_{\alpha\beta}^{ki}(\text{sym}) \quad (35)$$

Unlike homotopic elements that are related by a proper symmetric element, enantiotopic elements exhibit distinct order parameter in CLCs. Hence, the Saupe order matrix,  $S(\text{CLC})$  for an enantiotopic pair in CLC, is equal to  $S(\text{sym}) + S(\text{anti})$  and we have:

$$\Delta T^{ki}(\text{CLC}) = \frac{2}{3} \sum_{\alpha, \beta = a, b, c} S_{\alpha\beta}(\text{sym}) T_{\alpha\beta}^{ki}(\text{sym}) + \frac{2}{3} \sum_{\alpha, \beta = a, b, c} S_{\alpha\beta}(\text{anti}) T_{\alpha\beta}^{ki}(\text{anti}) \quad (36)$$

In Eq. (36), the elements,  $T_{\alpha\beta}^{ki}(\text{sym})$ , associated to enantiotopic pairs, pro- $R$  and pro- $S$ , are equal, while the elements,  $T_{\alpha\beta}^{ki}(\text{anti})$ , are of opposite signs (see Table 3),

$$T_{\alpha\beta}^{k, \text{pro-}R}(\text{sym}) = T_{\alpha\beta}^{k, \text{pro-}S}(\text{sym}) \text{ and } T_{\alpha\beta}^{k, \text{pro-}R}(\text{anti}) = -T_{\alpha\beta}^{k, \text{pro-}S}(\text{anti}) \quad (37)$$

Hence, for an enantiotopic pair in an achiral liquid crystal,

$$\Delta T^{k, \text{pro-}R}(\text{ALC}) = \Delta T^{k, \text{pro-}S}(\text{ALC}) = \Delta T^k(\text{ALC}) = \frac{2}{3} \sum_{\alpha, \beta = a, b, c} S_{\alpha\beta}(\text{sym}) T_{\alpha\beta}^k(\text{sym}), \quad (38)$$

while we have in a chiral liquid crystal:

$$\Delta T^{k, \text{pro-}R}(\text{CLC}) = \frac{2}{3} \sum_{\alpha, \beta = a, b, c} S_{\alpha\beta}(\text{sym}) T_{\alpha\beta}^k(\text{sym}) + \frac{2}{3} \sum_{\alpha, \beta = a, b, c} S_{\alpha\beta}(\text{anti}) T_{\alpha\beta}^k(\text{anti}) \quad (39)$$

and

$$\Delta T^{k, \text{pro-}S}(\text{CLC}) = \frac{2}{3} \sum_{\alpha, \beta = a, b, c} S_{\alpha\beta}(\text{sym}) T_{\alpha\beta}^k(\text{sym}) - \frac{2}{3} \sum_{\alpha, \beta = a, b, c} S_{\alpha\beta}(\text{anti}) T_{\alpha\beta}^k(\text{anti}). \quad (40)$$

Table 6 (see also Table 1 in Section 2) gives the expression of the  $S(\text{sym})$  and  $S(\text{anti})$  matrices for the four symmetry point groups of rigid molecules exhibiting enantiotopic elements, which can be discriminated using NMR in CLCs.

### 9.3. Enantiotopic discrimination investigated by $^2\text{H}$ or NAD NMR

Enantiotopic discriminations were first observed using  $^2\text{H}$  NMR in PBLG mesophases for perdeuterated flexible prochiral compounds with average  $C_s$  symmetry on the NMR timescale [128]. Later they were also reported for the rigid prochiral molecule acenaphthene- $\text{d}_{10}$  with  $C_{2v}$ -symmetry [48, 57]. In fact, the discrimination of enantiomers that are chiral as a result of  $^2\text{H}/^1\text{H}$  substitution (enantio-isotopomers) using NAD 2D NMR indicated the possibility of differentiating enantiotopic directions in their parent cyclic

prochiral compounds, which are rigid cyclic solutes with  $C_s$  symmetry (*endo*-bicyclo[2.2.2]oct-5-ene-2,3-dicarboxylic anhydride, dimethyloxirane, norbornene) and  $C_{2v}$  symmetries (acenaphthen norbornadien, quadricyclane) [41, 359, 360, 361, 362].

Prochiral rigid compounds having  $D_{2d}$  and  $S_4$  symmetries are rare in chemistry. However, ANAD 2D-NMR has allowed the discrimination of the enantio-isotopomers of spiropentane [41] and icosane [363], which demonstrates the possibility of discriminating enantiotopic directions in the parent rigid prochiral compound with  $D_{2d}$  and  $S_4$  symmetries, respectively. In a similar way, it has been shown that enantiotopic directions in 1,3,5,7-tetramethylcyclooctatetraene (TMCOT), which exhibits no dynamic effect at RT, can be discriminated using NMR in CLCs [363, 364]. As an illustration, Fig. 64 presents four examples of the discrimination of enantio-isotopomers using NAD NMR, which are related to the discrimination of enantiotopic C-H directions in rigid prochiral molecules with symmetries  $C_s$ ,  $C_{2v}$ ,  $D_{2d}$  and  $S_4$ .

The discrimination of enantio-isotopomers, and hence of enantiotopic directions in the parent prochiral compounds, has also been reported for other chiral weakly ordering media, such as DNA-based [111] or polyacetylene-based LCs [144], as well as stretched polysaccharide-based gels (i-carrageenan) [365] or swollen cross-linked gelatin [366].

**Table 6.** Explicit Saupe order matrices of rigid molecules with enantiotopic elements, which can be discriminated using NMR in CLCs.

Allowed group & (proper subgroup)	$C_s$	$(C_1)$	$S_4$	$(C_2)$	$C_{2v}$	$(C_2)$	$D_{2d}$	$(D_2)$
$S(\text{sym})^a$	$\begin{pmatrix} S_{aa} & 0 & 0 \\ 0 & S_{bb} & S_{bc} \\ 0 & S_{cb} & S_{cc} \end{pmatrix}$	$\begin{pmatrix} S_{aa} & 0 & 0 \\ 0 & -\frac{1}{2}S_{aa} & 0 \\ 0 & 0 & -\frac{1}{2}S_{aa} \end{pmatrix}$	$\begin{pmatrix} S_{aa} & 0 & 0 \\ 0 & -\frac{1}{2}S_{aa} & 0 \\ 0 & 0 & -\frac{1}{2}S_{aa} \end{pmatrix}$	$\begin{pmatrix} S_{aa} & 0 & 0 \\ 0 & S_{bb} & 0 \\ 0 & 0 & S_{cc} \end{pmatrix}$	$\begin{pmatrix} S_{aa} & 0 & 0 \\ 0 & -\frac{1}{2}S_{aa} & 0 \\ 0 & 0 & -\frac{1}{2}S_{aa} \end{pmatrix}$	$\begin{pmatrix} S_{aa} & 0 & 0 \\ 0 & -\frac{1}{2}S_{aa} & 0 \\ 0 & 0 & -\frac{1}{2}S_{aa} \end{pmatrix}$	$\begin{pmatrix} S_{aa} & 0 & 0 \\ 0 & -\frac{1}{2}S_{aa} & 0 \\ 0 & 0 & -\frac{1}{2}S_{aa} \end{pmatrix}$	$\begin{pmatrix} S_{aa} & 0 & 0 \\ 0 & -\frac{1}{2}S_{aa} & 0 \\ 0 & 0 & -\frac{1}{2}S_{aa} \end{pmatrix}$
$S(\text{anti})^b$	$\begin{pmatrix} 0 & S_{ab} & S_{ac} \\ S_{ba} & 0 & 0 \\ S_{ca} & 0 & 0 \end{pmatrix}$	$\begin{pmatrix} 0 & 0 & 0 \\ 0 & \frac{1}{2}S_{bb} & S_{bc} \\ 0 & S_{cb} & -\frac{1}{2}S_{bb} \end{pmatrix}$	$\begin{pmatrix} 0 & 0 & 0 \\ 0 & \frac{1}{2}S_{bb} & S_{bc} \\ 0 & S_{cb} & -\frac{1}{2}S_{bb} \end{pmatrix}$	$\begin{pmatrix} 0 & 0 & 0 \\ 0 & 0 & S_{bc} \\ 0 & S_{cb} & 0 \end{pmatrix}$	$\begin{pmatrix} 0 & 0 & 0 \\ 0 & \frac{1}{2}S_{bb-cc} & 0 \\ 0 & 0 & -\frac{1}{2}S_{bb-cc} \end{pmatrix}$	$\begin{pmatrix} 0 & 0 & 0 \\ 0 & \frac{1}{2}S_{bb-cc} & 0 \\ 0 & 0 & -\frac{1}{2}S_{bb-cc} \end{pmatrix}$	$\begin{pmatrix} 0 & 0 & 0 \\ 0 & \frac{1}{2}S_{bb-cc} & 0 \\ 0 & 0 & -\frac{1}{2}S_{bb-cc} \end{pmatrix}$	$\begin{pmatrix} 0 & 0 & 0 \\ 0 & \frac{1}{2}S_{bb-cc} & 0 \\ 0 & 0 & -\frac{1}{2}S_{bb-cc} \end{pmatrix}$
$S(\text{CLC})^c$	$\begin{pmatrix} S_{aa} & S_{ab} & S_{ac} \\ S_{ba} & S_{bb} & S_{bc} \\ S_{ca} & S_{cb} & S_{cc} \end{pmatrix}$	$\begin{pmatrix} S_{aa} & 0 & 0 \\ 0 & S_{bb} & S_{bc} \\ 0 & S_{cb} & S_{cc} \end{pmatrix}$	$\begin{pmatrix} S_{aa} & 0 & 0 \\ 0 & S_{bb} & S_{bc} \\ 0 & S_{cb} & S_{cc} \end{pmatrix}$	$\begin{pmatrix} S_{aa} & 0 & 0 \\ 0 & S_{bb} & S_{bc} \\ 0 & S_{cb} & S_{cc} \end{pmatrix}$	$\begin{pmatrix} S_{aa} & 0 & 0 \\ 0 & S_{bb} & 0 \\ 0 & 0 & S_{cc} \end{pmatrix}$	$\begin{pmatrix} S_{aa} & 0 & 0 \\ 0 & S_{bb} & 0 \\ 0 & 0 & S_{cc} \end{pmatrix}$	$\begin{pmatrix} S_{aa} & 0 & 0 \\ 0 & S_{bb} & 0 \\ 0 & 0 & S_{cc} \end{pmatrix}$	$\begin{pmatrix} S_{aa} & 0 & 0 \\ 0 & S_{bb} & 0 \\ 0 & 0 & S_{cc} \end{pmatrix}$
$\Delta T^k(\text{sym})^d$	$S_{aa}T_{aa}^k + \frac{1}{3}S_{bb-cc}T_{bb-cc}^k + \frac{4}{3}S_{bc}T_{bc}^k$	$S_{aa}T_{aa}^k$	$S_{aa}T_{aa}^k$	$S_{aa}T_{aa}^k + \frac{1}{3}S_{bb-cc}T_{bb-cc}^k$	$S_{aa}T_{aa}^k$	$S_{aa}T_{aa}^k$	$S_{aa}T_{aa}^k$	$S_{aa}T_{aa}^k$
$\Delta T^k(\text{anti})^e$	$ \frac{4}{3}(S_{ab}T_{ab}^k + S_{ac}T_{ac}^k) $	$ \frac{1}{3}S_{bb-cc}T_{bb-cc}^k + \frac{4}{3}S_{bc}T_{bc}^k $	$ \frac{1}{3}S_{bb-cc}T_{bb-cc}^k + \frac{4}{3}S_{bc}T_{bc}^k $	$ \frac{4}{3}S_{bc}T_{bc}^k $	$ \frac{1}{3}S_{bb-cc}T_{bb-cc}^k $	$ \frac{1}{3}S_{bb-cc}T_{bb-cc}^k $	$ \frac{1}{3}S_{bb-cc}T_{bb-cc}^k $	$ \frac{1}{3}S_{bb-cc}T_{bb-cc}^k $

<sup>a</sup>  $S(\text{sym}) = S(\text{ALC})$ ; <sup>b</sup>  $S(\text{anti}) = S(\text{CLC}) - S(\text{ALC})$ ; <sup>c</sup>  $S(\text{CLC}) = S(\text{sym}) + S(\text{anti})$ ; <sup>d</sup>  $\Delta T^k(\text{sym}) = \frac{1}{2}(\Delta T^{kr} + \Delta T^{ks})$ ;

<sup>e</sup>  $\Delta T^k(\text{sym}) = \frac{1}{2}(\Delta T^{kr} + \Delta T^{ks})$ .

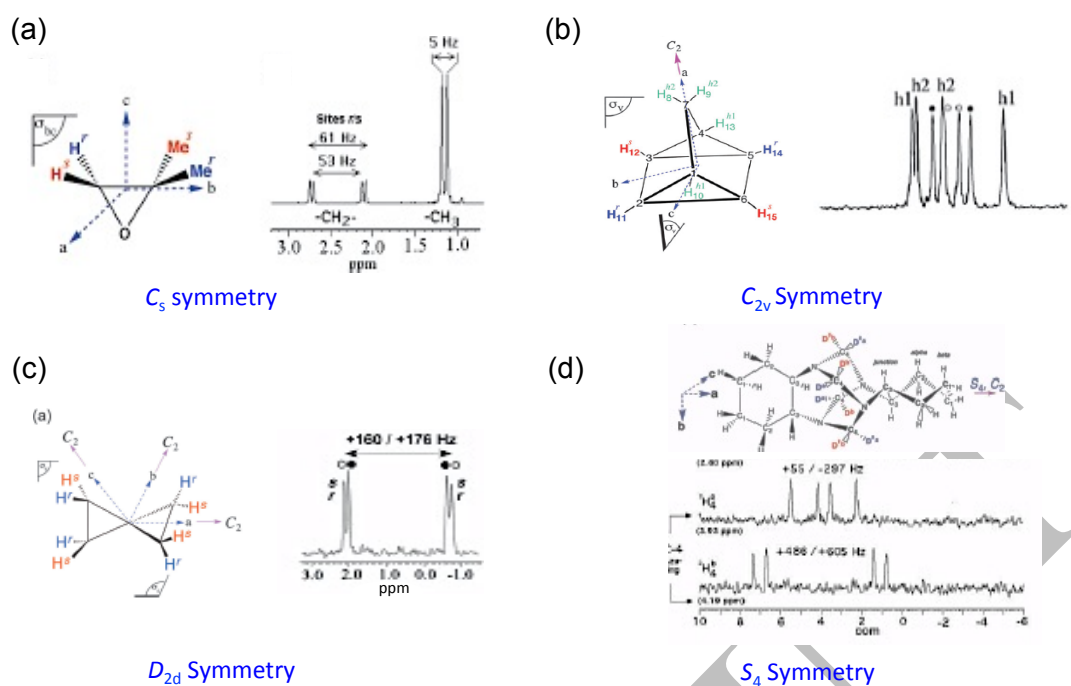


**Fig. 64.** Examples of  $C_s$ ,  $C_{2v}$ ,  $D_{2d}$  and  $S_4$  molecular structures along with axes of symmetry and associated NAD- $\{^1H\}$  enantiodiscriminated signals recorded in a PBLG system and extracted from 1D or 2D (QUOSY-type) spectra: (a) 1,1'-dimethoxyxylene ( $C_s$ ), (b) quadricyclane ( $C_{2v}$ ), (c) spiro[3.3]heptane  $D_{2d}$  and (d) icosane ( $S_4$ ). Figure adapted from Refs. [41], [373] and [361,363], with permission.

#### 9.4. Discrimination of enantiotopic elements in prochiral flexible compounds using NMR in CLCs

The examples of enantiotopic discrimination discussed above correspond to rigid prochiral solutes. Enantiotopic discrimination can also be observed using NMR in CLCs for flexible prochiral molecules. By “flexible” we mean that the molecule rapidly interconverts on the NMR time scale between several conformations. These molecules are often described by a prochiral average structure possessing enantiotopic directions.

For these compounds, a common simplification is to model the conformational exchange as an exchange between stable conformers, which correspond to the minima of the conformational potential energy surface. This assumption is known as the rotamer isomeric state (RIS) approximation [367, 368]. When these transformations are fast (on the NMR timescale, or “feasible” in Altmann’s terminology), the effective symmetry,  $S$ , of the resulting average structure corresponds to the group product of  $G$  and  $I$ , [41, 316,369].

$$S = G \times I \quad (41)$$

where  $G$  is the molecular symmetry group of the conformers and  $I$  the isodynamic group, i.e. the group of symmetry operations, which allows to permute one conformer into another. In a chiral environment, such as a CLC solution, the effective symmetry of the average molecule is reduced to  $S'$ , the proper subgroup of  $S$ , since the improper operations are irrelevant in a chiral environment. For instance, in the case of fast

exchange between the conformers of *cis*-decalin, we have  $G = C_2$  and  $I = C_s$  (see Fig. 54a). Eq. (41) yields an average symmetry  $S = C_{2v}$ , which is reduced to  $S' = C_2$  in CLC [329].

For flexible prochiral molecules, enantiotopic discrimination can be observed using NMR in CLCs, even when  $S$  differs from  $C_s$ ,  $C_{2v}$ ,  $D_{2d}$  and  $S_4$ . For instance,  $^2\text{H}$ - $\{^1\text{H}\}$  NMR in CLC allows discrimination of enantio-isotopomers of molecules with  $S = C_{3v}$ ,  $C_{3h}$  or  $D_{3h}$  symmetry, such as the crown isomer of tri(dioxyethylene) cyclotrimeratrylene [228], the saddle isomer of nonamethoxy cyclotrimeratrylene [369] or tridioxymethylenetriphenylene [370].

Enantiodiscrimination in these cases occurs because the interconverting species comprise different enantiomeric conformers that experience different orientational orderings in the chiral mesophases, and the theoretical treatment given in Section 2 must be generalized. Within the RIS approximation, in an uniaxial nematic phase with the director aligned with  $B_0$  field, the NMR observables, such as the CSA, dipolar coupling and quadrupolar coupling, are proportional to

$$\langle [A_{20}^\Lambda]^L \rangle = \frac{2}{3} \sum_{n=1}^N p_{\text{iso}}(\phi_n) \sum_{\alpha, \beta = a, b, c} [A_{20}^\Lambda]^M(\phi_n) S_{\alpha\beta}(\phi_n) \quad (42)$$

where  $[A_{20}^\Lambda]^L$  is the  $m = 0$  component of the spatial tensor of the anisotropic NMR interaction,  $\Lambda$ : CSA (chemical shift anisotropy),  $D$  (dipolar interaction) or  $Q$  (quadrupolar interaction) in the laboratory frame,  $L$ ,  $\langle \dots \rangle$  denotes the time average over the  $N$  different conformers, which rapidly exchange at the NMR time scale, and all the orientations of these conformers, a conformer  $n$  is characterized by the torsional angles  $\phi_n$ . Eq. (42) assumes that the conformer populations in CLC are identical to those in isotropic solvent,  $p_{\text{iso}}(\phi_n)$ . This assumption usually holds in weakly ordering media.  $[A_{20}^\Lambda]^M(\phi_n)$  denotes the  $m = 0$  component of the spatial tensor of the anisotropic NMR interaction  $\Lambda$  for the conformer  $n$  in the molecular frame  $M$  and  $S_{\alpha\beta}(\phi_n)$  represents the set of order parameters describing the orientation of the conformer  $n$  with respect to the  $B_0$  field.

### 9.5. Differentiation between enantiotopic H $\cdots$ H directions in $C_s$ molecules.

The first successful example of differentiation between enantiotopic directions using proton-coupled  $^{13}\text{C}$  NMR was reported in the case of ethanol, which is a flexible prochiral molecule (see Fig. 65a). In the PBLG/ $\text{CHCl}_3$  phase, the symmetric structure of  $^{13}\text{C}$  signal of C-1 carbon atom can be modelled assuming a AMNX<sub>3</sub> spin system where A is the carbon atom, M, N are the two methylene protons, and X<sub>3</sub> are the three methyl protons, respectively, while the one-bond ( $^{13}\text{C}$ - $^1\text{H}$ )-RDCs for the pro-*R* and pro-*S* C-H directions are different [371]. This result confirms the discrimination of C-D directions of the CD<sub>2</sub> group of [ $^2\text{H}_5$ ]-ethanol using  $^2\text{H}$  NMR in PBLG/ $\text{CHCl}_3$  phase. Furthermore, the asymmetric spectral pattern of the  $^{13}\text{C}$  signal of C<sub>1</sub> of isotopically unmodified ethanol in the PCBL/CHCl<sub>3</sub> phase revealed that the

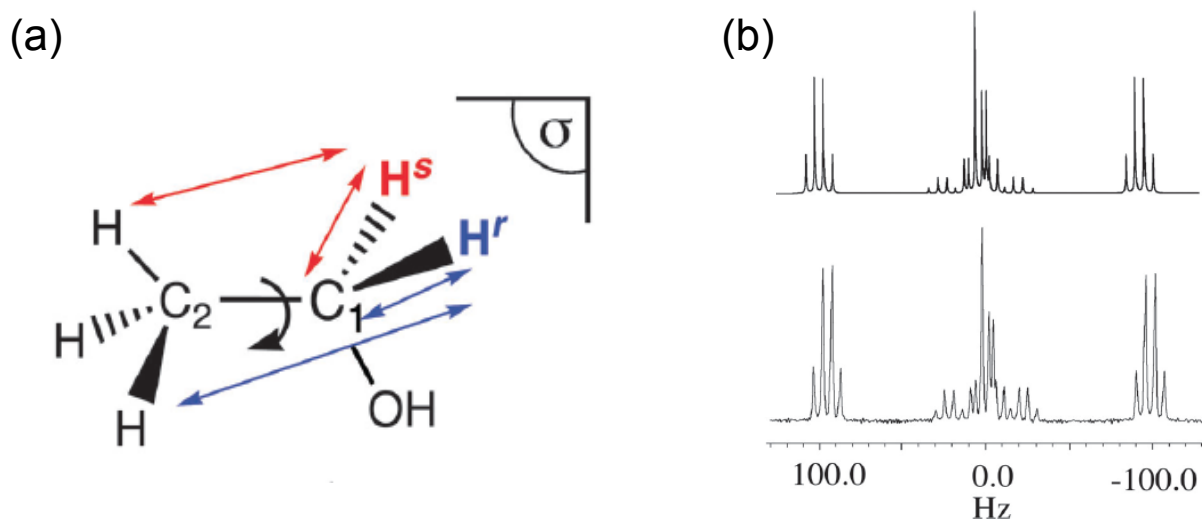


**Fig. 65.** (a) Structure of ethanol showing (by arrows) the pairs of  $^1\text{H}$ - $^1\text{H}$  and  $^{13}\text{C}$ - $^1\text{H}$  enantiotopic directions. (b) Experimental (bottom) and simulated (top) 100.6 MHz proton-coupled  $^{13}\text{C}$  NMR signals of the prostereogenic C-1 carbon obtained in PCBL/CHCl<sub>3</sub> at 300 K. Simulations was made on the basis of a AMNX<sub>3</sub> spin-system with  $\delta_M \neq \delta_N$ ,  $D_{AM} \neq D_{AN}$  and  $D_{MX_3} \neq D_{NX_3}$ . Figure adapted from Ref. [361] with permission.

enantiotopic hydrogens exhibit not only distinct one-bond and three-bond ( $^{13}\text{C}$ - $^1\text{H}$ )-RDCs but also slightly different chemical shifts (see Fig. 65b). This situation clearly indicates the inequivalence of enantiotopic directions between the methylene and methyl protons of ethanol in the CLC.

### 9.6. Differentiation between enantiotopic C-H Directions in $C_{2v}$ molecules containing no prostereogenic tetrahedral center

Rigid  $C_{2v}$ -symmetry molecules without a prostereogenic tetrahedral center are interesting model molecules. Two typical examples are difluoromethane (DFM) and malononitrile (MLN) (see Fig. 66). These non-prochiral molecules may be superimposed upon themselves by an overall rotation, thus producing a structure that is indistinguishable from the original. Consequently, the  $^{19}\text{F}$  and  $^1\text{H}$  nuclei in DFM as well as the  $^{13}\text{C}$ - $^1\text{H}$  nuclei (nitrile group) in MLN are isochronous whatever the solvent used. From the stereochemical viewpoint, the one-bond  $^{13}\text{C}$ - $^1\text{H}$  and  $^{13}\text{C}$ - $^{19}\text{F}$  directions in these molecules are homotopic and so cannot be differentiated even using a CLC. However the  $^{13}\text{C}\cdots^1\text{H}$  and  $^{13}\text{C}\cdots^{19}\text{F}$  (nonbonded) internuclear directions are enantiotopic, and so expected to be distinguished in a CLC. Theoretically an AA'XX' spin system ( $A/A' = ^{19}\text{F}$  and  $X/X' = ^1\text{H}$ ) and AXX' spin system ( $A = ^{13}\text{C}$  of nitrile group and  $X/X' = ^1\text{H}$ ) are expected to be seen for DFM and MLN, respectively. In the PBLG phase, no inequivalence in the ( $^1\text{H}$ - $^{19}\text{F}$ )-RDCs has been detected since the  $^1\text{H}$  and  $^{19}\text{F}$  spectral patterns correspond to those of  $A_2X_2$  spin system. Conversely a sufficient difference in ( $^1\text{H}$ - $^{13}\text{C}$ )-RDCs of MLN in CLC was observed leading to a typical second-order spectral pattern (AXX' spin system) for  $^{13}\text{C}$  signals (C-2/C-3) of nitrile group (that disappear in the PBG ALC) as displayed in Fig. 66b [361]. The transformation of the RAS (a,b,c) into the PAS (a',b',c') can be viewed as a simple rotation around the b axis. Here the tilting angle,  $\alpha$ , between the initial and final planes is equal to  $+14^\circ$  (see Fig. 66c).



The result obtained for MLN raises a fundamental stereochemical issue about the definition of the prochirality concept. Indeed, NMR results suggest that MLN can be regarded as a prochiral compound when interacting with the CLC, while for organic chemists (who generally define prochirality in terms of the practical possibility that an achiral molecule becomes chiral in the course of a single-step chemoselective chiral process), this molecule is not! In fact, the spectral differentiation in CLC of enantiotopic directions in  $C_{2v}$  symmetry molecules without a prostereogenic tetrahedral center has illustrated for the first time an old stereochemical hypothesis made by Mislow and Raban in 1967 which speculated that “for molecules of the type “CXXYY” ..., the two X groups as well as the Y groups are equivalent and cannot be distinguished in chiral or achiral circumstances. However, the relationships between X and Y groups are not all equivalent. The four X-Y relationships may be ordered into two enantiotopic sets of two equivalent relationships” [372]. The NMR result obtained with MLN has in fact validated also a more recent concept: the stereogenicity proposed in 1990 by Fujita who considers that “the compounds (CX<sub>2</sub>Y<sub>2</sub>) can be regarded as prochirals, since the four edges (X-Y) construct an enantiospheric  $C_{2v}(C_1)$  orbit” [373, 374, 375].

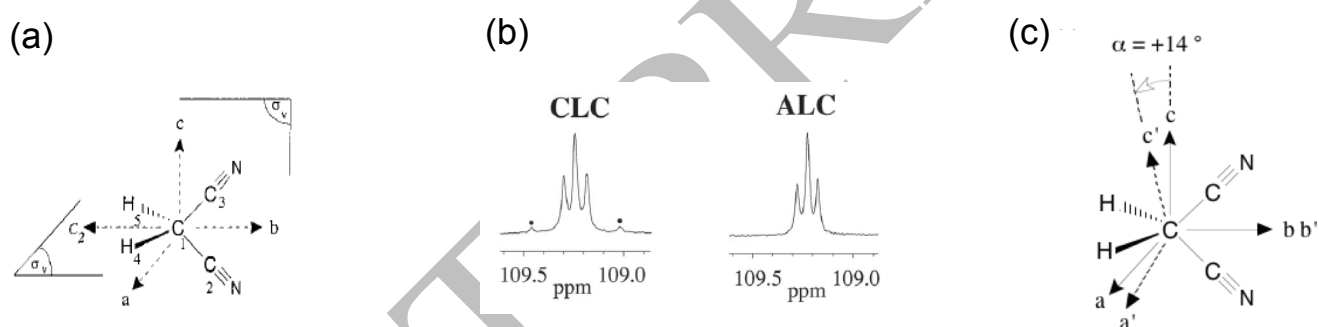


**Fig. 66.** Structure, atomic numbering and coordinates used in the analysis of the proton-coupled <sup>13</sup>C signal of the nitrile carbons of malononitrile. (b) 100.6 MHz proton coupled <sup>13</sup>C NMR spectra of the nitrile groups in CLC (PBLG/CHCl<sub>3</sub>) and ALC (PBG/CHCl<sub>3</sub>). Note the disappearance of external small peaks in the <sup>13</sup>C NMR spectrum in ALC. (c) Representation of the b'c' and a'b' planes relative to the initial bc and ab planes seen from the b axis. Figure adapted from Ref. [361] with permission.

## 10. Anisotropic NMR and structure determination

### 10.1. Using (<sup>13</sup>C-<sup>1</sup>H)-RDCs and <sup>13</sup>C-RCSAs

The determination of chemical structures of small organic molecules from isotropic 2D NMR data is an important challenge for chemists. Initially, this task uses a combination of homonuclear COSY, heteronuclear HMQC/HSQC, and HMBC data involving internuclear scalar couplings. In practice, connectivities obtained from <sup>1</sup>H-<sup>1</sup>H COSY 2D spectra describe the separation of vicinal protons (<sup>3</sup>J<sub>HH</sub>), while <sup>1</sup>H-<sup>13</sup>C HMBC connectivities represent <sup>1</sup>H protons separated from carbon atoms by two to three skeletal bonds (<sup>2,3</sup>J<sub>CH</sub>). Commonly, the set of coupling data is combined with NOE information extracted from NOESY/ROESY 2D maps to establish information on intranuclear distances (distance restraints) and relative angles between internuclear vectors [376].

To help with structure validation, various computer-assisted structure elucidation algorithms have been developed such as “STRUCELUC” or “CASE”, for instance [377, 378]. Interestingly, anisotropic NMR data such as (<sup>1</sup>H-<sup>1</sup>H)-RDCs, (<sup>13</sup>C-<sup>1</sup>H)-RDCs or <sup>13</sup>C-RCSAs (see Section 2) extracted from anisotropic NMR spectra with the help of various multinuclear 1D/2D NMR techniques are also highly structurally informative. Indeed, RDCs and RCSAs contain information on the orientation of various intramolecular directions with respect to the B<sub>0</sub> field, thus leading to the determination of the order matrix of the studied compound. In addition, because the orientation matrix is also directly linked to the molecular geometry, it allows access to the relative orientation of each internuclear vector between NMR active spins within a molecule. Consequently, the RDCs and RCSAs are able to extend the angular and distance range limits of scalar couplings and NOE information, respectively.

The potential of anisotropic data obtained from weakly ordered LC solvents was first explored for refining structures of biomolecules, such as proteins [87, 88, 89, 379, 380] and ribonucleic acids (RNAs) [381], following which the use of RDCs to elucidate the structure of small organic molecules oriented in polypeptide systems was proposed simultaneously by three groups in 2003 [382, 383, 384]. The usefulness of this approach was demonstrated by assigning the diastereotopic positions in methylene groups of chiral compounds (strychnine, menthol) or determining the relative configuration (*cis/trans* geometry) of chiral compounds (dihydropyridone derivatives).

Based on these pioneering results in the field, intensive work has since been carried out on the use of anisotropic data for robust determination of conformation and/or relative configuration of organic analytes (small molecules or drugs) containing multiple stereo-centres. However, a comprehensive overview of these studies (see Section 3) is beyond the scope of this review, and we only present a few salient examples. Interested readers may find many examples in literature, by reading, for example, the work of Luy, Griesenger, Gil, Reggelin, Thiele, Williamson, and collaborators, among many others [101 145, 384-392]. This list is obviously not exhaustive!

In the world of small molecules, both homo and/or heteronuclear RDCs have been used to elucidate the 3-dimensional structure of small molecules of interest, such as peptides [385], organometallics [387] and chiral drugs [344].

A crucial step for these studies is the calculation of the most probable conformer(s). This task is usually accomplished using molecular dynamics (MD) involving DFT calculations. In addition, predicting NMR data with DFT with gauge-including atomic orbital (GIAO) is also highly desirable to reach the right structure(s) of a given molecule of interest. In this context, a possible workflow has recently been proposed [105] for calculating structure(s) that leads to the best fit between NMR-derived and DFT calculated data (see Fig. 67). The first step is dedicated to the generation of the most probable conformers with MD or Monte Carlo (MC) procedures. In the next step these trial structures are

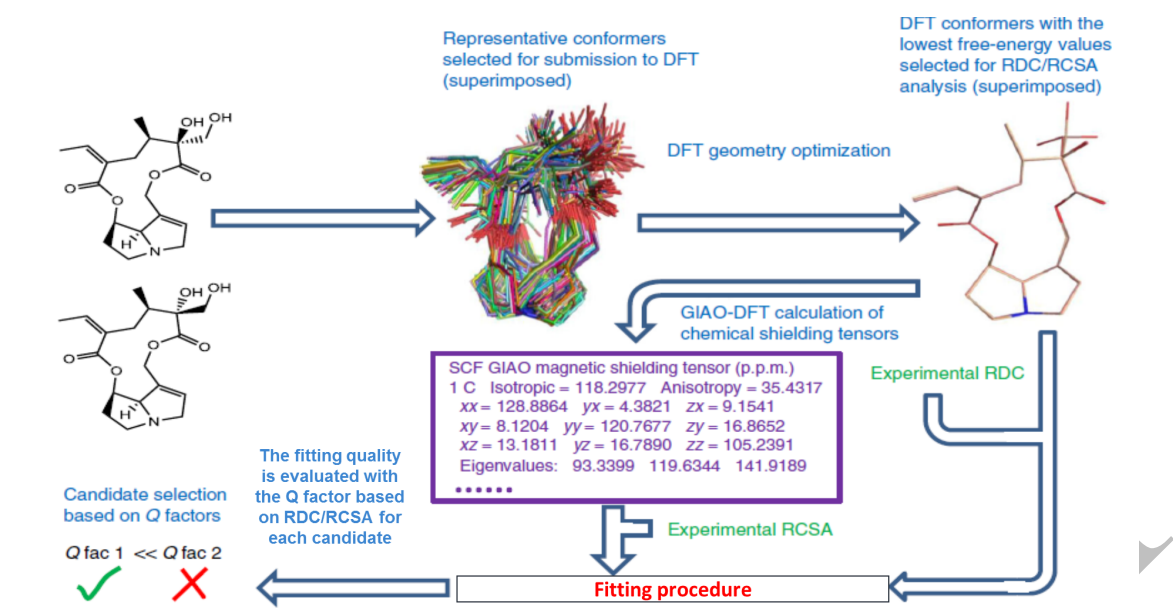


**Fig. 67.** Schematic general workflow for elucidating structure(s) based on anisotropic data. Here the pyrrolizidine alkaloid retrorsine is used as an illustrative example. Figure extracted from Ref. [105] with permission.

submitted to DFT calculations in order to establish the most abundant conformers. The latter are then used to calculate RDCs using, for instance, singular value decomposition (SVD) methods. In parallel, DFT/GIAO calculations give access to calculated RCSAs by considering the most stable conformers. The final step allows for comparing experimental and calculated anisotropic data through a fitting procedure. The best fitting structures having lower Cornilescu's quality factors,  $Q$ , (i.e. closer to zero) [393] are then considered as the best candidate(s) for the molecule under structural elucidation. This 3D structural validation has been exploited by using RDCs [98, 99, 103] or RCSAs [103, 104] or both [105] with natural products, but also to revise their complex structures [389, 390]. Using a set of  $n$  RDCs,  $D_n$ , the Cornilescu's quality factor can be calculated in its simplest form using Eq. (43).

$$Q = \sqrt{\frac{\sum_n (D_n^{exptl} - D_n^{calcd})^2}{\sum_n (D_n^{exptl})^2}} \quad (43)$$

In 2018, a new method implemented within the computational protocol (program ConArch+) was developed based on the use of RDC/RCSA parameters for configurational assignment of chiral compounds [391, 392]. In contrast to the existing calculation protocols [394], the new approach combines floating chirality in 4D- and 3D- distance bounds driven dynamics calculations (geometric constraints from the constitution) with structural information based on RDCs (experimental restraints). This novel procedure allows the simultaneous determination of both the configuration and conformation of analytes. With the same aim, the performance and capabilities of molecular dynamics with orientational constraints (MDOC implemented in COSMOS 6.0 programme) to assign the relative configuration of stereogenic and prochiral centres in small organic molecules was explored in 2019 [395].

## 10.2. Contribution of $^2\text{H}$ -RQCs to structural analysis

### 10.2.1. Structural assignment of RQCs

As with RDCs or RCSAs (see [Section 1](#)), the relevant  $^2\text{H}$ -RQC values can be related to the elements of the Saupe order matrix,  $S_{\alpha\beta}$ , and the molecular geometry of a solute through the orientation of the C-D bonds within an axis system fixed to the molecule (see [Fig. 1b](#)), using [\[329, 362\]](#):

$$\frac{2}{3} \frac{\Delta\nu_{Q_i}^{\text{exp}}}{K_{\text{C-D}_i}} = \sum_{\alpha,\beta=\text{a,b,c}} \cos\theta_{\text{C-D}_i}^{\alpha} \cos\theta_{\text{C-D}_i}^{\beta} S_{\alpha\beta} \quad (44)$$

where all terms have been defined in [Section 2](#).

As mentioned above, the experimental  $^2\text{H}$ -RQC data can be obtained by ANAD NMR. In terms of structure elucidation, this approach benefits from two advantages. First, the  $^2\text{H}$ -RQC are in general one order of magnitude larger than the RDCs (two orders larger than RCSAs), and hence are more sensitive to differences in molecular alignment and molecular structure (see [Section 2](#)). Thus it is possible to access RQCs associated with enantiotopic elements in prochiral molecules [\[41, 329, 362\]](#), or to extract separated sets of  $^2\text{H}$ -RQCs for enantiomeric pairs (in scalemic or racemic mixtures) in the same oriented sample [\[396\]](#).

This can be seen as a real advantage because only a single sample is needed, while two samples of pure enantiomer (*R* or *S*) must be prepared when using ( $^{13}\text{C}$ - $^1\text{H}$ )-RDCs [\[397, 398\]](#), introducing possible uncertainties in terms of sample composition, temperature, or physical homogeneity of the mesophase. Second, as only monodeuterated isotopomers are detected by ANAD NMR, the values of  $^2\text{H}$ -RQCs are not affected by all the  $^1\text{H}$ - $^1\text{H}$  strong coupling effects that frequently hamper an accurate determination of the ( $^{13}\text{C}$ - $^1\text{H}$ )-RDCs in  $\text{CH}_2$  group [\[361, 398, 399\]](#).

The molecular structure can be assessed by comparing the experimental  $^2\text{H}$ -RQC data to theoretical  $^2\text{H}$  values back-calculated from the  $S_{\text{op}}$ . If the experimental  $^2\text{H}$ -RQCs are inconsistent with the structure, a new assignment or a new geometry must be tested. This RQC-based strategy was first explored in 2003 [\[362\]](#), at the same time as strategies using RDCs in PBLG for structure elucidation [\[382, 383, 384\]](#). This approach was first applied to the analysis of rigid prochiral analytes, such as norbornene with  $C_s$  symmetry and quadricyclane with  $C_{2v}$  symmetry, and led to reassessment of some ambiguous  $^1\text{H}$  assignments [\[362\]](#).

[Fig. 68](#) shows the example of a  $^2\text{H}$ -RQC correlation plot ( $^2\text{H}\text{-RQC}^{\text{Calcd}}$  vs.  $^2\text{H}\text{-RQC}^{\text{Exptl}}$ ) obtained for norbornene oriented in the PBLG/ $\text{CHCl}_3$  system. In this example, it was possible to assign nuclei to each enantiotopic face in this  $C_s$  prochiral molecule. This approach proved to be an original tool for probing the diastereotopicity and/or enantiotopicity of solutes, thus providing an alternative to conventional

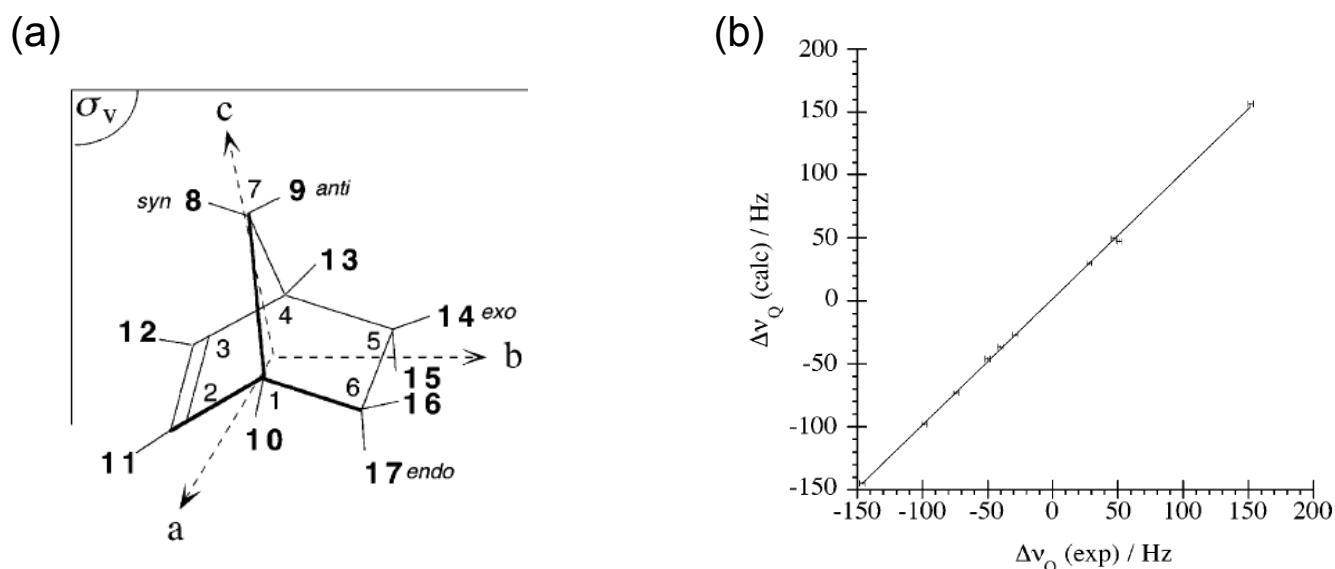


**Fig. 68.** (a) Definition of axes (a, b, c) of the reference molecular frame and numbering of atoms. (b) Correlation plot of back-calculated vs. experimental datasets ( ${}^2\text{H-RQC}^{\text{Calc}}$  vs.  ${}^2\text{H-RQC}^{\text{Exptl}}$ ). Figure adapted from Ref. [374] with permission.

isotropic 2D-NMR. Interestingly, the NAD data for this study had been obtained with a 9.4 T spectrometer equipped with a non-cryogenic classical selective  ${}^2\text{H}$  probe.

### 10.2.2. A hyphenated computational ${}^2\text{H}$ protocol

The above work resorted to manual procedures to calculate the Saupe order matrix. More recently, a hyphenated computational protocol, termed MSpin-RQC, and derived from the MSpin-RDC program developed by Navarro-Vazquez [394] has been proposed for analyzing natural abundance  ${}^2\text{H-RQC}$  data of fenchone (**FCH**), a chiral molecule in a scalemic mixture ( $ee = 30\%$ ), dissolved in PBLG CLCs [396]. This program integrates all steps of the analysis process, including the *ab-initio* calculations (DFT method) of the quadrupolar coupling,  $K_{C-D}$  (see Eq. (14)) and the minimized energy structure, as well as the iterative calculation to match experimental and back-calculated  ${}^2\text{H-RQC}$  data [396].

The general principle of this integrated computational program is schematically depicted in Fig. 69 [397]. In short, the  ${}^2\text{H-RQC}$ -based protocol proposed here can be divided into five key steps: i) the optimization of molecular structure by a DFT calculation; ii) the determination at the same DFT level of the EFG tensors for the  ${}^2\text{H}$  sites; iii) the calculation of the Saupe order parameters from DFT geometry and EFG tensors using the singular value decomposition procedure; iv) the back-prediction of  ${}^2\text{H-RQC}$  values from the calculated Saupe tensor and the prediction of quality factors; v) the calculation, through diagonalization, of Saupe tensor eigenvectors and eigenvalues and related properties, such as Euler angles and asymmetry parameters.

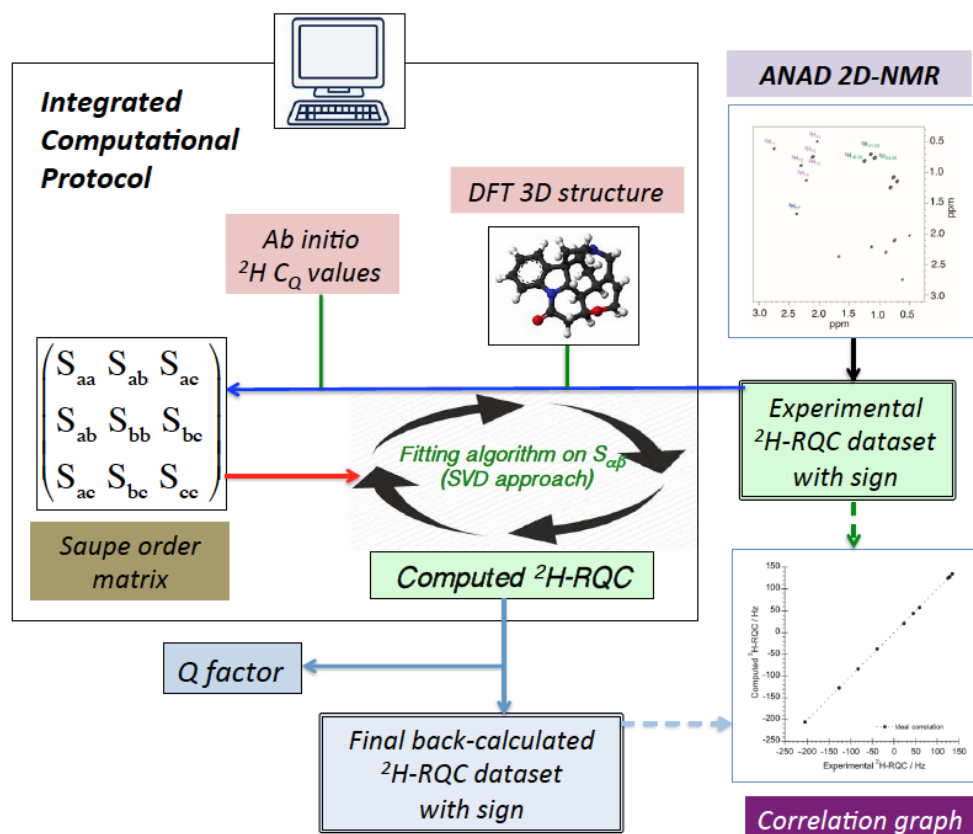


**Fig. 69.** Simplified flow chart showing the principle of molecular structural analysis through <sup>2</sup>H-RQCs extracted from ANAD 2D-NMR experiments, and using the integrated computational program “MSpin-RQC”. The correlation graph simply shows the quality of fit of experimental data (<sup>2</sup>H-RQC<sup>Calc</sup> vs. <sup>2</sup>H-RQC<sup>Exptl</sup>). Figure adapted from Ref. [397] with permission.

This hyphenated computational protocol provides all pertinent data relative to the alignment properties of the solute, including: i) the Sauepe matrix elements; ii) the Euler angles between molecular and PAS axis systems; iii) the axial and rhombic components, and the general degree of order (**GDO**) [394, 396, 401, 402]. Finally, the graphical interface of the program shows the optimized molecular structure and the PAS and/or inertia tensor principal axis. Additionally, the alignment tensor can be graphically represented as a 3D iso-surface corresponding to a particular (positive and negative) value [396].

Fig. 70 displays an example of the graphical screen for enantiomers of FCH, in which the principal axis systems of the Sauepe ( $S_{x'x'}$ ,  $S_{y'y'}$ ,  $S_{z'z'}$ ) and inertia tensors ( $I_{x'}$ ,  $I_{y'}$ ,  $I_{z'}$ ) are simultaneously displayed.

Whatever the source of anisotropic NMR parameters or the protocol used, it is possible to determine the “5D” angle theta,  $\theta$ , between any molecular tensors, for instance between those for enantiomers ( $\hat{S}^R$  and  $\hat{S}^S$ ) as well as between the molecular alignment and inertia tensors ( $\hat{I}^R$  and  $\hat{I}^S$ ). This angle between two tensors, noted  $\hat{A}$  and  $\hat{B}$ , is analogous to an angle between 3D vectors, and it is computed as:

$$\cos(\theta) = \left( \frac{\hat{A} \cdot \hat{B}}{\sqrt{\hat{A} \cdot \hat{A}} \times \sqrt{\hat{B} \cdot \hat{B}}} \right) \quad (45)$$

Here, the dot denotes the scalar product, that is, the sum over all pairwise products in the matrix representation. Using the order tensors  $S_{\alpha\beta}^S$  and  $S_{\alpha\beta}^R$ , for instance, Eq. (45) can be recast as:

$$\theta = \arccos \left( \frac{\sum_{\alpha, \beta = a, b, c} S_{\alpha\beta}^R S_{\alpha\beta}^S}{\sqrt{\sum_{\alpha, \beta = a, b, c} S_{\alpha\beta}^R S_{\alpha\beta}^R \times \sum_{\alpha, \beta = a, b, c} S_{\alpha\beta}^S S_{\alpha\beta}^S}} \right) \quad (46)$$

Interestingly, this angular parameter was used to quantify the efficiency of enantiodiscrimination mechanisms of a CLC towards a pair of enantiomers, to compare difference between Saupe ( $S_{\alpha\beta}$ ) and inertia tensors ( $I$ ), or analyzing two orienting (chiral or achiral) media. It provides an alternative to the Euler angles,  $\theta, \phi, \psi$ , used initially to compare the relative orientation of  $PAS^R$  and  $PAS^S$  in 90's [49, 190]. From a more theoretical viewpoint, the analysis of the inter-tensor angles between enantiomers in CLC or between CLC and ALC provides valuable insights for understanding the global alignment process and the parameters governing enantiodiscrimination mechanisms such as the molecular shape anisotropy or electronic effects. In practical terms, the analyses/rationalizations of experimental data could be of great help in determining the AC of solutes, but also in designing new enantiodiscriminatory liquid crystals [144, 415].

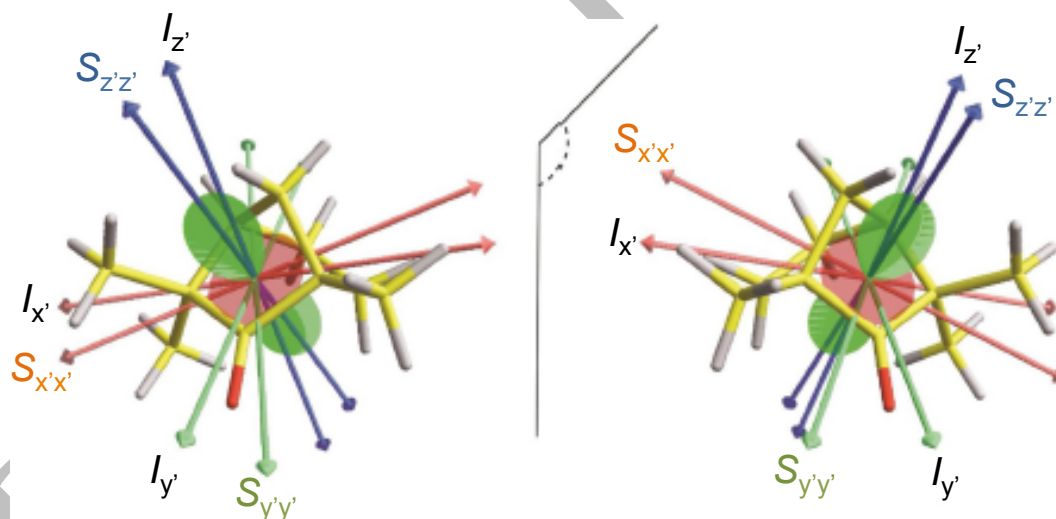


**Fig. 70.** The principal axis system ( $S_{x'x'}$ ,  $S_{y'y'}$ ,  $S_{z'z'}$ ) of the diagonalized Saupe matrix, the inertia tensor axes, ( $I_x$ ,  $I_y$ ,  $I_z$ ), and the Saupe tensor surface representation (red and green surfaces indicate positive and negative  $^2H$ -RQCs, respectively) for (left) (S)-FCH and (right) (R)-FCH oriented in PBLG/ $CHCl_3$ . Figure reproduced from Ref. [396] with permission.

### 10.2.3. Absolute configuration: a $^2H$ -NMR-based empirical approach

In contrast to the problem of relative configuration, the determination of the absolute configuration of enantiomers of small chiral compounds (one stereogenic center) or enantiotopic elements in prochiral molecules using anisotropic NMR is still an unsettled question and remains an analytical challenge, since a general method does not exist, so far [404, 405]. In fact, as the enantiodiscrimination process originates

from a difference in orientational ordering of enantiomers or enantiotopic elements, the *a priori* assignment of AC can be only envisaged *via ab initio* molecular dynamic simulations that could predict such ordering differences [406, 407] from the evaluation of interactions between a helicoidal system and a given analyte [408, 409].

Although interesting results were obtained for achiral oriented solvents, nematic [406, 407] or polypeptide-based systems (PBG) [314], the modelling of CLC as polypeptide systems is still problematic [407].

In mid 2019, the first formulation a mean torque potential sensitive to *P* and *M* chirality of helical solutes aligned in anisotropic media composed of helical particles has been described, leading to the absolute enantiorecognition, when combined with Monte-Carlo-simulated order parameters [412]

In 2007, an empirical approach combining NAD 2D-NMR and CLC for assigning the AC of small chiral molecules was explored [413]. The central concept of this approach relies on the fact that shape recognition plays an important role in molecular ordering/differentiation mechanisms. Thus, the relative magnitude of ordering for each enantiomer, and the difference in their ordering, is expected to be similar for a series of iso-structural chiral compounds dissolved in a given CLC, assuming the same experimental conditions (concentration and *T*). The strategy comprises three steps: i) the optimization of spectral enantiodiscriminations for the compound X1; ii) the analysis of NAD QUOSY 2D spectra for a series of *n* (enantio-enriched) mixtures (X2, X3, ... , Xn) of isostructural chiral molecules for which the AC of the major enantiomer is known; and iii) the assignment of the absolute stereochemistry of NAD signals of X1 from the analysis of NAD 2D spectra of reference molecules.

This empirical approach was first applied to determine the unknown absolute configuration of the major enantiomer in a prepared enantio-enriched mixture of 1,1,1-trifluoromethyl-2,3-epoxypropane (X1) (see Fig. 71a) that had been synthesized in both racemic and enantiopure series. As depicted in Fig. 71b, the analysis of spectral 2D fingerprints of enantio-enriched mixtures shows two important points: i) the relative position (inner/outer) of QDs can be correlated to the major/minor enantiomer (namely the higher/lower peak intensity) in the mixture for the three <sup>2</sup>H sites (2-4); ii) the correlation between the fingerprints and enantiomeric shapes is the same for the various mixtures tested. Based on these repetitive spectral patterns it was concluded that the mixture X1 is most probably enriched in the *R* enantiomer, as named according to the CIP (Cahn-Ingold-Prelog) rules. Interestingly, it has been pointed out that the CIP priority rules (based on the atomic numbers of atoms) classically used to define the *R* (or *S*) stereodescriptors for the two enantiomers are poorly adapted to classify molecules better described in terms of molecular topology. Thus, the problem of stereochemical assignment is approached in terms of iso-structural shapes (in relation with the shape anisotropy), instead of classical CIP rules [1] that do not have a real physical meaning in terms of van der Waals volumes and/or electronic distribution [233, 414].



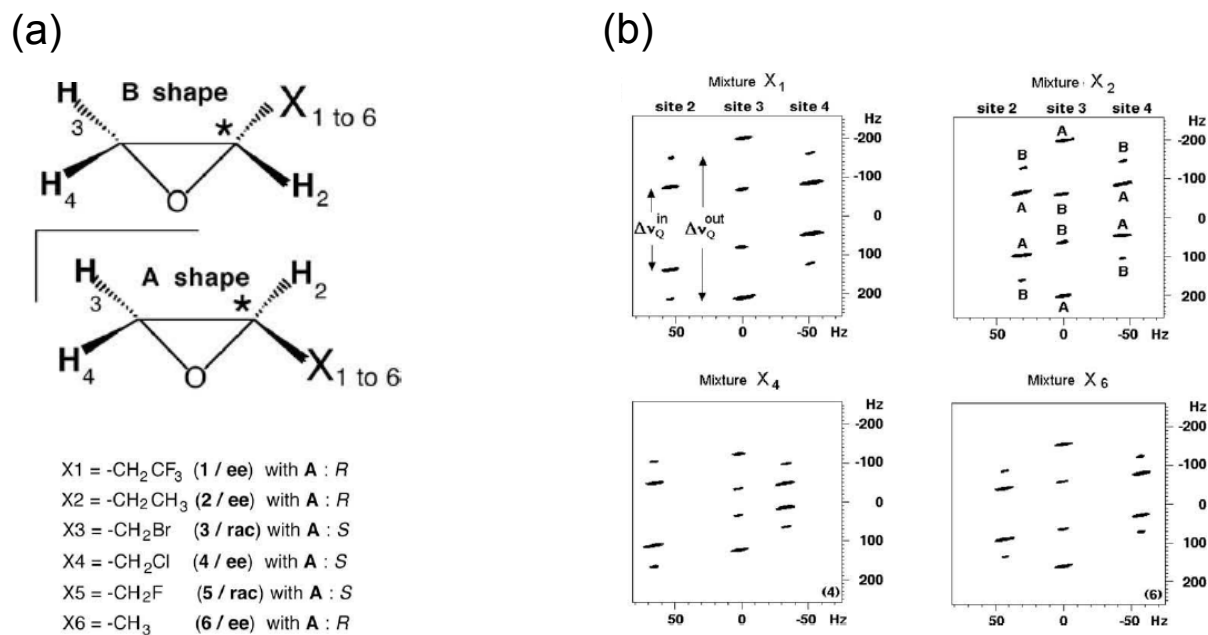


**Fig. 71.** (a) Structure of enantiomeric shapes denoted A and B and nature of substituents (X1-X6). The correspondence between the A shape and the stereodescriptors *R/S* is given. (b) The 92.1 MHz NAD spectral 2D fingerprints associated with three deuterons of the epoxyde ring in compounds 1, 2, 4 and 6 (ee = 33%). Figure adapted from Ref. [413] with permission.

## 11. Conclusion and prospects

NMR spectroscopy of samples dissolved in liquid crystals provides the simplest means to reveal all residual order-dependent intramolecular NMR interactions (RCSA, RDC, RQC) that are no longer averaged to zero as they would be in isotropic liquids. From such spectral data, a wide variety of global or local molecular information on solutes under investigation can be extracted and exploited in various fields of application: 3D structure, configuration and conformational analysis, internal dynamics, natural isotopic distribution determination, and finally molecular stereochemistry, if the alignment system is chiral and enantiopure. Despite these tremendous analytical advantages, NMR in (chiral) liquid crystals has remained relatively confined to the study of small organosoluble compounds because it has been considered as an obscure method by chemists for almost thirty years, mainly due to the complexity of spectral analyses. Clearly, the emergence and the use of weakly aligning media, such as polypeptide mesophases from end of 1980's, has been the starting point of a new adventure, thus leading to the renaissance of anisotropic NMR spectroscopy. The quantity and diversity of research worldwide combining NMR approaches and anisotropic systems since the 1990s have demonstrated the vitality of this exciting and vigorous analytical field.

Among the numerous alignment media used for NMR, those based on helical polypeptides occupy an historical and central place because of their practical convenience, and obviously their enantiodifferentiation properties with respect to the majority of organic chiral molecules. These advantages have been further enhanced by the development of specific NMR methods, including: i) the design of new <sup>1</sup>H, <sup>2</sup>H and <sup>13</sup>C NMR *n*D experiments for simplifying spectra and/or extracting useful data;

ii) the development of original (combined or not) analytical strategies for investigating dynamical behaviour, diastereomorphism of chiral molecules, and enantiotopicity relationships in prochiral molecules; iii) the development of hyphenated computational protocols for structural/configurational elucidation; iv) a toolkit for a better understanding of enantiodifferentiation mechanisms. Like an “analytical Grail”, the ultimate goal of these developments still remains the correlation between the anisotropic NMR signals and the absolute configuration of enantiomers of chiral molecules or enantiotopic positions in prochiral compounds.

Promoting a new NMR methodology to a large community of (non expert) users is a difficult but exciting challenge. Indeed, the reorientation of users' applications requires the evaluation and the demonstration of the advantages but also the disadvantages compared to previous methods. In this comprehensive review, we have tried to familiarize readers with many important aspects of anisotropic NMR, as well as to illustrate the wealth of NMR data that has been obtained in polypeptide CLCs. The sum of all successful results presented in this compendium clearly indicates that this tool is a powerful and original analytical approach that should no longer be ignored by the community of chemists.

Many developments of NMR as applied to polypeptide LC systems have been carried out successively over almost 30 years, based on instrumental (cryogenic probe, new electronics, three-axes gradients, fast and powerful CPU, etc.) and methodological (NUS protocol, spatially encoded experiments, ultra-fast, etc.) advances. New challenges remaining for the future are numerous. We can cite particularly the use of NAD 2D-NMR spectroscopy for the structural elucidation of natural products (a work in progress in 2019). From a more methodological aspect, the development of dissolution dynamic nuclear polarization (**DNP**) can open new avenues to boost the sensitivity of anisotropic NMR of low abundance nuclei as  $^{13}\text{C}$  or  $^2\text{H}$  in high-MW analytes, as well as abundant nuclei as  $^1\text{H}$  when analyzing natural products only available in sub-milligrams amounts amounts [250, 415, 416, 417, 418].

## 12. Acknowledgments

First of all, all the authors who have worked or are still working in the "RMN en milieu orienté" group located in Orsay (Université Paris-Sud/Paris-Saclay) would like to warmly thank Professor Jacques Courtieu to whom this compendium is dedicated. With the exception of N.G., all the authors obtained their doctoral degrees under the supervision of J. Courtieu, before obtaining academic positions (at the University or at the CNRS). Between 1992 and 2012, Jacques Courtieu has contributed to the development of NMR spectroscopy in chiral polypeptide-based liquid crystals dedicated to the chiral analysis and its many applications; twenty years of continuous interest for the anisotropic NMR [419].

The authors would also like to thank all local (ICMMO), national (CEA, ENSCP, ICSN, Universities of Lille, Nantes, Paris VI, Paris VII, Orléans, Rennes, Strasbourg, among others) and international (Brazil, Canada, England, Finland, Germany, India, Israel, Italy, Poland, among others) scientific partners

and colleagues who successfully contributed to all the work compiled in this overview of three-decades, and the help of all French or foreign outstanding students (from Master students to Post-doctoral fellows) and all visitors to our laboratory who also participated, as well.

Special acknowledgment is due to the CNRS and the Université Paris-Sud for their recurrent funding of fundamental research, as well as ANR agency for funding some specific projects.

Finally, P.L. thanks Dr. J.-P. Bayle for his careful reading of this manuscript and his fruitful comments. J.F. warmly thanks his partner S. Bouchet for unflinching daily assistance.

### 13. Special dedications

This article is dedicated to the 75<sup>th</sup> anniversary of Professor Jacques Courtieu in 2019, but a special dedication is also made to three pioneers of NMR in liquid crystals who have actively participated in the development of “NMR in PBLG” in collaboration with the French group. Chronologically, we will mention Professor Aharon Loewenstein (Technion, Haifa, Israel), Professor James W. Emsley (University of Southampton, UK), and finally, Professor Zeev Luz (Weizman Institute, Rehovot, Israel) who recently passed away in October 2018. Images of each of them appear in the last Figure of this review.



*Prof. Jacques Courtieu*



*Prof. James W. Emsley*



*Prof. Aharon Loewenstein*



*Prof. Zeev Luz*

**Fig. 72.** Images of Professors Aharon Loewenstein, James W. (Jim) Emsley and Zeev Luz. Photo Credit: Drs.C. Aroulanda and Philippe Lesot.

#### 14. References and notes

- [1] E.L. Eliel, S.H. Wilen, in *Stereochemistry of organic compounds*, John Wiley & Sons, New York, 1994.
- [2] G. Subramanian, Ed, in *Chiral separation technique, a practical approach*, 2<sup>nd</sup> Ed., Ed. G. Subramanian, Wiley-VCH, Weimheim, 2000.
- [3] T.J. Wenzel, in *Discrimination of chiral compounds using NMR spectroscopy*, John Wiley & Sons, INC. New Jersey, 2007.
- [4] T.J. Wenzel, C.D. Chisholm, Assignment of the absolute configuration of polyfunctional compounds by NMR using chiral derivatizing agents, *Prog. Nucl. Magn. Reson. Spectrosc.* 59 (2011) 1-63.
- [5] J.M. Seco, E. Quiñoá, R. Riguera, The assignment of absolute configuration by NMR, *Chem. Rev.* 112 (2012) 4603-4641.
- [6] S. Kumar Talapatra, B. Talapatra, *Fundamental stereochemical concepts and nomenclatures, in chemistry of plant natural products*, Springer, Berlin, Heidelberg, pp. 23-201, 2014.
- [7] T.B. Freedman, X. Cao, R.K. Dukor, L.A. Nafie, Absolute configuration determination of chiral molecules in the solution state using vibrational circular dichroism, *Chirality* 15 (2003) 743-758.
- [8] J.W. Emsley, J. Feeney, Milestones in the first fifty years of NMR, *Prog. Nucl. Magn. Reson. Spectrosc.* 28 (1995) 1-9.
- [9] R.R. Ernst, G. Bodenhausen, A. Wokaun, in *Principles of NMR in one and two dimensions*, Clarendon press, Oxford Science Publication, 1987.
- [10] M. Levitt in *Spin dynamics, basics of nuclear magnetic resonance*, 2<sup>nd</sup> Ed., Wiley, 2008.
- [11] J. Keller, in *Understand NMR spectroscopy*, 3<sup>rd</sup> Ed., John Wiley & Son, Ltd, 2010.
- [12] H. Günter, in *NMR spectroscopy*, 3<sup>rd</sup> Ed., Wiley-VCH, Weimheim, 2013.
- [13] M.J. Duer (Ed.) in *Solid state NMR spectroscopy: principles and application*, 1<sup>st</sup> Ed., Blackwell Science Ltd, 2001.
- [14] D.C. Apperley, R.K. Harris, P. Hodgkinson in *Solid state NMR: basic principles and practice*, Momentum Press, New York, 2012.
- [15] K. Muller, M. Geppi in *Solid state NMR: principles, methods and applications*, 1<sup>st</sup> Ed., Wiley 2018.
- [16] S.E. Ashbrook, D.M. Dawson, J.M. Griffin, in *Solid-state nuclear magnetic resonance spectroscopy*, Eds. D.W. Bruce, D. O'Hare, R.I. Walton Local structural characterization, John Wiley & Sons, Ltd, Chichester, pp. 1-88, 2014.
- [17] A.D. Buckingham, Chirality in NMR spectroscopy, *Chem. Phys. Lett.* 398 (2004) 1-5.
- [18] A.D. Buckingham, Chiral discrimination in NMR spectroscopy, *Q. Rev. Biophys.* 48 (2015) 421-423.
- [19] A.D. Buckingham, Direct chiral discrimination in NMR spectroscopy, *Chem. Phys.* 324 (2006), 111-116.
- [20] J.I. Santos, I. Rivilla, F. P. Cossío, J.M. Matxain, M. Grzelczak, S.K.S. Mazinani, J.M. Ugalde, V. Mujica, Chirality-induced electron spin polarization and enantiospecific response in solid-state cross-polarization nuclear magnetic resonance, *ACS Nano* 12 (2018) 11426-11433.
- [21] H.D.W. Hill, A.P. Zens, J. Jacobus, Solid-state NMR spectroscopy. Distinction of diastereomers and determination of optical purity, *J. Am. Chem. Soc.* 101 (1979) 7090-7091.

- [22] K.V. Andersen, H. Bildsoe, H.J. Jakobsen, Determination of enantiomeric purity from solid-state  $^{31}\text{P}$  MAS NMR of organophosphorus compounds, *Magn. Reson. Chem.* 28 (1990) S47-S51.
- [23] M.J. Potrzebowski, E. Tadeusiak, K. Misiura, W. Ciesielski, G. Bujacz, P. Tekely, A new method for Distinguishing between enantiomers and racemates and assignment of enantiomeric purity by means of solid-state NMR. Examples from oxazaphosphorinanes. *Chem. Eur. J.* 8 (2002) 5007-5011.
- [24] J.E. Tadeusiak, W. Ciesielski, S. Olejniczak, The determination of enantiomeric excess of valine by ODESSA solid-state NMR experiment, *Magn. Reson. Chem.* 44 (2006) 905-983.
- [25] M. J. Potrzebowski, A. Jeziorna, S. Kaźmierski, NMR studies of chiral organic compounds in non-isotropic phases, *Concept Magn. Reson.* 32A (2008) 201-208.
- [26] D. Parker, NMR determination of enantiomeric purity, *Chem. Rev.* 91 (1991) 1441-1457.
- [27] R. Rothchild, NMR methods for determination of enantiomeric excess, *Enantiomer* 5 (2000) 457-471.
- [28] T.J. Wenzel, J.D. Wilcox Chiral reagents for the determination of enantiomeric excess and absolute configuration using NMR spectroscopy, *Chirality* 15 (2003) 256-270.
- [29] To find information, an entire issue of Chemical Review was devoted to cyclodextrins: *Chem. Rev.* 98 (1998) 1751-2076.
- [30] E. Sackmann, S. Meiboom, L.C. Snyder, Nuclear magnetic resonance spectra of enantiomers in optically active liquid crystals, *J. Am. Chem. Soc.* 90 (1968) 2183-2184.
- [31] E. Lafontaine, J.-P. Bayle, J. Courtieu, High-resolution NMR in cholesteric medium: visualization of enantiomers, *J. Am. Chem. Soc.* 111 (1989) 8294-8296.
- [32] J.W. Emsley, J.C. Lindon, in *NMR spectroscopy using liquid crystal solvents*, Pergamon, Oxford, 1975.
- [33] C. Veracini, in *Nuclear magnetic resonance of liquid crystals*, NATO ASI Series C, 1985.
- [34] Ronald Y. Dong (Ed), in *Nuclear magnetic resonance spectroscopy of liquid crystals*, World Scientific, Singapore, 2010.
- [35] M. Sarfati, P. Lesot, D. Merlet, J. Courtieu, Theoretical and experimental aspects of enantiomeric differentiation using natural abundance multinuclear NMR spectroscopy in chiral polypeptide liquid crystals, *Chem. Commun.* (2000) 2069-2081.
- [36] A. Saupe, G. Englert, High-resolution nuclear magnetic resonance spectra of orientated molecules *Phys. Rev. Lett.* 11 (1963) 462-464.
- [37] A. Saupe, G. Englert, Proton magnetic resonance spectra of oriented molecules acetylenic compounds acetonitrile and methanol, *Mol. Cryst.* 1 (1966) 503-514.
- [38] A. Saupe, Average orientation of solute molecules in nematic liquid crystals by proton magnetic resonance measurements and orientation dependent intermolecular forces, *Mol. Cryst.* 1 (1966) 527-540.
- [39] A. Saupe, Recent results in the field of liquid crystals, *Angew. Chem., Int. Ed.* 7 (1968) 97-112.
- [40] J.-P. Bayle, J. Courtieu, E. Gabetty, A. Loewenstein, J.-M. Péchiné, Enantiomeric analysis in a polypeptide lyotropic liquid-crystal through proton decoupled deuterium NMR, *New J. Chem.* 16 (1992) 837-838.
- [41] P. Lesot, C. Aroulanda, H. Zimmermann, Z. Luz, Enantiotopic discrimination in the NMR spectrum of prochiral solutes in chiral liquid crystals, *Chem. Soc. Rev.* 44 (2015) 230-275.

- [42] F. Reinitzer, Beiträge zur Kenntnis des Cholesterins, *Monasth. Chem.* 9 (1888) 421-441.
- [43] P.G. De Gennes, J. Prost, in *The physics of liquid crystals*, Oxford University, Press, New York, 1995.
- [44] J.W. Emsley, NMR in anisotropic systems, theory, *Encyclopedia of spectroscopy and spectrometry*, 3<sup>rd</sup> Ed., Vol. 3, *Eds.* J. C. Lindon, G.E. Tranter, D.W. Koppenaal, 3 (2017) 134-139.
- [45] C. Zannoni, in *Quantitative description of orientational order: rigid molecules*, *Nuclear Magnetic Resonance of Liquid Crystals*, edited by J.W. Emsley, Reidel, Dordrecht, pp. 1 & 31, 1985.
- [46] C. Zannoni, in *The molecular physics of liquid crystals*, *Eds.* G.R. Luckhurst, G.W. Gray Academic, Chap. 3, New York, 1979.
- [47] P.H. Butler, in *Point group symmetry applications. Methods and tables*, Plenum Press, New York and London, Chap. 3, 1981.
- [48] D. Merlet, J.W. Emsley, P. Lesot, J. Courtieu, The relationship between molecular symmetry and second-rank orientational order parameters for molecules in chiral liquid crystalline solvents, *J. Chem. Phys.* 111 (1999) 6890-6896.
- [49] P. Lesot, Y. Gounelle, D. Merlet, A. Loewenstein, J. Courtieu, Measurement and analysis of the molecular ordering tensors of two enantiomers oriented in a polypeptide liquid crystalline system, *J. Phys. Chem. A*, 99 (1995) 14871-14875.
- [50] A. Meddour, P. Berdagué, A. Hedli, J. Courtieu, P. Lesot, Proton-decoupled carbon-13 NMR spectroscopy in a lyotropic chiral nematic solvent as an analytical tool for the measurement of the enantiomeric excess, *J. Am. Chem. Soc.* 119 (1997) 4502-4508.
- [51] G. Kummerlöwe, B. Luy, Residual dipolar couplings for the configurational and conformational analysis of organic molecules. *Ann. Rep. NMR Spectrosc.* 68 (2009) 193-232.
- [52] R.R. Gil, Residual dipolar couplings in small-molecules NMR, in *Encyclopedia of spectroscopy and spectrometry*, *Eds.* J.C. Lindon, G.E. Tranter, D.W. Koppenaal, 3<sup>rd</sup> Ed., Vol. 3, (2017) 946-955.
- [53] P. Lesot, D. Merlet, A. Meddour, J. Courtieu, A. Loewenstein, Visualization of enantiomers in a polypeptide liquid-crystal solvent through carbon-13 NMR spectroscopy, *J. Chem. Soc., Faraday Trans.* 91 (1995) 1371-1375.
- [54] P. Lesot, J. Courtieu, Natural abundance deuterium NMR spectroscopy: developments and analytical applications in liquids, liquid crystals and solid phase, *Prog. Nucl. Magn. Reson. Spectrosc.* 55 (2009) 128-159.
- [55] P. Lesot, O. Lafon, Natural abundance <sup>2</sup>H NMR spectroscopy, in *Encyclopedia of Spectroscopy and Spectrometry*, *Eds.* J. Lindon, G.E. Tranter and D.W. Koppenaal, Elsevier / Academic Press. 3<sup>rd</sup> Ed., Vol. 3 (2017) 1-14.
- [56] E. Graf, R. Graff, W. Hosseini, C. Huguenard, F. Taulelle, Probing peristatic chirality of alkaline cations: NMR study of alkaline borocryptates, *Chem. Commun.* (1997) 1459-1460.
- [57] D. Merlet, J.W. Emsley, J. Jokisaari, J. Kaski Characterisation of the structure, deuterium quadrupolar tensors, and orientational order of acenaphtene, a rigid, prochiral molecule, from the NMR spectra of samples dissolved in nematic and chiral nematic liquid crystalline solvents, *Phys. Chem. Chem. Phys.* 3 (2001) 4918-4925.
- [58] E.H. Hardy, R. Witt, M.D. Zeidler, A new method for the determination of the dynamic isotope effect and the deuterium quadrupole coupling constant in liquids, *J. Magn. Reson.* 34 (1998) 300-307.
- [59] Private communication, Internal report, (1997).

- [60] M. Rivard, F. Guillen, J.-C. Fiaud, C. Aroulanda, P. Lesot, Efficient enantiodiscrimination of chiral monophosphine oxides and boranes by phosphorus coupled carbon-13 NMR spectroscopy in the presence of chiral ordering agents, *Tetrahedron: Asymmetry* 14 (2003) 1141-1152.
- [61] Lesot, C. Aroulanda, in *NMR Spectroscopy of Liquid Crystals*, 1<sup>st</sup> Print edition, *Ed.* R.Y. Dong, World Scientific Publishing Co. Pte. Ltd, Chap. 2, (Analytical potentials of natural abundance deuterium NMR spectroscopy in achiral thermotropics and polypeptide chiral liquid crystals), pp. 37-78, (2010).
- [62] D. Merlet, B. Ancian, J. Courtieu, P. Lesot, Two-dimensional deuterium NMR spectroscopy of chiral molecules oriented in a polypeptide liquid crystal: application for the enantiomeric analysis through natural abundance deuterium NMR, *J. Am. Chem. Soc.* 121 (1999) 5249-5258.
- [63] E. Sackmann, S. Meiboom, L.C. Snyder, A.E. Meixner, R.E. Dietz, On the structure of the liquid crystalline state of cholesterol derivatives, *J. Am. Chem. Soc.* 90 (1968) 3567-3569.
- [64] I. Canet, J. Iovschall, J. Courtieu. Visualization of enantiomers through deuterium NMR in cholesterics optimization of the chiral liquid-crystal solvent, *Liq. Crystals*, 16 (1994) 405-412.
- [65] J.W. Emsley, J.C. Lindon, J.M. Tabony, T.H. Wilmshurst, Simplification of H-1 nuclear magnetic resonance spectra of partially oriented molecules by partial deuteration and deuterium decoupling *Chem. Commun.* (1971) 1277-1278.
- [66] J.W. Emsley, J.C. Lindon, J.M. Tabony, NMR-spectra of ethanol and partially deuterated ethanols as solutes in a nematic phase, *Mol. Phys.* 26 (1973) 1485-1498.
- [67] Longeri, G. Celebre in *Encyclopedia of NMR*, *Eds.* D.M. Grant, R.K. Harris, J. Wiley & Sons, Chichester, pp. 2774-2781, 1996.
- [68] E.E. Burnell, C.A. de Lange, in *NMR of ordered liquids*, *Eds.* E.E. Burnell, C.A. de Lange Kluwer Academic Publishers, Chap.10, Dordrecht, 2003.
- [69] B. Baishya, U.R. Prabhu, N. Suryaprakash, Binuclear spin state selective detection of <sup>1</sup>H single quantum transitions using triple quantum coherence: A novel method for enantiomeric discrimination. *J. Magn. Reson.* 192 (2008) 92-100.
- [70] P. Lesot, D. Merlet, J. Courtieu, J.W. Emsley, Discrimination and analysis of the NMR spectra of enantiomers dissolved in chiral liquid crystal solvents through 2D correlation spectroscopy, *Liq. Crystals*, 21, (1996) 427-435.
- [71] M. Gochin, D. Hugiely, H. Zimmermann, A. Pines, Two-dimensional multiple quantum NMR of isotopic mixtures in liquid-crystals, *Mol. Phys.* 60 (1987) 205-212.
- [72] M. Mehring in *Principle of high-resolution NMR in solids*, 2<sup>nd</sup> Ed., Chap. 3, Springer Verlag, New York, 1983,
- [73] J.-M. Ouvrard, B.N. Ouvrard, J. Courtieu, C.L. Maine, D.M. Grant, Coherent reduction of dipolar interactions in molecules dissolved in liquid-crystal solvents using a new multiple-pulse technique during acquisition, *J. Magn Reson.* 93 (1991) 225-241.
- [74] P. Lesot, J.-M. Ouvrard, B.N. Ouvrard, J. Courtieu, Coherent reduction of dipolar interactions in molecules dissolved in anisotropic media using a new multiple-pulse sequence in a cosy experiment *J. Magn. Reson. A*, 107 (1994) 141-150.
- [75] P. Lesot, F. Nielsen, J.M. Ouvrard, J. Courtieu, Multiple-pulse COSY NMR spectroscopy of oriented molecules in thermotropic cholesterics *J. Phys. Chem. A*, 98 (1994) 12849-12855.
- [76] J. Courtieu, D.W. Alderman, D.M. Grant, Spinning near the magic angle - a means of obtaining 1<sup>st</sup>-order dipolar NMR-spectra of molecules dissolved in nematic liquid-crystals, *J. Am. Chem. Soc.* 103 (1981) 6783-6784.

- [77] J. Courtieu, J.-P. Bayle, B.M. Fung, Variable-angle sample-spinning NMR in liquid-crystals, *Prog. Nucl. Magn. Reson. Spectrosc.* 26 (1994) 141-169.
- [78] J. Courtieu, Spinning liquid crystalline samples, in *Encyclopedia of Magnetic Resonance*, Eds. R.K. Harris, R. Wasylishen, John Wiley: Chichester, pp. 4545 (1996).
- [79] R.W. Martin, J.E. Kelly, K.A. Colier, Spatial reorientation experiments for NMR of solids and partially oriented liquids, *Prog. Nucl. Magn. Reson. Spectrosc.* 90/91(2015) 92-122.
- [80] R.G. Laughlin, in *The aqueous phase behaviour of surfactants*. London: Academic Press, (1996), ISBN 0-12-437760-2.
- [81] IUPAC. *Compendium of Chemical Terminology*, 2<sup>nd</sup> Ed. (the "Gold Book"). Compiled by A.D. McNaught and A. Wilkinson. Blackwell Scientific Publications, Oxford (1997). Online version (2019-) created by S. J. Chalk, ISBN 0-9678550-9-8, DOI: 10.1351/goldbook.
- [82] M. Barón, R.F.T. Stepto, Definitions of basic terms relating to polymer liquid crystals, *Pure Appl. Chem.*, 74 (2002) 493-509.
- [83] A.S. Tracey, Lyotropic liquid crystalline samples, *eMagRes*, Online, John Wiley & Sons, Ltd, (2007).
- [84] J.P. Straley, The gas of long rods as a model for lyotropic liquid crystals, *Mol. Cryst., Liq. Cryst.* 22 (1973) 3-4, 333-357.
- [85] C. Guha, W.A. Hines, E.T. Samulski, Polypeptide liquid crystals: magnetic susceptibility, twist elastic constant, rotational viscosity coefficient, and PBLG sidechain conformation, *J. Chem. Phys.*, 61 (1974) 947-953.
- [86] I.W. Hamley, Liquid crystal phase formation by polymer, *Soft Matter*, 6 (2010) 1863-1871.
- [87] N. Tjandra, A. Bax, Direct measurement of distances and angles in biomolecules by NMR in a dilute liquid crystalline medium, *Science* 278 (1997) 1111-1114.
- [88] E. de Alba, N. Tjandra, NMR dipolar couplings for the structure determination of biopolymers in solution, *Prog. Nucl. Magn. Reson. Spectrosc.* 40 (2002) 175-197.
- [89] J.H. Prestegard, C.M. Bougault, A.I. Kishore, Residual dipolar couplings in structure determination of biomolecules, *Chem. Rev.* 104 (2004) 3519-3540.
- [90] J.A. Losonczi, J.H. Prestegard, Improved dilute bicelle solutions for high-resolution NMR of biological macromolecules, *J. Biomol. NMR* 12 (1998) 447-451.
- [91] S. Gaemers, A. Bax, Morphology of three lyotropic liquid crystalline biological NMR media studied by translational diffusion anisotropy, *J. Am. Chem. Soc.* 123 (2001) 12343-12352.
- [92] M. Ottiger, A. Bax, Characterization of magnetically oriented phospholipid micelles for measurement of dipolar couplings in macromolecules, *J. Biomol. NMR* 12 (1998) 361-372.
- [93] G.M. Clore, M.R. Starich, A.M. Gronenborn, Measurement of residual dipolar couplings of macromolecules aligned in the nematic phase of a colloidal suspension of rod-shaped viruses, *J. Am. Chem. Soc.* 120 (1998) 10571-105782.
- [94] G.A. Nagana Gowda, H. Chen, C.L. Khetrpal, R.G. Weiss, Amphotropic ionic liquid crystals with low order parameters, *Chem. Mat.* 16 (2004), 2101-2106.
- [95] M. Rückert, G. Otting, Alignment of biological macromolecules in novel nonionic liquid crystalline media for NMR experiments, *J. Am. Chem. Soc.* 122 (2000) 7793-7797.
- [96] R. Tycko, F.J. Blanco, Y. Ishii, Alignment of biopolymers in strained gels: a new way to create detectable dipole-dipole couplings in high-resolution biomolecular NMR, *J. Am. Chem. Soc.* 122 (2000) 9340-9341.



- [97] J.H. Ma, G.I. Goldberg, N. Tjandra, Weak alignment of biomacromolecules in collagen gels: an alternative way to yield residual dipolar couplings for NMR Measurements. *J. Am. Chem. Soc.* 130 (2008) 16148-16149.
- [98] C.-M. Thiele, Use of RDCs in rigid organic compounds and some practical considerations concerning alignment media, *Concepts in Magn. Reson. A.* 30 (2007) 65-80.
- [99] C-M. Thiele, Residual dipolar couplings (RDCs) in organic structure determination, *Eur. J. Org. Chem.*, 34 (2008) 5673-5685.
- [100] G. Kummerlöwe, B. Luy, Residual dipolar couplings as a tool in determining the structure of organic molecules *TrAC Trends in Analytical Chemistry* 28 (2009) 483-493.
- [101] A. Navarro-Vazquez, R.R. Gil, K. Blinov, Computer-assisted 3D structure elucidation (CASE-3D) of natural products combining isotropic and anisotropic NMR parameters, *J. Nat. Prod.* 81 (2018) 203-210.
- [102] G.-W. Li, H. Liu, F. Qiu, X.-J. Wang, X.-Xi. Lei, Residual dipolar couplings in structure determination of natural products, *Natural Products and Bioprospecting*, 8 (SI) (2018) 279-295.
- [103] F. Hallwass, M. Schmidt, Manuel, H. Sun, Han, A Mazur, G. Kummerloewe, Grit, B. Luy, A. Navarro-Vazquez, Armando, C. Griesinger, U.M. Reinscheid, Residual chemical shift anisotropy (RCSA): A tool for the analysis of the configuration of small molecules, *Angew. Chem., Ed. Int.* 50 (2011) 9487-9490.
- [104] N. Nath, Nilamoni, M Schmidt, R.R Gil, R.T. Williamson, R. Thomas, G.E. Martin, A. Navarro-Vazquez, C. Griesinger, Y. Liu, Determination of Relative Configuration from Residual Chemical Shift Anisotropy, *J. Am. Chem. Soc.* 138 (2016) 9548-9556.
- [105] Y. Liu, A. Navarro-Vázquez, R.R. Gil, C. Griesinger, G.E. Martin, R.T. Williamson, Application of anisotropic NMR parameters to the confirmation of molecular structure, *Nature Protocol* 14 (2018) 217-247.
- [106] A. Tracey, P. Diehl, The interaction of *D* and *L*-alanine with an optically active model membrane system, *FEBS Lett.* 59 (1975) 131-132.
- [107] A.S. Tracey, K. Radley, Effects of composition on cholesteric behavior in the lyotropic mesophase system of potassium *N*-dodecanoyl-*L*-alaninate, *J. Phys. Chem.* 88 (1984) 6044-6048.
- [108] A. Solgadi, A. Meddour, J. Courtieu, Enantiomeric discrimination of water soluble compounds using deuterium NMR in a glucopon/buffered water/*n*-hexanol chiral lyotropic liquid crystal, *Tetrahedron: Asymmetry* 15 (2004) 1315-1318.
- [109] K. Baczko, C. Larpent, P. Lesot, New amino acid based on anionic surfactants and their use as enantiodiscriminating lyotropic liquid crystalline NMR solvent, *Tetrahedron: Asymmetry* 15 (2004) 971-982.
- [110] S.P. Sau, K.V. Ramanathan, Visualization of enantiomers in the liquid-crystalline phase of a fragmented DNA solution, *J. Phys. Chem. B.* 113 (2009) 1530-1535.
- [111] P. Lesot, U. Venkateswara Reddy, N.S. Suryaprakash, Exploring the enantiodiscrimination potentialities of DNA-based orienting media using deuterium NMR spectroscopy, *Chem. Commun.* 47 (2011) 11736-11738.
- [112] E. Lafontaine, J.M. Péchiney, J. Courtieu, C.L. Maine, Visualization of enantiomers in cholesteric solvents through deuterium NMR, *Liq. Crystals* 7 (1990) 293-298.
- [113] C. Aroulanda, M. Sarfati, J. Courtieu, P. Lesot, Investigation of enantioselectivity of three polypeptide liquid-crystalline solvents using NMR spectroscopy, *Enantiomer.* 6 (2001) 281-287.

- [114] K. Czarniecka, E.T. Samulski, Polypeptide liquid crystals: a deuterium NMR study, *Mol. Cryst. Liq. Cryst.* 63 (1981) 205-214.
- [115] M. Panar, W. D. Phillips, Magnetic ordering of poly( $\gamma$ -benzyl-*L*-glutamate) solutions, *J. Am. Chem. Soc.* 90 (1968) 3880-3882.
- [116] E.T. Samulski, A.V. Tobolsky, Some unusual properties of poly( $\gamma$ -benzyl-*L*-glutamate) films cast in strong magnetic fields, *Macromolecules* 1 (1968) 555-557.
- [117] M.D. Poliks, Y.W. Park, E.T. Samulski, Poly- $\gamma$ -benzyl-*L*-glutamate: order parameter, oriented gel, and novel derivatives, *Mol. Cryst. Liq. Cryst.* 153 (1987) 321-345.
- [118] C.-M. Thiele, Simultaneous assignment of all diastereotopic protons in strychnine using RDCs: PELG as alignment medium for organic molecules, *J. Org. Chem.* 69 (2004) 7403-7413.
- [119] S. Hansmann, T. Larem, C.-M. Thiele, Enantiodifferentiating properties of the alignment media PELG and PBLG - a comparison, *Eur. J. Org. Chem.* 7 (2016) 1324-1329.
- [120] J.W. Emsley, G.R. Luckhurst, H.S. Sachdev, The orientational ordering of a biaxial solute in mixtures of nematic solvents, *Mol. Phys.* 67 (1989) 151-160.
- [121] P. Lesot, O. Lafon, C. Aroulanda, R. Dong,  $^2\text{H}$  NMR studies of two-homopolypeptide lyotropic mesophases: toward the quantification of solute-fiber interactions, *Chem. Eur. J.* 14, (2008) 4082-4092.
- [122] T. Montag, C.-M. Thiele, Cross-linked helically chiral poly( $\gamma$ -benzyl-*L*-glutamate) as enantiodiscriminating alignment medium, *Chem. Eur. J.* 19 (2013) 2271-2274.
- [123] M. Schwab, D. Herold, C.-M. Thiele, Polyaspartates as thermoresponsive enantiodifferentiating helically chiral alignment media for anisotropic NMR spectroscopy, *Chem. Eur. J.* 23 (2017) 14576-14584.
- [124] M. Hirschmann, M. Schwab, C.-M. Thiele, Molecular weights: the key of lyotropic liquid crystalline of Poly- $\beta$ -benzyl-*L*-Aspartate, *Macromolecules* (2019) 52 6025-6034.
- [125] S. Jeziorowski, C.-M. Thiele, Poly- $\gamma$ -*p*-biphenylmethyl-glutamate as enantiodifferentiating alignment medium for NMR spectroscopy with temperature-tunable properties, *Chem Eur. J.* 24 (2018) 15631-15637.
- [126] M. Schwab, V. Schmidts, C.-M. Thiele, Thermoresponsive alignment media in NMR spectroscopy: helix reversal of a co-polyaspartate at ambient temperatures, *Chem. Eur. J.* 24 (2018) 14373-14377.
- [127] S. Hansmann, V. Schmidts, C.-M. Thiele, Synthesis of poly- $\gamma$ -*S*-2-methylbutyl-*L*-glutamate and poly- $\gamma$ -*S*-2-methylbutyl-*D*-glutamate and their use as enantiodiscriminating alignment media in NMR spectroscopy, *Chem. Eur. J.* 23 (2017) 9114-9121.
- [128] A. Meddour, I. Canet, A. Loewenstein, J.-M. Péchiné, J. Courtieu, Observation of enantiomers, chiral by virtue of isotopic substitution, through deuterium NMR in a polypeptide liquid crystal, *J. Am. Chem. Soc.* 116 (1994) 9652-9656.
- [129] B.D. Dupré, R.W. Duke, Temperature, concentration, and molecular weight dependence of the twist elastic constant of cholesteric poly- $\gamma$ -benzyl-*L*-glutamate, *J. Chem. Phys.* 63 (1975), 143-148.
- [130] P.G. De Gennes, Calcul de la distorsion d'une structure cholestérique par un champ magnétique, *Solid State Commun.* 6 (1968) 163-165.
- [131] S. Sobajima, NMR studies on orientation of liquid crystals of poly- $\gamma$ -benzyl-*L*-glutamate in magnetic fields, *J. Phys. Soc. Jpn.* 23 (1967) 1070-1078.
- [132] P. Trigo-Mourino, C. Merle, M.R.M. Koos, B. Luy, R.R. Gil, Probing spatial distribution of alignment by deuterium NMR Imaging, *Chem. Eur. J.* 19 (2013) 7013-7019.

- [133] A. Marx, B. Boettcher, Benjamin, C.-M. Thiele, Enhancing the orienting properties of poly( $\gamma$ -benzyl-*L*-glutamate) by means of additives, *Chem. Eur. J.* 16 (2010) 1656-1660.
- [134] C.-M. Thiele, W.C. Pomerantz, N.L. Abbott, S.H. Gellman, Lyotropic liquid crystalline phases from helical  $\beta$ -peptides as alignment media, *Chem. Commun.* 47 (2011) 502-504.
- [135] C. Canlet, D. Merlet, P. Lesot, A. Meddour, A. Loewenstein, J. Courtieu, Deuterium NMR stereochemical analysis of threo-erythro isomers bearing remote chiral centres in racemic and non-racemic liquid crystalline solvents, *Tetrahedron: Asymmetry* 11 (2000) 1911-1918.
- [136] Z. Serhan, C. Aroulanda, P. Lesot, Investigation of solute-fiber affinity and orientational ordering of norbornadiene interacting with two-polypeptide chiral liquid crystalline solvents by NAD NMR, *J. Phys. Chem. A* 120 (2016) 6076-6088.
- [137] L. Arnold, A. Marx, C.-M. Thiele, M. Reggelin, Polyguanidines as chiral orienting media for organic compounds, *Chem. Eur. J.* 16 (2010) 10342-10346.
- [138] M. Dama, S. Berger, Polyisocyanides as a new alignment medium to measure residual dipolar couplings for small organic molecules. *Org. Lett.* 14 (2012) 241-243.
- [139] N.-C. Meyer, A. Krupp, V. Schmidts, C.-M. Thiele, M. Reggelin, Polyacetylenes as enantiodifferentiating alignment media, *Angew. Chem., Int. Ed.* 51 (2012) 8334-8338.
- [140] A. Krupp, M. Reggelin, Phenylalanine-based polyarylacetylenes as enantiomer-differentiating alignment media, *Magn. Reson. Chem.* 50 (2012) S45-S52.
- [141] M. Dama, S. Berger, Polyacetylenes as a new alignment medium to measure residual dipolar couplings for chiral organic molecules, *Tetrahedron Lett.* 53 (2012) 6439-6442.
- [142] G.W. Li, J.M. Cao, W. Zong, L. Hu, M.L. Hu, X. Lei, H. Sun, R.X. Tan, Helical polyisocyanopeptides as lyotropic liquid crystals for measuring residual dipolar couplings, *Chem. Eur. J.* 23 (2017) 7653-7656.
- [143] M. Reller, S. Wesp, M. R. M. Koos, M. Reggelin, B. Luy, Biphasic liquid crystal and the simultaneous measurement of isotropic and anisotropic parameters by spatially resolved NMR spectroscopy, *Chem. Eur. J.* 23 (2017) 13351-13359.
- [144] P. Lesot, P. Berdagué, A. Meddour, A. Kreiter, M. Noll, M. Reggelin,  $^2\text{H}$  and  $^{13}\text{C}$  NMR-based enantiodetection using polyacetylene *versus* polypeptide aligning media: versatile and complementary tools for chemists, *ChemPlusChem* 84 (2019) 144-155.
- [145] B. Luy, K. Kobzar, H. Kessler, An easy and scalable method for the partial alignment of organic molecules for measuring residual dipolar couplings, *Angew. Chem., Int. Ed.* 43 (2004) 1092-1094.
- [146] G. Kummerlöwe, J. Auernheimer, A Lendlein, B. Luy, Stretched poly(acrylonitrile) as a scalable alignment medium for DMSO, *J. Am. Chem. Soc.* 129 (2007) 6080-6081.
- [147] G. Kummerlöwe, F. Halbach, B. Laufer, B. Luy, Precise measurement of RDCs in water and DMSO based gels using a silicone rubber tube for tunable stretching, *The Open Spectroscopy Journal*, 2 (2008) 29-33.
- [148] B.E. Chapman, N. Muller, W.A. Bubb, D.J. Philip, A.M Torres, Apparatus for rapid adjustment of the degree of alignment of NMR samples in aqueous media: verification with residual quadrupolar splittings in  $^{23}\text{Na}$  and  $^{133}\text{Cs}$  spectra, *J. Magn. Reson.* 180 (2006) 256-265.
- [149] C. Naumann, W.A. Bubb, B.E. Chapman, P.W. Kuchel, Tunable-alignment chiral system based on gelatin for NMR spectroscopy, *J. Am. Chem. Soc.*, 129 (2007) 5340-5341.
- [150] R.R. Gil, C. Gayathri, N.V. Tsarevsky, K. Matyjaszewski, Stretched poly(methyl methacrylate) gel aligns small organic molecules in chloroform. stereochemical analysis and diastereotopic proton NMR assignment in ludartin using residual dipolar couplings and  $^3\text{J}$  coupling constant analysis, *J.*

Org. Chem. 73 (2008) 840-848.

- [151] C. Gayathri, N.V. Tsarevsky, R.R. Gil, Residual dipolar couplings (RDCs) analysis of small molecules made easy: fast and tuneable alignment by reversible compression/relaxation of reusable PMMA gels, *Chem. Eur. J.* 16 (2010) 362-3626.
- [152] K. Kobzar, H. Kessler, B. Luy, Stretched gelatin gels as chiral alignment media for the discrimination of enantiomers by NMR spectroscopy, *Angew. Chem., Int. Ed.* 44 (2005) 314-3147.
- [153] G. Kummerlöwe, M.U. Kiran, B. Luy, Covalently cross-linked gelatin allows chiral distinction at elevated temperatures and in DMSO, *Chem. Eur. J.* 15 (2009) 12192-12195.
- [154] J.H. Ma, G.I. Goldberg, N. Tjandra, Weak alignment of biomacromolecules in collagen gels: an alternative way to yield residual dipolar couplings for NMR measurement, *J. Am. Chem. Soc.* 130 (2008) 16148-16149.
- [155] M. Schmidt, H. Sun, A. Leonov, C. Griesinger, U.M. Reinscheid, Chiral discrimination of amines by anisotropic NMR parameters using chiral polyacrylamide-based gels, *Magn. Reson. Chem.* 50 (2012) S38-S44.
- [156] B. Plainchont, D. Pitoux, M. Cyrille, N. Giraud, Accurate quantitative analysis of enantiomeric mixtures from spatially, *Anal. Chem.* 90 (2018) 1595-1600.
- [157] N. Giraud, J. Farjon, Analyses of enantiomeric mixtures using chiral liquid crystals, *Current Opinion in Colloid & Interface Science* 33 (2018) 1-8.
- [158] T. Facke, S. Berger, SERF, A new method for H,H spin-coupling measurement in organic-chemistry, *J. Magn. Reson. A*, 113 (1995) 114-116.
- [159] S. Berger, A quarter of a century of SERF: the progress of an NMR pulse sequence and its application, *Prog. Nucl. Magn. Reson. Spectrosc.* 108 (2018) 74-114.
- [160] W.P. Aue, J. Karhan, R.R. Ernst, Homonuclear broad band decoupling and two-dimensional J-resolved NMR spectroscopy, *J. Chem. Phys.* 64 (1976) 4226-4227.
- [161] J. Farjon, D. Merlet, P. Lesot, J. Courtieu, Enantiomeric excess measurements in weakly oriented chiral liquid crystal solvents through 2D <sup>1</sup>H selective refocusing experiments, *J. Magn. Reson.* 158 (2002) 169-172.
- [162] L. Beguin, J. Courtieu, L. Ziani, D. Merlet, Simplification of the H-1 NMR spectra of enantiomers dissolved in chiral liquid crystals, combining variable angle sample spinning and selective refocusing experiments. *Magn. Reson. Chem.* 44 (2006) 1096-1101.
- [163] L. Beguin, N. Giraud, J.-M. Ouvrard, J. Courtieu, D. Merlet, Improvements to selective refocusing phased (SERFph) *J. Magn. Reson.* 199 (2009) 41-47.
- [164] J. Farjon, D. Merlet, SERF-filtered experiments: New enantio-selective tools for deciphering complex spectra of racemic mixtures dissolved in chiral oriented media, *J. Magn. Reson.* 210 (2011) 24-30.
- [165] D. Merlet, L. Beguin, J. Courtieu, N. Giraud, Spin-spin coupling edition in chiral liquid crystal NMR solvent, *J. Magn Reson*, 209 (2011) 315-322.
- [166] K. Zangger, H. Sterk, Homonuclear broadband-decoupled NMR spectra, *J. Magn. Reson.* 124 (1997) 486-489.
- [167] N. Giraud, L. Beguin, J. Courtieu, D. Merlet, Nuclear magnetic resonance using a spatial frequency encoding: application to J-edited spectroscopy along the sample, *Angew. Chem., Int. Ed.* 49 (2010) 3481-3484.

- [168] S. Kumar Mishra, N. Suryaprakash, Pure shift edited ultra high-resolution NMR spectrum with complete eradication of axial peaks and unwanted couplings, *J. Magn. Reson.* 279 (2017) 74-80.
- [169] A. Fredi, P. Nolis, T. Parella, Accurate measurement of  $J_{\text{HH}}$  in overlapped signals by a TOCSY-edited SERF Experiment, *Magn. Reson. Chem.* 55 (2017) 525-529.
- [170] M. Foroozandeh, G.A. Morris, M. Nolson, PSYCHE pure shift NMR spectroscopy, *Chem. Eur. J.* 24 (2018) 13988-14000.
- [171] K. Zangger, Pure shift NMR, *Prog. Nucl. Magn. Reson. Spectrosc.* 86-87 (2015) 1-20.
- [172] N. Giraud, M. Joos, J. Courtieu, D. Merlet, Application of a  $^1\text{H}$  delta-resolved 2D NMR experiment to the visualization of enantiomers in chiral environment, using sample spatial encoding and selective echoes, *Magn. Reson. Chem.* 47 (2009) 300-306.
- [173] B. Bikash, N. Suryaprakash, Spin state selective detection of single quantum transitions using multiple quantum coherence: simplifying the analyses of complex NMR spectra, *J. Phys. Chem. A*, 111 (2007) 5211-5217.
- [174] B. Baishya, U.R. Prabhu, N. Suryaprakash, Enantiomeric discrimination by double quantum excited selective refocusing (DQ-SERF) Experiment, *J. Phys. Chem. B*, 111 (2007) 12403-12410.
- [175] B. Baishya, U.R. Prabhu, N. Suryaprakash, Spin state selective coherence transfer: A method for discrimination and complete analyses of the overlapped and unresolved  $^1\text{H}$  NMR spectra of enantiomers, *J. Magn. Reson.* 192 (2008) 101-111.
- [176] U.R. Prabhu, B. Baishya, N. Suryaprakash, Chemical shift anisotropy edited complete unraveling of overlapped  $^1\text{H}$  NMR spectra of enantiomers: application to small chiral molecules, *J. Magn. Reson.* 191 (2008) 259-266.
- [177] U.R. Prabhu, N. Suryaprakash, Band selective small flip angle COSY: a simple experiment for the analyses of  $^1\text{H}$  NMR spectra of small chiral molecules, *J. Magn. Reson.* 195 (2008) 145-152.
- [178] U.R. Prabhu, N. Suryaprakash, Application of z-COSY experiment and its variant for accurate chiral discrimination by  $^1\text{H}$  NMR, *J. Magn. Reson.* 202 (2010) 217-222.
- [179] N. Nath, N. Suryaprakash, Selective detection of single-enantiomer spectrum of chiral molecules aligned in the polypeptide liquid crystalline solvent: Transition selective one-dimensional  $^1\text{H}$ - $^1\text{H}$  COSY, *J. Magn. Reson.* 202 (2010) 34-37.
- [180] S. Hebbar, U.R. Prabhu, N. Suryaprakash, Selective double quantum resolved correlation experiment for the complete separation of entire proton NMR spectra of enantiomers, *J. Magn. Reson.* 215 (2012) 23-26.
- [181] N. Lokesh, N. Suryaprakash, CH-RES-TOCSY: Enantiomers spectral resolution and measurement of heteronuclear residual dipolar couplings, *Chem. Phys. Lett.* 625 (2015) 10-13.
- [182] M. Perez-Trujillo, L. Castanar, E. Monteagudo, L.T. Kuhn, P. Nolis, A. Virgili, R.T. Williamson, T. Parella, Simultaneous  $^1\text{H}$  and  $^{13}\text{C}$  NMR enantiodifferentiation from highly-resolved pure shift HSQC spectra, *Chem. Commun.* 50 (2014) 10214-10217.
- [183] L. Paudel, R.W. Adams, P. Király, A. Aguilar, M. Foroozandeh, M.J. Cliff, M. Nilsson, P. Sándor, J.P. Waltho, G.A. Morris, Simultaneously enhancing spectral resolution and sensitivity in heteronuclear correlation NMR spectroscopy, *Angew. Chem., Int. Ed.* 52 (2013) 11616-11619.
- [184] M. Foroozandeh, D. Jeannerat, Reconstruction of full high-resolution HSQC using signal split in aliased spectra, *Magn. Reson. Chem.* 53 (2015) 894-900.
- [185] D.M. Korzhnev, I.V. Ibraghimov, M. Billeter, V.Y. Orekhov, MUNIN: Application of three-way decomposition to the analysis of heteronuclear NMR relaxation data. *J. Biomol. NMR.* 21 (2001) 263-268.

- [186] N. Nath, N. Suryaprakash, Quantification of enantiomeric excess by  $^1\text{H}$ -detected heteronuclear refocusing and homonuclear multiple quantum NMR experiments, *Chem. Phys. Lett.* 502 (2011) 136-143.
- [187] H.O. Kalinowski, S. Berger, S. Braun, in *Carbon-13 NMR spectroscopy*; Wiley and Sons: Chichester, 1984.
- [188] L. Ziani, J. Courtieu, D. Merlet, Visualisation of enantiomers via insertion of a BIRD module in X-H correlation experiments in chiral liquid crystal solvent, *J. Magn. Reson.* 183 (2006) 60-67.
- [189] H. Kovacs, D. Moskau, M. Spraul, Cryogenically cooled probes, a leap in NMR technology, *Prog. Nucl. Magn. Reson. Spectrosc.* 45 (2005) 131-155.
- [190] P. Lesot, D. Merlet, J. Courtieu, J.W. Emsley, T.T. Rantala, J. Jokisaari, Calculation of the molecular ordering parameters of ( $\pm$ )-3-butyn-2-ol dissolved in an organic solution of poly( $\gamma$ -benzyl-L-glutamate), *J. Phys. Chem. A* 101 (1997) 5719-5724.
- [191] A.J. Shaka, J. Keeler, R. Freeman, Evaluation of a new broadband decoupling sequence: WALTZ-16, *J. Magn. Reson.* 53 (1983) 313-340.
- [192] E. Tenailleau, S. Akoka, Adiabatic  $^1\text{H}$  decoupling scheme for very accurate intensity measurements in  $^{13}\text{C}$  NMR, *J. Magn. Reson.* 185 (2007) 50-58.
- [193] P. Tzvetkova, B. Luy, S. Simova, Chemical shift anisotropy-based measurement of enantiomeric excess for selected tetrasubstituted pyrrolidines, *Topics in Chemistry and Material Science Vol. 5* (2011) pp. 70-77 of *Current Issues in Organic Chemistry*, Eds. R.D. Nikolova, S. Simova, P. Denkova, G.N. Vayssilov, Heron Press Ltd, Birmingham, 2011.
- [194] V.M. Marathias, P.A. Tate, N. Papaioannou, W. Masefski An improved method for determining enantiomeric excess by  $^{13}\text{C}$ -NMR in chiral liquid crystal media, *Chirality* 22 (2010) 838-843.
- [195] V. Madiot, D. Grée, R. Grée, P. Lesot, J. Courtieu, Highly enantioselective propargylic monofluorination established by carbon-13 and fluorine-19 NMR in chiral liquid crystals, *Chem. Commun.* (2000) 169-170.
- [196] G.A. Morris, in *Two-dimensional J-resolved 2D spectroscopy*, *Encyclopedia of Magnetic Resonance*, Eds. R.K. Harris, R.E. Wasylishen, Wiley, Chichester, DOI: 10.1002/9780470034590.emrstm0579.pub2, 2009.
- [197] M. Sugiura, A. Kimura, H. Fujiwara, Discrimination of enantiomers by means of NMR spectroscopy using chiral liquid crystalline solution: application to triazole fungicides, uniconazole and diniconazole, *Magn. Reson. Chem.* 44 (2006) 121-126.
- [198] P. Berdagué, J.-E. Herbert-Pucheta, V. Jha, A. Panossian, F.R. Leroux, P. Lesot, Multi-nuclear NMR of axially chiral biaryls in polypeptide orienting solvents: spectral discriminations and enantiorecognition mechanisms, *New J. Chem.* 39 (2015) 9504-9517.
- [199] J.W. Emsley, P. Lesot, D. Merlet, The orientational order and conformational distributions of the two enantiomers in a racemic mixture of a chiral, flexible molecule dissolved in a chiral nematic liquid crystalline solvent, *Phys. Chem. Chem. Phys.* 6 (2004) 522-530.
- [200] J. Farjon, J.-P. Baltaze, P. Lesot, D. Merlet, J. Courtieu, Heteronuclear selective refocusing 2D NMR experiments for the spectral analysis of enantiomers in chiral oriented solvents, *Magn. Reson. Chem.* 42 (2004) 594-599.
- [201] J. Farjon, *Nouvelle méthodologie RMN en milieu cristal liquide chiral: contribution à l'analyse stéréochimique en chimie structurale organique*, Thèse N° 7293, Université de Paris-Sud, Orsay, France (2003).

- [202] R.R. Ernst, G. Bodenhausen, A. Wokaun, in Principles of nuclear magnetic resonance in one and two dimensions, Clarendon Press, Oxford, 1987.
- [203] A. Bax, R. Freeman, S.P. Kempel, Natural abundance carbon-13-carbon-13 coupling observed via double-quantum coherence, *J. Am. Chem. Soc.* 102 (1980) 4849-4851.
- [204] J. Buddrus, J. Lambert, Connectivities in molecules by INADEQUATE: recent developments, *Magn. Reson. Chem.* 40 (2002) 3-23.
- [205] D. Urin, Recent development in liquid-state INADEQUATE studies, *Ann. Rep. on NMR Spectrosc.* 70 (2010) 1-33.
- [206] N. Merchak, J. Bejjani, T. Rizk, V. Silvestre, G.S. Remaud, S. Akoka,  $^{13}\text{C}$  isotopomics of triacylglycerols using NMR with polarization transfer techniques, *Anal. Meth.* 7 (2015) 4889-1891.
- [207] N. Nath, N. Suryaprakash, Enantiodiscrimination and extraction of short and long range homo- and hetero-nuclear residual dipolar couplings by a spin selective correlation experiment, *Chem. Phys. Lett.* 496 (2010) 175-182.
- [208] A. Marx, V. Schmidts, C.-M. Thiele, How different are diastereomorphous orientations of enantiomers in the liquid crystalline phases of PBLG and PBDG: a case study, *Magn. Reson. Chem.* 47 (2009) 734-740.
- [209] A. Marx, C.-M. Thiele, Orientational properties of poly- $\gamma$ -benzyl-*L*-glutamate: influence of molecular weight and solvent on order parameters of the solute, *Chem. Eur. J.* 15 (2009) 254-260.
- [210] N. Nath, B. Baishya, N. Suryaprakash, Visualization of enantiomers using natural abundant  $^{13}\text{C}$ -filtered single and double quantum selective refocusing experiments: Application to small chiral molecules, *J. Magn. Reson.* 200 (2009) 101-108.
- [211] N. Nath, N. Suryaprakash, Enantiodiscrimination and extraction of short and long-range homo- and hetero-nuclear residual dipolar couplings by a spin selective correlation experiment, *Chem. Phys. Lett.* 496 (2010) 175-182.
- [212] U.R. Prabhu, S.R. Chaudhari, N. Suryaprakash, Visualization of enantiomers and determination of homo- and hetero-nuclear residual dipolar and scalar couplings: The natural abundant  $^{13}\text{C}$  edited J/D-resolved NMR techniques, *Chem. Phys. Lett.* 500 (2010) 334-341.
- [213] O. Dirat, C. Kouklovsky, Y. Langlois, P. Lesot, J. Courtieu, Double diastereoselection in asymmetric [2+3] cycloadditions reactions of chiral oxazoline *n*-oxides and application to the kinetic resolution of a racemic  $\alpha,\beta$ -unsaturated  $\delta$ -lactone, *Tetrahedron: Asymmetry* 10 (1999) 3197-3207.
- [214] D. Riegert, J. Collin, A. Meddour, E. Schulz, A. Trifonov, Enantioselective intramolecular hydroamination catalysed by lanthanide ate complexes coordinated by *N*-Substituted (*R*)-1,1'-binaphthyl-2,2'-diamido ligands, *J. Org. Chem.* 71 (2006) 2514-2517.
- [215] C. Queffelec, F. Boeda, A. Pouilhès, A. Meddour, C. Kouklovsky, J. Hannedouche, J. Collin, E. Schulz, Enantioselective intramolecular hydroamination of secondary amines catalyzed by easily accessible ate and neutral rare-earth complexes, *ChemCatChem* 3 (2011) 122-126.
- [216] D. Didier, A. Meddour, S. Bezenine-Lafollée, J. Collin, Samarium iodobinaphtholate: an efficient catalyst for enantioselective aza-michael additions of *O*-benzylhydroxylamine to *N*-alkenoyloxazolidinones, *Eur. J. Org. Chem.* (2011) 2678-2684.
- [217] O. Lafon, P. Lesot, M. Rivard, M. Chavarot, F. Rose-Munch, E. Rose, Enantiomeric analysis of planar chiral ( $\eta^6$ -arene) chromium tricarbonyl complexes using NMR in oriented solvents, *Organometallics*, 24 (2005) 4021-4028.

- [218] A. Eloi, F. Rose-Munch, E. Rose, A. Pillet, P. Lesot, P. Herson, Cationic planar chiral ( $\eta^6$ -arene) $\text{Mn}(\text{CO})_3^+$  complexes: resolution, NMR study in chiral oriented solvents and applications to the enantioselective syntheses of 4-substituted cyclohexenones and of ( $\eta^6$ -phosphinoarene) $\text{Mn}(\text{CO})_3^+$  complexes, *Organometallics*, 29 (2010) 3876-3886.
- [219] S. Prevost, S. Gauthier, M.C. Caño De Andrade, C. Mordant, A.R. Touati, P. Lesot, P. Savignac, T. Ayad, P. Phansavath, V. Ratovelomanana-Vidal, J.-P. Genet, Dynamic kinetic resolution of  $\alpha$ -chloro  $\beta$ -keto esters and phosphonates: hemisynthesis of taxotere® through Ru-difluorophos asymmetric hydrogenation, *Tetrahedron: Asymmetry* 21 (2010) 1436-1446.
- [220] I. Canet, J. Courtieu, A. Loewenstein, A. Meddour, J.-M. Péchiné, Enantiomeric analysis in a polypeptide lyotropic liquid crystal by deuterium NMR, *J. Am. Chem. Soc.* 117 (1995) 6520-6526.
- [221] A. Meddour, D. Atkinson, A. Loewenstein, J. Courtieu, Enantiomeric analysis of homologous series of secondary alcohols by deuterium NMR spectroscopy in a chiral nematic liquid crystal: influence of molecular geometry on chiral discrimination, *Chem. Eur. J.* 4 (1998) 1142-1147.
- [222] M. Tavasli, J. Courtieu, R.J.M. Goss, A. Meddour, D. O'Hagan, Extreme enantiomeric discrimination of fluoroalkanes using deuterium NMR in chiral liquid crystalline media, *Chem. Commun.* (2002) 844-845.
- [223] G. Szalontai, Spectroscopy in partially oriented phases. Routine H-2 NMR of small to medium sized molecules, *Magn. Reson. Chem.* 38 (2000) 872-876.
- [224] A. Solgadi, L. Jean, M.C. Lasne, J. Rouden, J. Courtieu, A. Meddour, NMR in chiral polypeptide liquid crystals: the problem of amines, *Tetrahedron: Asymmetry* 18 (2007) 1511-1516.
- [225] P. Lesot, M. Sarfati, J. Courtieu, Natural abundance deuterium NMR spectroscopy in polypeptide liquid crystals as a new and incisive means for enantiodifferentiation of chiral hydrocarbons, *Chem. Eur. J.* 9 (2003) 1724-1745.
- [226] G. Szalontai, Routine H-2 NMR in ternary mixtures of poly( $\gamma$ -benzyl-L-glutamate) - a useful tool for studying molecular shape, symmetry, and conformational motions, *Eur. J. Org. Chem.* 18 (2000) 3511-3518.
- [227] W. Smadja, S. Auffret, P. Berdagué, D. Merlet, C. Canlet, J. Courtieu, J.-Y Legros, A. Boutros, J.-C. Fiaud, Visualisation of axial chirality using  $^2\text{H}\{-^1\text{H}\}$  NMR in poly- $\gamma$ -benzyl-L-glutamate, a chiral liquid crystal solvent, *Chem. Commun.* (1997) 2031-2032.
- [228] P. Lesot, D. Merlet, M. Sarfati, J. Courtieu, H. Zimmermann, Z. Luz, Enantiomeric and enantiotopic analysis of cone-shaped compounds with  $C_3$  and  $C_{3v}$  symmetry using NMR spectroscopy in chiral anisotropic solvents, *J. Am. Chem. Soc.* 124 (2002) 10071-10082.
- [229] E. Chureau, A. Meddour, J. Courtieu, Enantiomeric visualization of metallic tris-(acetylacetonate) chiral complexes by NMR in a chiral liquid crystal, Internship report, University of Paris-Sud, (1999), unpublished results in the literature.
- [230] L. Huynh, A. Meddour, J. Courtieu, Visualization of enantiomers of hexacoordinate Co(III), Al(III) chiral by  $^2\text{H}$ -NMR in chiral liquid crystals, Internship report, University of Paris-Sud, (2000), unpublished results in the literature.
- [231] G. Szalontai, M. Kovacs, Distinction of tris(diimine)ruthenium(II) enantiomers chiral by virtue of helical chirality: Temperature-dependent deuterium NMR spectroscopy in partially oriented phases, *Magn. Reson. Chem.* 44 (2006) 1044-1050.
- [232] I. Canet, A. Meddour, J. Courtieu, J.-L. Canet, J. Salaün, New and accurate method to determine the enantiomeric purity of amino acids based on deuterium NMR in a cholesteric lyotropic liquid crystal, *J. Am. Chem. Soc.* 116 (1994) 2155-2156.



- [233] A. Meddour, A. Loewenstein, J.-M. Péchiné, J. Courtieu An achiral deuterated derivatizing agent for enantiomeric analysis through NMR in a liquid crystalline solvent, *Tetrahedron: Asymmetry* 8 (1997) 485-494.
- [234] J.-L. Canet, I. Canet, J. Courtieu, S. Da Silva, J. Gelas, Y. Troin, Acetyl-d<sub>3</sub> chloride: a convenient non chiral derivatizing agent (NCDA) for a facile enantiomeric excess determination of amines through deuterium NMR, *J. Org. Chem.* 61 (1996) 9035-9037.
- [235] A. Meddour, J. Courtieu, Achiral deuterated derivatizing agent for enantiomeric analysis of carboxylic acids by NMR in a chiral liquid crystalline solvent, *Tetrahedron: Asymmetry* 11 (2000) 3635-3644.
- [236] <sup>2</sup>H NMR spectrum not published, but results have been reported in reference 6.150.
- [237] A.R. Phillips, G.J. Sharman, The measurement of high enantiomeric excesses in chiral liquid crystals using <sup>19</sup>F NMR and exchangeable protons in <sup>2</sup>H NMR, *Chem. Commun.* (2004) 1330-1331.
- [238] M. Palomino, H. Khudr, J. Courtieu, D. Merlet, A. Meddour, The use of exchangeable nuclei to observe enantiomers through deuterium NMR in chiral liquid crystalline solvents, *Magn. Reson. Chem.* 50 (2012) S12-S16.
- [239] P. Lesot, O. Lafon, J. Courtieu, P. Berdagué, Analysis of the <sup>13</sup>C NMR spectra of molecules, chiral by isotopic substitution, dissolved in a chiral oriented environment: toward the absolute assignment of the pro-*R*/pro-*S* character of enantiotopic ligands in prochiral molecules, *Chem. Eur. J.* 10 (2004) 3741-3746.
- [240] P. Lesot, D. Merlet, A. Loewenstein, J. Courtieu, Enantiomeric visualisation using proton-decoupled natural abundance deuterium NMR in poly( $\gamma$ -benzyl-L-glutamate) liquid crystalline solutions, *Tetrahedron: Asymmetry* 9 (1998) 1871-1881.
- [241] D. Merlet, B. Ancian, W. Smadja, Courtieu, P. Lesot, Analysis of the natural abundance deuterium NMR spectra of enantiomers in chiral liquid crystals through 2D auto-correlation experiments, *Chem. Commun.* (1998) 2301-2302.
- [242] D. Merlet, M. Sarfati, B. Ancian, J. Courtieu, P. Lesot, Description of natural abundance deuterium 2D NMR experiments in weakly ordered liquid crystalline solvents using a tailored cartesian spin-operator formalism, *Phys. Chem. Chem. Phys.* 2 (2000) 2283-2290.
- [243] O. Lafon, P. Lesot, Deuterium three-dimensional NMR experiments for analysing weakly aligned, isotopically enriched molecules, *Chem. Phys. Lett.* 404 (2005) 90-94.
- [244] P. Lesot, O. Lafon, Enantiomeric analysis using natural abundance deuterium 3D NMR spectroscopy in polypeptide chiral oriented media, *Chem. Phys. Lett.* 458 (2008) 219-222.
- [245] P. Lesot, M. Sarfati, D. Merlet, B. Ancian, J.W. Emsley, B.A. Timimi, 2D-NMR strategy dedicated to the analysis of weakly ordered, fully deuterated enantiomers in chiral liquid crystals, *J. Am. Chem. Soc.* 125 (2003) 7689-7695.
- [246] O. Lafon, P. Berdagué, P. Lesot, Use of two-dimensional correlation between <sup>2</sup>H quadrupolar splittings and <sup>13</sup>C CSA's for assignment of NMR spectra in chiral nematics, *Phys. Chem. Chem. Phys.* 6 (2004) 1080-1084.
- [247] P. Lesot, O. Lafon, Experimental detection of achiral and chiral naturally abundant <sup>13</sup>C-<sup>2</sup>H isotopomers by 2D-NMR in liquids and chiral oriented solvents, *Anal. Chem.* 84 (2012) 4569-4573.
- [248] P. Tzvetkova, B. Luy, Q.E.COSY: determining sign and size of small deuterium residual quadrupolar couplings using an extended E.COSY principle, *Magn. Reson. Chem.* 54 (2016) 351-357.

- [249] O. Lafon, P. Lesot, D. Merlet, J. Courtieu, Modified z-gradient filtering as a new mean to obtain phased deuterium autocorrelation 2D NMR spectra in oriented solvents, *J. Magn. Reson.* 171 (2004) 135-142.
- [250] B. Plainchont, P. Berruyer, J.-N. Dumez, S. Jannin, P. Giraudeau, Dynamic nuclear polarization opens new perspectives for NMR spectroscopy in analytical chemistry, *Anal. Chem.* 90 (2018) 3639-3650.
- [251] R. Tycko, NMR at low and ultra low temperatures, *Acc. of Chem. Res.* 46 (2013) 1923-1932.
- [252] J. Farjon, How to face the low intrinsic sensitivity of 2X heteronuclear NMR with fast repetition techniques: go faster to go higher, *Magn. Reson. Chem.* 55 (2017) 883-892.
- [253] D. Marion, Fast acquisition of NMR spectra using Fourier transform of non-equispaced data, *J. Biomol. NMR*, 32 (2005) 149-151.
- [254] N.M. Balsgart, T. Vosegaard, Fast forward maximum entropy reconstruction of sparsely sampled data, *J. Magn. Reson.* 223 (2012) 164-169.
- [255] M. Mobli, J.C. Hoch, Non-uniform sampling and non-Fourier signal processing methods in multidimensional NMR, *Prog. Nucl. Magn. Reson. Spectrosc.* 83 (2014) 21-41.
- [256] O. Lafon, B. Hu, J.-P. Amoureux, P. Lesot, Fast and high-resolution stereochemical analysis by non-uniform sampling and covariance processing of anisotropic natural abundance 2D  $^2\text{H}$ -NMR datasets, *Chem. Eur. J.* 17 (2011) 6716-6724.
- [257] K. Kazmierczuk, O. Lafon, P. Lesot, Criteria for sensitivity enhancement by compressed sensing: practical application to anisotropic NAD 2D-NMR spectroscopy, *Analyst* 139 (2014) 2702-2713.
- [258] P. Lesot, K. Kazmierczuk, J. Trebosc, J.-P. Amoureux, O. Lafon, Fast acquisition of multidimensional NMR spectra of solids and mesophases using alternative sampling methods, *Magn. Reson. Chem.* 53 (2015) 927-939.
- [259] L. Frydman, A. Lupulescu, T. Scherf, Principles and features of single scan two-dimensional NMR spectroscopy, *J. Am. Chem. Soc.* 125 (2003) 9204-9217.
- [260] P. Giraudeau, L. Frydman, Ultrafast 2D NMR: an emerging tool in analytical spectroscopy, *Ann. Rev. Anal. Chem.* 7 (2014) 129-1061.
- [261] P. Giraudeau, T. Montag, B. Charrier, C.M. Thiele, Fast access to residual dipolar couplings by single-scan 2D NMR in oriented media, *Magn. Reson. Chem.* (2012), 50, S53-S57.
- [262] P. Lesot, P. Berdagué, P. Giraudeau, Detection of quadrupolar nuclei by ultrafast 2D-NMR: exploring the case of deuterated analytes aligned in chiral oriented solvents, *Chem. Commun.* 52 (2016) 2122-2125.
- [263] P. Pelupessy, Adiabatic single scan two-dimensional NMR spectroscopy, *J. Am. Chem. Soc.* 125 (2003) 12345-12350.
- [264] P. Mansfield, Spatial mapping of the chemical shift in NMR, *Magn. Reson. Med.* 1 (1984) 370-386.
- [265] H. Eyring, Activated Complex in Chemical Reactions, *Chem. Rev.* 17 (1935) 65-77.
- [266] A.D. Bain, Chemical exchange in NMR, *Prog. Nucl. Magn. Reson. Spectrosc.* 43 (2003) 63-103.
- [267] O. Lafon, P. Lesot, C.A. Fan, H.B. Kagan, Analysis of intramolecular dynamic processes in enantiomeric diaryl atropisomers and related derivatives through  $^2\text{H}$  NMR in polypeptide liquid crystals, *Chem. Eur. J.* 13 (2007) 3772-3786.
- [268] P. Lesot, O. Lafon, H.B. Kagan, P. Fan, Study of molecular rotational isomerism using deuterium NMR in chiral oriented solvents, *Chem. Commun.* (2006) 389-391.

- [269] M. Sarfati, C. Aroulanda, J. Courtieu, P. Lesot, Enantiomeric recognition of chiral invertomers through NMR in chiral oriented solvents: a study of the *cis*-decalin, *Tetrahedron: Asymmetry* 12 (2001) 737-744.
- [270] P. Lesot, C. Aroulanda, P. Berdagué, H. Zimmerman Z. Luz, Conformation and dynamics of 18-membered hexathia-metacyclophanes: The two steps chirality averaging as studied by deuterium NMR in chiral liquid crystalline solutions *J. Phys. Chem. B.* 115 (2011) 11793-11804.
- [271] J.-L. Canet, A. Fadel, J. Salaün, I. Canet-Fresse, J. Courtieu, Enantiomeric excess analysis of sesquiterpene precursors through proton-decoupled deuterium NMR in cholesteric lyotropic liquid crystal, *Tetrahedron: Asymmetry* 4 (1993) 31-34.
- [272] I. Canet, J. Courtieu, G. Dauphin, J.-G. Gourcy, H. Veschambre, Enantiomeric excess analysis of (2*R*,3*S*)-3-deuterio-2-methylcyclohexanone and (1*S*,2*R*,3*S*)-3-deuterio-2-methylcyclohexanol, through deuterium NMR in a polypeptide lyotropic liquid crystal, *Tetrahedron: Asymmetry* 6 (1995) 333-336.
- [273] A. Meddour, A. Haudrechy, P. Berdagué, W. Picoul, Y. Langlois, J. Courtieu, Analysis of the diastereoselectivity of a Diels-Alder cycloaddition through <sup>2</sup>H NMR in chiral liquid crystals, *Tetrahedron: Asymmetry* 7 (1996) 2489-2492.
- [274] A. Français, O. Bedel, W. Picoul, A. Meddour, J. Courtieu, A. Haudrechy, Highly enantioselective sequential Claisen-Ireland/metathesis: synthesis of cycloalkenes bearing two contiguous highly functionalized asymmetric centres, *Tetrahedron: Asymmetry* 16 (2005) 1141-1155.
- [275] F. Escalettes, D. Florentin, A. Marquet, C. Canlet, J. Courtieu, Desulfurization of biotin and epibiotin sulfoxides with nickel boride: analysis of the stereoselectivity through <sup>2</sup>H NMR in a polypeptide liquid crystal, *Tetrahedron Lett.* 39 (1998) 7499-7502.
- [276] A.A. Mitrochkine, I. Blain, C. Canlet, S. Pierre, J. Courtieu, M. Reglier, Enantioselective synthesis of *cis*- and *trans*-2(s)-amino-1-d-indane: debrominative [1,2]-hydride shift rearrangement by reduction of *cis*-2-azido-1-bromoindane with LiAlD<sub>4</sub>, *J. Org. Chem.* 62 (1997) 6204-6209.
- [277] A.V. Malkov, L. Gouriou, G.C. Lloyd-Jones, I. Starý, V. Langer, P. Spoor, V. Vinader, P. Kočovský, Asymmetric allylic substitution catalyzed by C<sub>1</sub>-symmetrical complexes of molybdenum: structural requirements of the ligand and the stereochemical course of the reaction, *Chem. Eur. J.* 12 (2006) 6910-6929.
- [278] M. Assié, A. Meddour, J.-C. Fiaud, J.-Y. Legros, Enantiodivergence in alkylation of 1-(6-methoxynaphth-2-yl)ethyl acetate by potassium dimethyl malonate catalyzed by chiral palladium-DUPHOS complex, *Tetrahedron: Asymmetry* 21 (2010) 1701-1708.
- [279] A.E. Leyes, C.D. Poulter, Synthesis of (*R*)-[2-<sup>2</sup>H] isopentenyl diphosphate and determination of its enantiopurity by <sup>2</sup>H NMR spectroscopy, *Org. Lett.* 1 (1999) 1067-1070.
- [280] D. O'Hagan, R.J.M. Goss, A. Meddour, J. Courtieu, Assay for enantiomeric analysis of [<sup>2</sup>H<sub>1</sub>]-fluoroacetic acid: insight into the stereochemical course of fluorination during fluorometabolite biosynthesis in *Streptomyces cattleya*, *J. Am. Chem. Soc.* 125 (2003) 379-387.
- [281] C.D. Cadicamo, J. Courtieu, H. Deng, A. Meddour, D. O'Hagan, Enzymatic fluorination in *Streptomyces cattleya* takes place with an inversion of configuration consistent with an S<sub>N</sub>2 reaction mechanism, *ChemBioChem.* 5 (2004) 685-690.
- [282] A. Amadasi, M. Bertoldi, R. Contestabile, S. Bettati, B. Cellini, M.L. di Salvo, C. Borri-Voltattorni, F. Bossa, A. Mozzarelli, Cloning, expression, purification, crystallization and preliminary X-ray studies of a pyridoxine 5'-phosphate oxidase from *Mycobacterium smegmatis*, *Curr. Med. Chem.* 14 (2007) 1291-1324.

- [283] M. Chan-Huot, P. Lesot, P. Pelupessy, L. Duma, P. Duchambon, G. Bodenhausen, M. D. Toney, U.V. Reddy, N. Suryaprakash, 'On-the-fly' kinetics of enzymatic racemization using deuterium NMR in DNA-based, oriented chiral solvents, *Anal. Chem.* 85 (2013) 4694-4697.
- [284] P. Lesot, Natural abundance deuterium NMR in chiral liquid crystals: technological evolutions methodological improvements and new analytical applications, *Spectra Analyse* 260 (2008) 16-22.
- [285] P. Lesot, Deuterium NMR of liquid-crystalline samples at natural abundance, *Encyclopedia of Magnetic Resonance (eMagRes)* 2 (2013) 315-334, J. Wiley: Chichester, *Eds.* R.K. Harris, R.E. Wasylishen.
- [286] C.A. Fan, B. Ferber, H.B. Kagan, O. Lafon, P. Lesot, Two aspects of the desymmetrization of selected prochiral aromatic or vinylic dihalides: enantioselective halogen-lithium exchange and prochiral recognition in chiral liquid crystals, *Tetrahedron: Asymmetry* 19 (2008) 2666-2677.
- [287] A. Parenty, J.-M. Campagne, C. Aroulanda, P. Lesot, Routine use of natural abundance deuterium NMR in a polypeptidic chiral oriented solvent for determination of the enantiomeric composition of chiral building blocks, *Org. Lett.* 4 (2002) 1663-1666.
- [288] A. Lemetay, Y. Bourdeux, P. Lesot, J. Farjon, J.-M. Beau, Synthesis of a mycobacterium tuberculosis tetra-acylated sulfolipid analogue and characterization of the chiral acyl chains using anisotropic NAD 2D-NMR spectroscopy, *J. Org. Chem.* 78 (2013) 7648-7657.
- [299] M. Sarfati, J. Courtieu, P. Lesot, First successful enantiomeric discriminations of chiral alkanes using NMR spectroscopy. *Chem. Commun.* (2000) 1113-1114.
- [290] E.E. Burnell, C.A. de Lange, Prediction from molecular shape of solute orientational order in liquid crystals. *Chem. Rev.* (1998) 98 2359-2388.
- [291] A. Masarwa, L. Oskar, A. Loewenstein, H.P. Reisenauer, D. Gerbig, P. Lesot, R. Schreiner, I. Marek, Probing the limits of NMR and VCD spectroscopy in the stereochemical assignment of chiral  $^2\text{H}_6$ -neopentane, *Angew. Chem., Int. Ed.* 54 (2015) 13106-13109.
- [292] G. Martin M.L. Martin, Deuterium labelling at natural abundance level as studied by high field quantitative  $^2\text{H}$  NMR, *Tetrahedron Lett.* 22 (1981) 3525-3528.
- [293] M.L. Martin, G.J. Martin, in *NMR basic principles and progress*, Ed. P. Diehl, Springer-Verlag Vol. 23, pp. 1-61, (1990).
- [294] D.A. Singleton, A.A. Thomas, High-precision simultaneous determination of multiple small kinetic isotope effects at natural abundance, *J. Am. Chem. Soc.* 117 (1995), 9357-93.
- [295] G. Martin, B.-L. Zhang, N. Naulet, M. Martin, Deuterium transfer in the bioconversion of glucose to ethanol studied by specific isotope labeling at the natural abundance level. *J. Am. Chem. Soc.* 108 (1986) 5116-5122.
- [296] S. Pionnier, R.J. Robins B.-L. Zhang, Natural abundance hydrogen isotope affiliation between the reactants and the products in glucose fermentation with yeast, *J. Agr. Food Chem.* 51 (2003) 2076-2082.
- [297] G.J. Martin, M.L. Martin, F. Mabon, J. Bricout, A new method for the identification of the origin of natural products. Quantitative  $^2\text{H}$  NMR at the natural abundance level applied to the characterization of anetholes, *J. Am. Chem. Soc.* 104 (1982) 2658-2659.
- [298] G.S. Remaud, M.L. Martin, G.G. Martin, G.J. Martin, Detection of sophisticated adulterations of natural vanilla flavors and extracts: application of the SNIF-NMR method to vanillin and *p*-hydroxybenzaldehyde, *J. Agric. Food Chem.* 45 (1997) 859-866.

- [299] G.S. Remaud, A.A. Debon, Y.-L. Martin, G.G. Martin, G.J. Martin, Authentication of bitter almond oil and cinnamon oil: application of the SNIF-NMR method to benzaldehyde. *J. Agric. Food Chem.* 45 (1997) 4042-4048.
- [300] J.-R. Duan, I. Billault, F. Mabon, R.J. Robins, Natural deuterium distribution in fatty acids isolated from peanut seed oil: a site-specific study by quantitative  $^2\text{H}$  NMR spectroscopy, *ChemBioChem*. 3 (2002) 752-759.
- [311] E. Tenailleau, P. Lancelin, R.J. Robins, S. Akoka, Authentication of the origin of vanillin using quantitative natural abundance C-13 NMR, *J. Agric. Food Chem.* 52 (2004) 7782-7787.
- [302] T. Jézéquel, V. Joubert, P. Giraudeau, G.S. Remaud, S. Akoka, The new face of isotopic NMR at natural abundance. *Magn. Reson. Chem.* 55 (2017) 77-90.
- [303] P. Lesot, C. Aroulanda, I. Billault, Exploring the analytical potential of NMR spectroscopy in chiral anisotropic media for the study of the natural abundance deuterium distribution in organic molecules, *Anal. Chem.* 76 (2004) 2827-2835.
- [304] V. Baillif, I. Billault, R.J. Robins, P. Lesot, Assignment of absolute configuration of natural abundance deuterium signals associated with (*R*)- and (*S*)-enantiomers in a fatty acid aligned in a chiral liquid crystal: enantioselective synthesis and NMR analysis, *J. Am. Chem. Soc.* 128 (2006) 11180-11187.
- [305] P. Lesot, V. Baillif, I. Billault, Combined analysis of four C-18 unsaturated fatty acids using natural abundance deuterium 2D NMR spectroscopy in chiral oriented solvents, *Anal. Chem.* 80 (2008) 2963-2972.
- [306] Z. Serhan, L. Martel, I. Billault, P. Lesot, Complete determination of natural site-specific enantiomeric excesses in linoleic acid using natural abundance deuterium 2D NMR in polypeptide mesophases, *Chem. Commun.* 46 (2010) 6599-6601.
- [307] P. Lesot, Z. Serhan, I. Billault, Recent advances in the analysis of the site-specific isotopic fractionation of metabolites such as fatty acids using anisotropic natural abundance  $^2\text{H}$  NMR spectroscopy: application on conjugated linolenic methyl esters, *Anal. Bioanal. Chem.* 399 (2011) 1187-1200.
- [308] P. Lesot, Determination of the natural deuterium distribution of fatty acids by application of  $^2\text{H}$  2D-NMR in liquid crystals: fundamentals, progresses, abroad and beyond, *Liq. Crystals*, online, DOI:10.1080/02678292.2019.1613685 (2019).
- [309] V. Baillif, R. Robins, S. Le Feunten, P. Lesot, I. Billault, Investigation of fatty acid elongation and desaturation steps in *Fusarium lateritium* by quantitative two-dimensional deuterium NMR spectroscopy in chiral oriented media, *J. Biol. Chem.* 284 (2009) 10783-10792.
- [310] R.S. Cahn, C. Ingold, V. Prelog, Specification of molecular chirality, *Angew. Chem., Int. Ed.* 5 (1966) 385-385.
- [311] I. Billault, A. Ledru, M. Ouetrani, Z. Serhan, P. Lesot, R.J. Robins, Probing substrate-product relationships by natural abundance deuterium 2D NMR spectroscopy in liquid-crystalline solvents: the case of the epoxidation of linoleate to vernoleate by two different plant enzymes, *Anal. Bioanal. Chem.* 402 (2012) 2985-2998.
- [312] E. Blée, U. Stahl, F. Schuber, S. Stymne, Regio- and stereo-electivity of cytochrome P-450 and peroxxygenase dependent formation of *cis*-12,13-epoxy-9(*Z*)-octadecenoic acid (vernolic acid) in *Euphorbia lagascae*, *Biochem. Biophys. Res. Commun.* 197 (1993) 778-784.
- [313] M. Lee, M. Lenman, A. Banas, M. Bafor, S. Singh, M. Schweizer, R. Nilsson, C. Liljenberg, A. Dahlqvist, P.O. Gummesson, S. Sjodahl, A. Green, S. Stymne, Identification of non-heme diiron proteins that catalyze triple bond and epoxy group formation, *Science* 280 (1998) 915-918.

- [314] Z. Serhan, I. Billault, A. Borgogno, A. Ferrarini, P. Lesot, Analysis of NAD 2D-NMR spectra of saturated fatty acids in polypeptide aligning media by experimental and modeling approaches, *Chem. Eur. J.* 18 (2012) 117-126.
- [315] P. Lesot, Z. Serhan, C. Aroulanda, I. Billault, Analytical contribution of NAD 2D-NMR spectroscopy in polypeptide mesophases to the investigation of triglycerides, *Magn. Reson. Chem.* 50 (2012) S2-S11.
- [316] S.I. Altmann, The summary of nonrigid molecules: the Schrödinger supergroup, *Proc. Roy. Soc. (London)* A298 (1967) 184-203.
- [317] J. Jacob, J.-R. Disnar, G. Bardoux G., Carbon isotope evidence for sedimentary miliacin as a tracer of *Panicum miliaceum* (broomcorn millet) in the sediments of Lake le Bourget (French Alps), *Org. Geochem.* 39 (2008) 1077-1080.
- [318] P. Berdagué, P. Lesot, J. Jacob, V.-J. Terwilliger, C. Lemilbeau, Contribution of NAD 2D-NMR in liquid crystals to the determination of hydrogen isotope profile of methyl groups in miliacin, *Geochim. Cosmochim. Acta.* 173 (2016) 337-351.
- [319] B. Toulemonde, I. Horman, H. Egli, M. Derbesy, Differentiation between natural and synthetic vanillin samples using  $^2\text{H}$  NMR. *Helv. Chim. Acta.* 66 (1983) 2342-2345.
- [320] G.S. Remaud, S. Akoka, A review of flavors authentication by position specific isotope analysis by nuclear magnetic resonance spectrometry: the example of vanillin, *Flavour Fragrance J.* 32 (2016) 77-84.
- [321] T. Texier-Bonniot, P. Berdagué, R.J. Robins, G. Remaud, P. Lesot, Analytical contribution of deuterium 2D-NMR in oriented solvents to  $^2\text{H}/^1\text{H}$  isotopic characterization: the case of vanillin, *Flavour Fragrance J.* 34 (2018) 217-229.
- [322] A. Bax, G. A. Morris, An Improved method for heteronuclear chemical-shift correlation by two-dimensional NMR, *J. Magn. Reson.* 42 (1981) 501-505.
- [323] P. Caravatti, L. Braunschweiler, R.R. Ernst, HETCOR spectroscopy in rotating solids, *Chem.*
- [324] O. Lafon, P. Berdagué, P. Lesot, Use of two-dimensional correlation between  $^2\text{H}$  quadrupolar splittings and  $^{13}\text{C}$  CSA's for assignment of NMR spectra in chiral nematics, *Phys. Chem. Chem. Phys.* 6 (2004) 1080-1084.
- [325] P. Lesot, O. Lafon, P. Berdagué, Correlation 2D-NMR experiments involving both  $^{13}\text{C}$  and  $^2\text{H}$  isotopes in oriented media: methodological developments and analytical applications, *Magn. Reson. Chem.* 52 (2014) 595-613.
- [326] P. Lesot, O. Lafon, Experimental detection of achiral and chiral naturally abundant  $^{13}\text{C}$ - $^2\text{H}$  isotopomers by 2D-NMR in liquids and chiral oriented solvents, *Anal. Chem.* 84 (2012) 4569-4573.
- [327] C. Auger, A. Lesage, S. Caldarelli, P. Hodgkinson, L. Emsley, Deuterium-carbon NMR correlation spectroscopy in oriented materials, *J. Am. Chem. Soc.* 119 (1997) 12000-12001.
- [328] C. Auger, A. Lesage, S. Caldarelli, P. Hodgkinson, L. Emsley. Assignment and measurement of deuterium quadrupolar couplings in liquid crystals by deuterium-carbon NMR correlation spectroscopy, *J. Phys. Chem. B.* 120 (1998) 3718-3723.
- [329] C. Aroulanda, O. Lafon, P. Lesot, Enantiodiscrimination of flexible cyclic solutes using deuterium NMR spectroscopy in polypeptide chiral mesophases: investigation of cis-decalin and THF, *J. Phys. Chem. B.* 113 (2009) 10628-10640.
- [330] H. Villar, F. Guibé, C. Aroulanda, P. Lesot, Investigation of  $\text{SmI}_2$  mediated cyclisation process of  $\delta$ -iodo- $\alpha$ ,  $\beta$ -unsaturated esters by deuterium 2D NMR in oriented solvents, *Tetrahedron: Asymmetry* 13 (2002) 1465-1475.

- [331] O. Lafon, P. Lesot. Theoretical and experimental investigation of  $^{13}\text{C}$  relayed  $^2\text{H}$ - $^2\text{H}$ -COSY 2D experiments: application to the analysis of weakly aligned solutes, *J. Magn. Reson.* 174 (2005) 254-264.
- [332] K. Benali, O. Lafon, H. Zimmermann, E. Guittet, P. Lesot, Homo- and heteronuclear 2D NMR approaches to analyse a mixture of deuterated unlike/like compounds using weakly ordering chiral liquid crystals, *J. Magn. Reson.* 187 (2007) 205-215.
- [333] M.A. Delsuc, E. Guittet, N. Trotin, J.-Y. Lallemand, Two-dimensional correlation spectroscopy with heteronuclear relay, *J. Magn. Reson.* 56 (1984) 163-166.
- [334] D. Neuhaus, G. Wider, K. Wagner, K. Wüthrich, X-relayed  $^1\text{H}$ - $^1\text{H}$  correlated spectroscopy, *J. Magn. Reson.* 57 (1984) 164-168.
- [335] M.R. Bendall, D.T. Pegg, D.M. Doddrell, Polarization transfer pulse sequences for two-dimensional NMR by Heisenberg vector analysis, *J. Magn. Reson.* 45 (1981) 8-29.
- [336] M.H. Levitt, in *Encyclopedia of Magnetic Resonance*, Vol. 2, Eds. D.M. Grant, R.K Harris, Wiley, Chichester, U.K. pp. 1396. (1996).
- [337] M.H. Levitt, Composite Pulses, in *Encyclopedia of Nuclear Magnetic Resonance*, Eds. D.M. Grant, R.K. Harris, Wiley, Chichester, U.K., pp. 1396, 1996.
- [338] P.E. Hansen, Isotope effects in nuclear shielding, *Prog. Nucl. Magn. Reson. Spectrosc.* 64 (1988) 207-255.
- [339] M. Jakubcova, A. Meddour, J.-M. Péchiné, A. Baklouti, J. Courtieu, Measurement of the optical purity of fluorinated compounds using proton decoupled  $^{19}\text{F}$ -NMR spectroscopy in a chiral liquid crystal solvent, *J. Fluorine Chem.* 86 (1997) 149-153.
- [340] L. Pauling, The nature of the chemical bond. IV. The energy of single bonds and the relative electronegativity of atoms, *J. Am. Chem. Soc.* 54 (1932) 3570-3582.
- [341] L. Pauling, *Nature of the Chemical Bond*, pp. 88-107, (1960), Cornell University Press. ISBN 978-0-8014-0333-0.
- [342] W.B. Jensen, Electronegativity from Avogadro to Pauling: Part 1: origins of the electronegativity concept, *J. of Chem. Educ.* 73 (1996) 11-20.
- [343] A. Bondi, Van der Waals volumes and radii, *J. Phys. Chem.* 68 (1964) 441-451.
- [344] M.E Di Pietro, G. Celebre, G. De Luca R.A Salvino. C. Aroulanda, D. Merlet, G. De Luca, The use of residual dipolar couplings for conformational analysis of non-steroidal anti-inflammatory drugs dissolved in weakly ordering media liquid crystals, *Liq. Crystals* 45 (2018) 2033-2047.
- [345] M.E. Di Pietro, C. Aroulanda, D. Merlet, G. Celebre, G. De Luca, Conformational investigation in solution of a fluorinated anti-inflammatory drug by NMR spectroscopy in weakly ordering, *J. Phys. Chem. B* 118 (2014) 9007-9016.
- [346] M.E. Di Pietro, C. Aroulanda, G. Celebre, D. Merlet, G. De Luca, The conformational behaviour of naproxen and flurbiprofen in solution by NMR spectroscopy, *New J. Chem.* 39 (2015) 9086-9097.
- [347] J.W. Emsley, G.R. Luckhurst, C.P. Stockley, A theory of orientational ordering in uniaxial liquid-crystals composed of molecules with alkyl chains, *Proc. R. Soc. Lond. A.* 381 (1982) 117-138.
- [348] J.W. Emsley, I.D. Wallington, D. Catalano, C. A. Veracini, G. Celebre, M. Longeri, Comparison of the maximum entropy and additive potential methods for obtaining rotational potentials from the NMR spectra of samples dissolved in liquid crystalline solvents. The case of 4-nitro-1-(beta.,beta.,beta.-trifluoroethoxy)benzene, *J. Phys. Chem.* 97 (1993) 6518-6523.
- [349] G. Celebre, G. De Luca, J.W. Emsley, E.K. Foord, M. Longeri, F. Lucchesini, G. Pileio, The conformational distribution in diphenylmethane determined by nuclear magnetic resonance

- spectroscopy of a sample dissolved in a nematic liquid crystalline solvent, *J. Chem. Phys.* 118 (2003) 6417-6426.
- [350] M.E. Di Pietro, C. Aroulanda, D. Merlet, A new gradient encoded SERF experiment for the trivial edition of  $^1\text{H}$ - $^{19}\text{F}$  couplings, *J. Magn. Reson.* 234 (2013) 101-105.
- [351] A. Meddour, J. Uziel, J. Courtieu, S. Jugé, Enantiodifferentiation of acyclic phosphonium salts in chiral liquid-crystalline solutions, *Tetrahedron: Asymmetry* 17 (2006) 1424-1429.
- [352] C. Brevard, in *Handbook of high resolution multinuclear NMR*, New York, Wiley-Interscience, (1981).
- [353] C. Huguenard, F. Taulelle, E. Graf, NMR in a liquid crystal solvent: study of the chirality of borocryptates, *J. Chim. Phys.* 95 (1998) 341-349.
- [354] E. Graf, M.W. Hosseini, A. De Cian, J. Fischer, Simultaneous binding of boron and alkaline metal cations by a macrocyclic ligand bearing catechol units: structural analysis of borocryptates, *Bull. Soc. Chim. Fr.* 133 (1996) 743-748.
- [355] R.R. Fraser, M.A. Petit, M. Miskow, Separation of nuclear magnetic resonance signals of internally enantiotropic protons using a chiral shift reagent. Deuterium isotope effect on geminal proton-proton coupling constants, *J. Am. Chem. Soc.* 94 (1972) 3253-3254.
- [356] R.W. Lang, H.J. Hansen,  $^1\text{H}$ -NMR. Spectroscopic analysis of prochiral allenic esters using optically active europium shift reagents, *Helv. Chem. Acta* 62 (1979) 1458-1465.
- [357] A. Bilz, T. Stork, G. Helmchen, New chiral solvating agents for carboxylic acids: discrimination of enantiotopic nuclei and binding properties, *Tetrahedron: Asymmetry* 8 (1997) 3999-4002.
- [358] J. Huskens, R. Goddard, M.T. Reetz, Direct observation of stereotopic group recognition in solution and solid state, *J. Am. Chem. Soc.* 120 (1998) 6617-6618.
- [359] P. Lesot, C. Aroulanda, Z. Luz, Analysis of the enantiotopic discrimination in the NMR spectra of prochiral solutes dissolved in chiral liquid crystals by symmetry factorization of the Saupe ordering matrix, *J. Chem. Phys.* 131 (2009) 104501/1-16.
- [360] D. Merlet, J.W. Emsley, J. Jokisaari, J. Kaski, Characterisation of the structure, deuterium quadrupolar tensors, and orientational order of acenaphthene, a rigid, prochiral molecule, from the NMR spectra of samples dissolved in nematic and chiral nematic liquid crystalline solvents, *Phys. Chem. Chem. Phys.* 3 (2001) 4918-4925.
- [361] C. Aroulanda, D. Merlet, J. Courtieu, P. Lesot, NMR experimental evidence of the differentiation of enantiotopic directions in  $C_s$  and  $C_{2v}$  molecules using partially oriented, chiral media, *J. Am. Chem. Soc.* 123 (2001) 12059-12066.
- [362] C. Aroulanda, P. Lesot, D. Merlet, J. Courtieu, Structural ambiguities in bridged ring systems resolved using natural abundance deuterium NMR in chiral liquid crystals, *J. Phys. Chem. A.* 107 (2003) 10911-10918.
- [363] C. Aroulanda, H. Zimmermann, Z. Luz, P. Lesot, Enantiotopic discrimination in the deuterium NMR spectrum of solutes with  $S_4$  symmetry in chiral liquid crystals, *J. Chem. Phys.* 134 (2011) 134502-1/8.
- [364] F.A. Cotton, in *Chemical applications of group theory*, 3<sup>rd</sup> Ed., J. Wiley & Sons, New York, pp. 58. (1990).
- [365] C. Naumann, P.W. Kuchel, NMR (pro)chiral discrimination using polysaccharide gels, *Chem. Eur. J.* 15 (2009) 12189-12191.
- [366] G. Kummerlöwe, M. Udaya Kiran, B. Luy, Covalently cross-linked gelatin allows chiral distinction at elevated temperatures and in DMSO, *Chem. Eur. J.* 15 (2009) 12192-12195.



- [367] P.J. Flory, Foundations of rotational isomeric state theory and general methods for generating configurational averages, *Macromolecules* 7 (1974) 381-392.
- [368] V.M. Gil, A.J.C. Varandas, J.N. Murrell, On the use of the rotational isomeric state approximation in studies of internal rotation, *Can. J. Chem.* 61 (1983) 163-170.
- [369] P. Lesot, O. Lafon, H. Zimmermann, Z. Luz, Enantiodiscrimination in deuterium NMR spectra of flexible chiral molecules with average axial symmetry dissolved in chiral liquid crystals: the case of tridioxymethylenetriphenylene, *J. Am. Chem. Soc.* 130 (2008) 8754-8761.
- [370] O. Lafon, P. Lesot, H. Zimmermann, R. Poupko, Z. Luz, Chiral discrimination in the  $^{13}\text{C}$  and  $^2\text{H}$  NMR of the crown and saddle isomers of nonamethoxy-cyclotrimeratrylene in chiral liquid-crystalline solutions, *J. Am. Chem. Soc.* 111 (2007) 9453-9467.
- [371] D. Merlet, A. Loewenstein, W. Smadja, J. Courtieu, P. Lesot, Quantitative description of the facial discrimination of molecules containing a prochiral group oriented in a chiral liquid crystalline solution, *J. Am. Chem. Soc.* 120 (1998) 963-969.
- [372] K. Mislow, M. Raban, in *Topics in stereochemistry*, Vol. 1, Eds. N.L. Allinger, E.L. Eliel, Wiley, New York, (1967).
- [385] S. Fujita, Chirality fittingness of an orbit governed by a coset representation. Integration of point-group and permutation-group theories to treat local chirality and prochirality, *J. Am. Chem. Soc.* 112 (1990) 3390-3397.
- [386] S. Fujita, Promolecules for characterizing stereochemical relationships in non-rigid molecules, *Tetrahedron* 47 (1991) 31-46.
- [375] S. Fujita, Systematic characterization of prochirality, prostereogenicity, and stereogenicity by means of the sphericity concept, *Tetrahedron* 56 (2000) 735-740.
- [376] J.D. Baleja, J. Moulton, B.D. Sykes, Distance measurement and structure refinement with NOE data, *J. Magn Reson.* 87 (1990) 375-384.
- [377] S.G. Molodtsov, M.E. Elyashberg, K.A. Blinov, A.J. Williams, E.E. Martirosova, G.E. Martin, B. Lefevre, Structure elucidation from 2D NMR spectra using the *struceluc* expert system: detection and removal of contradictions in the data, *J. Chem. Inf. Comput. Sci.* 44 (2004) 1737-1751.
- [378] M.E. Elyashberg, K.A. Blinov, S.G. Molodtsov, A.J. Williams, G.E. Martin, Fuzzy structure generation: A new efficient tool for computer-aided structure elucidation (CASE), *J. of Chem. Inform. Model.* 47 (2007) 1053-1066.
- [379] R. Lipsitz, N. Tjandra, Residual dipolar couplings in NMR structure analysis, *Ann. Rev. Biophys. Biomol. Struct.* 33 (2004) 387-413.
- [380] C. Kang, N. Tjandra, The use of residual dipolar coupling in studying proteins by NMR, *Topics in current chemistry*, 326 (2012) 47-67.
- [381] L. Salmon, G. Bascom, I. Andricioaei, H.M. Al-Hashimi, A general method for constructing atomic-resolution RNA ensembles using NMR residual dipolar couplings: the basis for interhelical motions revealed, *J. Am. Chem. Soc.* 135 (2013) 5457-5466.
- [382] C. Aroulanda, V. Boucard, E. Guibé, J. Courtieu, D. Merlet, Weakly oriented liquid-crystal NMR solvents as a general tool to determine relative configurations, *Chem. Eur. J.* 9 (2003) 4536-4539.
- [383] C.-M. Thiele, S. Berger, Probing the diastereotopicity of methylene protons in strychnine using residual dipolar couplings, *Org. Lett.* 5 (2003) 705-708.

- [384] L. Verdier, P. Sakhaii, M. Zwecktetter, C. Griesinger, Measurement of long range H,C couplings in natural products in orienting media: a tool for structure elucidation of natural products, *J. Magn. Reson.* 163 (2003) 353-359.
- [385] J. Farjon, M. Radzom, P. Haberz, A. Zeeck, M. Blackledge, C. Griesinger, U.M. Reinscheid, Effect of the solvent on the conformation of a depsipeptide: NMR-derived solution structure of hormaomycin in DMSO from residual dipolar couplings in a novel DMSO-compatible alignment medium, *ChemBioChem.* 7 (2006) 287-296.
- [386] C.-M. Thiele, V. Schmidts, B. Böttcher, I. Louzao, R. Berger, A. Maliniak, B. Stevensson, On the treatment of conformational flexibility when using residual dipolar coupling for structure determination, *Angew. Chem., Int. Ed.* 48 (2009) 6708-6712.
- [387] B. Böttcher, V. Schmidts, J. A. Raskatov, C.-M. Thiele, Determination of the conformation of the key intermediate in an enantioselective palladium-catalyzed allylic substitution from residual dipolar couplings, *Angew. Chem., Int. Ed.* 49 (2010) 205-209.
- [388] J.A.A. Franca, A. Navarro-Vazquez, XX Lei, H. Sun, C. Griesinger, F. Hallwass, Complete NMR assignment and conformational analysis of 17- $\alpha$ -ethinylestradiol by using RDCs obtained in grafted graphene oxide, *Magn. Reson Chem.* 55 (2017) 297-303.
- [389] Y. Liu, J. Saurí, E Mevers, M.W. Pecuh, H. Hiemstra, J. Clardy, G.E. Martin, R.T. Williamson, Unequivocal determination of complex molecular structures using anisotropic NMR measurements, *Science* 356 (2017) eaam5349.
- [390] D.J. Milanowski, N. Oku, L.K. Cartner, H.R. Bokesch, R.T. Williamson, J. Saurí, Y. Liu, K.A. Blinov, Y. Ding, X.-C. Li, D. Ferreira, L.A Walker, S. Khan, M.T. Davies-Coleman, J.A. Kelley, J.B. McMahon, G.E. Martin, K.R. Gustafson, Unequivocal determination of caulamidines A and B: application and validation of new tools in the structure elucidation tool box, *Chem. Sci.* 9 (2018) 307-314.
- [391] S. Immel, M. Koeck, M. Reggelin, Configurational analysis by residual dipolar couplings: A critical assessment of diastereomeric differentiabilitys, *Chirality* 31 (2019) 384-400.
- [392] S. Immel, M. Köck, M. Regelin, Configurational analysis by residual dipolar coupling driven floating chirality distance geometry calculations, *Chem. Eur. J.* 24 (2018) 13918-13930.
- [393] G. Cornilescu, A. Bax, Measurement of proton, nitrogen, and carbonyl chemical shielding anisotropies in a protein dissolved in a dilute liquid crystalline phase, *J. Am. Chem. Soc.* 122 (2000) 10143-10154.
- [394] A. Navarro-Vázquez, MSpin-RDC. A program for the use of residual dipolar couplings for structure elucidation of small molecules, *Magn. Reson. Chem.* 50 (S1) (2012) S73-S79.
- [395] P. Tzvetkova, U. Sternberg, T. Gloge, A. Navarro-Vázquez, B. Luy, Configuration determination by residual dipolar couplings: accessing the full conformational space by molecular dynamics with tensorial constraints, *Chem. Sci.* (2019). Advance Article, DOI: 10.1039/C9SC01084J.
- [396] A. Navarro-Vazquez, P. Berdagué, P. Lesot, Integrated computational protocol for analyzing quadrupolar splittings from natural abundance deuterium NMR Spectra in (chiral) oriented media, *ChemPhysChem.* 18 (2017) 1252-1266.
- [397] P. Lesot, Nuclear Magnetic Resonance Spectroscopy | Hydrogen Isotopes:  $^2\text{H}$  NMR, *Encyclopedia of Analytical Science*, 3<sup>rd</sup> Edition, (2019), 152-167. DOI: 10.1016/B978-0-12-409547-2.14084-3.
- [398] S. Hansmann, T. Larem, C.-M. Thiele, Enantiodifferentiating properties of the alignment media PELG and PBLG - A comparison, *Eur. J. Org. Chem.* 7 (2016) 1324-1329.

- [399] A. Marx, V. Schmidts, C.-M. Thiele, How different are diastereomorphous orientations of enantiomers in the liquid crystalline phases of PBLG and PBDG: a case study, *Magn. Reson. Chem.* 47 (2009) 724-740.
- [400] B. Yu, H. van Ingen, S. Vivekanandan, C. Rademacher, S.E. Norris, D.I. Freedberg, More accurate  $^1J_{\text{CH}}$  coupling measurement in the presence of  $^3J_{\text{HH}}$  strong coupling in natural abundance, *J. Magn. Reson.* 215 (2012) 10-22.
- [401] F. Kramer, M.V. Deshmukh, H. Kessler, S.J. Glaser, Residual dipolar coupling constants: An elementary derivation of key equations, *Concepts Magn. Reson. A.* 21 (2004) 10-21.
- [402] J.R. Tolman, H.M. Al-Hashimi, L.E. Kay, J.H. Prestegard, Structural and dynamic analysis of residual dipolar coupling data for proteins, *J. Am. Chem. Soc.* 123 (2001) 1416-1424.
- [403] J. Courtieu, C. Aroulanda, P. Lesot, A. Meddour, D. Merlet, Evolution of the Saupe order parameters of enantiomers from a non-chiral to a chiral liquid crystal solvent: an original light on the absolute configuration problem, *Liq. Crystals* 37 (2010) 903-912.
- [404] V.M. Marathias, G.J. Tawa, I. Goljer, A.C. Bach, Stereochemical identification of (*R*)- and (*S*)-ibuprofen using residual dipolar couplings, NMR, and modeling, *Chirality* 19 (2007) 741-750.
- [405] R. Berger, J. Courtieu, R.R. Gil, C. Griesinger, M. Köck, P. Lesot, B. Luy, D. Merlet, A. Navarro-Vazquez, M. Reggelin, U.M. Reinscheid, C.-M. Thiele, M. Zweckstetter, Is the determination of absolute configuration possible by using residual dipolar couplings from chiral-non-racemic alignment media? - A critical assessment, *Angew. Chem., Int. Ed.* 51 (2012) 2-5.
- [406] J. Helfrich, R. Hentschke, U.M. Apel, Molecular-dynamics simulation study of poly( $\gamma$ -benzyl *L*-glutamate) in dimethylformamide, *Macromolecules* 2 (1994) 472-482.
- [407] A.O. Frank, J.C. Freudenberger, A.K. Shaytan, H. Kessler, B. Luy, Direct prediction of residual dipolar couplings of small molecules in a stretched gel by stochastic molecular dynamics simulations, *Magn. Reson. Chem.* 53 (2015) 213-217.
- [408] E. Alvira, J. Breton, J. Plata, Chiral discrimination - a model for the interaction between a helicoidal system and an amino-acid molecule, *Chem. Phys.* 155 (1991) 7-18.
- [409] N. Nandi, Role of secondary level chiral structure in the process of molecular recognition of ligand: Study of model helical peptide, *J. Phys. Chem. B* 108 (2004) 789-797.
- [410] G. Celebre, On the anisotropic intermolecular potential of biaxial apolar solutes in nematic solvents: Monte Carlo predictions and experimental data, *J. Chem. Phys.* 115 (2001) 9552-9556.
- [411] J. Photinos, in *NMR of ordered liquids*, Eds. E.E. Burnell, C.A. de Lange, Kluwer Academic Publisher, Dordrecht, Chap. 12, (2003).
- [412] G. Celebre, G. De Luca, C. D'Urso, M.E. Di Pietro, Helical solutes orientationally ordered in anisotropic media composed of helical particles: Formulation of a mean torque potential sensitive to *P* and *M* chirality as a tool for the assignment of the absolute configuration of enantiomers, *J. Mol. Liquids*, (2019) 288, 111044 (1-5).
- [413] L. Ziani, P. Lesot, A. Meddour, J. Courtieu, Empirical determination of the absolute configuration of small chiral molecules using natural abundance  $^2\text{H}$  NMR in chiral liquid crystals, *Chem. Commun.* (2007) 4737-4739.
- [414] H.J. Krabbe, H. Heggemeir, B. Schrader, E.H. Korte, Determination of the absolute-configuration of chiral molecules from the infrared rotatory-dispersion of their liquid-crystalline solutions, *J. Chem. Res. (S)* (1978) 238-238.

- [415] C. Griesinger, M. Bennati, H.M. Vieth, C. Luchinat, G. Parigi, P. Höfer, F. Engleke, S.J. Glaser, V. Denysenkov, T.F. Prisner, Dynamic nuclear polarization at high magnetic fields in liquids, *Prog. Nucl. Magn. Reson. Spectrosc.* 64 (2012) 4-28.
- [416] A.J. Rossini, J. Schlagnitweit, A. Lesage, L. Emsley, High-resolution NMR of hydrogen in organic solids by DNP enhanced natural abundance deuterium spectroscopy, *J. Magn. Reson.* 259 (2015) 192-198.
- [417] A.S.L. Thankamony, J.J. Wittmann, M. Kaushik, B. Corzilius, Dynamic nuclear polarization for sensitivity enhancement in modern solid-state NMR, *Prog. Nucl. Magn. Reson. Spectrosc.* 102/103 (2017) 120-195.
- [418] A. Rankin, J. Trébosc, F. Pourpoint, J.-P. Amoureux, O. Lafon, Recent developments in MAS DNP-NMR of materials, *Solid-State Nucl. Magn. Reson.* In press DOI: 10.1016/j.ssnmr.2019.05.009.
- [419] J. Courtieu, Forty-five years of stubborn dedication to NMR in partially ordered solvents, *Encyclopedia of Magnetic Resonance (eMagRes)*, (2010), DOI: 10.1002/9780470034590.emrhp1009.

POST-PRINT

Acronyms & notations of NMR and analytical methods

<sup>1</sup> H:	Proton	HMBC:	Heteronuclear multiple bond correlation
<sup>2</sup> H:	Deuterium	HMQC:	Heteronuclear multiple quantum coherence
<sup>10,11</sup> B:	Boron-10 and Boron-11	HPLC:	High pressure liquid chromatography
<sup>13</sup> C:	Carbon-13	HSQC:	Heteronuclear single quantum coherence
<sup>14</sup> N:	Nitrogen-14	INADEQUATE:	Incredible natural abundance DQ transfer experiment
<sup>19</sup> F:	Fluorine-19	IRMS (irMS)	Isotopic ratio mass spectroscopy
<sup>31</sup> P:	Phosphorus-31	K <sub>C-D</sub> :	<sup>2</sup> H-quadrupolar coupling constant
<sup>133</sup> Cs:	Cesium-133	MAS:	Magic angle spinning
2D:	Two dimensional	MC:	Monte Carlo
3D:	Three dimensional	MD:	Molecular dynamics
AC:	Absolute configuration	MQ:	Multi-quanta
ADUF:	Anisotropic deuterium ultra fast	MW:	Molecular weight
ANAD:	Anisotropic natural abundance deuterium	N*:	Chiral nematic
BIRD:	Bilinear rotation decoupling	NAD:	Natural abundance deuterium
B <sub>0</sub> :	Static magnetic field of spectrometer	NAD-{ <sup>1</sup> H}:	Natural abundance deuterium with <sup>1</sup> H decoupling
B <sub>1</sub> :	Radiofrequency field of the probe	NASDAC:	Natural abundance spectroscopy for deuterium and carbon
CDCOM:	Carbon-deuterium correlation in oriented media	NMR:	Nuclear magnetic resonance
CIP:	Cahn, Ingold and Prelog's rules	NOE:	Nuclear Overhauser effect
CISS:	Chiral-induced spin selectivity	NOESY:	Nuclear Overhauser effect spectroscopy
Cov:	Covariance transformation	NUS:	Non uniform sampling
CP:	Cross polarization	n:	Director of the mesophase
CPD:	Composite pulse decoupling	ORD:	Optical rotatory dispersion
CS:	Compressed sensing	PAS:	Principal axis system
CSA:	Chemical shift anisotropy	PFG:	Pulse field gradient
DCD:	Deuterium-carbon-deuterium transfer	QCC:	Quadrupolar coupling constant
DECADENCY:	Deuterium carbon deuterium nuclear correlation spectroscopy	Q-COSY:	Quadrupolar correlation spectroscopy
DFT:	Density functional theory	Q-COSY Fz:	Quadrupolar correlation spectroscopy with z- gradient filter
DIE:	Diastereo-isotopomeric excess	QD:	Quadrupolar doublet
DKR:	Dynamic kinetic resolution	QS:	Quadrupolar splitting (Hz)
DNP:	Dynamic nuclear polarization	QUOSY:	Quadrupole ordered spectroscopy
DOE:	Differential ordering effect	Q-resolved:	Quadrupolar resolved experiment
DP:	Degree of polymerization	Q-resol. Fz:	Quadrupolar resolved experiment with z-gradient filter
DQ:	Double quantum	RAS:	Initial axis system
EE (ee):	Enantiomeric excess	RC:	Relative configuration
EFG:	Electric field gradient	RCSA:	Residual chemical shift anisotropy
EIE (eie):	Enantio-isotopomeric excess	RDC:	Residual dipolar coupling
EPSI:	Echo-planar spectroscopic-maximum imaging	r <sub>ij</sub> :	Internuclear vector i-j
FID:	Free induction decay	RIS:	Rotational isomeric state
FT:	Fourier transformation	R-NASDAC:	Refocussed natural abundance spectroscopy for deuterium and carbon
FWHM:	Full width at half maximum	ROA:	Raman optical activity
GC:	Gas chromatography	ROESY:	Rotating-frame Overhauser effect spectroscopy
GDO:	General degree of orientation	RQC:	Residual quadrupolar coupling
GET-SERF:	Gradient encoded heteronuclear SERF		
GIAO:	Gauge-including atomic orbital		
G-SERF:	Gradient encoded selective Excitation refocussing		
HETCOR:	Heteronuclear correlation		
HETSERF:	Heteronuclear selective excitation refocusing		

### Acronyms & notations of NMR and analytical methods (continued)

RT:	Room temperature	T <sub>2</sub> :	Transverse relaxation time
SAPS:	Spectral aliased pure shift	UF:	Ultrafast
S <sub>αβ</sub> :	αβ elements of the Saupe order matrix	VASS:	Variable angle spinning sample
SEF:	Spatial encoding frequency	T <sub>R</sub> :	Recycling delay
SERF:	Selective excitation refocussing	T <sub>1</sub> :	Longitudinal relaxation time
SNIF:	Site-specific natural isotopic fractionation	T <sub>2</sub> :	Transverse relaxation time
SNR:	Signal-to-noise ratio	UF:	Ultrafast
SSNMR:	Solid-State NMR	VASS:	Variable angle spinning sample
SVD:	Singular value decomposition	VCD:	Vibrational circular dichroism
T <sub>exp</sub> :	Experimental time	r <sub>ij</sub> :	Internuclear vector i-j
T <sub>R</sub> :	Recycling delay	V-SMOW:	Vienna standard mean ocean water
T <sub>1</sub> :	Longitudinal relaxation time		

### Acronyms & notations of molecules or class of molecules

5CB:	4-n-pentyl-4'-cyanobiphenyl	MLn:	Methyl linolenate
ADDA:	Achiral deuterated derivatizing	MM:	Methyl myristate
AINS:	Anti-inflammatory non stereoidal	NMP:	N-methyl-2-pyrrolidone
ALA:	(L/D)-alanine	MO:	Methyl oleate
ALC:	Achiral liquid crystal	MP:	Methyl palmitate
AR:	Alanine racemase	MPu:	Methyl punicate
BPTH:	1,1'-bis-phenylthiohexane	MS:	Methyl stearate
CDA:	Chiral derivatizing agent	MV:	Methyl vernoleate
CDC:	Cis-decalin	PDMS:	Poly(dimethylsiloxane)
Ch:	Cholesteric	PB(L/D)G:	Poly-γ-benzyl-(L/D)-glutamate
CLC:	Chiral liquid crystal	PM:	Phenyl methanol
CLSR:	Chiral lanthanide-induced shift reagent	PBPM(L/D)G:	Poly-γ-p-biphenylmethyl-(L/D)-glutamate
CP:	Cross polarization	PCB(L/D)L:	Poly-ε-carbobenzyloxy-(L/D)-Lysine
COA:	Chiral ordering agent	PE(L/D)G:	Poly-γ-ethyl-(L/D)-glutamate
CSA:	Chiral solvating agent	PMB(L/D)G:	Poly-γ-(S)-2-methylbutyl-(L/D)-glutamate
CUFA:	Conjugated unsaturated fatty acid	PP(L/D)A:	Poly-β-phenethyl-(L/D)-aspartate
DFM:	Difluoromethane	PYR (Py)	Pyridine
DHEA:	Dehydroepiandrosterone	RNA:	Ribonucleic acid
DMF:	Dimethylformamide	SFA:	Saturated fatty acid
DMSO:	Dimethylsulphoxide	TB:	Tributyrin
DNA:	Deoxyribonucleic acid	TCE:	1,1,2-Trichloroethylene
FAME:	Fatty acid methyl ester	THF:	Tetrahydrofuran
FCH:	Fenchone	TG:	Triglyceride
HTMC:	Dodeca-methoxyhexathia-meta cyclophane	TM:	Trimyristin
LC:	Liquid crystal	TMCOT:	1,3,5,7-tetramethylcycloocta-tetraene
LLC:	Lyotropic liquid crystal	TMU:	Tetramethylurea
ML:	Methyl linoleate	UFA:	Unsaturated fatty acid
MLN:	Malononitrile		

Greek Symbol notations used			
$\Delta\delta^{R/S}$	Difference of $\delta$ between enantiomers	$\Delta\sigma$ :	Residual chemical shift anisotropy
$\Delta\Delta\nu_Q^{R/S}$	Difference of quadrupolar splitting between enantiomers	$\delta$ :	Chemical shift
$\Delta\nu_Q$ :	Quadrupolar splitting	$\gamma_i$ :	Gyromagnetic ratio
$\Delta\chi_m$ :	Molecular magnetic susceptibility anisotropy	$\theta_m$ :	Magic angle (54.73°)

POST-PRINT